

MAE 154A

Preliminary Design of Aircraft

Oddvar O. Bendiksen

Department of Mechanical and Aerospace Engineering
University of California, Los Angeles



Winter Quarter 2017

Course Overview

Texts:

1. McCormick, B.W., *Aerodynamics, Aeronautics, and Flight Mechanics*, 2nd ed., John Wiley & Sons.
2. Raymer, D.P., *Aircraft Design: A Conceptual Approach*, AIAA Education Series.

Other References:

3. Torenbeek, E., *Synthesis of Subsonic Airplane Design*, Delft University Press, Nijhoff Publishers, 1982.
4. Nicolai, L.M., *Fundamentals of Aircraft Design*, University of Dayton, OH, 1975.
5. Nicolai, L.M. and Carichner, G.E., *Fundamentals of Aircraft and Airship Design*, (in 2 volumes), AIAA Education Series, 2010.

Course Requirements:

- Preliminary Design Report (30%)
- Final Design Report (60%)
- Design Presentation (5%)
- Design Review (5%)



Topics

1. Overview of Aircraft Design Process; History of Flight.
2. Review of Basic Aerodynamics and Flight Mechanics.
3. Preliminary Design Layouts; Configuration Studies;
Structural and Mechanical Design Considerations.
4. Airfoil Aerodynamics; Airfoil Selection.
5. Subsonic and Transonic Wing Aerodynamic Design.
6. Supersonic Wing Aerodynamic Design.
7. Drag Estimation; Drag Reduction; Minimization of Induced Drag.
8. Propulsion: Reciprocating Engines; Gas Turbines; Engine Selection.
9. Airplane Performance Analysis; Design for Optimum Performance.
10. Airplane Stability and Control; Design of Empennage and Canards.



1.0 Overview of Aircraft Design Process



1.1 Introduction

- What is “*Preliminary Design*”?
- How does it differ from
 - Conceptual Design?
 - Detail Design?
 - Analysis?
- How is the “design” conveyed to (the) manufacturing (division) so that the individual parts can be made and assembled into a complete aircraft?
- Is this process different in the aircraft/aerospace industry than in, say, the automobile industry?
- What role does CAD/CAM play?
- Can “*Virtual Reality*” and “*Virtual Prototyping*” ever replace “real” modeling?



Design Process

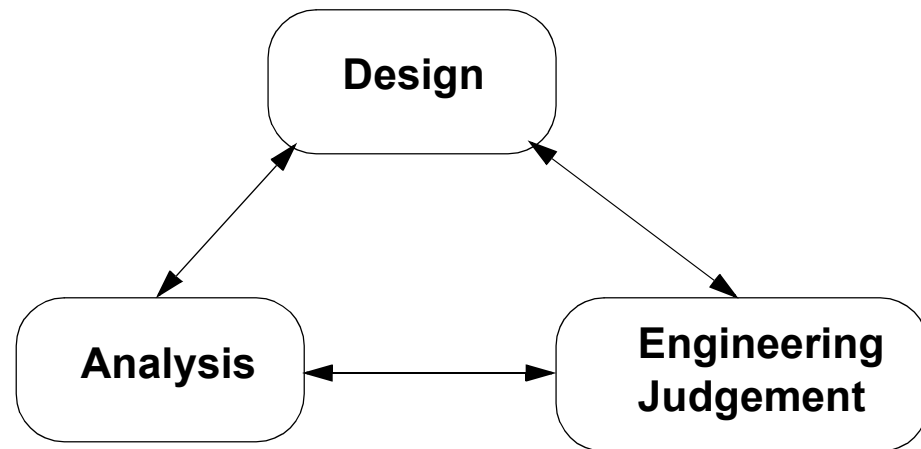
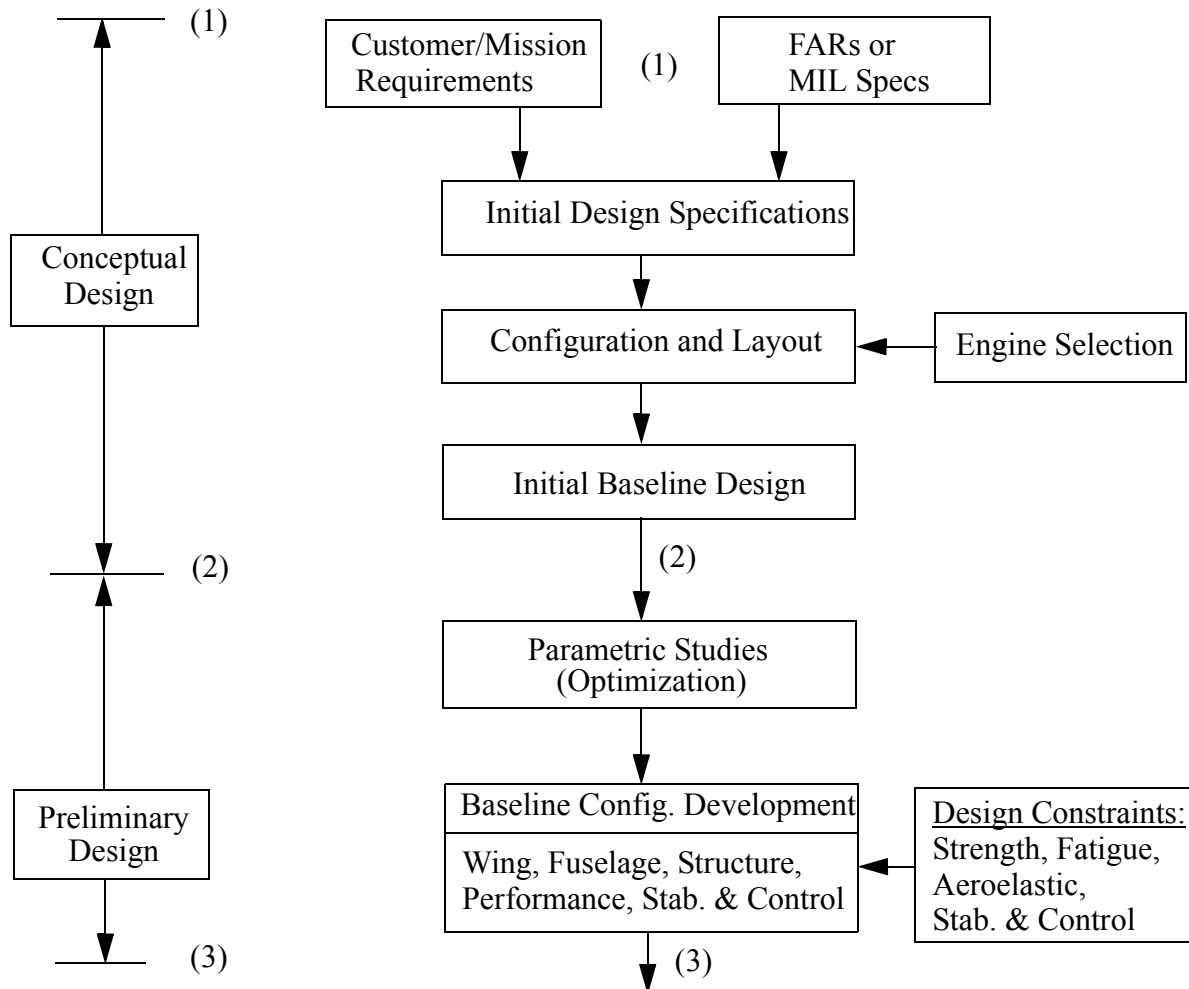


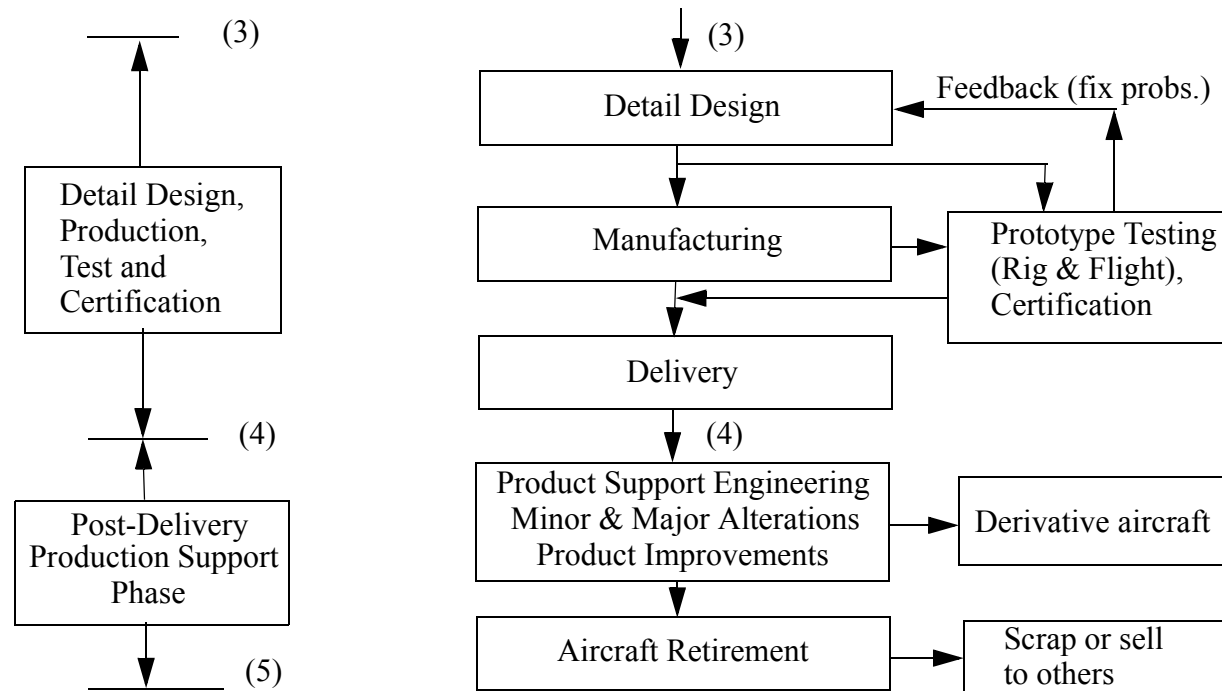
Fig. 1.1 Iterative nature of design process.



Aircraft Design & Development



Detail Design, Production, Test & Certification



Important Design Considerations

Civil Transport Aircraft

- Operating Cost
 - Fuel
 - Crew
 - Maintenance
 - Insurance, interest, etc. (not design related)
- Powerplant Selection
 - Jet vs. piston engines (reliability, fuel efficiency, passenger comfort)
 - Turbofan vs. turbojet (high vs. low BPR, fuel efficiency)
 - Turboprop and propfans (fuel efficiency vs. noise; new technology)
- Structural and Mechanical Integrity
 - Strength and buckling considerations
 - Fatigue and corrosion fatigue
 - Creep (high temperatures)
 - Aeroelastic problems (flutter, divergence, aileron reversal)
- Introduction of New Technologies (composite materials; fly-by-wire controls, ...)
- Attention to Customer Needs



Role of Optimum Design

- In “*Optimum Design*”, one attempts to cast the design problem as a *mathematical optimization problem*:

$$\text{Min } W(x_i)$$

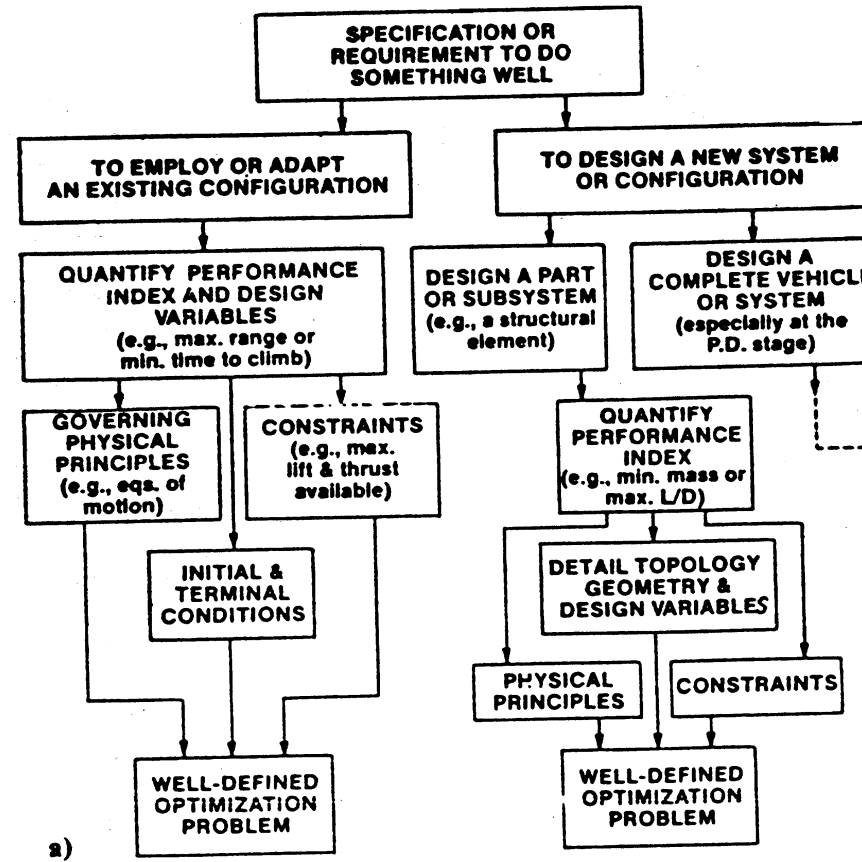
subject to *constraints*

$$C_k(x_i) \geq 0; \quad k = 1, 2, \dots, r$$

- Here, $W(x_i)$ is the objective function (typically the gross weight), x_i are the design variables, and the functions C_k represent design constraints.
- For a review of the use of optimum design principles in aircraft design, see H. Ashley, "On Making Things the Best - Aeronautical Uses of Optimization," *Journal of Aircraft*, Jan. 1982.



Optimum Design: Formulation



Optimum Design: Solution Phase

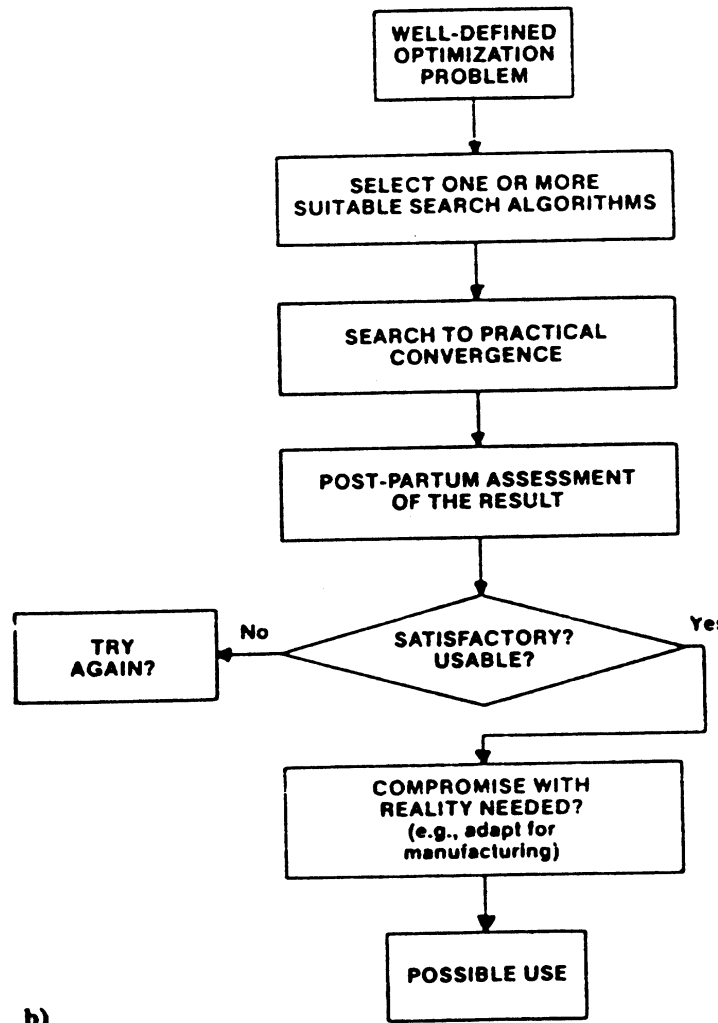


Fig. 1 Morphology of optimization in aeronautics. (From H. Ashley, JA)



JANUARY 1982

AERONAUTICAL USES OF OPTIMIZATION



A-7 WING
AR = 4
SWEEP = 35°
T/C = .07



WING NO. 1
AR = 4
SWEEP = 35°
T/C = .12



WING NO. 2
AR = 5
SWEEP = 20°
T/C = .09

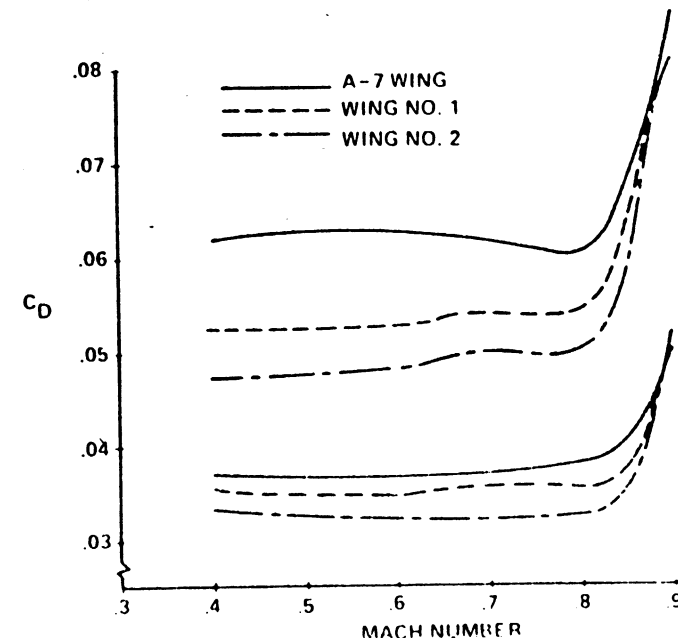
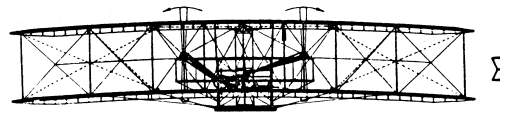
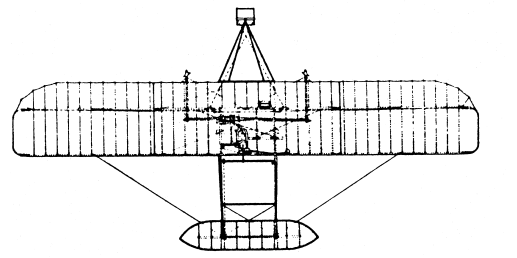


Fig. 7 Dependence of drag coefficient on Mach number, at two values of lift coefficient for the wings of Fig. 6.

Fig. 6 Plan views and other details for original A-7 wing and two reduced-drag substitutes designed by Haney and Johnson (Ref. 51).

(From H. Ashley, JA)



A BRIEF HISTORY OF FLIGHT



O. O. Bendiksen
MAE Department, UCLA



Introduction

The Beginning

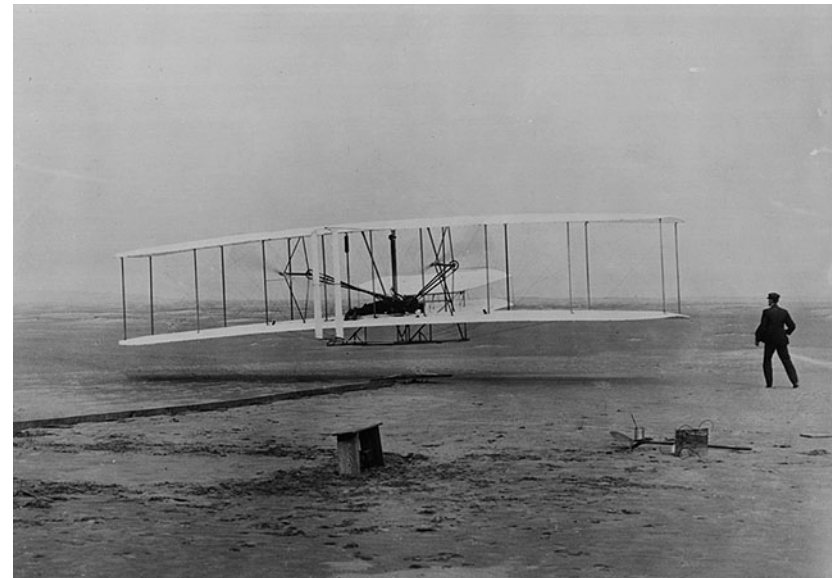
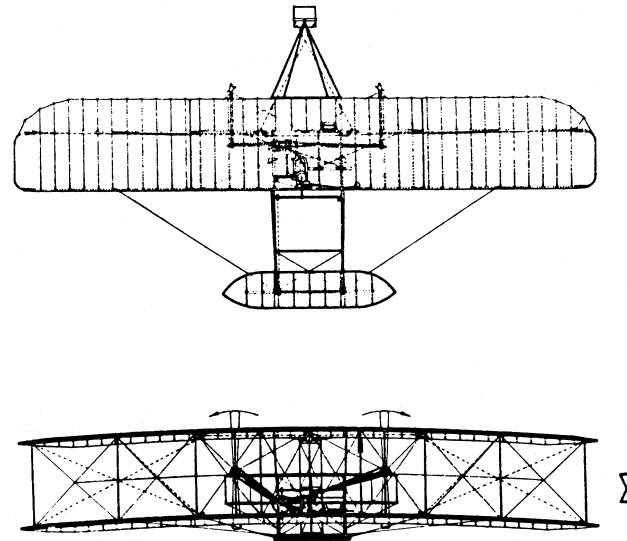
- *Once upon a time*, two brothers decided to build an airplane that could fly under its own power
- They were not aeronautical engineers, not even engineers, but rather bicycle mechanics, and this may have been their lucky break, since ignorance is often bliss when one must venture into uncharted waters
- Thus, they did not know that a great British scientist and Nobel laureate had just recently proclaimed human flight “infeasible” and an utter folly



The Wright Flyer

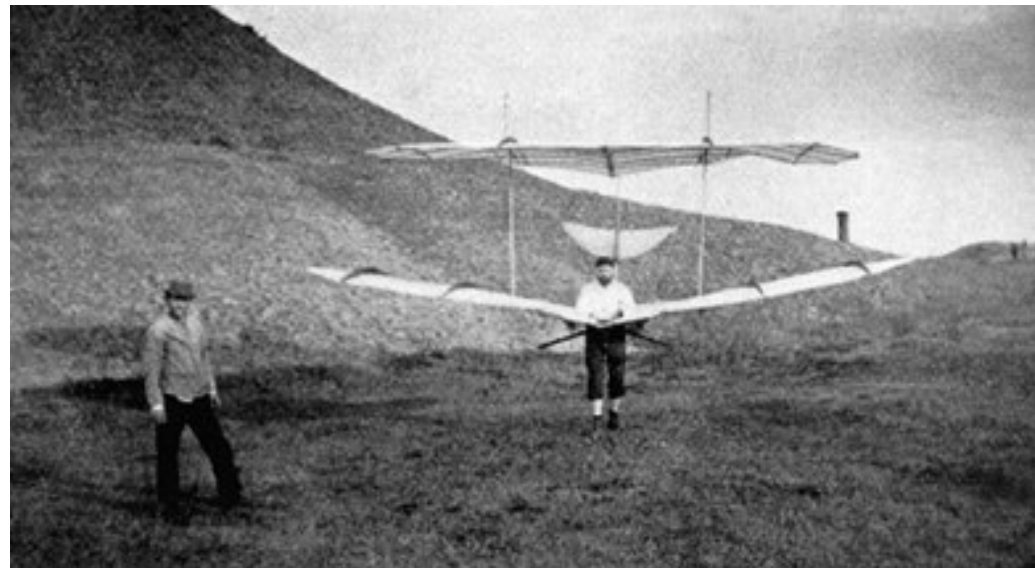
Multiply Braced Biplanes

- The Wright Brothers had been lucky. Ignorant as they were about the dangers of aeroelastic phenomena (divergence and flutter) they had the serendipitous luck to select the best design of the day: *The Multiply Braced Biplane*
- Their chief competitor for the price, Professor Samuel P. Langley, was not so fortunate
- Importance of sufficient *torsional stiffness* was not appreciated at that time



But Before the Beginning, there was Otto...

- 1889 - The German engineer Otto Lilienthal publishes the book "Der Vogelflug als Grundlage der Fliegekunst" (Bird Flight as the Basis of Aviation), the first book on flight based on science and experiments
- 1891 - Otto Lilienthal starts his glider flights, first in a series of 2000(!), until he crashes and breaks his neck in 1896. During this period, he built and flew 18 gliders: 15 monoplanes and 3 biplanes

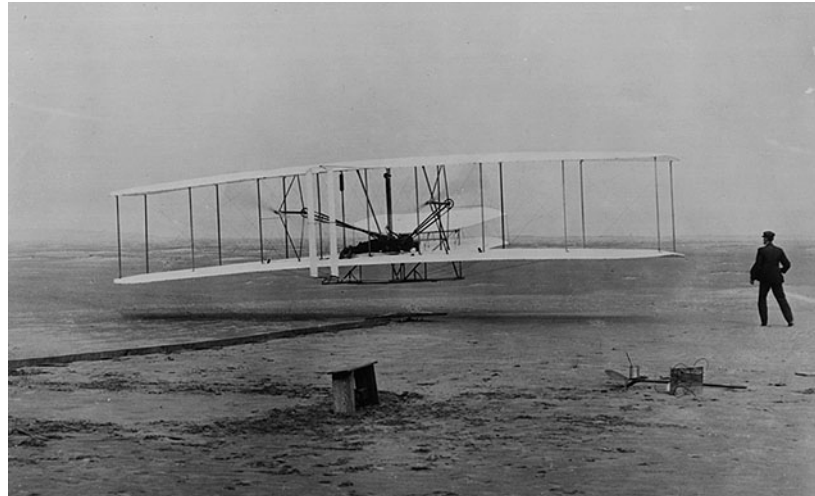


The Wright Brothers

First Flight at Kitty Hawk

1903 - Orville and Wilbur Wright make the first successful powered flight in their Wright Flyer on December 17, 1903 at Kitty Hawk, NC

After a promotional tour in Europe (there being no interest in airplane flight in the US at that time), the brothers sell their Flyer to the US Army for lots of cash



A long and bitter (and wrongful) lawsuit against Curtiss ensues, in an attempt to claim priority on the invention of the aileron

1912+ Their goodwill pretty much used up, they slowly fade into the sunset



World War I

Biplanes and Triplanes

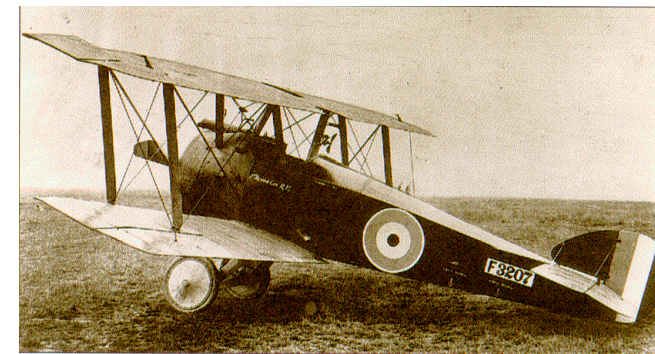
WWI (1914-1918): The military use of the airplane provides a needed *kick-in-the-pants* to stimulate developments

Ludwig Prandtl sets up his famous aeronautical research institute at the University of Göttingen in Germany, and develops the 3D lifting line wing theory that is still used by engineers in preliminary design

Structural innovations are modest: Aircraft spruce is the material of choice for wing spars and ribs, covered with fabric and doped and lacquered to finished strength



Fokker D-VII.



Sopwith Camel.

1919 - The US Army starts dumping - at fire sale prices - all of its WWI aircraft, as they are no longer needed in peacetime. The military brass and the civilian experts at MIT don't have the foresight to see that the airplane has a future

World War I

Aeroelastic Divergence Phenomenon is Discovered

- The high-performance monoplane Fokker D-8 enters service in October 1918 and is given to the top German aces
- Wing failures immediately start to occur in high-speed power dives
- Fokker himself diagnoses the problem as a new phenomenon caused by the interactions between the airloads and the flexible wing structure
- Problem is essentially one of *insufficient wing torsional stiffness*



Lindbergh

The Savior of Aviation

1927 - The Kool Absolut Grandson of a Swede, Charles Lindbergh, rescues aviation from oblivion by performing the ultimate stunt of flying solo nonstop from New York to Paris (May 20-21)

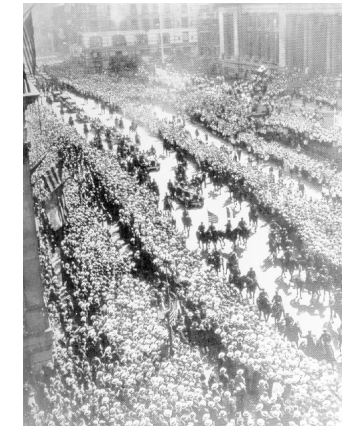
Lindbergh is famous overnight and doesn't have to worry about his next paycheck ever again. But the wise men still don't see any commercial value in the airplane, except to haul mail



The Spirit of St. Louis.

Note lack of forward windows

A periscope was used when needed



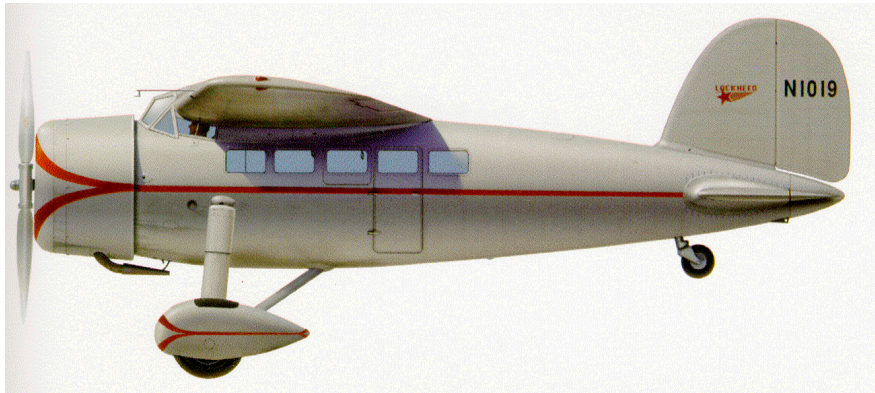
A New York parade awaits the hero

Lockheed Vega

Smooth Plywood Fuselage Construction

1927 - On July 4, the Loughead brothers (by then renamed *Lockheed* at the advice of their clever PR man), together with Jack Northrop, roll out the aircraft that starts modern aviation: the *Lockheed Vega*

It is beautifully streamlined unbraced monoplane, with an NACA cowl around a reliable Wright Whirlwind engine, with shock struts and hydraulic brakes on the main landing gear, and a price of less than \$20k



The Lockheed Vega.



Wiley Post's Vega, the *Winnie Mae*.

The Vega quickly becomes the aircraft of choice for all pilots of adventure (Wiley Post, Amelia Earhart, ...) and the rich and famous (Hearst, ...)

Boeing 247

First Smooth-Skin All-Metal Monocoque Construction

1933 - Boeing delivers the *B247*, the first smooth-skin, all-metal monocoque transport aircraft, with NACA cowls, two-position propellers, and a *retractable* landing gear. The entire production is pledged to United Airlines, which turns out to be a lucky break for Douglas

The chief design engineer has made a *bad mistake*: The main wing spar running through the cabin extends more than *two feet* above the cabin floor, causing passengers to stumble and spill their drinks ...



Douglas

Southern California Emerges as the Center of Aviation

1933 - Jack Frye, the 29-year-old VP of operations at TWA, asks Douglas to develop an airplane that can compete with the B247

Douglas answers by rolling out the 12-passenger DC-1 on July 1, 1933. It has Wright 1820 engines, adjustable-pitch propellers, with Karman wing fillets and split flaps ($V_L < 65$ mph)

Only one DC-1 was produced, but it gave rise to the most successful aircraft in aviation history: the DC-3. Before getting there, 220 of the 14-passenger (20 ft longer) DC-2 model were produced and delivered to the airlines. More than 11,000 DC-3 aircraft were built



The DC-1



The DC-2

The DC-3

(The DC-2 is still around)

1935 - The DC-3 arrives and changes aviation forever, by making passenger transport economically feasible and freeing the airlines from having to depend on the US Mail to make money

It carried 21 passengers, and could fly Los Angeles to New York in 24 hours (3 stops and 18 hrs of flying, cruising at 180 mph with the new P&WA 1830 engines

The modern semi-monocoque aluminum aircraft structure is established



The DC-3. Look at the streamlined design of this baby



Buffalo Airways - Northwest Territories in Canada

**Still going strong ...
and able to make money for its owners!**



World War II

A Turning Point for Aviation

WWII - Aviation gets another kick in the pants, and the value of the airplane in the commercial and military arenas is never again questioned

The *science* of aeronautics is finally becoming of age. NACA's Langley Research Center leads the way in the US, but the Germans are ahead in many respects



The Messerschmitt 109F



The *Me-262* was the first jet fighter. Very far ahead of its time, capable of reaching speeds of Mach 0.8. Fortunately for us, Hitler and Göring only believed in propellers

WWII Aircraft

On the Allied Side



The Supermarine *Spitfire* played a decisive role in the Battle of Britain. An elliptic wing and a Rolls-Royce Merlin engine made it a top performer



The *P-51 Mustang* was USA's best fighter of the WWII era



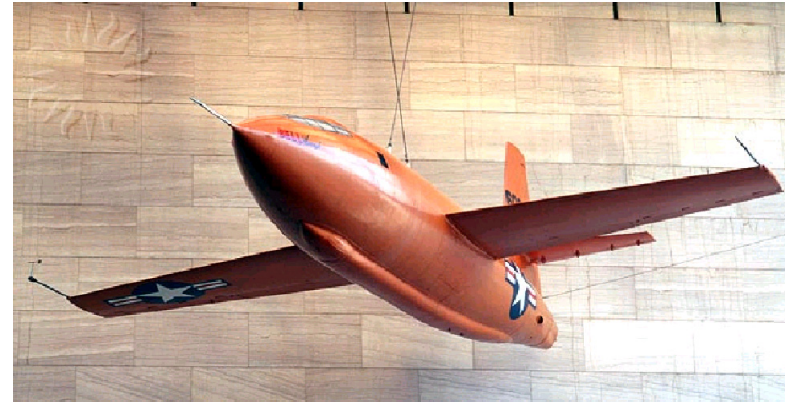
The Sound Barrier That Did Not Exist...

1947 - The Bell X-1 rocket-powered research aircraft breaks the sound barrier



NASA Dryden Flight Research Center Photo Collection
<http://www.dfrc.nasa.gov/gallery/photo/index.html>
NASA Photo: E49-007 Date: Sep 1949 Photo by: NASA photo

X-1-2 mounted under B-29 for launch



The Golden Era of Military Aircraft R&D

1950-1970

1947 - Boeing delivers the first jet bomber, the B-47. The cold war is under way, and with it comes money from Washington in a torrent never seen before. New military jet aircraft are developed and tested at Edwards AFB at an incredible rate

Some represented breakthroughs and went on to become classic aircraft; others are just as soon forgotten



One of the classics: *The B-52*.

Still in service, because of its capability to drop lots of "dumb" bombs and "bomb the enemy into the Stone Age" (to quote a US general during the Vietnam War)

The Golden Era

Two Notable Jet Fighters



The *F-100 Super Sabre* is the first jet capable of sustained level flight at above Mach 1. But the original aircraft has a nasty disposition



The *F-15* marks the end of the Golden Era

The Cold War is On

The Russians are Busy as Well...



A family portrait:

a) *MIG-29*

b) *MIG-21*

c) *MIG-15*



The Jet Age

What You Don't Know Can Hurt You

1952 - On the civilian side of business, the first jet powered transport enters service, the DH Comet 1, with BOAC, between London and Johannesburg, South Africa

The next year (1953), BOAC, UAT, and AF start operating the Comet on additional routes to the Far East, India, and Africa



1954 - Two Comet 1 aircraft suffer fatal and mysterious crashes

After the wreckage of one is recovered, the cause is determined to be metal fatigue of the fuselage structure around the window cutouts, resulting in massive structural breakup in flight

The Comet is withdrawn from service. Although redesigned and reintroduced as the Comet 4 in 1958, its reputation is shot and it never recovers to become a commercial success



The Race is On

A Revolution in Aviation

1956 - The Soviet Tupolev Tu-104 becomes the first jet transport in sustained service

1954-60 Boeing and Douglas work desperately to catch up and deliver their own passenger jets, the B-707 and DC-8, respectively

Pan Am places the first order on October 13, 1955, for 20 B-707's and 25 DC-8's



The Boeing 707

1958 - BOAC starts transatlantic jet service with a B-707-120, beating out Pan Am by three weeks(!). The nerve of those Brits

1960 - KLM starts transatlantic service with the DC-8-30. The jet age of commercial aviation is in full swing. The piston-powered civilian passenger aircraft's goose is cooked. Five years later, it is completely cooked

The Age of Speed

Mach 3+

1964 - The SR-71 Blackbird rolls out of Lockheed's (Kelly Johnson's) Skunk Works in Burbank. It is capable of sustained flight at Mach 3+ at altitudes of over 85,000 feet

Top speed and absolute ceiling remain classified



Dryden Flight Research Center EC97-43933-2 Feb1997
NASA Dryden's SR-71A #844 is pictured over the Southern
Sierra Nevada mountains during a recent pilot
proficiency flight. (NASA/Jim Ross)



Kelly Johnson's Skunk Works

Lockheed's Facility at Burbank Airport



But the End is Near And the Ending is Spectacular

1964 - North American Aviation rolls out the first of two XB-70A prototype Mach 3+ bombers. The second aircraft is destroyed in a midair collision in 1966

The No. 1 aircraft continued its research flights at the NASA Flight Research Center at Edwards until it was retired and flown to the AF Museum on February 4, 1969



NASA Dryden Flight Research Center Photo Collection
<http://www.dfrc.nasa.gov/gallery/photo/index.html>
NASA Photo: ECN-792 Date: August 17, 1965

XB-70A during take-off



Dryden Flight Research Center EC68-2131 Photographed 1968
XB-70 NASA photo



The Golden Era of Military R&D in aviation is over and out

The Jumbo Jets

2nd Generation of Jet Transports

1969-72 The second generation of jet transports enters service; the "jumbo" or "wide-body" aircraft: B-747, L-1011, and DC-10. These designs represented high-risk ventures, because of the unknown scaling problems involved in more than doubling the size of the aircraft and its engines!

Only Boeing was successful from an economic standpoint, and the B747 is still flying

But the company almost went under in 1970



Dryden Flight Research Center ECN 4245 Photographed 1974
747 vortex study NASA photo



An American Airlines *B-747* used in flight tests at Dryden



Dryden Flight Research Center EC95-43145-4 Photographed June, 1995
A NASA F-18 chase plane accompanies Orbital Science's L-1011
TriStar on a baseline data flight prior to the start of NASA's
Adaptive Performance Optimization project. (NASA/Carla Thomas)



The *L-1011*

The Dark Decade

1970-1980

1973 The US is hit with the first of two OPEC oil price shocks, just as the bills from the Vietnam War are coming due and Lockheed is facing bankruptcy

1974 - The Concorde represents the only bright light of the decade. Alas, in the OPEC era, the aircraft is no longer economically feasible to operate

The Russians enter the supersonic game as well, with the Tu-144 (the "Konkordski"). It is at the height of the cold war

But the Tu-144 meets with grief during the 1973 Paris Air Show, breaking up in flight during a low altitude pull-up



Guess which is which...



NASA Dryden Flight Research Center Photo Collection
<http://www.dfrc.nasa.gov/gallery/photo/index.html>
NASA Photo: EC97-44203-5 Date: July 1997 Photo by: NASA/IBP
Russian Tu-144LL SST Flying Laboratory Landing at Zhukovsky Air Development Center

The Decade of Diminishing Returns

1980-1990

New airplanes are introduced, but they represent small perturbations involving little or no risk. The risk is further reduced by *scaling down* rather than up in size.

On the military side, *stealth* replaces speed as the design objectives change.



The B-2 stealth bomber

Jack Northrop finally gets his revenge (from the grave) as his flying wing concept is finally taken seriously



Fifth Generation Fighters

F-22 and F-35

1997 - The F-22 Raptor starts flight testing at Edwards AFB. According to everyone with a dog in this fight, this is *the ultimate fighter*, to replace the F-15



The *F-22* side by side with an aging *F-15*
How can you tell them apart?
(Hint: The wing taper and tail dihedral
are different ...)

If the money doesn't run out, we'll soon have the F-35 (JSF) fully operational as well

F-35 Joint Strike Fighter

Ready for Prime Time?

The JFS is an impressive bird, but has suffered multiple setbacks from engine problems (blade failures), aircraft fires, schedule delays, and cost overruns

Some pilots say it will come up short in a dogfight with a 4th generation F-16!



2000 - Present Day

Now What?

Bold ideas are finally back in vogue:

Boeing: The Sonic Cruiser (alas, a Flash in the Pan)

Airbus: The A-380 Super Jumbo

Boeing: The 7E7 (later renamed the 787 Dreamliner)

Many airframers: UAVs for civilian and military purposes



Alas, the beautiful *Sonic Cruiser* bird became extinct before it was even born



The solar powered *Helios* bird, before it met with grief

Airbus 380

Luxury at 35,000 feet



Boeing 787

After a Difficult Birthing Process, Success at Last



- Extensive use of composites
- Extensive use of subcontractors for primary structure and systems
- Extensive delays
- Battery fires and other grief

What's Next?

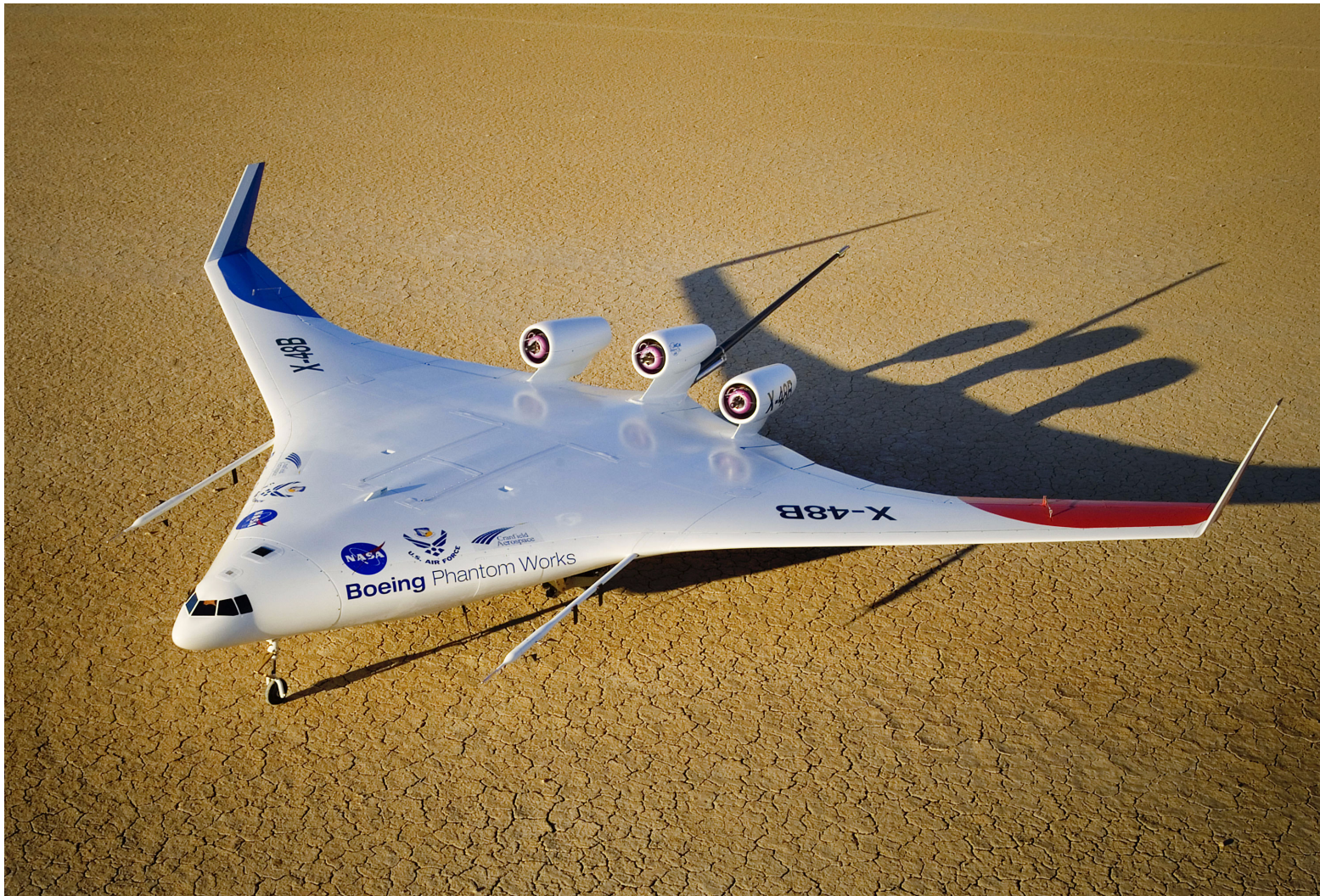
Opinions Differ...

Here are some of the ideas floating around



Blended Wing Body Design

Boeing



Supersonic Aircraft

Business and Passenger Jets



Boom Mach 2.2 SST (50 passengers)



Spike Aerospace Mach 1.6 S-512 SSBJ



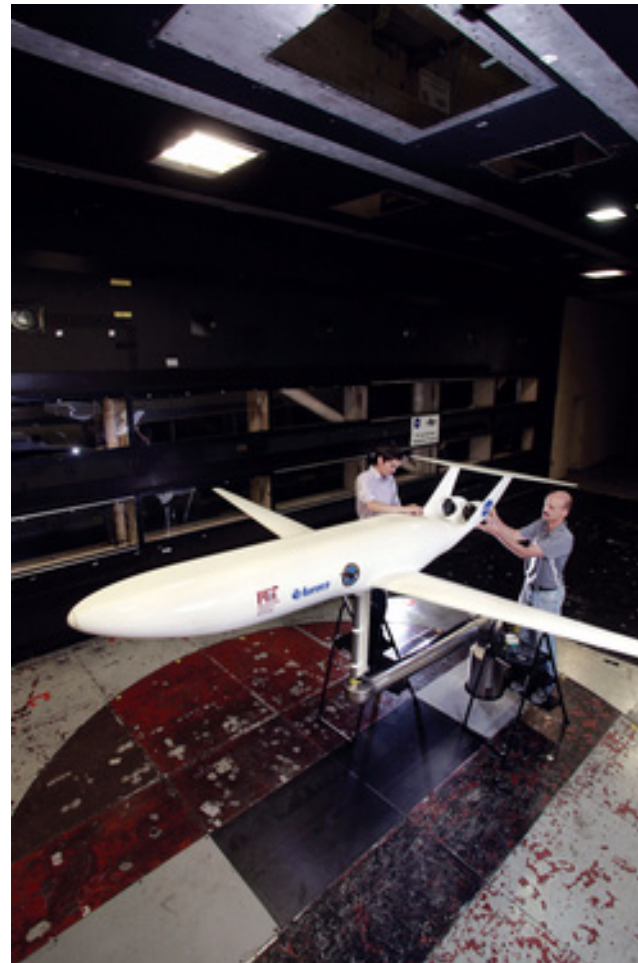
Aerion Mach 1.4 AS2 SSBJ



NASA QueSST Mach 1.4+ X-plane
(Lockheed Martin design)

Boundary Layer Ingestion for Drag Reduction

Poor Engines: Engines Don't Like Distorted Inlet Flow



2.0 Review of Basic Aerodynamics and Flight Mechanics



2.1 Introduction

Purpose of Chapter

- The purpose of this chapter is to present a summary of the more important formulas that will be used in the preliminary design calculations in this course.
- First, by pulling the basic aerodynamics and performance equations all in one section, students do not have to search through several texts to get started.
- Second, by reviewing the assumptions behind the various equations, students will be in a better position to determine the adequacy of these assumptions in a preliminary design environment, and as applied to their design in particular.



2.2 Steady Flight

Equilibrium Equations

- Consider an aircraft flying along a straight flight path with a constant velocity.
- The equations of motion then reduce to the *static equilibrium equations*

$$\sum F_x = T \cos \alpha - D - W \sin \gamma = 0 \quad (2.1)$$

$$\sum F_z = W \cos \gamma - L - T \sin \alpha = 0 \quad (2.2)$$

$$\sum M_y = M_{cg} = 0 \quad (2.3)$$

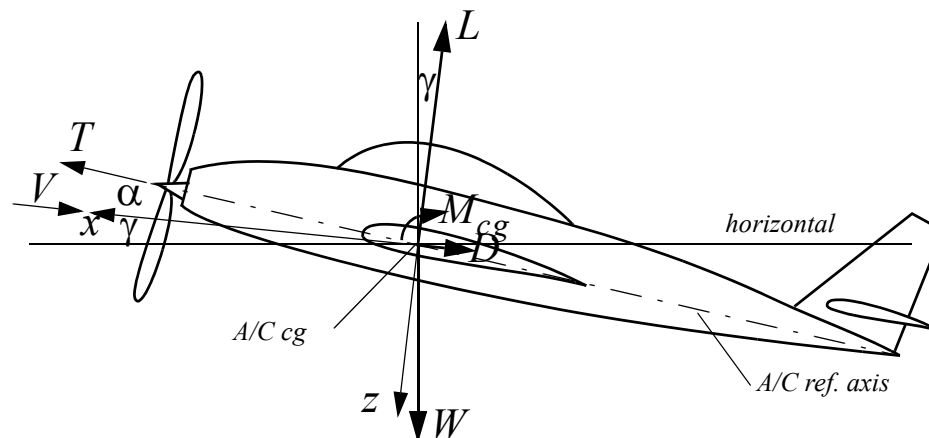


Fig. 2.1 Aircraft in steady flight.

a) Level Flight ($\gamma = 0$)

- The equilibrium equations become

$$\begin{aligned} T\cos\alpha &= D \\ L &= W - T\sin\alpha \\ M_{cg} &= 0 \end{aligned} \tag{2.4}$$

- If the angle of attack is small, $\cos\alpha \approx 1$, $\sin\alpha \approx \alpha \approx 0$, and the first two equations become

$$T = D$$

and

$$L = W,$$

respectively.



b) Steady Climb: ($\gamma = \text{const.} > 0$)

- Assuming $\alpha \ll 1$, $\cos\alpha \approx 1$, $\sin\alpha \approx \alpha \approx 0$,

$$\begin{aligned} T - D &= W \sin\gamma \\ L &= W \cos\gamma \\ M_{cg} &= 0 \end{aligned} \tag{2.5}$$

- The rate of climb can be obtained directly from the vector diagram below:

$$\begin{aligned} R/C &= V \sin\gamma \\ \sin\gamma &= \frac{T - D}{W} \end{aligned}$$

Fig. 2.2 Rate of climb.

$$R/C = \frac{(T - D)V}{W} \tag{2.6}$$



b) Steady Glide/Descent: ($\gamma = \text{const.} < 0$)

- From Eqs. (2.5), it follows that

$$\begin{aligned} T - D &< 0 \\ \tan \gamma &= \frac{T - D}{L} \end{aligned} \tag{2.7}$$

- The power-off glide slope is entirely determined by the drag to lift ratio:

$$\tan \gamma = -\frac{D}{L} \tag{2.8}$$

- The rate of descent R/D follows immediately from Eq. (2.6),

$$R/D = \frac{(D - T)V}{W} \tag{2.9}$$

and does depend on V , even in the case $T = 0$.



Trimmed Flight

- In trimmed flight, Eqs. (2.5) must be satisfied and this imposes two constraints on V :
 - *First, V must be higher than the stall speed, to make flight possible.*
 - *Second, V and angle of attack (or lift coefficient) must satisfy 2nd of Eqs. (2.5),*

$$L = \frac{1}{2}\rho V^2 C_L S = W \cos\gamma \quad (2.10)$$

- Solving for V ,

$$V = \sqrt{\frac{2 \cos\gamma}{\rho C_L}} \left(\frac{W}{S} \right) \quad (2.11)$$

- For a given flight path angle and wing loading W/S , and density altitude (ρ), the flight speed V and lift coefficient C_L are therefore related as follows:

$$V = \frac{\text{const.}}{\sqrt{C_L}} \quad (2.12)$$



2.3 Basic Aerodynamics

Aerodynamic Forces

- Aerodynamic forces are referred to the *aerodynamic center (AC)*, see Fig. 2.3.
- Aerodynamic forces (lift, drag, and pitching moment) acting on a wing can be written in terms of nondimensional aerodynamic coefficients, as follows:

$$\begin{aligned} L &= C_L q S \\ D &= C_D q S \\ M_{AC} &= C_{M_{AC}} q S \bar{c} \end{aligned} \quad (2.13)$$

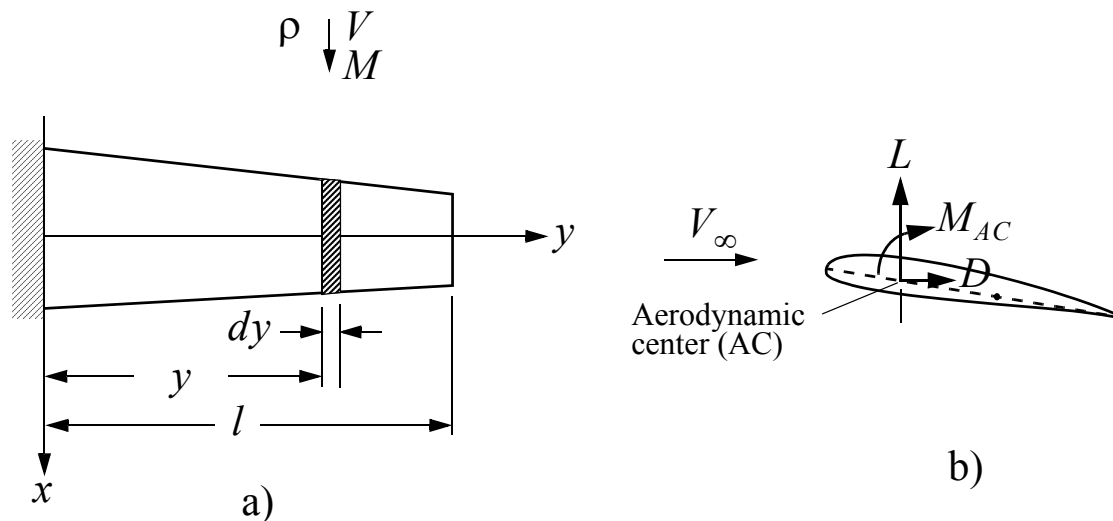


Fig. 2.3 a) 3D wing; b) typical chordwise section.

Aerodynamic Coefficients

C_L = lift coefficient

C_D = drag coefficient

$C_{M_{AC}}$ = moment coefficient about AC

(2.14)

$q = \frac{1}{2}\rho V^2$ = dynamic pressure

\bar{c} = wing mean aerodynamic chord (MAC)

S = wing area

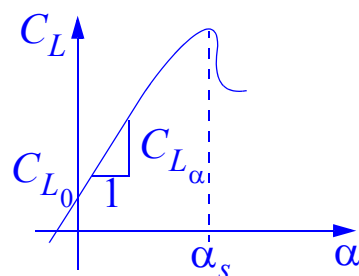


Fig. 2.4 Lift coefficient vs. α .

Over the linear part of the lift curve, Fig. 2.4, well below the stall angle α_s , the lift coefficient can be written as

$$C_L = \frac{\partial C_L}{\partial \alpha} \alpha + C_{L_0} \quad (2.15)$$

where $C_{L_0} = C_L|_{\alpha=0}$ is a constant independent of α .
($C_{L_0} \equiv 0$ for symmetric airfoils).



Linear Theory

- For a thin uncambered airfoil (e.g., a flat plate) in incompressible flow, linearized airfoil theory gives the following values for the lift and moment coefficients:

$$C_L = 2\pi\alpha; \quad C_{M_{AC}} = 0 = C_{L_0} \quad (2.16)$$

and the *aerodynamic center is at quarter-chord*.

- *Camber affects lift but not the lift curve slope or the location of the aerodynamic center.*
- The drag is zero in the two-dimensional inviscid case, on account of the appearance of a so-called “leading edge suction” force that precisely cancels the component of lift in the flow direction (d’Alembert’s Paradox).



2.4 Prandtl-Glauert Compressibility Corrections

Effect of Mach Number

- The effect of Mach number (or compressibility) on the aerodynamic coefficients can be determined using the *Prandtl-Glauert transformation*
- Corrections basically involve a stretching of the streamwise x -coordinate by the factor $1/\sqrt{1 - M^2}$.
- The corrections are valid in subsonic and supersonic flows, but not in transonic flows.



Compressibility Corrections - Subsonic Flow ($M < 1$)

$$C_p \equiv \frac{p - p_\infty}{\frac{1}{2} \rho_\infty V_\infty^2} = \frac{(C_p)_{M=0}}{\sqrt{1 - M^2}} \quad (2.17)$$

$$C_L = \frac{(C_L)_{M=0}}{\sqrt{1 - M^2}} \quad (2.18)$$

$$C_{L_\alpha} = \frac{(C_{L_\alpha})_{M=0}}{\sqrt{1 - M^2}} \quad (2.19)$$

$$C_{M_{AC}} = \frac{(C_{M_{AC}})_{M=0}}{\sqrt{1 - M^2}} \quad (2.20)$$

where the Mach number

$$M = \frac{V}{a} = \frac{V_\infty}{a_\infty} \quad (2.21)$$

refers to the Mach number of the undisturbed flow (i.e. at upstream infinity).



Flow Patterns in Sub-Transonic and Transonic Flows

- Figure 2.5 shows the flow patterns about an airfoil or wing as the Mach number is increased into the transonic region.

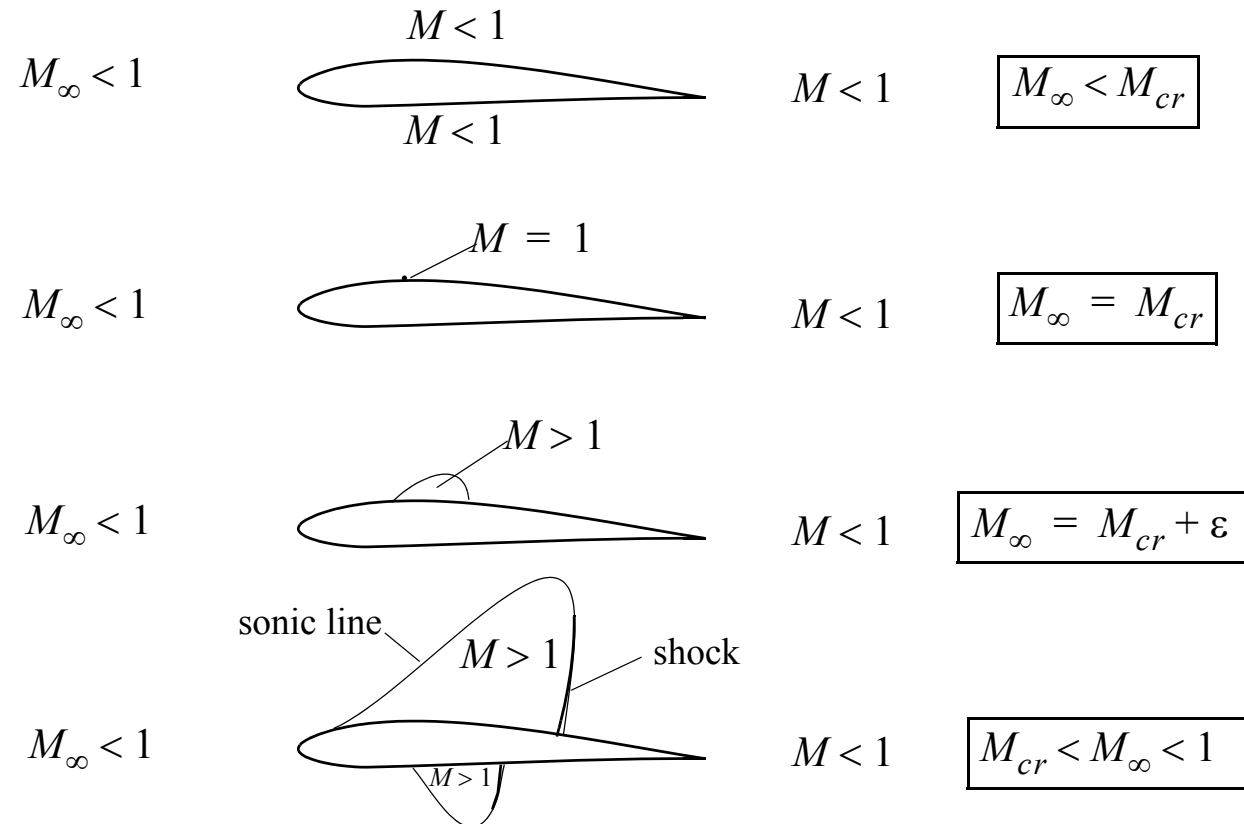


Fig. 2.5 Flow patterns about airfoils and wings in sub-transonic and transonic flows.

Drag Divergence

- When strong shocks occur on the airfoil, C_D increases rapidly, Fig. 2.6, because of wave drag + increased parasite drag due to shock-boundary layer interactions.
- As the angle of attack (or C_L) increases, so does the drag.

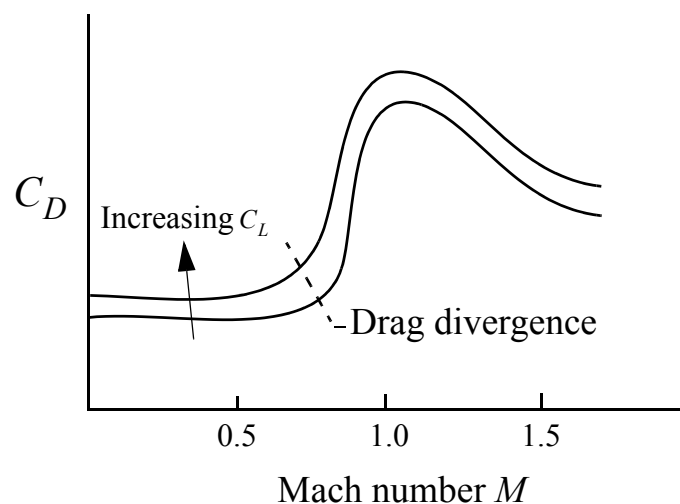


Fig. 2.6 Typical behavior of drag vs. Mach number.



Shock-Free Solutions

- Smooth acceleration from subsonic flow to supersonic flow (across the *sonic lines* indicated in Fig. 2.5) is possible both theoretically and in practice
- The reverse is not true:
Smooth shock-free (isentropic or loss-free) deceleration from supersonic to subsonic flow is only possible in theory.
- In all practical situations involving airfoils and wings in transonic flow, the deceleration occurs through a nearly normal shock wave.



Supercritical Wing

- If a given wing shape is capable of admitting a shock-free solution from a theoretical standpoint, the "real" wing may be expected to have only **weak shocks**.
- This is the basic idea behind so-called "supercritical wings", which allow near shock-free operation at Mach numbers beyond the critical Mach number.

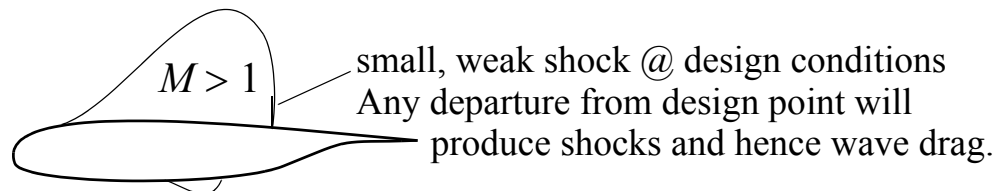


Fig. 2.7 Supercritical airfoil.

- These wings have the additional advantage that they permit the use of greater airfoil thickness ratios, providing more room for the structure, fuel tanks, etc.
- Supercritical sections typically have a cusp-like thin trailing-edge region, which brings in its own structural design problem.

Compressibility Corrections - Supersonic Flow ($M > 1$)

- In this case the natural reference Mach number is $M = \sqrt{2}$ (where no coordinate stretching occurs).
- The corresponding compressibility corrections are

$$C_p = \frac{(C_p)_{M=\sqrt{2}}}{\sqrt{M^2 - 1}} \quad (2.22)$$

$$C_L = \frac{(C_L)_{M=\sqrt{2}}}{\sqrt{M^2 - 1}} \quad (2.23)$$

$$C_{L_\alpha} = \frac{(C_{L_\alpha})_{M=\sqrt{2}}}{\sqrt{M^2 - 1}} \quad (2.24)$$

$$C_{M_{AC}} = \frac{(C_{M_{AC}})_{M=\sqrt{2}}}{\sqrt{M^2 - 1}} \quad (2.25)$$



Supersonic Wave Structure

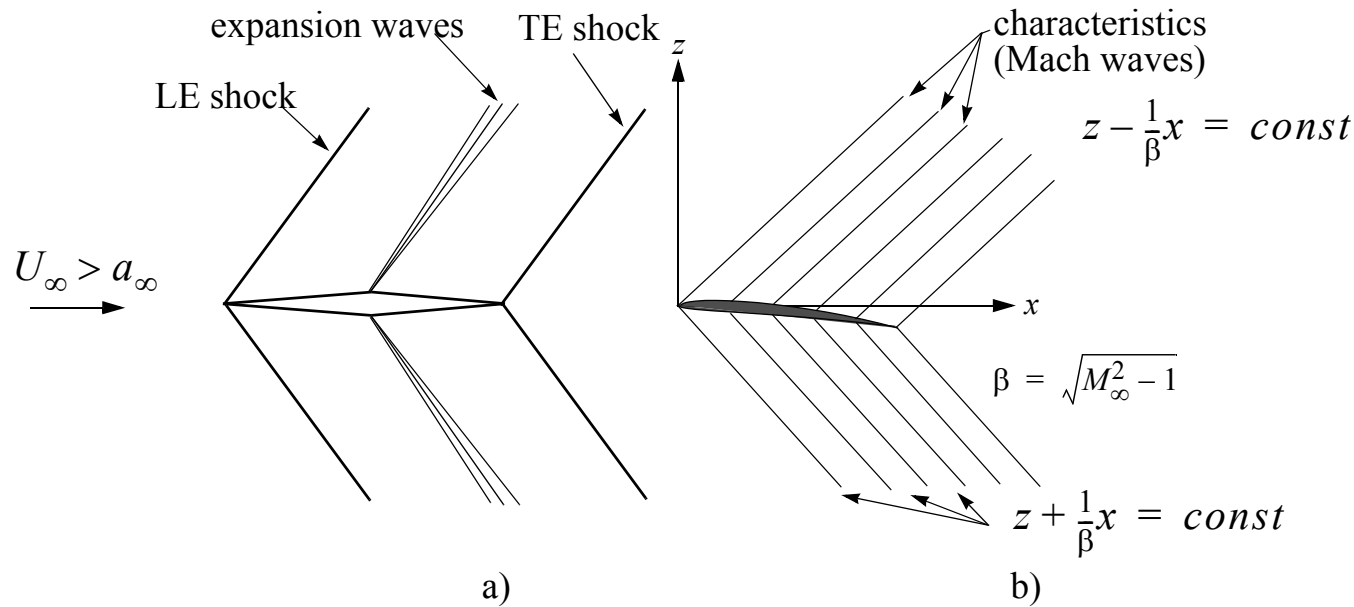


Fig. 2.8 Waves in supersonic flow: a) about a double wedge; b) about a smooth airfoil, according to the concepts of *linearized* supersonic flow (shocks become Mach waves)

- Supersonic flows are characterized by waves, Fig. 2.8, even in the steady case, and these waves extend to infinity.
- The waves carry energy away from the wing or body and give rise to an additional drag (*wave drag*) not present in subcritical subsonic flows.

2.5 Drag

Nomenclature

- For design purposes, it is customary to split the drag of an airplane (or a wing) into *induced* and *parasite* drag, as follows:

$$D = D_p + D_i \quad (2.26)$$

where

$$D_i = D_i(L) = \text{induced drag (associated with lift } L) \quad (2.27)$$

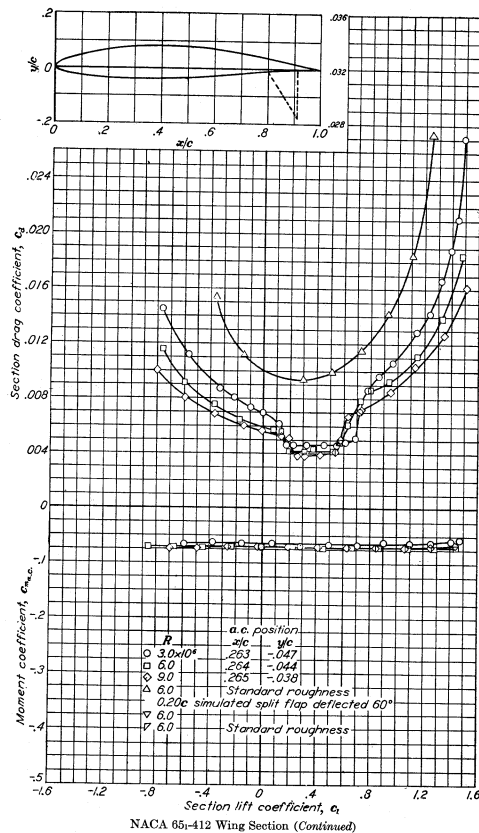
$$D_p = D - D_i = \text{parasite drag}$$

- Although D_p is not associated with lift, it still depends on the angle of attack and hence L , because of the sensitivity of the boundary layer to α and L .

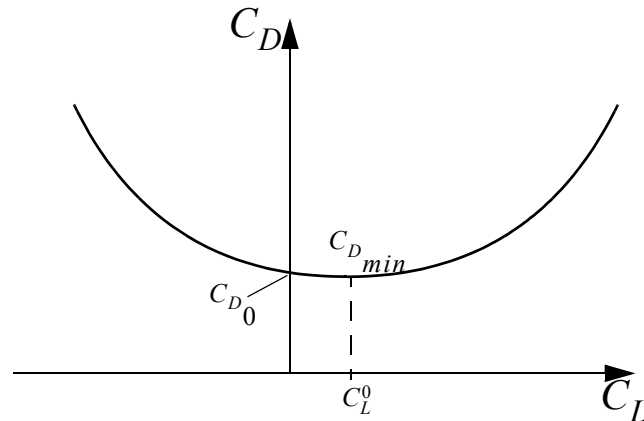


Drag Polar

- If we look at a typical drag polar for a wing or a two-dimensional airfoil, Fig. 2.9, the dominant behavior is essentially parabolic in C_L or α , for relevant values.



a) Laminar flow airfoil with “drag bucket”



b) Nomenclature

Fig. 2.9 Typical drag polars.

Drag Approximations

- A natural starting point for fitting curves to drag data obtained in wind tunnel tests would be to consider a Taylor expansion about $C_{D_{min}}$:

$$C_D = C_{D_{min}} + \frac{\partial C_D}{\partial C_L} \Big|_{C_L^0} (C_L - C_L^0) + \frac{1}{2} \frac{\partial^2 C_D}{\partial C_L^2} \Big|_{C_L^0} (C_L - C_L^0)^2 + \dots \quad (2.28)$$

$$C_D = C_{D_{min}} + K(C_L - C_L^0)^2 + \dots \quad (2.29)$$

valid to second order in the lift coefficient, where K is a constant.

- For symmetric airfoils and wings,

$$\begin{aligned} C_L^0 &= 0 \\ C_{D_0} &= C_{D_{min}} \end{aligned} \quad (2.30)$$

and the drag polar can be written as

$$C_D = C_{D_0} + K C_L^2 \quad (2.31)$$



Simplified Formula

- This symmetric form is typically used in preliminary design calculation, even for unsymmetric airfoils (error is small except for highly cambered sections).
- In some text, Eq. (2.31) is also used as the basis for splitting the drag into parasite and induced drag.
- But this is sloppy; instead, we will write

$$C_{D_P} = C_{D_{min}} + k'' C_L^2 \quad (2.32)$$

- Here k'' is a small constant (of order 0.01) that can be determined directly from curve-fitting a parabola to the two-dimensional wind tunnel data for the airfoil.
- Because of the considerable cost of obtaining relevant airplane drag data, most of this type of data is considered confidential and is typically as closely guarded as “trade secrets”.



Induced Drag

- For subsonic wings, the induced drag can be estimated based on the vortex theory of lift (formulas simple enough to be used in preliminary design).
- In supersonic flow, the situation is complicated by the fact that the wave drag is partly “induced” and partly “parasite”, in the above definition of the terms:
Part of the wave drag it associated with the production of lift.
- In most cases this “induced” part of the wave drag cannot be represented by a simple formula suitable for use in preliminary design.



2.6 Subsonic Wings

2.6.1 Prandtl's Lifting Line Theory

- For straight wings of moderate to high aspect ratio, the lifting line theory developed by Prandtl yields results of sufficient accuracy for use in preliminary design.
- The lifting line approximation is *based on the vortex theory of lift*, which associates lift with the establishment of a circulation about the wing.
- In the two-dimensional case, the *Kutta-Joukowski relation (or theorem)* states that the lift L is directly proportional to the circulation Γ around the airfoil:

$$L = \rho_\infty V_\infty \Gamma \quad (2.33)$$

- The generalization to a three-dimensional wing, Fig. 2.10, can be written as

$$\text{Lift per unit span: } l(y) \equiv \frac{dL}{dy} = \rho V \Gamma(y) \quad (2.34)$$



Horseshoe Vortices

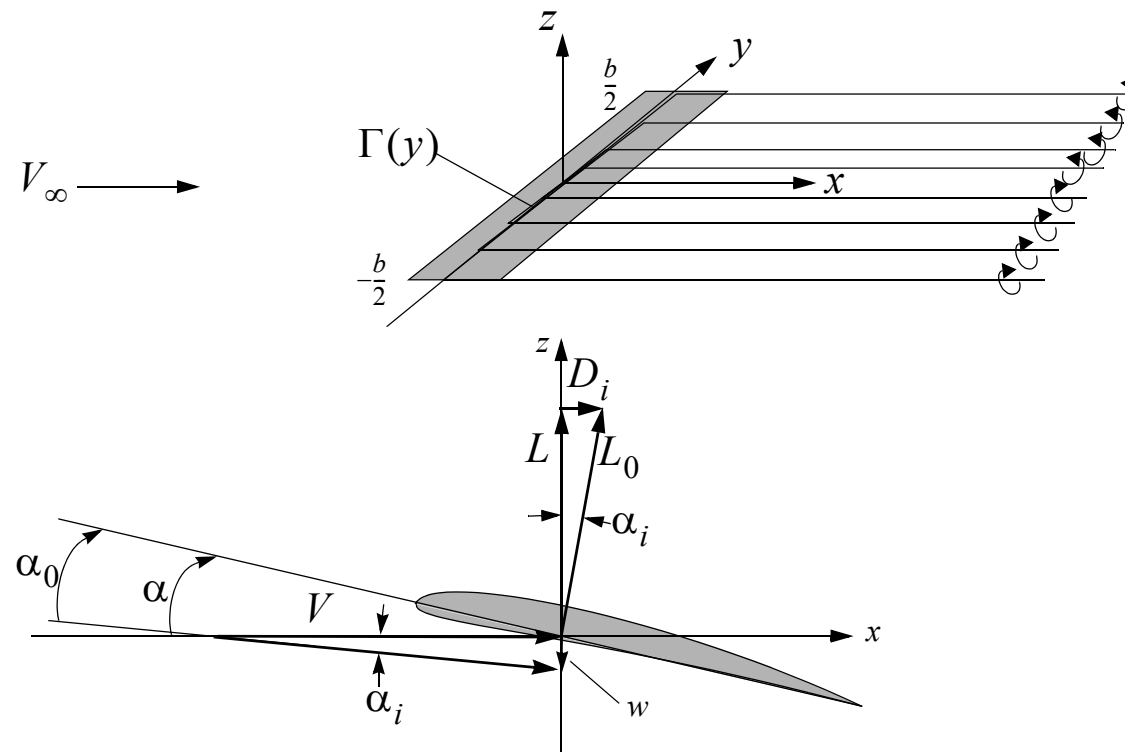


Fig. 2.10 Prandtl's lifting line theory.

- The problem of finding the spanwise lift distribution over the wing then reduces to the problem of determining the bound vortex strength $\Gamma(y)$ as a function of the span variable y .

Prandtl's Integral Equation

- Prandtl's theory links $\Gamma(y)$ it to the downwash $w(y)$ on the wing along the quarter-chord line (aerodynamic centers), to produce tangent flow on the wing surface.
- The result is Prandtl's integral equation:

$$w(y) = \frac{1}{4\pi} \int_{-b/2}^{b/2} \frac{d\Gamma(y_1)}{dy_1} \frac{dy_1}{y - y_1} \quad (2.35)$$

- From Fig. 2.10 we see that the induced downwash at the quarter chord gives rise to a corresponding reduction of the local angle of attack,

$$\alpha = \alpha_0 + \alpha_i \quad (2.36)$$

- Here α_0 is the “effective” angle of attack and α_i is the “induced angle of attack”, given by

$$\tan \alpha_i = \frac{w}{V} \quad (2.37)$$



Small Angle Approximation

- For small angles of attack, we can set

$$\alpha_i \approx \frac{w}{V} \quad (2.38)$$

and from Eq. (2.35), we obtain

$$\alpha_i(y) = \frac{1}{4\pi V} \int_{-b/2}^{b/2} \frac{d\Gamma(y_1)}{dy_1} \frac{dy_1}{(y - y_1)} \quad (2.39)$$

- The induced drag arises from this redefinition of the local flow angle.
- Locally the sectional lift is normal to the flow relative velocity at an angle α_0 with respect to the wing section, which means that it is no longer orthogonal to the flow velocity at upstream infinity.



Lift and Induced Drag

- From Fig. 2.10 we see that

$$D_i = L_0 \sin \alpha_i \approx L_0 \alpha_i \approx L_0 \frac{w}{V} \quad (2.40)$$

where

$$L_0 = C_{L_0} q S \quad (2.41)$$

based on the effective angle of attack α_0 .

- Also,

$$L = L_0 \cos \alpha_i \approx L_0 \quad (2.42)$$

for small induced angles of attack.



Integro-Differential Equation

- It remains to link the LHS of Eq. (2.39) to the local geometric angle of attack of the wing. For wings of high aspect ratio, it is reasonable to assume

$$l(y) = c_{l_\alpha} q c [\alpha_{zL}(y) - \alpha_i(y)] \quad (2.43)$$

where α_{zL} is the local geometric angle of attack, measured w.r.t the zero lift angle of attack, and c_{l_α} is the local two-dimensional lift curve slope of the wing.

- Substituting back into Eq. (2.39) and using Eq. (2.34), we obtain the integro-differential equation due to Prandtl,

$$\Gamma = \frac{1}{2} c_{l_\alpha} V c \left[\alpha_{zL}(y) - \frac{1}{4\pi V} \int_{-b/2}^{b/2} \frac{d\Gamma(y_1)}{dy_1} \frac{dy_1}{(y-y_1)} \right] \quad (2.44)$$



Analytical and Numerical Solutions

- For preliminary calculations, a two-dimensional lift curve slope of 2π may be assumed.
- If experimental data is available for the airfoil section, the experimentally determined lift curve slope c_{l_α} should be used.
- The solution of Eq. (2.44) for arbitrary wing geometries must be obtained numerically, as exact solutions are known only for a few special cases.
- It was noted by Prandtl and his students that solutions can be most easily obtained by the *inverse method*; namely, assume a given spanwise lift distribution $l(y)$, or what is equivalent, $\Gamma(y)$, then the required wing geometric twist distribution $\alpha_{zL}(y)$ can be calculated from Eq. (2.44).



Elliptic Wings and Lift Distributions

- One of Prandtl's students, Max Munk, showed that the *elliptic lift distribution* corresponding to

$$\Gamma(y) = \Gamma_0 \sqrt{1 - \left(\frac{2y}{b}\right)^2} \quad (2.45)$$

yields a constant downwash w and hence also a constant induced angle of attack α_i over the wing span.

- Using heavy-duty mathematics (calculus of variations), Munk was able to prove that *this lift distribution is optimal in the sense that it minimizes the induced drag, for a given total lift L*.
- This result is not limited to a lifting line theory, but applies to a more general lifting surface theory as well - as expressed through his famous *Stagger Theorem*.



Lift

- The total lift on the wing is, in the case of an *elliptic lift distribution*, given by

$$L = \rho V \Gamma_0 \int_{-b/2}^{b/2} \sqrt{1 - \left(\frac{2y}{b}\right)^2} dy \quad (2.46)$$

- The integral can be evaluated by using the trigonometric substitution

$$y = \frac{b}{2} \cos \theta; \quad dy = -\frac{b}{2} \sin \theta d\theta \quad (2.47)$$

$$\int_{-b/2}^{b/2} \sqrt{1 - \left(\frac{2y}{b}\right)^2} dy = \int_{\pi}^0 \sqrt{1 - \cos^2 \theta} \left(-\frac{b}{2}\right) \sin \theta d\theta = \frac{b}{2} \int_0^{\pi} \sin^2 \theta d\theta = \frac{b\pi}{4} \quad (2.48)$$

- Hence the lift becomes

$$L = \frac{\pi}{4} b \rho V \Gamma_0 = \frac{1}{2} \rho V^2 C_L S \quad (2.49)$$



Solution for Elliptic Lift Distribution

- Solving for the lift coefficient, we obtain

$$C_L = \frac{\pi}{2} \frac{\Gamma_0 b}{V S} \quad (2.50)$$

$$\Gamma_0 = \frac{2 V S}{b \pi} C_L \quad (2.51)$$

- The induced angle of attack becomes, using the trig substitution (2.47),

$$\begin{aligned} \alpha_i(y) &= \frac{1}{4\pi V} \int_{-b/2}^{b/2} \frac{d\Gamma(y_1)}{dy_1} \frac{dy_1}{(y - y_1)} = \frac{1}{4\pi V} \int_{\pi}^0 \frac{\Gamma_0 \cos \theta d\theta}{[y - (b/2) \cos \theta]} \\ &= -\frac{\Gamma_0}{4\pi V} \int_0^\pi \frac{\cos \theta d\theta}{(y - (b/2) \cos \theta)} = \frac{\Gamma_0}{2\pi b V} \int_0^\pi \frac{\cos \theta d\theta}{(\cos \theta - \cos \varphi)} \end{aligned} \quad (2.52)$$

where $\cos \varphi = 2y/b$.



Glauert's Integral

- The last integral in Eq. (2.52) can be shown to be equal to π , since it is a form of *Glauert's integral*,

$$\int_0^{\pi} \frac{\cos n\theta d\theta}{(\cos \theta - \cos \varphi)} = \frac{\pi \sin n\varphi}{\sin \varphi} \quad , \quad n = 0, 1, 2, \dots \quad (2.53)$$

- With this result, the induced angle of attack becomes

$$\alpha_i = \frac{w}{V} = \frac{\Gamma_0}{2bV} \quad (2.54)$$

- Substituting from (2.51),

$$\alpha_i = \frac{2VS}{2b\pi bV} C_L = \frac{C_L}{\pi A} \quad (2.55)$$
$$A = b^2/S = \text{aspect ratio}$$



Induced Drag - Elliptic Wing

- The induced drag becomes

$$D_i = C_L q S \alpha_i = \frac{C_L^2}{\pi A} q S = C_{D_i} q S \quad (2.56)$$

from which it follows that

$$C_{D_i} = \frac{C_L^2}{\pi A} \quad (2.57)$$

for an elliptic wing, or more precisely, *for a wing with elliptic lift distribution.*

- Note that $C_{D_i} \rightarrow 0$ as $A \rightarrow \infty$ (no induced drag in 2D flows).



Optimal Properties of Elliptic Lift Distribution

- It was proved by Max Munk that the elliptic spanwise lift distribution is optimal in the following sense:
 1. For a given lift, the optimal spanwise distribution of lift is that which results in a constant downwash velocity w and hence a constant induced angle of attack α_i over the wing span.
- The elliptic distribution results in the min. induced drag for a given L .
- 2. It can be shown that this result also applies to *general* lifting surfaces in subsonic flow, i.e., it is not limited by the high aspect ratio assumption of Prandtl's lifting line theory.

This result follows directly from Munk's *Stagger Theorem*.

- For most wings, a judicious choice of wing taper ratio (about 1/3+) will result in a wing with induced drag of only a few percent above the theoretical minimum.



Wing Efficiency

- Most wings are not of the elliptic type, because the improvement in induced drag cannot typically be justified by the added manufacturing costs
- Oswald (Ref. 7) introduced a “wing efficiency factor” to account for the drag penalty incurred for nonelliptic wings, as follows

$$C_{D_i} = \frac{C_L^2}{\pi e A} \quad (2.58)$$

$$\begin{aligned} e &= \text{wing efficiency factor} \\ eA &= \text{effective aspect ratio} \end{aligned} \quad (2.59)$$

- For straight subsonic wings, e generally falls in the range 0.7-0.85, with low-wing designs typically at the bottom of this range.



Glauert's Correction Factors

- Glauert (Ref. 8) introduced the following correction factors to account for a non-elliptic lift distribution:

$$\alpha_i = \frac{C_L}{\pi A} (1 + \tau) \quad (2.60)$$

$$C_{D_i} = \frac{C_L^2}{\pi A} (1 + \delta) \quad (2.61)$$

- Figure 2.11 shows plots of τ and δ for a rectangular wing of aspect ratio of 6.

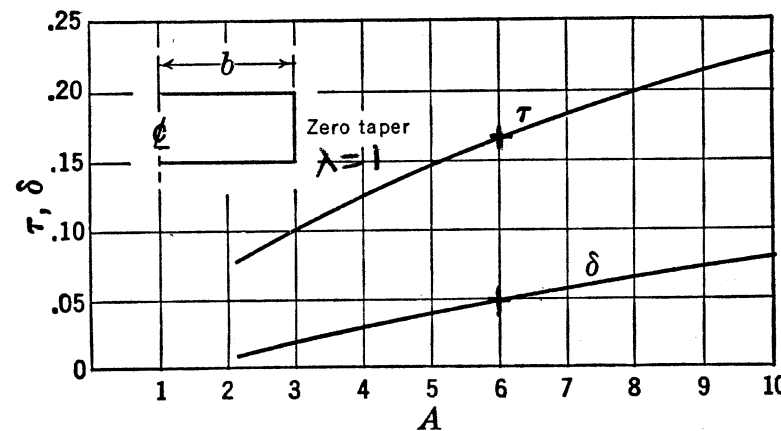


Fig. 2.11 Wing correction factors. (From Ref. 5).

Effect of Wing Taper

- Figure 2.12 shows the effect of wing taper ratio $\lambda = c_t/c_r$ for a wing of aspect ratio of 6.
- Note that the minimum of δ corresponds to the minimum of the induced drag.

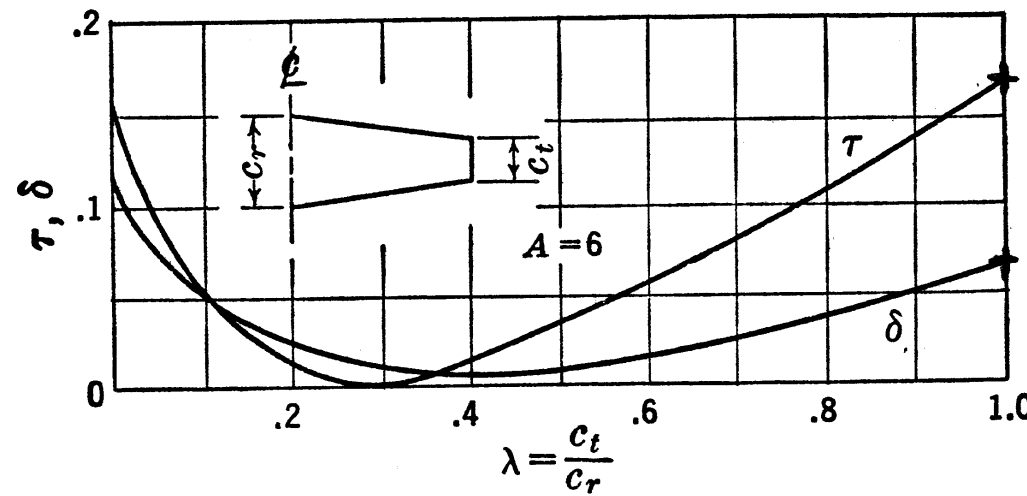
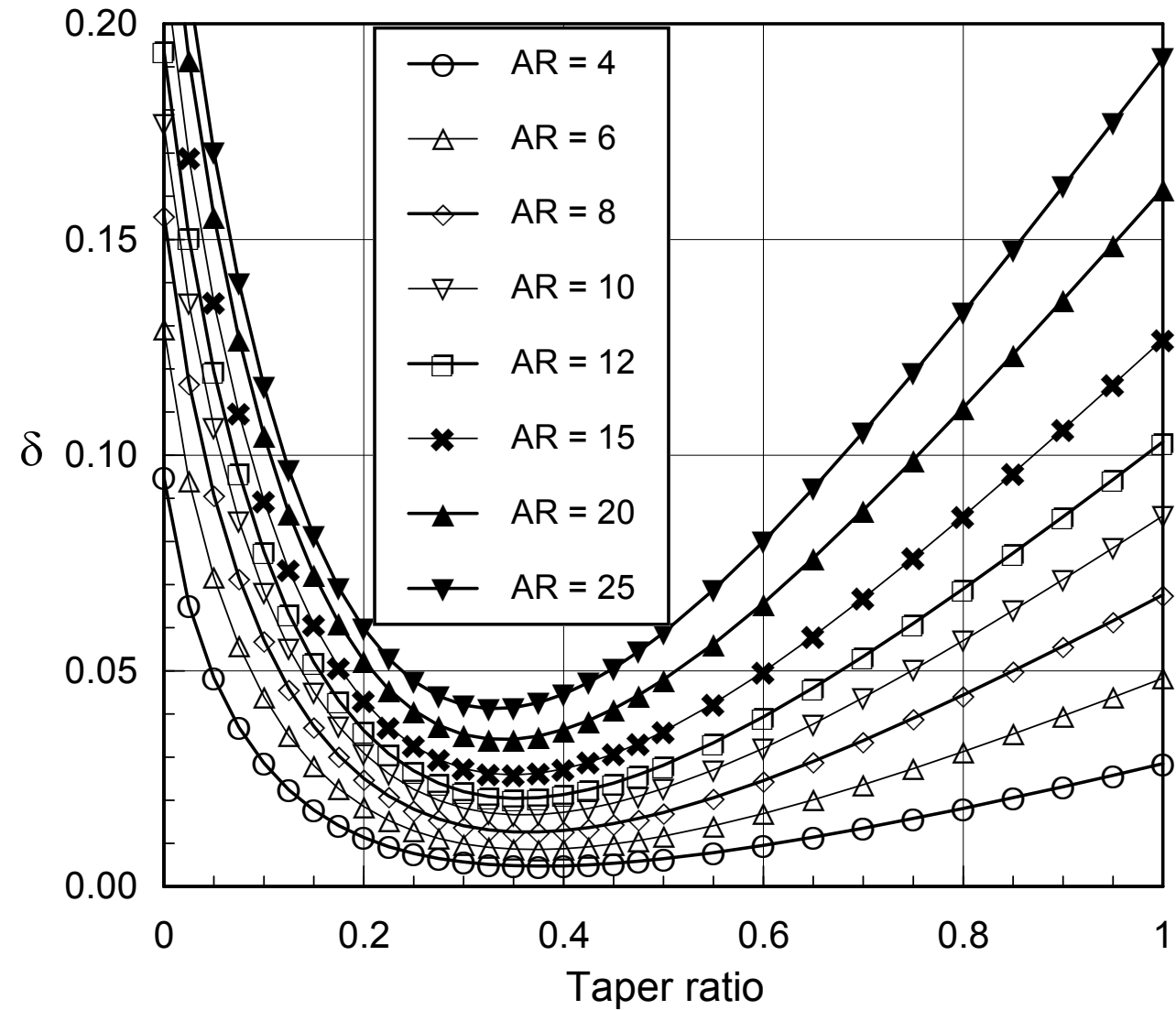


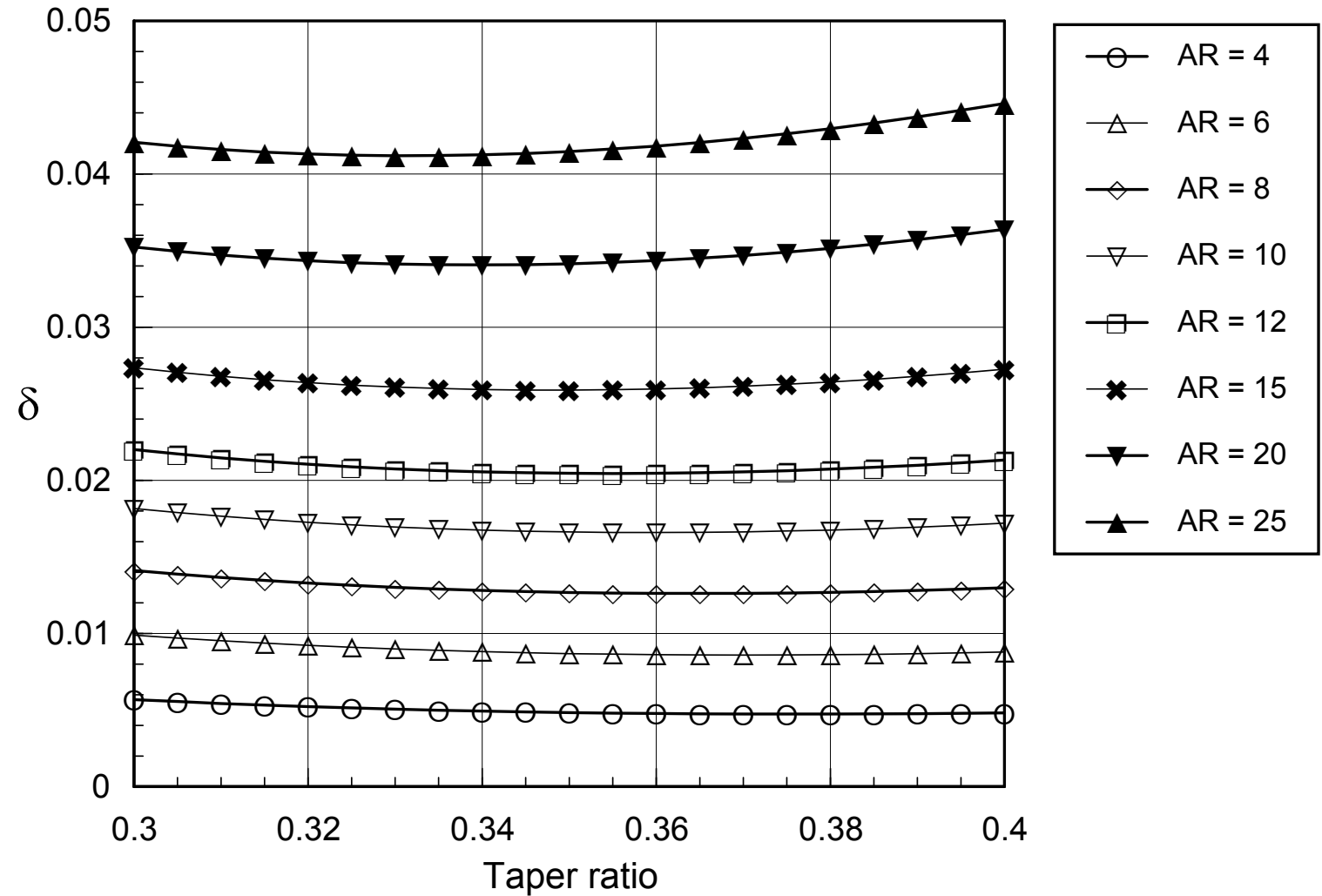
Fig. 2.12 Effect of wing taper (Ref 5).



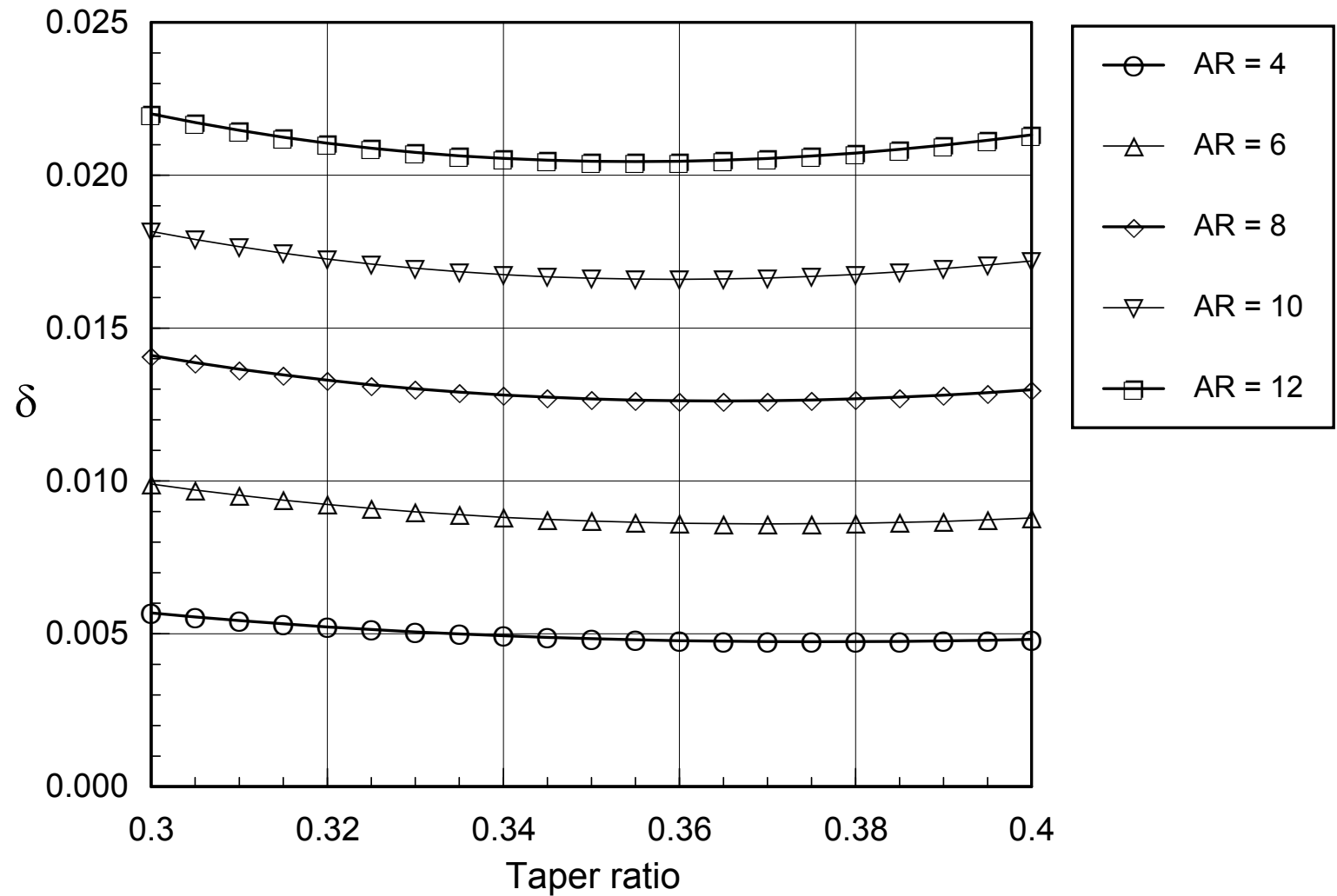
Effect of Taper: More Accurate DP Calculations



Optimum Taper vs. Aspect Ratio



Optimum Taper: AR = 4-12



Example: Untapered Straight Wing

- Let $A = 6$, then $\delta \approx 0.05$ and

$$e = \frac{1}{1 + \delta} = \frac{1}{1 + 0.05} \approx 0.95 \quad (2.62)$$

which is highly optimistic for this aspect ratio.

- In preliminary design calculations, an upper limit of $e \leq 0.85$ should be imposed in most cases, except for wings of very high aspect ratio.
- Note that this wing efficiency is the theoretical value based on the Glauert correction factors and does not include the contribution from the k'' parasite term.



Oswald's Wing Efficiency

- The parasite drag typically contains a small term that depends on the angle of attack and hence L , because of the sensitivity of the boundary layer to α and L .
- In Oswald's definition, this term is included in the wing efficiency:

$$C_{D_P} = C_{D_{min}} + k'' C_L^2 \quad (2.63)$$

$$C_D = C_{D_{min}} + k'' C_L^2 + \frac{C_L^2}{\pi A} (1 + \delta) = C_{D_{min}} + \frac{C_L^2}{\pi e A} \quad (2.64)$$

$$e = \frac{1}{1 + \delta + \pi A k''} \quad (2.65)$$

- Example: $A = 6$ wing and assuming $k'' = 0.01$,

$$e = \frac{1}{1 + 0.05 + \pi(6)(0.01)} = 0.8074 \quad (2.66)$$

- Note: Eq. (2.65) may give unreasonable (too low) values for high- A wings.



Lift Curve Slope

- The lift curve slope can be obtained as follows. From Eqs. (2.36) and (2.60),

$$\alpha = \alpha_0 + \alpha_i = \alpha_0 + \frac{C_L}{\pi A}(1 + \tau) \quad (2.67)$$

- Differentiating both sides with respect to C_L , we obtain

$$\frac{1}{a} = \frac{1}{a_0} + \frac{1}{\pi A}(1 + \tau) \quad (2.68)$$

$$a = \frac{dC_L}{d\alpha} = C_{L\alpha} = \text{3D lift curve slope} \quad (2.69)$$

$$a_0 = \frac{dC_L}{d\alpha_0} = \text{2D lift curve slope}$$

- Solving for the lift curve slope of the 3D wing, we obtain

$$a = \frac{a_0}{1 + \frac{a_0}{\pi A}(1 + \tau)} \quad (2.70)$$



Irrational Flow Assumption

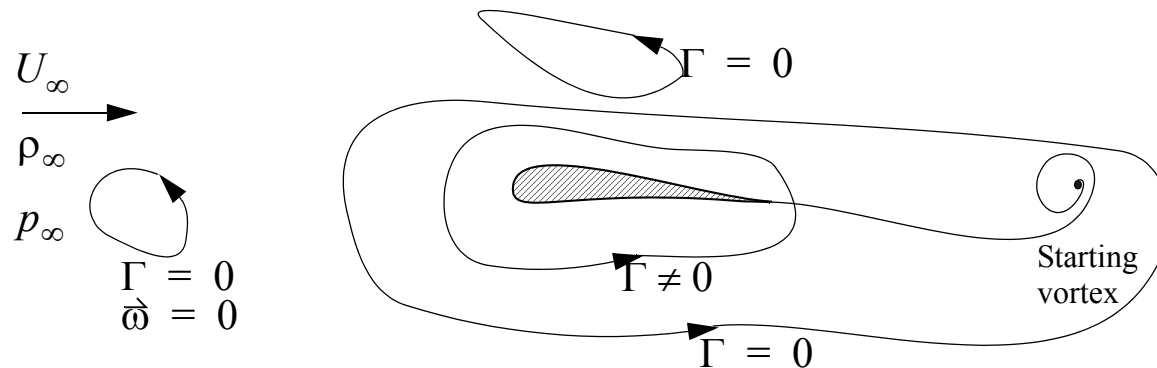


Fig. 2.13 The generation of circulation about a wing through the shedding of a vortex wake.

- Most linearized aerodynamic theories suitable for use in preliminary design are based on the assumption of *irrotational flow*.
- Basically this means that viscosity has been neglected, and so has the entropy production at shocks (if present), since these would produce vorticity.
- If a barotropic fluid starts out irrotational at $t = 0$ and is subjected only to conservative forces, then by Kelvin's theorem it will remain irrotational for all time.

The Kutta Condition

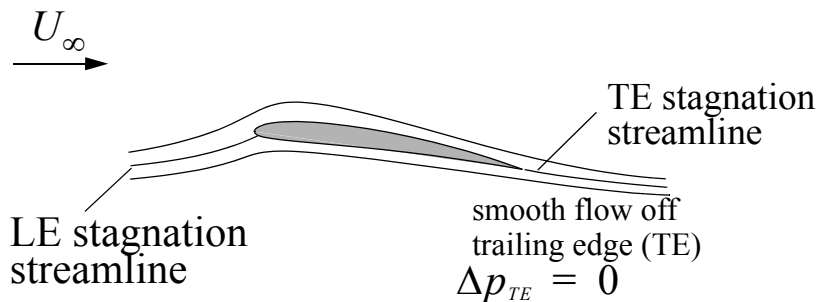


Fig. 2.14 Kutta-Joukowski condition at the trailing edge.

- For subsonic flow the lifting problem does not have a unique solution, because potential theory admits an arbitrary circulation about the airfoil or wing.
- Uniqueness is restored by imposing the *Kutta-Joukowski condition* at the trailing edge:

$$\Delta p_{TE} = 0 \quad (2.71)$$

$$\Delta p(x, y, t) = -[p] = p_l - p_u \quad (2.72)$$

2.6.2 Subsonic Lifting Surface Theories

- For wings of low to moderate aspect ratio, the chordwise loading distribution is also of importance in determining the characteristics of the wing.
- Falkner (1948), Watkins, et al. (1959), and others developed integral equation methods for calculating steady and unsteady loads on subsonic wings.
- Since around 1970, more direct “*vortex lattice*” or “*doublet lattice*” methods have been developed and implemented on high speed computers.
- These methods are still used extensively in preliminary design.



Design Charts

- In NACA Report No. 921 (1948), Ref. 9, DeYoung and Harper have presented an approximate lifting surface method for subsonic wings of arbitrary planform.
- Design charts are presented that allow a rapid determination of the lift curve slope, Fig. 2.15, as well as the spanwise lift distribution for real wings with built-in washout.
- The NACA Rept. 921 charts are more accurate than the various C_{L_α} formulas based on the so-called Helmbold equation,

$$a = \frac{a_0}{\sqrt{1 + (a_0/\pi A)^2} + a_0/\pi A} \quad (2.73)$$

- This formula was obtained by a German aerodynamicist in 1942 for straight wings in incompressible flow, applicable to moderate to low aspect ratios, where formulas based on Prandtl's theory are not applicable.



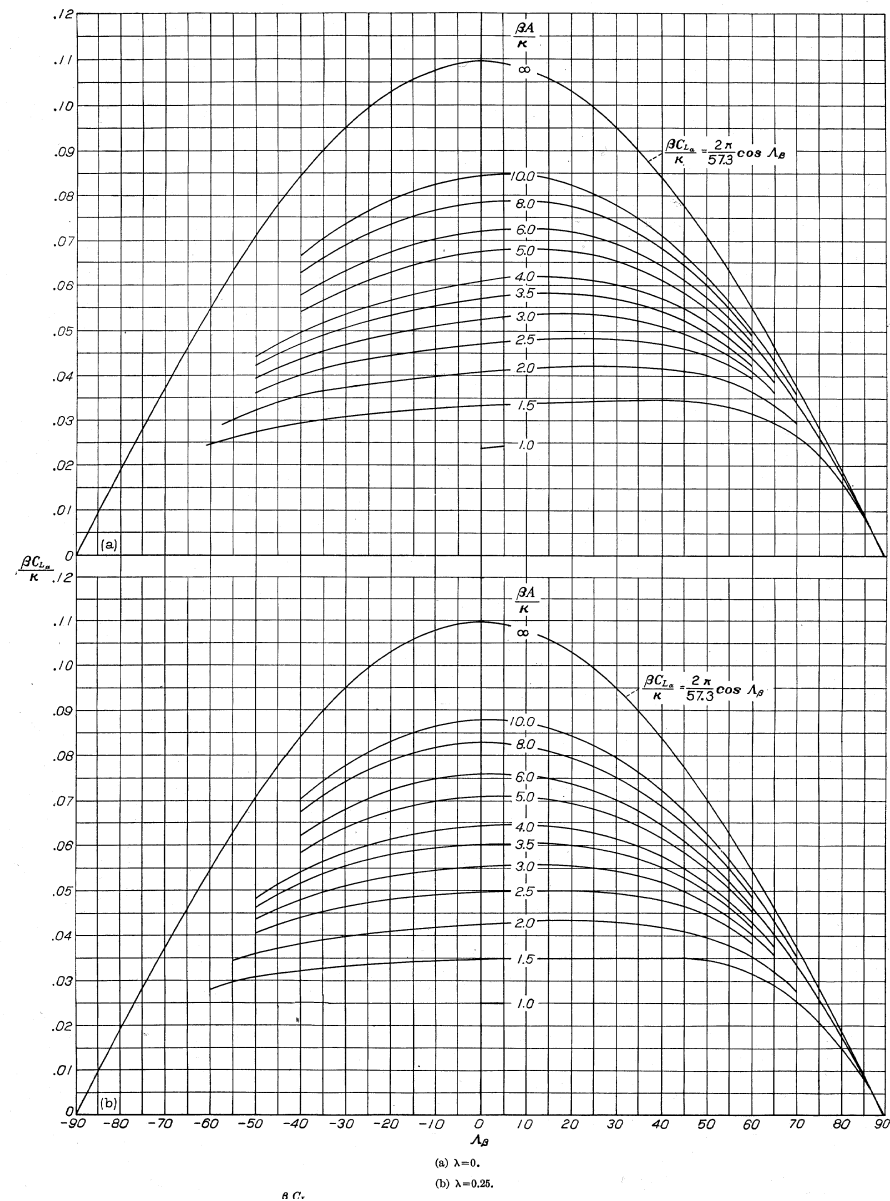


Fig. 2.15 Design charts for calculating the wing lift curve slope, using the approximate lifting surface method of NACA Rept. 921 [9]. ($\lambda = 0$ and $\lambda = 0.25$).

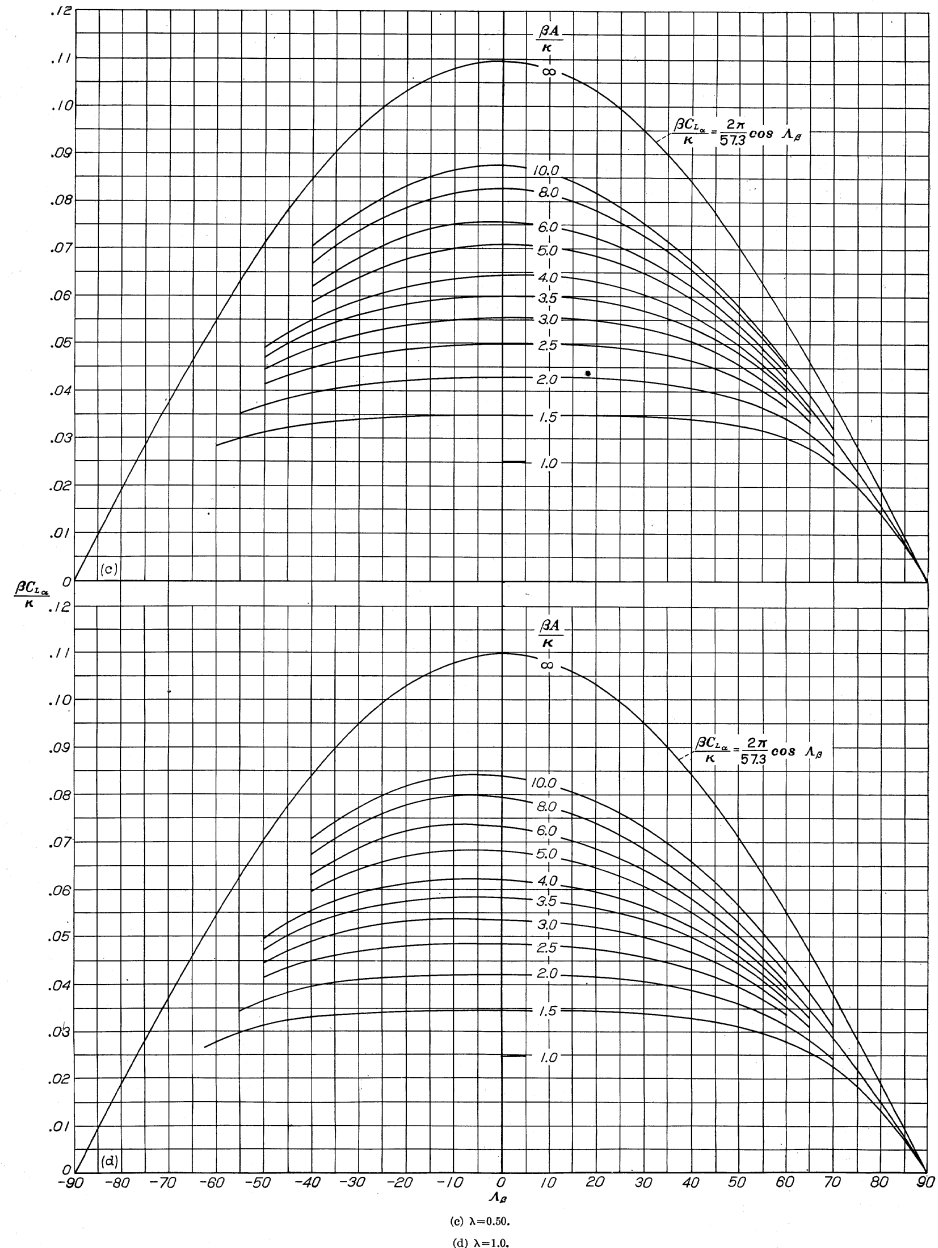


Fig. 2.15 (continued): Design charts for calculating the wing lift curve slope, using the approximate lifting surface method of NACA Rept. 921 ($\lambda = 0.50$ and $\lambda = 1.0$).



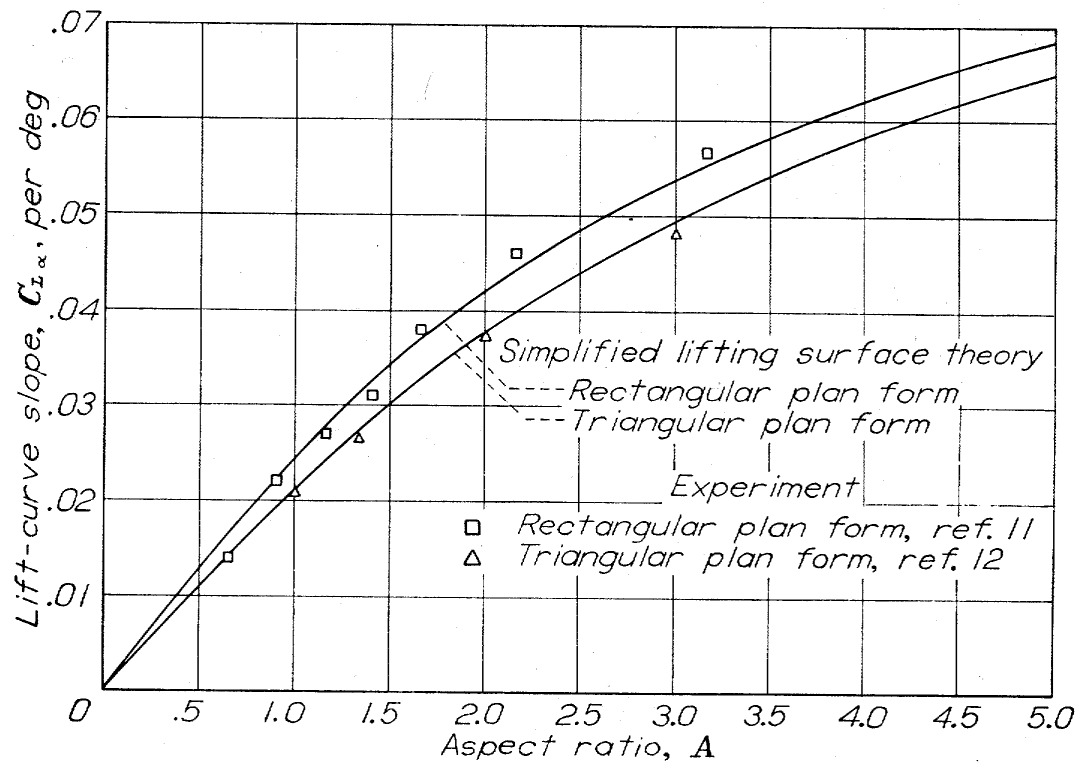


Fig. 2.16 Comparison of calculated vs. experimental lift curve slopes for rectangular and triangular wings. (From Ref. 9).

Diedrich's Formula

- Diedrich (Ref. 10) noted that this formula works well over the entire range of Mach numbers, recovering Prandtl's formula as $A \rightarrow \infty$.
- To account for sweep, he applied *classical sweepback theory*,

$$a_{n_0} = a_0 \cos \Lambda \quad (2.74)$$

to get the following formula

$$a = \frac{a_0 \cos \Lambda}{\sqrt{1 + (a_0 \cos \Lambda / \pi A)^2} + a_0 \cos \Lambda / \pi A} \quad (2.75)$$

- Equation (2.75) agrees surprisingly well with experimental data over the entire range of aspect ratios.
- Unfortunately, Eq. (2.75) is based on junk science.



Mach Number Corrections

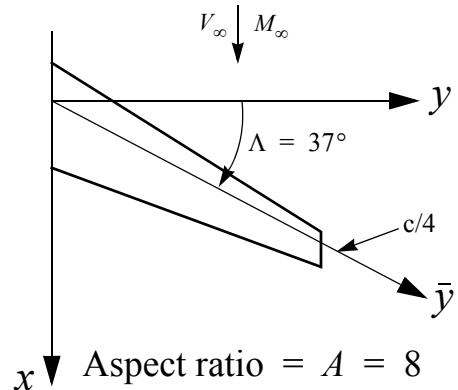
- Several authors have extended the formula to include Mach number (compressibility) effects, by applying the classical Prandtl-Glauert corrections, to obtain

$$a = \frac{a_0 A}{\sqrt{(A/\cos \Lambda)^2 + (a_0/\pi)^2 - (AM)^2} + a_0/\pi} \quad (2.76)$$

- Two back-to back sins cancel everything and you are blessed once again, e.g., Eq. (5.85) in McCormick, or Eq. (12.6) in Raymer.
- In addition to the lack of a scientific foundation, these formulas do not account for taper, or the spanwise lift distribution.



Example 1: Swept Tapered Wing



$$\text{Taper ratio} = \lambda = c_t/c_r = 0.5$$

Fig. 2.17 Swept tapered wing.

From Fig. 2.15c, we obtain

$$\frac{\beta C_{L\alpha}}{\kappa} \cong 0.064/\text{deg} = 3.67 \text{ per radian} \quad (2.78)$$

$$C_{L\alpha} = \frac{3.67}{0.866} = 4.24$$

At Mach 0.5,

$$\tan \Lambda_\beta = \frac{\tan \Lambda}{\beta} = \frac{\tan 37^\circ}{\sqrt{1 - 0.5^2}} = 0.8701 \quad (2.77)$$

$$\Lambda_\beta = 41.03^\circ; \frac{\beta A}{\kappa} = \frac{0.866(8)}{1.0} = 6.928$$

If experimental airfoil data is available, then use

$$\kappa = \frac{(c_{l\alpha})_{\text{exp}}}{2\pi/\beta}$$

for the corresponding Mach number.

Same Wing at Mach 0.8

$$\beta = \sqrt{1 - 0.8^2} = 0.60; \quad \Lambda_\beta = \tan^{-1}\left(\frac{\tan 37^\circ}{0.6}\right) = 51.47^\circ$$

$$\frac{\beta A}{\kappa} = \frac{(0.6)(8)}{1} = 4.8; \quad \frac{\beta C_{L_\alpha}}{\kappa} \approx 0.055/\text{deg} = 3.15 \text{ per radian (Fig. 2.15c)} \quad (2.79)$$

$$C_{L_\alpha} = \frac{3.15}{0.60} = 5.25$$

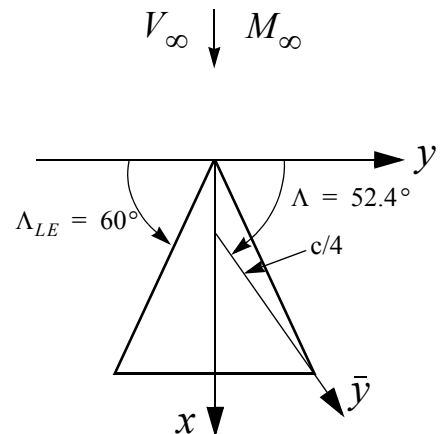
If the aspect ratio is reduced from 8 to 4, we obtain

$$\begin{aligned} \frac{\beta A}{\kappa} &= \frac{0.866(4)}{1.0} = 3.464 @ M = 0.5 \\ \frac{\beta A}{\kappa} &= \frac{0.600(4)}{1.0} = 2.400 @ M = 0.8 \end{aligned} \quad (2.80)$$

$$\begin{aligned} \frac{\beta C_{L_\alpha}}{\kappa} &\approx 0.054/\text{deg} \Rightarrow C_{L_\alpha} = 3.57 @ M = 0.5 \\ \frac{\beta C_{L_\alpha}}{\kappa} &\approx 0.042/\text{deg} \Rightarrow C_{L_\alpha} = 4.01 @ M = 0.8 \end{aligned} \quad (2.81)$$



Example 2: Delta Wing



Aspect ratio = $A = 2.31$

Taper ratio = $\lambda = c_t/c_r = 0$

Fig. 2.18 Delta wing.

- Wing aspect ratio

$$A = \frac{b^2}{S} = \frac{b^2}{\left(\frac{b}{2}\right)^2 \tan \Lambda_{LE}} = 4 \cot 60^\circ = 2.31 \quad (2.82)$$

Wing Aerodynamics

$$\Lambda_\beta = \tan^{-1} \left(\frac{\tan 52.4^\circ}{\sqrt{1 - 0.5^2}} \right) = 56.3^\circ \text{ @ } M = 0.5$$

$$\frac{\beta A}{\kappa} = \frac{0.866(2.31)}{1.0} = 2.000 \text{ @ } M = 0.5 \quad (2.83)$$

$$\frac{\beta A}{\kappa} = \frac{0.600(2.31)}{1.0} = 1.386 \text{ @ } M = 0.8$$

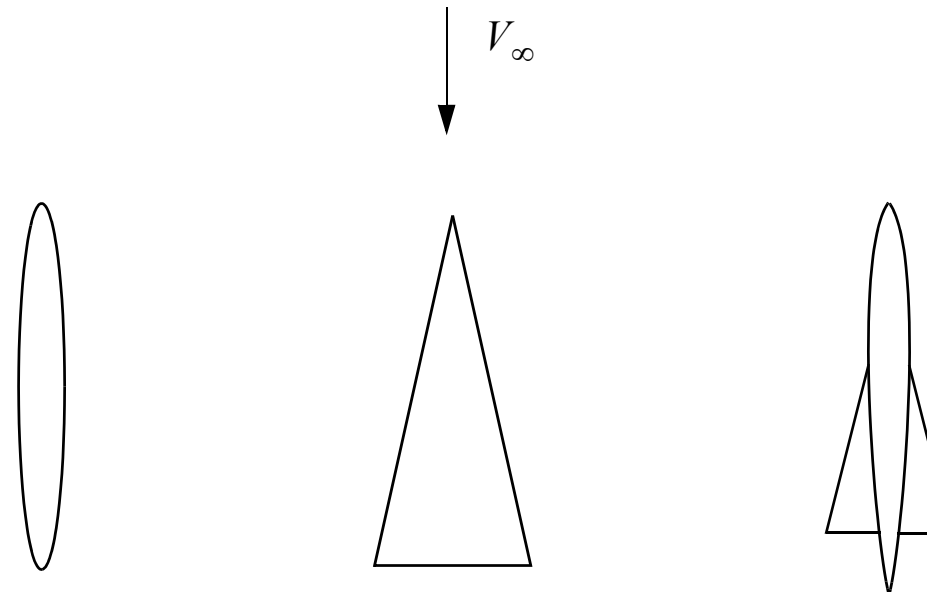
$$\frac{\beta C_{L_\alpha}}{\kappa} \cong 0.038/\text{deg} \Rightarrow C_{L_\alpha} = 2.51 \text{ @ } M = 0.5 \quad (2.84)$$

$$\frac{\beta C_{L_\alpha}}{\kappa} \cong 0.028/\text{deg} \Rightarrow C_{L_\alpha} = 2.67 \text{ @ } M = 0.8$$



2.6.3 Delta Wings: Slender Body Approximation

- By a “slender body” we mean a body whose dimensions normal to the longitudinal axis of the body are small compared to the length of the body, Fig. 2.19.
- The so-called *slender body theory* provides simple formulas for calculating lift and drag of such bodies, based on linearized subsonic and supersonic flows.



a) Body of revolution

b) Delta wing

c) Wing-body combination

Fig. 2.19 Slender bodies.

Asymptotic Solutions

- From a mathematical standpoint, one can think of Prandlt's lifting line theory and the slender body theory as representing *asymptotic solutions in the limits of large and small values of the wing aspect ratio*, respectively.
- In the lifting line theory the emphasis is on the spanwise distribution of lift, in slender body theory the emphasis is on the *chordwise* distribution of lift.
- What is remarkable is that the corresponding spanwise load distribution in the latter case approaches the *elliptic distribution*, corresponding to minimum induced drag!



Example

- Consider the slender delta wing depicted in Fig. 2.19b).
- Assume that the wing has camber, defined by some distribution $z_c(x)$, so that the “local” angle of attack on the mean camber line at a chordwise location x is

$$\alpha(x) \cong \alpha_0 + \frac{dz_c}{dx} \quad (2.85)$$

which we will assume is independent of the spanwise coordinate y .

- Slender body theory then yields the following simple formula for the spanwise lift distribution on the wing:

$$l(y) \equiv \frac{dL}{dy} = 2\rho V^2 \alpha_{TE} \sqrt{\left(\frac{b}{2}\right)^2 - y^2} \quad (2.86)$$

where $\alpha_{TE} = \alpha(c)$ is the *local angle of attack at the trailing edge*.



Slender Body Lift

- The lift becomes

$$L = \int_{-b/2}^{b/2} l(y)dy = \rho V^2 \alpha_{TE} b \int_{-b/2}^{b/2} \sqrt{1 - \left(\frac{2y}{b}\right)^2} dy \quad (2.87)$$

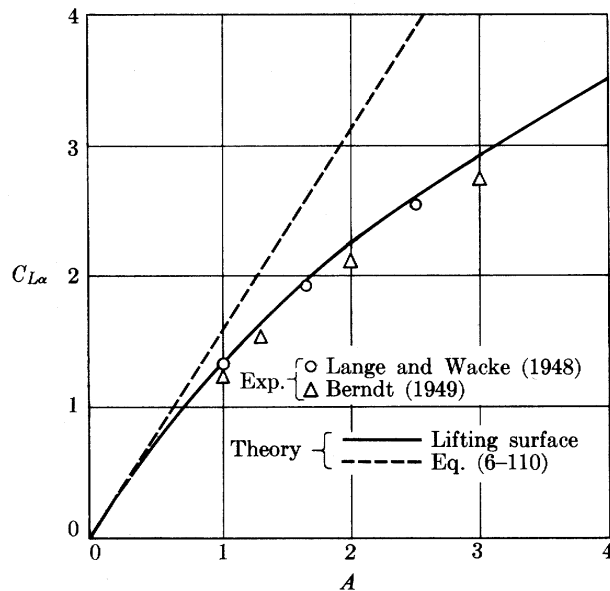
- The integral on the RHS is the same integral that we encountered in Prandtl's lifting line theory, which was evaluated by trig substitution to get $\pi b/4$.
- Substituting into (2.87), we obtain

$$\begin{aligned} L &= \frac{\pi}{4} \rho V^2 \alpha_{TE} b^2 = C_L q S \\ C_L &= \frac{\pi}{2} A \alpha_{TE} \\ C_{L_\alpha} &= \frac{\pi}{2} A \end{aligned} \quad (2.88)$$

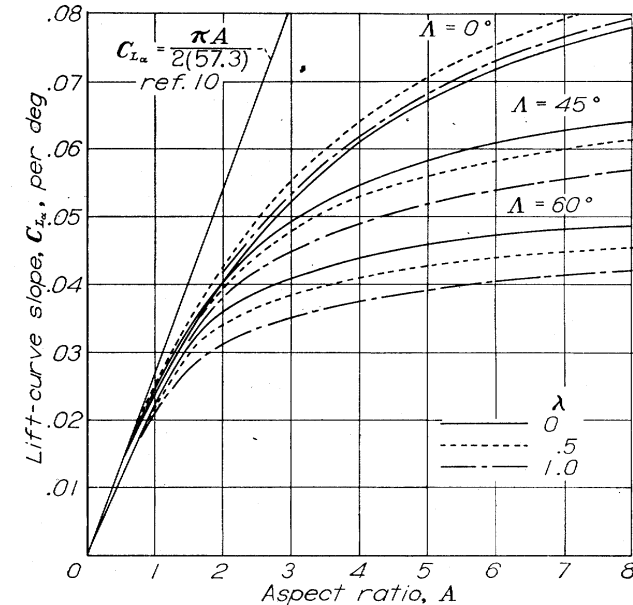
- Note that *the lift does not depend on the wing area, only on the wing span, and only on the angle of attack immediately in front of the trailing edge!*



Slender Body Lift Curve Slope



a) Fig. 6-10 from Ref. 12



b) Fig. 23 from NACA Rept 921

Fig. 2.20 $C_{L\alpha}$ predictions for low aspect ratio wings, and comparison to wind tunnel data.

- The lift coefficient and the lift curve slope are relatively insensitive to Mach number, both in subsonic and supersonic flow.
- Figure 2.20 compares the prediction of slender body theory to lifting surface calculations and experimental data, and with the predictions of NACA Rept. 921.

Remarks

- From Fig. 2.20 we conclude that the slender body approximation should not be used for aspect ratios above one.
- For a triangular delta wing, the slender body approximation overestimates the lift curve slope by about 10% at $A = 1$.
- Because the spanwise lift distribution is elliptical, and applying Munk's stagger theorem, it follows that the induced drag coefficient is simply

$$C_{D_i} = \frac{C_L^2}{\pi A} \quad (2.89)$$



Strange Stuff

- If the “local” span $s(x)$, Fig. 2.21, is not monotonically increasing, then one can show that *the section behind the maximum span point generates no lift*.

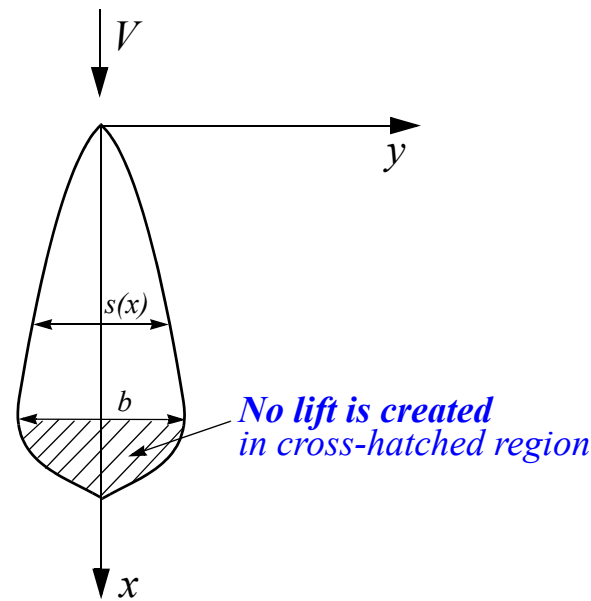


Fig. 2.21 General wing planform (slender body).

Leading Edge Vortices (LEVs)



a) Concorde



b) XB-70

Fig. 2.22 Example where leading edge vortices (LEVs) are clearly visible in flight.

- An important aspect of delta wings at moderate to high angles of attack is the creation of *additional lift due to leading edge vortices (LEVs)*.
- Thin wings and “strakes” will generate strong vortices at the leading edge, Fig. 2.22, where the flow separates due to high adverse pressure gradients.

Nonlinear Vortex Lift

- The LEVs effectively change the shape of the wing, increasing the effective camber and thickness in the LE region (high angles of attack without stalling).
- The result is that an additional nonlinear “vortex lift” is produced; see, for example Fig. 3.74 in McCormick’s text [1], reproduced below as Fig. 2.23.

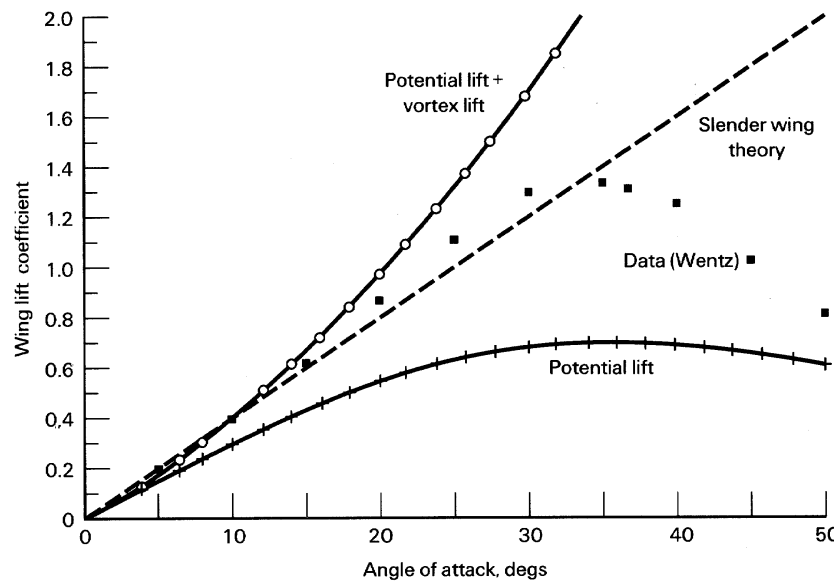


Fig. 2.23 Lift vs. angle of attack on delta wing with 70 deg sweep ($A = 4 \cot 70^\circ = 1.456$); experimental data vs. predictions of various theories. (From McCormick [1], Fig. 3.74).



2.7 Supersonic Wings

2.7.1 Two-dimensional steady supersonic flow

- Supersonic airfoil and wing theories are simpler in many respects than the corresponding subsonic theories, because in all 2D and many 3D cases, the upper and lower wing surfaces operate independently of each other.
- This allows us to obtain individual solutions for the upper and lower surfaces.

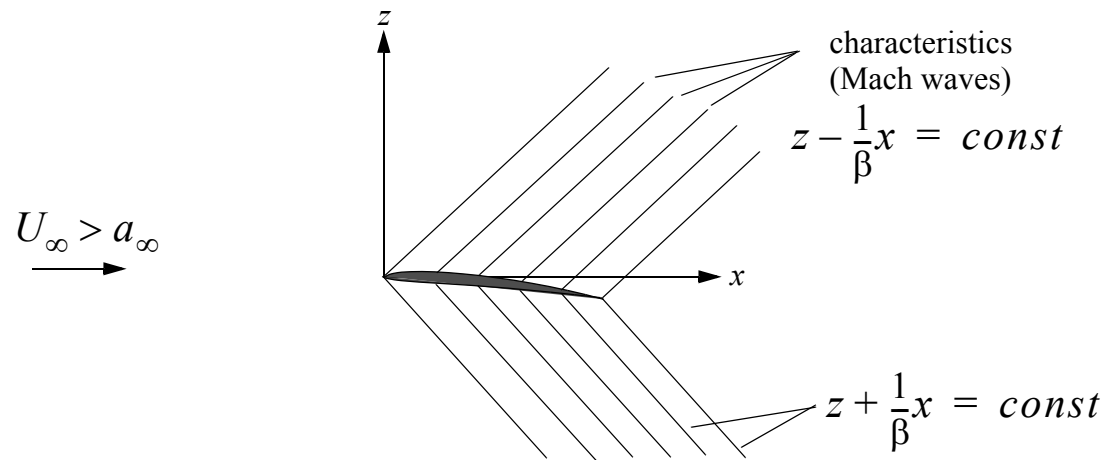


Fig. 2.24 Two-dimensional wing in steady supersonic flow.

2D Lift and Moment

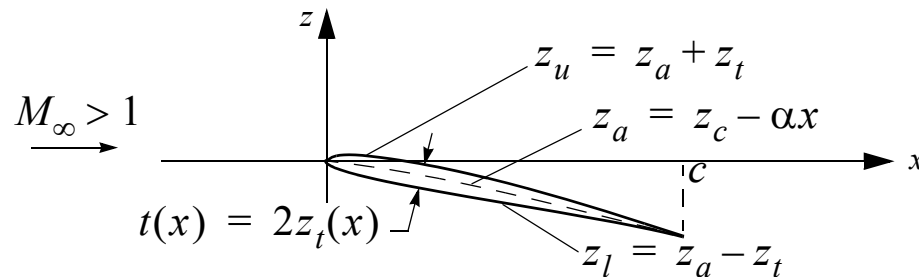


Fig. 2.25 General airfoil in supersonic flow.

- The pressure at the wing surface is given by the simple formula

$$\Delta p(x) = -\frac{\rho_\infty U_\infty^2}{\beta} \left\{ \frac{dz_l}{dx} + \frac{dz_u}{dx} \right\} \quad (2.90)$$

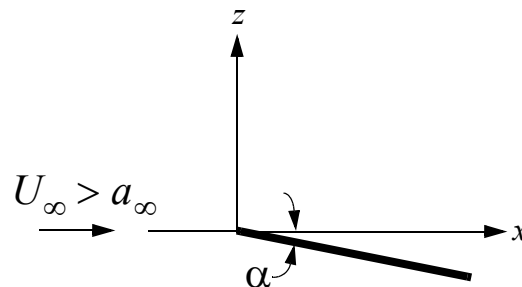
- The lift and moment about the leading edge, positive nose up, per unit span, are

$$L = \int_0^c \Delta p(x) dx; \quad M_{LE} = - \int_0^c x \Delta p(x) dx \quad (2.91)$$

Example 1: Flat Plate in Supersonic Flow

- For a flat plate airfoil or wing exposed to supersonic flow on both surfaces,

$$z = -\alpha x ; \quad \frac{dz_l}{dx} = \frac{dz_u}{dx} = -\alpha \quad (2.92)$$



$$\Delta p = \frac{2\rho_\infty U_\infty^2}{\beta} \alpha = \frac{4\alpha}{\sqrt{M_\infty^2 - 1}} q_\infty \quad (2.93)$$

where $q_\infty = \frac{1}{2}\rho_\infty U_\infty^2$. The lift per unit span is

$$L = \frac{4\alpha c}{\sqrt{M_\infty^2 - 1}} q_\infty \quad (2.94)$$

Fig. 2.26 Flat plate in supersonic flow.

$$C_L = \frac{4\alpha}{\beta} = \frac{4\alpha}{\sqrt{M_\infty^2 - 1}} \quad (2.95)$$
$$C_{L_\alpha} = \frac{4}{\beta} = \frac{4}{\sqrt{M_\infty^2 - 1}}$$

Example 2: General Airfoil of Arbitrary Shape

- Because no signal can travel from the upper surface to the lower surface, or vice versa, the two surfaces are independent
- The aerodynamic solution can be calculated for each surface and then added to get the complete solution, and we get

$$C_L = \frac{4}{\sqrt{M_\infty^2 - 1}} \left[\frac{z_a(0)}{c} - \frac{z_a(c)}{c} \right] \quad (2.96)$$

Note that, unlike in the subsonic case, *camber does not produce lift, only drag.*

- The drag is readily worked out using Eq. (2.90) and considering the surface slope to get the force component in the flow direction, and we obtain

$$C_D \equiv C_{D_W} = \frac{4}{c \sqrt{M_\infty^2 - 1}} \int_0^c \left\{ \left(\frac{dz_u}{dx} \right)^2 + \left(\frac{dz_l}{dx} \right)^2 \right\} dx = \frac{4}{c \sqrt{M_\infty^2 - 1}} \int_0^c \left\{ \left(\frac{dz_a}{dx} \right)^2 + \left(\frac{dz_t}{dx} \right)^2 \right\} dx \quad (2.97)$$

$$C_{D_W} = \frac{4}{\sqrt{M_\infty^2 - 1}} \left\{ \overline{\left(\frac{dz_a}{dx} \right)^2} + \overline{\left(\frac{dz_t}{dx} \right)^2} \right\} \quad (\text{wave drag}) \quad (2.98)$$



2.7.2 Three-dimensional steady supersonic flow

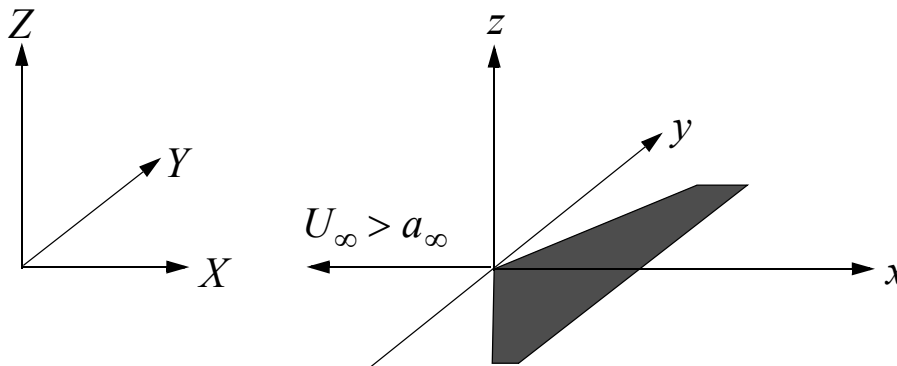


Fig. 2.27 Supersonic wing in steady flight.

- Since 3D supersonic wing theory is not covered in the undergraduate aerospace engineering curriculum at UCLA, there is nothing to review at this point.
- What we will do instead is to consider special cases, where the wing aerodynamics can be solved or approximated using 2D supersonic theory.

Wings of Simple Planforms

- Simple planforms have no subsonic edges, and the upper and lower surfaces are therefore completely independent of each other; see Fig. 2.28.
- Depending on the shape of the wing planform, a significant region of the wing may be operating in two-dimensional supersonic flow,

$$\Delta p = \frac{2\rho_\infty U_\infty^2}{\beta} \alpha = \frac{4\alpha}{\sqrt{M_\infty^2 - 1}} q_\infty \quad (2.99)$$

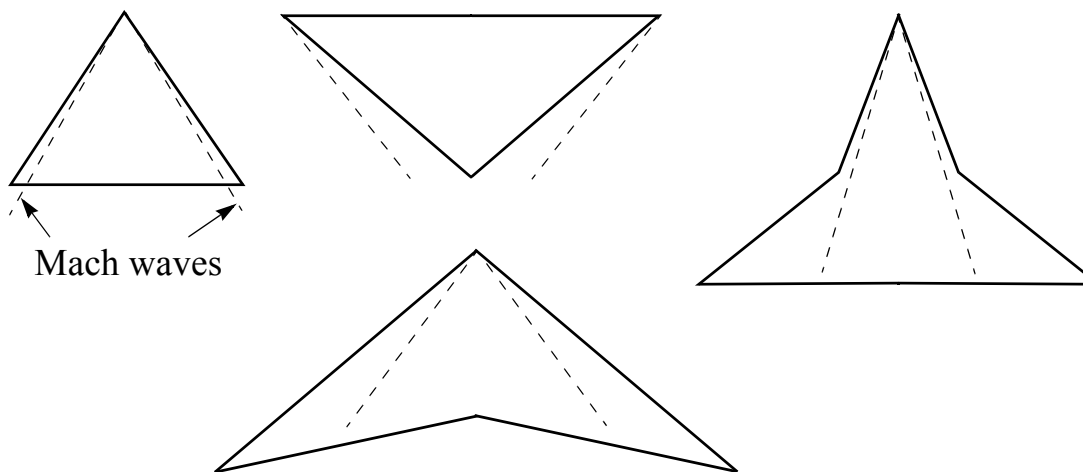


Fig. 2.28 Supersonic wings of simple planforms.

Lift and Drag Coefficient

- The local lift coefficient at y is then simply

$$c_l(y) = \frac{4\alpha}{\sqrt{M_\infty^2 - 1}} \quad (2.100)$$

based on the local chord $c(y)$.

- In these 2D regions of the wing the local induced drag coefficient is

$$c_{d_i}(y) = c_l(y)\alpha = \frac{4\alpha^2}{\sqrt{M_\infty^2 - 1}} \quad (2.101)$$

- If the entire wing planform is in 2D supersonic flow, it follows that the induced drag coefficient for the entire wing is

$$C_{D_i} = \alpha C_L = \alpha^2 C_{L_\alpha} = C_L^2 / C_{L_\alpha} \quad (2.102)$$



Wings with 2D Flow Regions

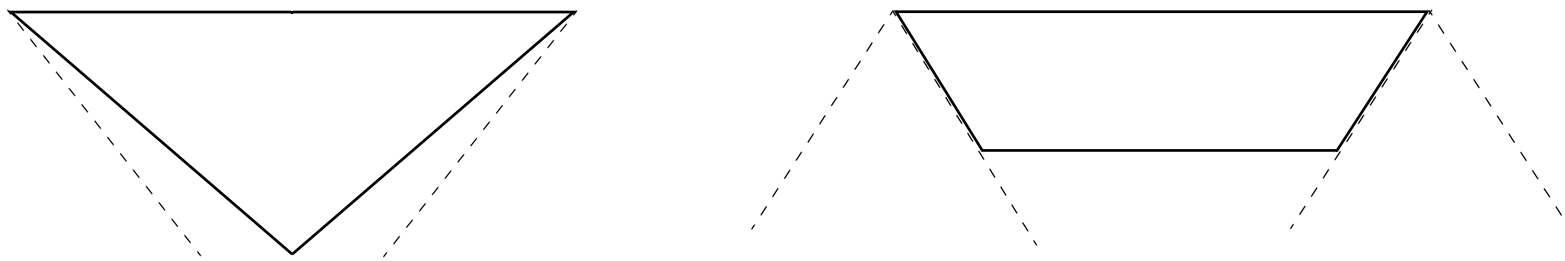


Fig. 2.29 Examples of wings where the 2D solution applies over the entire planform.

Supersonic LE and TE

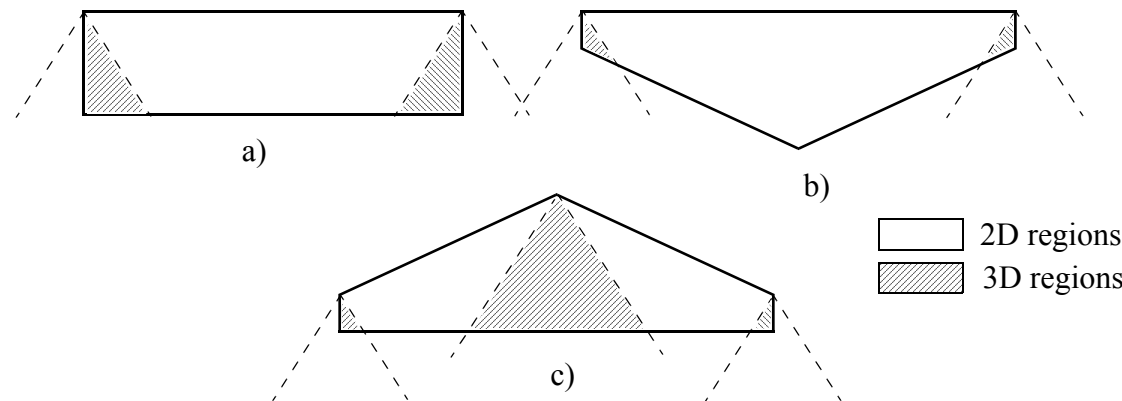


Fig. 2.30 Wings with supersonic leading and trailing edges.

- Another important class of wing planforms is shown in Fig. 2.30. Here, the leading and trailing edges are supersonic, but the wing tips are subsonic.
- In the case of a rectangular untapered wing, Fig. 2.30a), the formulas are very simple (for $\beta A > 2$)

$$C_L = \frac{4\alpha}{\sqrt{M_\infty^2 - 1}} \left[1 - \frac{1}{2A \sqrt{M_\infty^2 - 1}} \right], \quad C_{D_i} = \alpha C_L \quad (2.103)$$

Remarks

- Note that the induced drag has a very different dependence on the aspect ratio than in subsonic flow. In fact, as A increases, the induced drag at a given angle of attack actually *increases*.
- This interesting behavior has been misinterpreted by some authors to mean that a low-aspect ratio wing is better from a wave drag standpoint.
- But C_L also decreases, and the wave drag *at constant lift* is

$$C_{D_w} = \frac{\beta C_L^2}{4 - 2/(\beta A)} = C_L^2 / C_{L_a} \quad (2.104)$$

and this equation shows that the drag *decreases* with increasing aspect ratio.

- In the limit $A \rightarrow \infty$, the 2D result is approached from above.



2.8 Aircraft Performance Calculations

- Only a brief overview and discussion of the key formulas and approximate methods for estimating aircraft performance in the early stages of preliminary design, at the level required for the preparation of the midterm reports.
- A more detailed analysis will be presented later in the course.



2.8.1 Thrust and Power Required

a) Level Flight (Steady)

- In this case, thrust must equal drag, and

$$\begin{aligned} T &= D = D_p + D_i \\ &= qS \left(C_{D_{min}} + \frac{C_L^2}{\pi e A} \right) \cong qS \left(C_{D_0} + \frac{C_L^2}{\pi e A} \right) \end{aligned} \quad (2.105)$$

- Here, C_{D_0} represent the drag coefficient at zero lift, and is easily determined in wind tunnel tests.
- The corresponding power required is then

$$P = DV = TV = \frac{1}{2} \rho V^3 S \left(C_{D_0} + \frac{C_L^2}{\pi e A} \right) \quad (2.106)$$

- For $\gamma = 0$ and small α , the equilibrium equation in the vertical direction yields $L = W$, and

$$C_L = \frac{L}{qS} = \frac{W}{qS} = \frac{2W}{\rho V^2 S} \quad (2.107)$$



Required Thrust and Power

- Substituting back into Eqs. (2.105) and (2.106), we obtain the following expressions for the *required thrust* T_R and *required power* P_R :

$$T_R = \frac{1}{2}\rho C_{D_0} SV^2 + \frac{2}{\pi\rho e} \left(\frac{W}{b}\right)^2 \frac{1}{V^2} \quad (2.108)$$

$$P_R = \frac{1}{2}\rho C_{D_0} SV^3 + \frac{2}{\pi\rho e} \left(\frac{W}{b}\right)^2 \frac{1}{V} \quad (2.109)$$

- In the case of aircraft powered by jet engines, the thrust formula is used for design - there being no need to calculate the required power, per se.
- *Turbojet and turbofan engine ratings* (Takeoff, Max. Climb, Max. Cruise, etc.) are always stated in terms of the net uninstalled thrust.
- *Piston (reciprocating) engines and turboprop engines*, on the other hand, are rated in brake horse power (BHP) for the corresponding flight conditions.



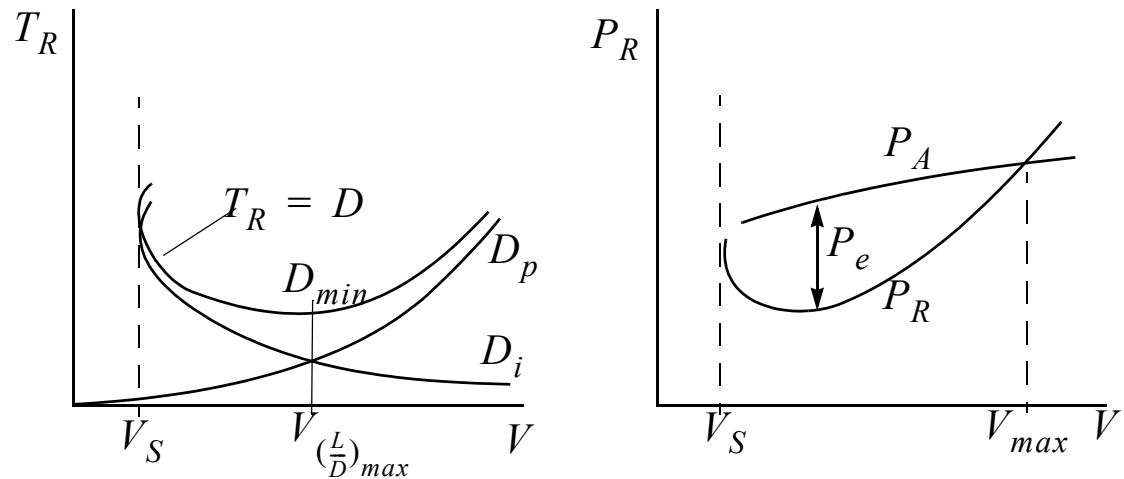


Fig. 2.31 Thrust and power required as a function of airspeed.

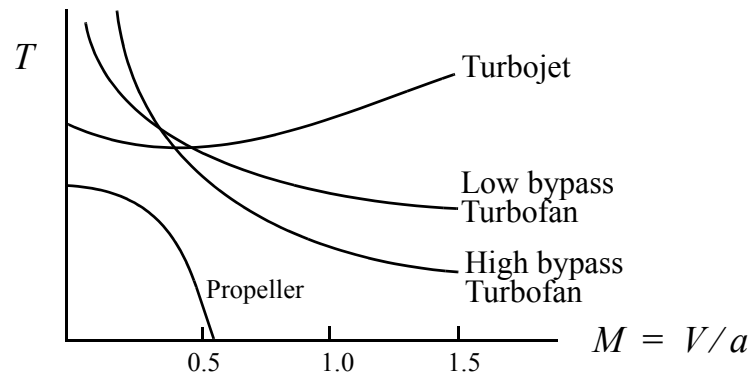


Fig. 2.32 Typical behavior of thrust vs. airspeed for different types of aircraft propulsion.

b) Steady Climb

- The appropriate formula has already been derived in Sec.2.2, Eq. (2.6):

$$R/C = \frac{(T-D)V}{W} = \frac{P_A - P_R}{W} \quad (2.110)$$

where $P_A = TV$ represents the available power.

- The difference $P_A - P_R$ is often referred to as “excess power”, and is therefore available for increasing the energy of the aircraft, either by increasing the potential energy Mgh , or by increasing the kinetic energy $\frac{1}{2}MV^2$.
- By plotting P_A and P_R vs. V or M for different altitudes, the performance envelope of the aircraft can be assessed.
- For jet-powered aircraft, one plots T_A and T_R , as illustrated in Fig. 2.33.
- Figure 2.34 shows typical rate of climb performance vs. altitude for two extreme types of aircraft, a light general aviation propeller airplane and a large jumbo jet.



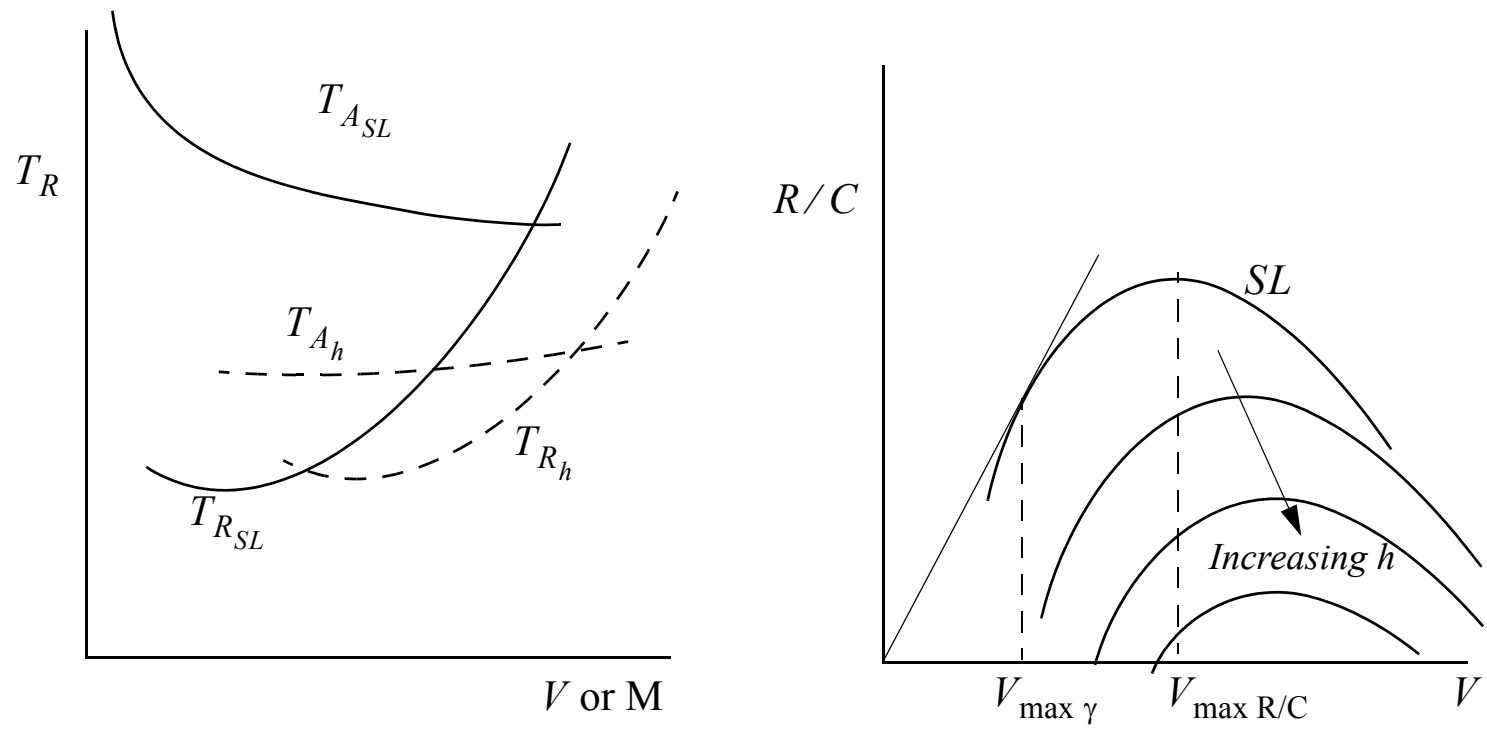
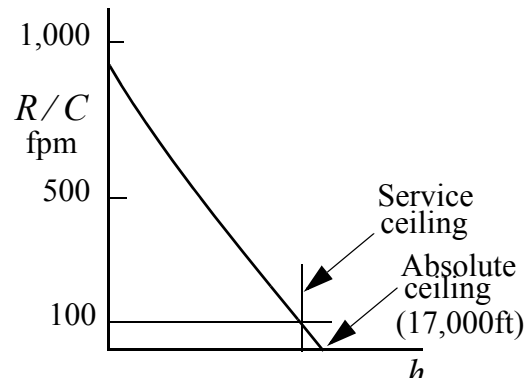
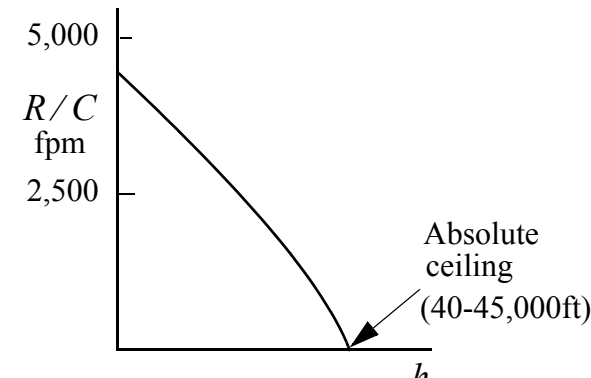


Fig. 2.33 a) T_A and T_R at SLSD and at altitude; b) R/C vs. V and h .



(a) PA-28 Cherokee



(b) Boeing 747

Fig. 2.34 Typical rate of climb for (a) a light propeller A/C and (b) a heavy jumbo jet.

2.8.2 Range

- Let

$$\begin{aligned}\dot{W}_f &= \text{fuel flow rate (lbs/hr)} \\ &= (BSFC) \cdot BHP \text{ (piston engines)} \\ &= (TSFC) \cdot T \text{ (jet engines)}\end{aligned}\tag{2.111}$$

$BSFC$ = Brake Specific Fuel Consumption

BHP = Engine Brake Horsepower

$TSFC$ = Thrust Specific Fuel Consumption

T = Engine thrust

- Range formulas depend on propulsion.



a) Propeller Airplanes

- The overall (engine + propeller) propulsive efficiency is defined as

$$\eta = \frac{\text{Net propulsive thrust power}}{\text{Engine brake power}} = \frac{DV}{BHP} \quad (2.112)$$

- Assuming that the only loss of weight of the aircraft occurs through the fuel burn, the rate of change of the aircraft weight W is

$$\frac{dW}{dt} = -\frac{P_R c}{\eta} = -\frac{DVc}{\eta} \quad (2.113)$$

where c denotes the *BSFC*, in lbs/HP/hr, if P_R is expressed in HP.

- Rearranging and assuming $\alpha, \gamma \ll 1$, we can write

$$\frac{dW}{dt} = -\left(\frac{D}{L}\right) \frac{LVc}{\eta} = -\frac{DWVc}{L\eta} \quad (2.114)$$



Breguet Equation

- Separating variables and integrating

$$\int_{W_0}^{W_1} \frac{dW}{W} = - \int_0^R \left(\frac{D}{L} \right) \left(\frac{c}{\eta} \right) ds \quad (2.115)$$

- If we assume that the integrand on the RHS is constant, we can take it outside the integral sign and immediately obtain

$$\ln W \Big|_{W_0}^{W_1} = - \left(\frac{D}{L} \right) \left(\frac{c}{\eta} \right) R \quad (2.116)$$

- Solving for R , we obtain the *Breguet equation*

$$R = \left(\frac{L}{D} \right) \left(\frac{\eta}{c} \right) \ln \left(\frac{W_0}{W_1} \right) \quad (2.117)$$



Maximum Range

- All ratios occurring in this equation except η/c are dimensionless.
- The specific fuel consumption rate c has the dimension of inverse length (l^{-1}).

$$[c] = \frac{[\dot{W}_f]}{[BHP]} = \frac{\text{lbs/hr}}{\text{ft-lbs/hr/[198 x } 10^4\text{]}} = \frac{1}{\text{ft}} \quad (2.118)$$

where brackets mean “dimension of”.

- From the Breguet equation, it is clear that the range is maximized (for a given weight ratio) when the product of L/D and η/c is maximized.



Propeller Efficiency

- Propeller efficiency is a function of two primary variables, the blade angle β and the nondimensional advance ratio J ,

$$J = \frac{V}{nD} \quad (2.119)$$

- If a variable pitch (constant-speed) propeller is used, then the blade angle is automatically controlled to extract a fixed amount of power from the engine (e.g., 65% of rated power, for economy cruise), at a constant RPM.
- For a fixed pitch propeller, on the other hand, there will be a single V at which the propeller efficiency is maximized, for a given power setting (rps).
- This airspeed would not necessarily coincide with the airspeed that maximizes (L/D) .
- Furthermore, for many light aircraft the optimum airspeed corresponding to $(L/D)_{max}$ is much slower than what the aircraft is capable of at reasonable cruise power settings, say 65%-75% of rated power.
-



Momentum Theory

- The ideal propeller efficiency η_i is defined as the ratio between the net propulsive power TV and the “ideal” input (shaft) power to the propeller:

$$\eta_i = \frac{TV}{P} = \frac{TV}{T(V+w)} = \frac{1}{1+w/V} \quad (2.120)$$

- Using elementary fluid mechanics (Bernoulli eq. + continuity), can show that

$$\frac{w}{V} = \frac{\sqrt{1+T_c} - 1}{2} \quad (2.121)$$

where T_c is a nondimensional thrust coefficient for the propeller, defined as

$$T_c = \frac{T}{qA} \quad (2.122)$$

- Here $q = \frac{1}{2}\rho V^2$ is the dynamic pressure and $A = \pi D^2/4$ is the propeller disk area.
- Substituting into Eq. (2.120), the ideal efficiency becomes

$$\eta_i = \frac{2}{1 + \sqrt{1 + T_c}} \quad (2.123)$$



b) Jet Aircraft

- Let

$$c_t = TSFC = \text{true specific fuel consumption} \quad (2.124)$$

then the fuel burned during a time interval dt is

$$dW_f = c_t T dt = -dW \quad (2.125)$$

and is equal to the weight decrease dW of the aircraft.

- The distance traveled during dt is

$$ds = V dt = -\frac{V dW}{c_t T} \quad (2.126)$$

and the range is obtained by integration

$$R = \int_0^R ds = - \int_{W_0}^{W_1} \frac{V dW}{c_t T} \quad (2.127)$$



Range Equation - Jet Aircraft

- Assuming $\alpha, \gamma \ll 1$ and steady unaccelerated flight,

$$T = D = \frac{1}{2} \rho V^2 C_D S = \frac{D}{L} W \quad (2.128)$$

and the following formula for the range is obtained:

$$R = - \int_{W_0}^{W_1} \left(\frac{V}{c_t} \right) \left(\frac{L}{D} \right) \frac{dW}{W} \quad (2.129)$$

- If the cruise portion of flight is carried out at a constant velocity *and* a constant L/D , and if we assume that the TSFC remains constant, the integration of Eq. (2.169) yields the following range formula:

$$R = \left(\frac{V}{c_t} \right) \left(\frac{L}{D} \right) \ln \left(\frac{W_0}{W_1} \right) \quad (2.130)$$

- To maximize the range under these assumptions, we should cruise at a speed somewhat higher than the speed that yields maximum L/D .



Climb Cruise

- Note that to keep the aircraft trimmed at a constant flight speed as the aircraft burns fuel and gets lighter, C_L and hence α cannot be kept constant, but must decrease as fuel is burned, for cruising flight at a fixed altitude h .
- But that would change L/D , violating our assumption that L/D is constant.
To keep both V and L/D fixed, we must continually change altitude during cruise.
- As the aircraft burns fuel, we simply climb to a higher altitude, where the air is thinner and the lift generated for a given C_L and V is less, allowing $L = W$ to remain satisfied.

This process is referred to as *climb cruise*, for obvious reasons.

- The range formula (2.170) is also valid under the single assumption

$$\left(\frac{V}{c_f}\right)\left(\frac{L}{D}\right) = \text{const.} \quad (2.131)$$



Range vs. Flight Mach Number

- Let

$$\begin{aligned} M &= \frac{V}{a} \\ a &= a_0 \sqrt{\theta} \\ \theta &= T_a / T_0 \end{aligned} \tag{2.132}$$

where a_0 is the speed of sound at sea level standard day (SLSD) conditions, and T_a is the ambient outside temperature (absolute) at the cruising altitude.

- The 1976 U.S. Standard Atmosphere sets $T_0 = 59^\circ + 459.67^\circ = 518.67^\circ R$ on the Rankine scale.
- The corresponding Kelvin temperature is $15 + 273.15 = 288.15^\circ K$.¹ The range formula can now be expressed as

$$\frac{R}{a_0} = \frac{M(L/D)}{c_t / \sqrt{\theta}} \ln\left(\frac{W_0}{W_1}\right) \tag{2.133}$$

1. The Kelvin scale is based on the triple point of water, which is at 0.01 deg C, and which is assigned the arbitrary value of 273.16 deg. K. Absolute zero is at -273.15 (*not* -273.16) deg. C. Much confusion exists in aerodynamics texts on this point, many of the texts incorrectly equating 273.16 deg C with the freezing point of water (0 deg C).



Range Parameter

- Now $c_t/\sqrt{\theta}$ is the “corrected” TSFC, and is therefore constant at a given engine thrust and Mach number, and roughly constant over the small range of Mach number variations expected to occur in a typical subsonic/transonic cruise.
- Then best range is obtained when the so-called *range parameter*

$$M\left(\frac{L}{D}\right) \quad (2.134)$$

is maximized.

- This will result in an optimum Mach number for subsonic cruise that is higher than the Mach number at which $(L/D)_{max}$ occurs. We will show later that, at a constant altitude,

$$M_{opt} = \sqrt[4]{3} M_{\left(\frac{L}{D}\right)_{max}} \cong 1.316 M_{\left(\frac{L}{D}\right)_{max}} \quad (2.135)$$



Optimum Cruise Mach Number

- Conclude: Subsonic transport aircraft cruising in the transonic region should cruise slightly into the drag divergence region, for best range.
- *In fact, if transonic drag divergence is ignored, one can show that there is no optimum, because the range continues to increase with altitude.*
- Only when the (real) transonic drag increase is modeled do we obtain a specific optimum value for the range parameter and a definite optimal Mach number.
- Although no simple analytical formula for the optimum can be written down (because of the highly nonlinear behavior of transonic drag), the corresponding optimum values for M and ML/D can be determined graphically or numerically.



2.8.3 Takeoff Distance

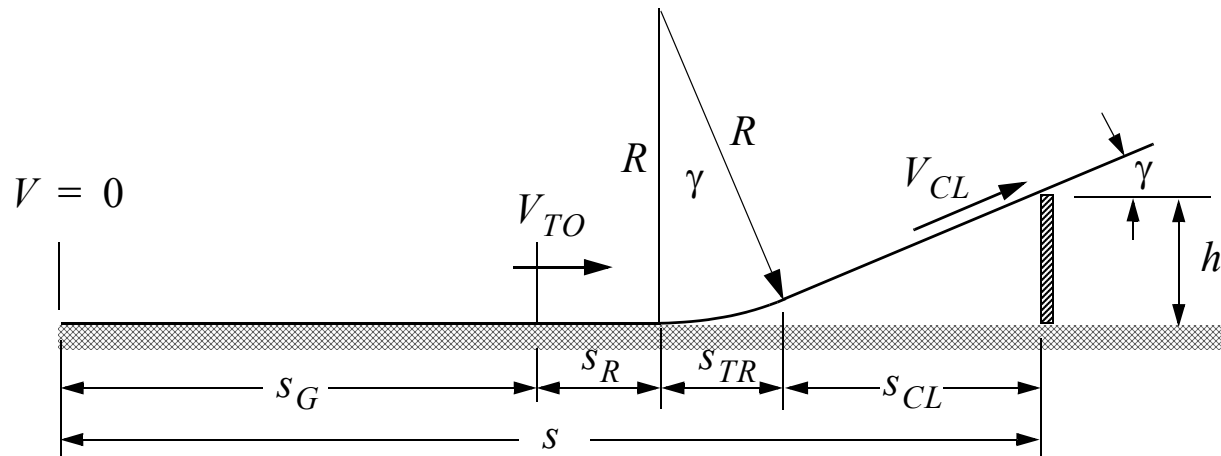


Fig. 2.35 Total takeoff distance to clear an obstacle of height h .

- The total takeoff distance to clear an obstacle of $h = 35$ feet (or 50 feet, for FAR Part 23) can be broken into four different parts, Fig. 2.35:
 - the ground run (roll) distance s_G ,*
 - the rotation distance s_R ,*
 - the transition distance s_{TR} ,*
 - and the climb-out distance s_{CL} :*

$$s = s_G + s_R + s_{TR} + s_{CL} \quad (2.136)$$

Takeoff Roll

- The ground roll distance is calculated by applying Newton's 2nd law in the x -direction:

$$\sum F_x = T - D - \mu(W - L) = Ma_x = M \frac{dV}{dt} \quad (2.137)$$

- Lift and drag during the ground roll must be based on the flap and slat settings for takeoff, and include the parasite drag associated with a retractable landing gear,

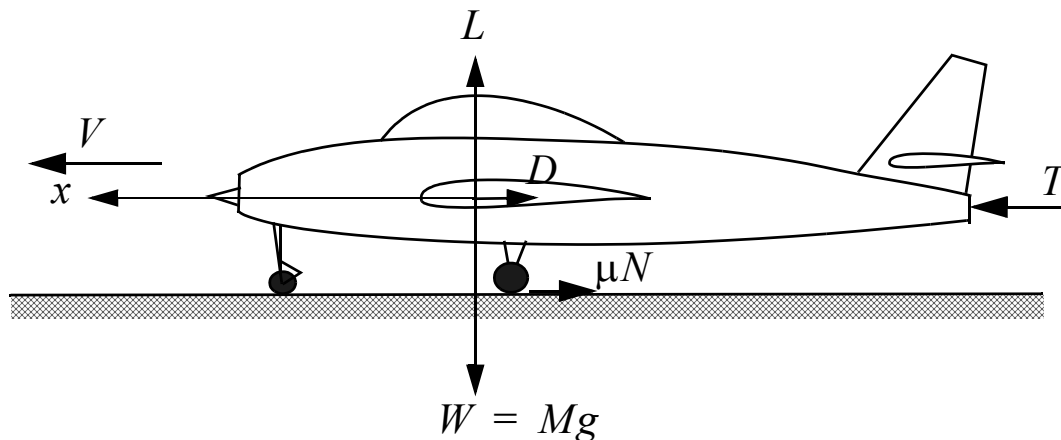


Fig. 2.36 Takeoff run.

Lift and Drag During Ground Roll

$$L = C_{L_G} q S = \frac{1}{2} \rho V^2 S C_{L_G} \quad (2.138)$$

$$D = C_{D_G} q S = \frac{1}{2} \rho V^2 S \left[C_{D_0} + \Delta C_{D_{flaps}} + \Delta C_{D_{gear}} + \frac{C_{L_G}^2}{\pi e A} \right] \quad (2.139)$$

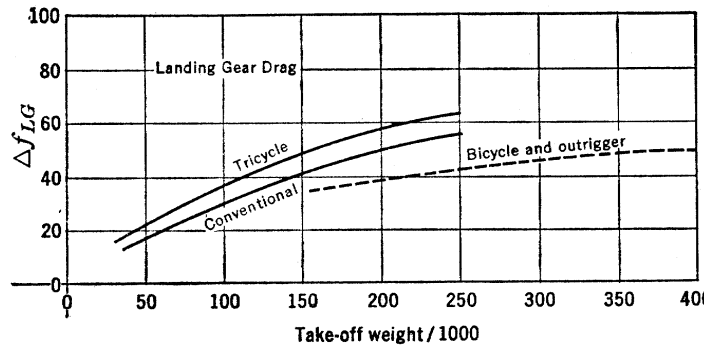
- Estimates for the added drag due to the landing gear has been presented in the classic text by Perkins and Hage (ref. 5), Fig. 2.37.
- This figure presents curves for the parasite drag area for different types of landing gears, and

$$\Delta C_{D_{gear}} = \Delta f_{LG} \frac{A_{LG}}{S_W} \quad (2.140)$$

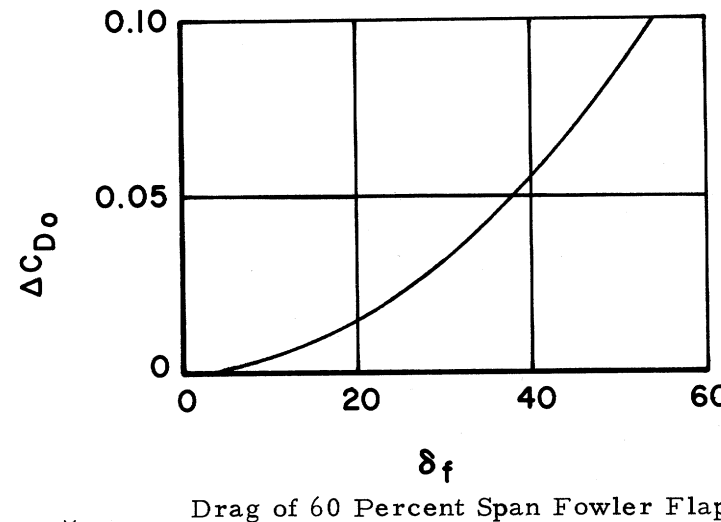
where A_{LG} is the frontal area of the landing gear and S_W is the wing area.

- As regards the induced drag, Perkins and Hage suggest that one should set $e \approx 1$, on account of the ground effect and the redistribution of the spanwise loading due to flap deflection, while McCormick suggests that the induced drag should be ignored altogether.





(From Perkins
and Hage)



(From Niclолai)

Fig. 2.37 Landing gear and flap drag during takeoff ground roll.

- However, ignoring induced drag is not a conservative assumption, and thus reduces any safety margin that may have been built into the takeoff calculations.
- In fact, many departure crashes have occurred because the pilot has misjudged the ability of the aircraft to fly - once out of the ground effect!



a) Ground Roll Distance

- In preliminary calculations, the Hartman approximation [14] is often sufficient.
- It is based on a semi-empirical relation for the acceleration during the ground roll, and can be established as follows. From

$$ds = Vdt = V \left(\frac{dV}{a} \right) \quad (2.141)$$

$$s = \int_0^{V_{TO}} \frac{V}{a} dV = \frac{1}{2} \int_0^{V_{TO}} \frac{1}{a} d(V^2) \quad (2.142)$$

- Based on test data from several different category aircraft, Hartman observed that *the inverse of the acceleration was roughly a linear function of V^2* during the ground roll,

$$\frac{1}{a} = \alpha V^2 \quad (2.143)$$

where α is a constant.



Hartman Approximation

$$s = \frac{1}{2} \int_0^{V_{TO}} \alpha V^2 dV^2 = \frac{1}{4} \alpha V_{TO}^4 = \frac{1}{2} \left(\alpha \frac{V_{TO}^2}{2} \right) V_{TO}^2 = \frac{1}{2} \frac{V_{TO}^2}{\alpha \Big|_{V_{TO}/\sqrt{2}}} \quad (2.144)$$

- The ground roll distance then becomes

$$s_G = \frac{1}{2} \frac{M V_{TO}^2}{T_e \Big|_{V_{TO}/\sqrt{2}}} \quad (2.145)$$

where

$$T_e = T - D - \mu(W - L) \quad (2.146)$$

- Typical values of the coefficient of friction are in the range 0.03 - 0.05, for concrete or macadam runways, with the higher value representing wet runways.
- Experience indicates that the Hartman approximation is reasonably accurate (sometimes surprisingly so), provided that certain conditions are met:
 - (1) The excess thrust T_e at $V_{TO}/\sqrt{2}$ must be greater than 10% of W_{TO} , and
 - (2) The takeoff speed V_{TO} must not be greater than 1.2 times the stalling speed in the *takeoff configuration* (flaps and slat settings, etc.).



Thrust Lapse During Takeoff

- If these conditions are not met, the equation of motion (2.137) should be integrated numerically to obtain s_G .
- In order to do this, we need to be able to estimate the *thrust lapse* as a function of V during the ground roll, i.e., we need T as a function of V .
- For propeller aircraft, this can be done once a propeller-engine combination has been selected, using propeller design charts.
- For jet aircraft, the situation is more difficult. If an engine has been selected, the required thrust lapse data would be available from the manufacturer in graphical or numerical form.
- However, the engine to be used may not exist yet, because it also need to be designed and manufactured.



Jet Engine Thrust Lapse

- Torenbeek has considered this problem in Appendix H of his text [3], where the following approximate but useful equation for estimating the thrust lapse during takeoff is presented (Eq. H-35, Appendix H):

$$\frac{T}{T_{TO}} = 1 - \frac{0.454(1 + \lambda)}{\sqrt{(1 + 0.75\lambda)G}} M + \left(0.6 + \frac{0.13\lambda}{G}\right) M^2 \quad (2.147)$$

where

$$\begin{aligned} M &= \text{Mach number} \\ T &= T(M) = \text{thrust as a function of } M \\ T_{TO} &= \text{takeoff thrust (static)} \\ \lambda &= \text{engine bypass ratio} \\ G &= \text{gas generator function (Eq. H-8)} \\ &\approx 0.9 \text{ for turbojets and low BPR turbofans} \\ &\approx 1.1 \text{ for high BPR turbofans} \end{aligned} \quad (2.148)$$

- Torenbeek states that this equation is accurate up to (approx.) Mach 0.3.
- Using engine data for the P&WA JT9D-7A engine, I obtained errors of less than 2% over this Mach number range. At Mach 0.45, the error was still only 2.5%.



General Thrust Calculations

- The installed thrust at any Mach number and altitude can be calculated by subtracting the ram drag (and miscellaneous engine losses that affect thrust).
- As an example, consider a turbojet (for simplicity). The net thrust F_n can be written as

$$F_n = \dot{m}_a[(1+f)V_j - V] + A_j(p_j - p_\infty) \quad (2.149)$$

where

$$\begin{aligned} \dot{m}_a &= \text{engine airflow rate (mass)} \\ f &= \dot{m}_f/\dot{m}_a = \text{fuel/air ratio} \\ V_j &= \text{exhaust nozzle exit (jet) velocity} \\ A_j &= \text{exhaust nozzle area} \\ p_j &= \text{exhaust jet nozzle exit pressure} \\ p_\infty &= \text{atmospheric pressure} \\ V &= \text{aircraft velocity (airspeed)} \end{aligned} \quad (2.150)$$

- The fuel/air ratio is small (of the order 1/60) and can be neglected in preliminary calculations.



Optimum Nozzle

- Assuming optimum nozzle expansion, $p_j = p_\infty$, the net thrust can be written

$$\begin{aligned} F_n &= F_g - \dot{m}_a V \\ &= \text{gross thrust} - \text{ram drag} \end{aligned} \tag{2.151}$$

- Under static conditions, $F_g = F_n$ (net thrust as measured in an engine test cell).
- Engine airflow and fuel flow are typically expressed as weight flow rates (lbs/sec or lbs/hr), and we write Eq. (2.151) using standard engine notation as

$$F_n = F_g - \left(\frac{W_a \sqrt{\theta_{t2}}}{\delta_{t2}} \right) \left(\frac{\delta_{t2}}{\sqrt{\theta_{t2}}} \right) \left(\frac{V}{g} \right) \tag{2.152}$$

where

$$\begin{aligned} \frac{W_a \sqrt{\theta_{t2}}}{\delta_{t2}} &= \text{engine airflow, corrected to SLSD} \\ \delta_{t2} &= p_{t2}/p_0 \\ \theta_{t2} &= T_{t2}/T_0 \\ g &= \text{acceleration due to gravity} \end{aligned} \tag{2.153}$$



Sea Level Standard Day (SLSD)

- The standard sea level conditions are

$$\begin{aligned}T_0 &= 518.67^{\circ}R = 288.15^{\circ}K \\p_0 &= 14.7 \text{ psi} = 29.92 \text{ "Hg}\end{aligned}\tag{2.154}$$

- Note that the zero subscript is also used to refer to the condition far upstream (sta. 0), i.e., atmospheric conditions.
- To avoid confusion, we will use the “ ∞ ” or “am” subscript whenever we need to refer to free-stream conditions.



Corrections to SLSD

- Engine data is then corrected to SLSD conditions, as follows

$$\begin{aligned}\frac{F_n}{\delta_{t2}} &= \text{corrected thrust} \\ \frac{N_1}{\sqrt{\theta_{t2}}}, \frac{N_2}{\sqrt{\theta_{t2}}} &= \text{corrected rotor speeds} \\ \frac{T_n}{\theta_{t2}} &= \text{corrected temperature at station n} \\ \frac{W_a \sqrt{\theta_{t2}}}{\delta_{t2}} &= \text{corrected airflow} \\ \frac{W_f}{\delta_{t2} \sqrt{\theta_{t2}}} &= \text{corrected fuel flow} \\ \frac{TSFC}{\sqrt{\theta_{t2}}} &= \text{corrected TSFC at constant thrust}\end{aligned}\tag{2.155}$$

- Unless noted otherwise, the corrections apply to a fixed engine pressure ratio (EPR) point.



Thrust (Power) Settings - Aircraft Engines

- Most engines use EPR to set engine power, which for a twin-spool engine is

$$EPR = \frac{p_{t7}}{p_{t2}} \quad (2.156)$$

where p_{t7} is the total pressure at the exit of the low pressure turbine, immediately in front of the exhaust nozzle.

- The corrected weight flow is a function of the corrected low pressure compressor speed $N_1 / \sqrt{\theta_{t2}}$, which is a unique function of engine pressure ratio (EPR).
- For a given power setting, the ram drag can be calculated from Eq. (2.152), using the engine performance data/curves, and the net thrust obtained for any combination of altitude and airspeed.
- It is convenient to use the flight Mach number M instead of V ,

$$M = \frac{V}{a} = \frac{V}{a_0 \sqrt{\theta}} \quad (2.157)$$

where a_0 is the speed of sound at SLSD conditions.



Thrust Formula

- Substituting into Eq. (2.152) and dividing both sides by δ_{t2} yields the following equation for the net thrust corrected to SLSD conditions:

$$\frac{F_n}{\delta_{t2}} = \frac{F_g}{\delta_{t2}} - \left(\frac{W_a \sqrt{\theta_{t2}}}{\delta_{t2}} \right) \left(\frac{a_0 \sqrt{\theta}}{\sqrt{\theta_{t2}}} \right) \left(\frac{M}{g} \right) = \frac{F_g}{\delta_{t2}} - \left(\frac{W_a \sqrt{\theta_{t2}}}{\delta_{t2}} \right) \left(\frac{a_0}{g} \right) \left(\frac{M}{\sqrt{1 + \frac{1}{2}(\gamma - 1)M^2}} \right) \quad (2.158)$$

- The actual thrust F_n at any altitude and Mach number can then be calculated using this formula.
- It should be noted that the corrected (or observed) gross thrust at altitude is not the same as would be obtained in a test cell at SL static conditions, because the engine exhaust nozzle operates at a higher pressure ratio because of the ram effect.
- The gross thrust must be calculated using nozzle charts provided by the manufacturer.



b) Rotation Distance

- The rotation distance is calculated by multiplying the takeoff speed by the time it takes to rotate the aircraft to an angle of attack that will generate a lift coefficient of $0.8C_{L_{max}}$,

$$s_R = V_{TO} t_R \quad (2.159)$$

- It is customary to assume that rotation takes 1-3 seconds, with 3 seconds being typical for a large transport and 1 second for a light propeller aircraft.
- The lift buildup is not in phase with the angle of attack, because it takes some time to change the circulation around the wing to produce the lift increase; hence the aircraft does not reach $0.8L_{max}$ immediately after the rotation has been completed.
- This time lag between change in α and the resulting change in L must be included in t_R .



c) Transition Distance

- During transition, the aircraft leaves the ground and flies along a circular arc, until it reaches the climb angle γ_{CL} to clear the obstacle of height h , Fig. 2.48.
- Assuming that the velocity remains constant during this phase, at liftoff the normal acceleration is directed straight up and Newton's 2nd law requires that

$$L - W = Ma_n = MV_{TO}^2/R \quad (2.160)$$

$$L = W + \frac{W}{gR}V_{TO}^2 = W \left(1 + \frac{V_{TO}^2}{gR} \right) \quad (2.161)$$

- Assuming that the takeoff speed is $V_{TO} = 1.2V_S$, and with $C_L = 0.8C_{L_{max}}$, we obtain

$$\frac{L}{W} = (0.8)(1.2) = 1.152 \quad (2.162)$$

$$R = \frac{V_{TO}^2}{0.152g} \quad (2.163)$$

$$s_{TR} = R \sin \gamma_{CL} \quad (2.164)$$

$$\sin \gamma_{CL} = \frac{T - D}{W} \quad (2.165)$$



d) Climb Distance

- The climb distance is obtained directly from Fig. 2.35, as follows:

$$s_{CL} = \frac{h - R(1 - \cos\gamma_{CL})}{\tan\gamma_{CL}} \quad (2.166)$$

- If the altitude at the end of transition, $R(1 - \cos\gamma_{CL})$, is greater than h , then $s_{CL} = 0$.



2.9 References

1. McCormick, B. W., *Aerodynamics, Aeronautics, and Flight Mechanics*, John Wiley & Sons, 2nd ed., 1995.
2. Raymer, D. P., *Aircraft Design: A Conceptual Approach*, AIAA Education Series.
3. Torenbeek, E., *Synthesis of Subsonic Airplane Design*, Delft University Press, Martinus Nijhoff Publishers, 1982.
4. Nicolai, L. M., *Fundamentals of Aircraft Design*, University of Dayton, Ohio, 1975.
5. Perkins, C.D. and Hage, R.E., *Airplane Performance, Stability and Control*, John Wiley & Sons, 1949.
6. Abbott, I.H. and von Doenhoff, A.E., *Theory of Wing Sections*, Dover Publications, 1959.
7. Oswald, W.B., *General Formulas and Charts for the Calculations of Airplane Performance*, NACA TN 408, 1932.
8. Glauert, H., *The Elements of Aerofoil and Airscrew Theory*, Cambridge University Press, New York, 1926.
9. DeYoung, J., and Harper, C., *Theoretical Symmetric Span Loading at Subsonic Speeds for Wings Having Arbitrary Plan Form*, NACA Report No. 921, 1948.
10. Diedrich, F.W., *A Planform Parameter for Correlating Certain Aerodynamics of Swept Wings*, NACA TN 2335, 1951.
11. Lowry, J.G., and Polhamus, E.C., *A Method for Predicting Lift Increments Due to Flap Deflection at Low Angles of Attack*, NACA TN 3911, 1957.
12. Ashley, H., and Landahl, M., *Aerodynamics of Wings and Bodies*, Dover Edition, 1985.
13. Vincenti, W.G., *Comparison Between Theory and Experiment for Wings at Supersonic Speeds*, NACA Report No. 1033, 1951.
14. Hartman, E.P., *Consideration of the Take-Off Problem*, NACA TN 557, 1936.

MAE 154A

Preliminary Design of Aircraft

Oddvar O. Bendiksen

Department of Mechanical and Aerospace Engineering
University of California, Los Angeles



Winter Quarter 2015

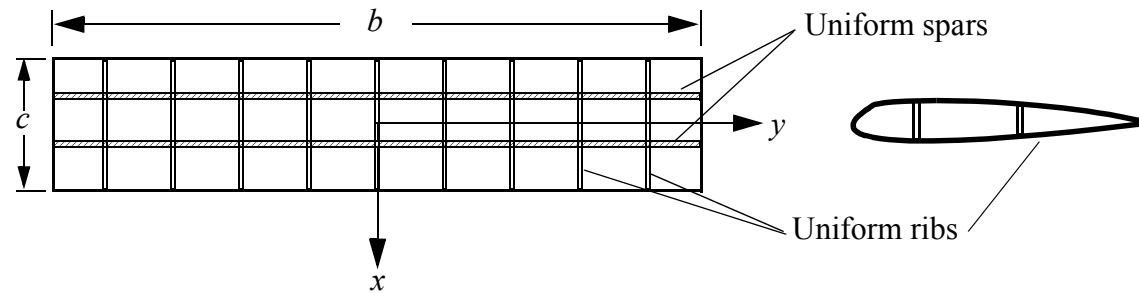
3.0 Configuration Studies: Aerodynamic, Structural and Mechanical Design Considerations



3.1 Configuration Studies

a) Wing Planform

(1) Straight, uniform wing: Suitable for light, low-speed aircraft.



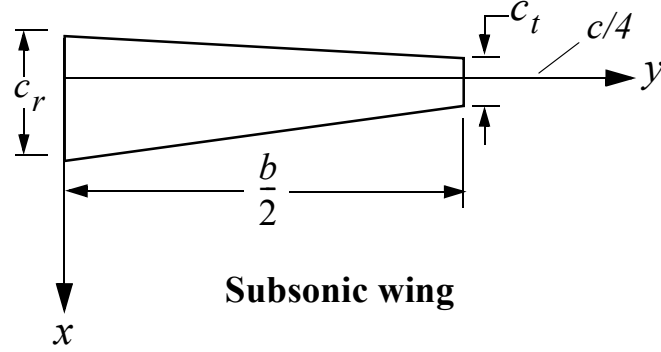
Advantages:

- Easy to analyze (aero and structure).
- Easy to fabricate (low cost).

Disadvantages:

- Structurally not optimum (not min. Wt.).
- Aerodynamically not optimum (not min. D).

(2) Straight, tapered wing: Subsonic and supersonic aircraft



$$\begin{aligned}\lambda &= \frac{c_t}{c_r} \\ A &= \frac{b^2}{S} = \frac{2b}{c_r(1 + \lambda)} \\ \bar{c} &= MAC = \frac{2}{S} \int_0^{\frac{b}{2}} c^2(y) dy \\ &= \frac{2}{3} c_r \left(\frac{1 + \lambda + \lambda^2}{1 + \lambda} \right)\end{aligned}$$

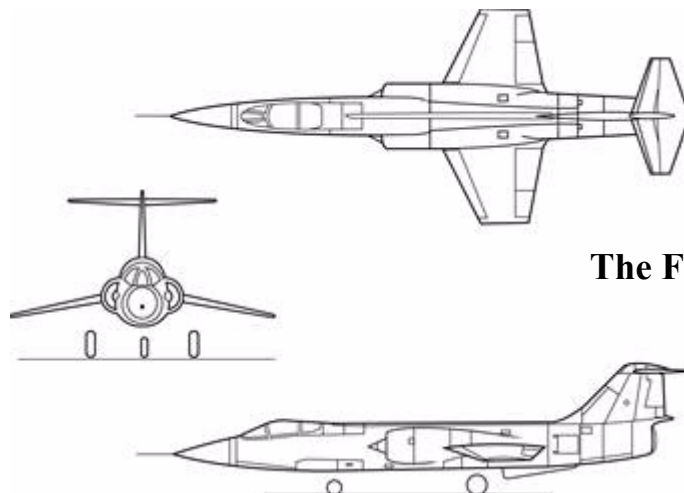
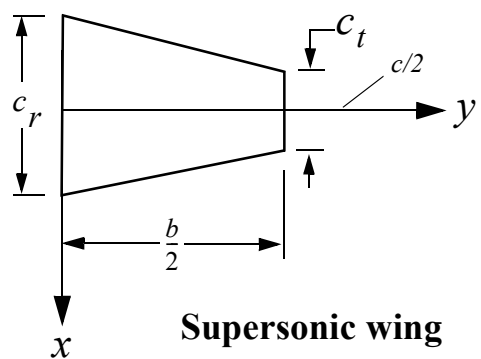
Advantages: (compared to a straight uniform wing)

- Has improved lift distribution, resulting in lower induced drag.
- Is structurally more efficient than uniform wing.

Disadvantages:

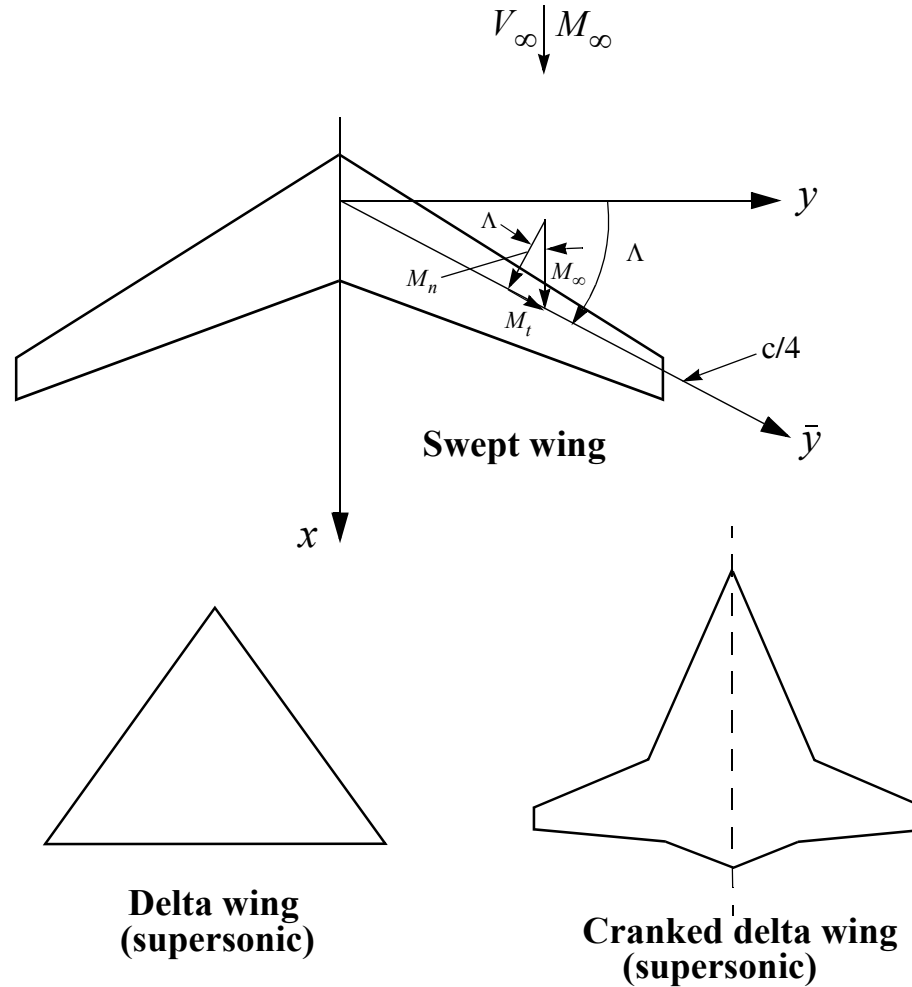
- More difficult to fabricate (higher manufacturing cost).
- Not optimum for transonic Mach numbers.





The F-104 Starfighter (a.k.a. the widowmaker)

(3) Swept, tapered wing: Subsonic and supersonic aircraft



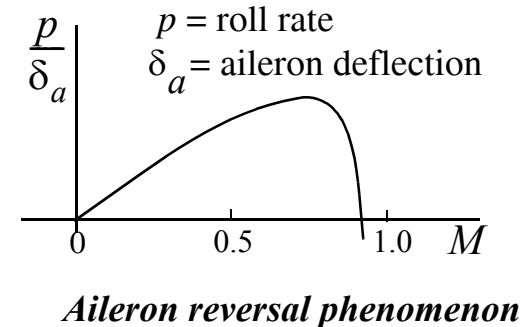
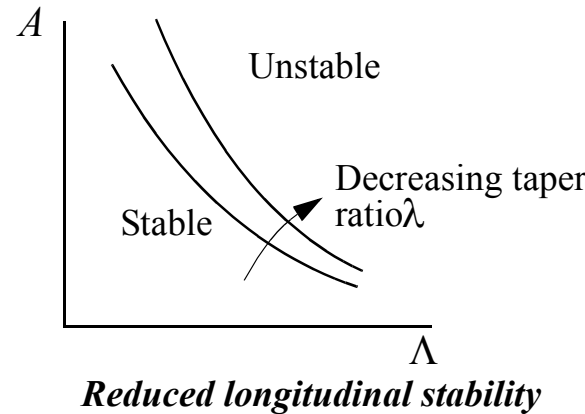
Aft sweep ($\Lambda > 0$)

Advantages:

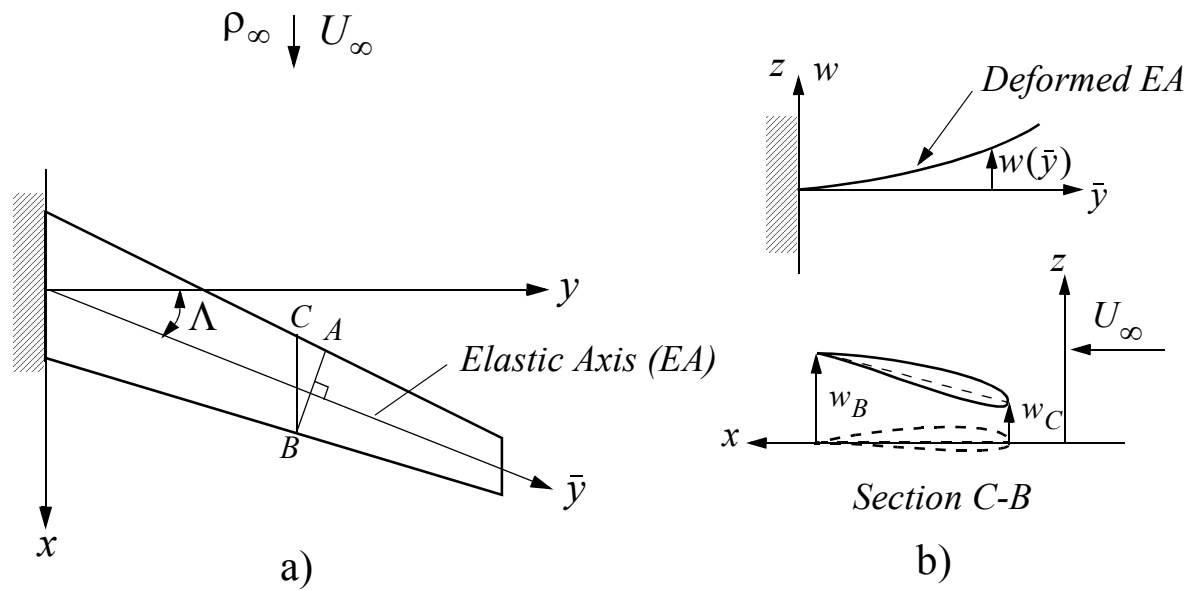
- Delays drag divergence (increases M_{crit} proportional to $1/\cos\Lambda$).
- Increases aeroelastic divergence speed.

Disadvantages:

- Reduces control effectiveness (aileron reversal problem). Structural washout plays an important role.
- Reduces longitudinal stability (limits Λ for high aspect ratio wings; introduces pitch-up tendency at stall).

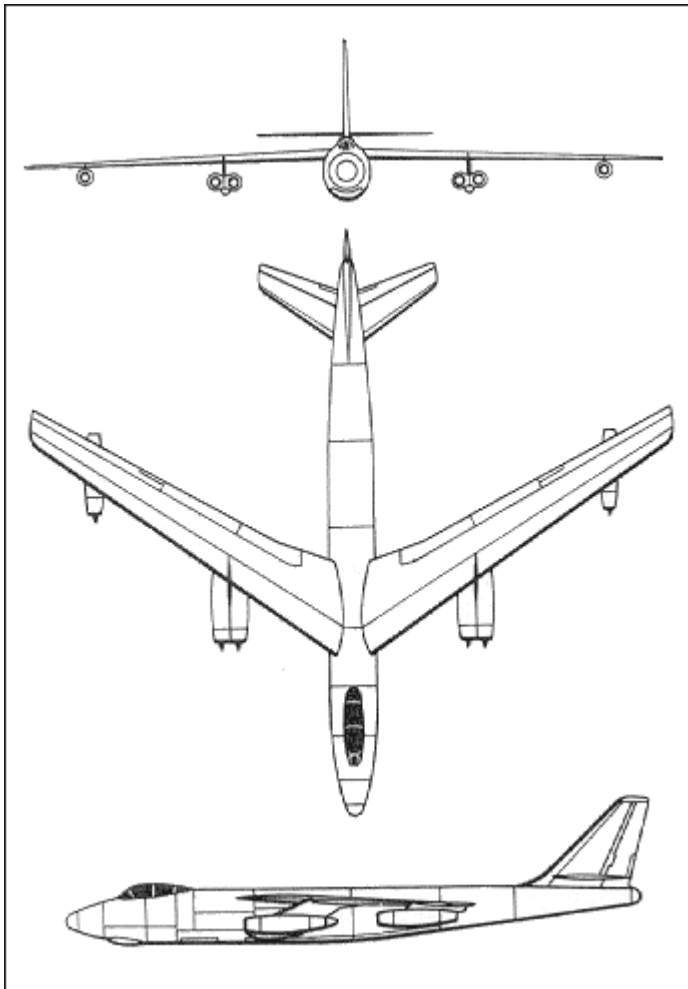


Structural Washout Effect



Structural washout effect: a) Chordwise segment $A-B$ vs. streamwise segment $C-B$ of a swept wing; b) structural washout effect (reduction of angle of attack of streamwise segment $C-B$, since $w_C < w_B$).

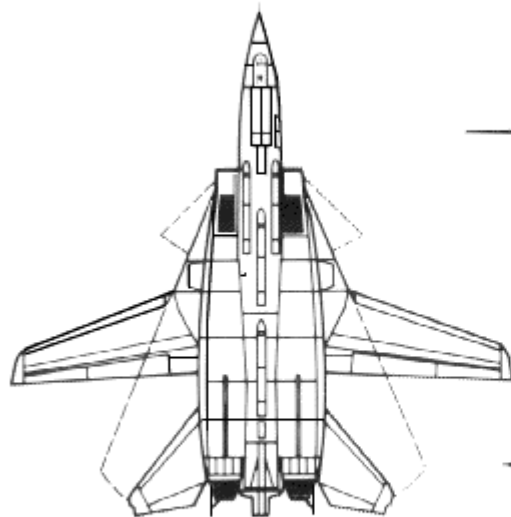
B-47 Bomber



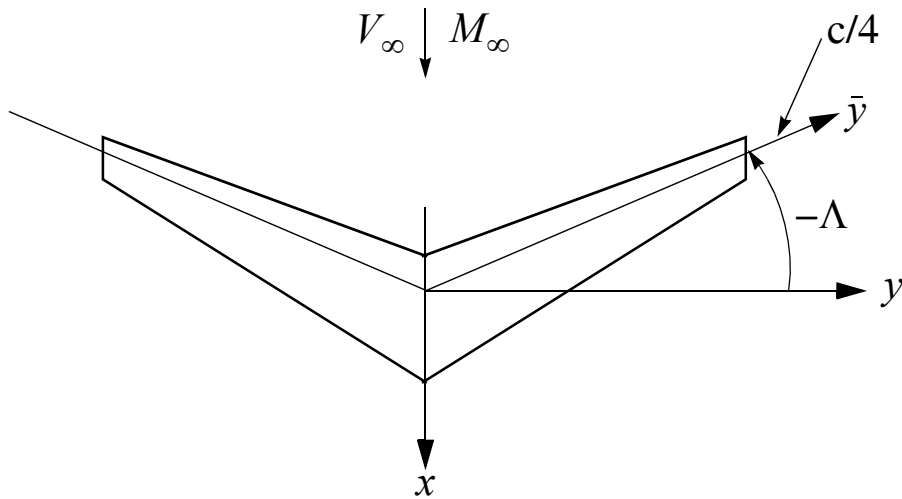
First US aircraft incorporating Busemann's ideas of swept wings. Also the first documented case of an aircraft encountering aileron reversal within the flight envelope.



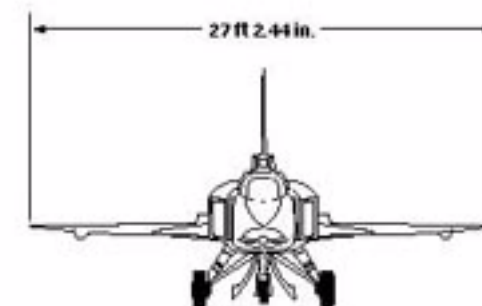
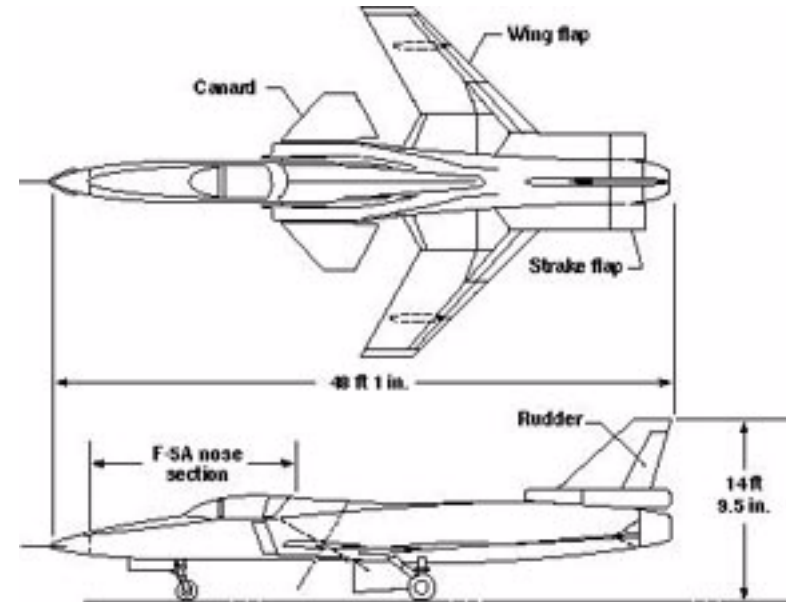
F-14



Forward sweep ($\Lambda < 0$)



Highly maneuverable military aircraft



X-29

X-29 and Su-47 Comparison



X-29



Su-47

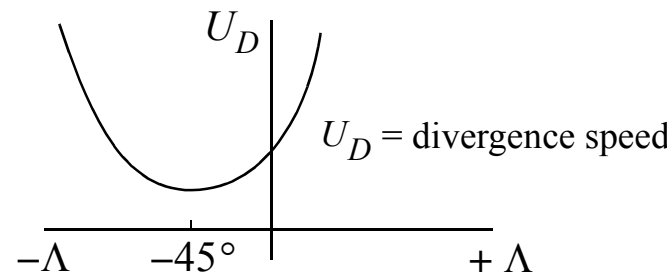
Forward Sweep: Advantages and Disadvantages

Advantages:

- Improves aerodynamic efficiency (increases M_{crit} and M_D).
- Increases control effectiveness significantly (eliminates aileron reversal).

Disadvantages:

- Aircraft becomes statically and dynamically unstable (need highly redundant active control computers to fly aircraft).
- Wing becomes very susceptible to aeroelastic divergence (need composites and aeroelastic tailoring).
- High complexity and cost.



Effect of sweep on divergence.

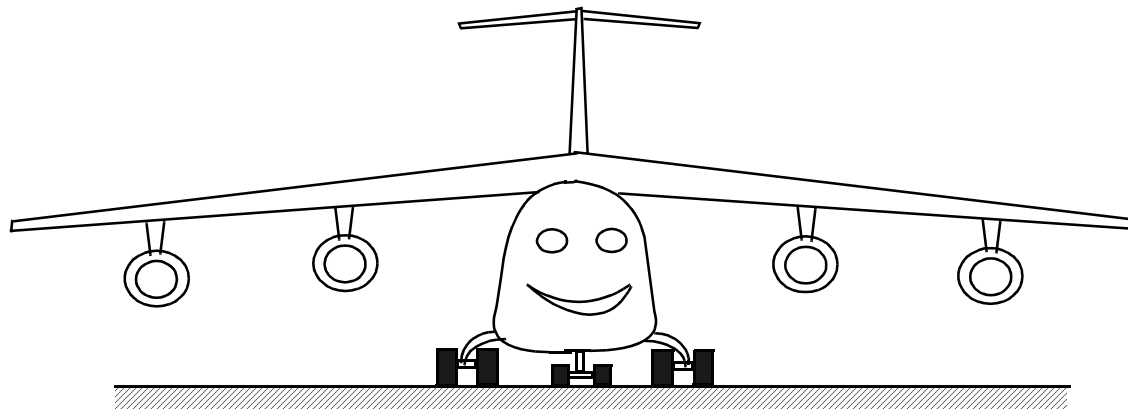


b) Airfoil selection

- Dictated by application/specs - esp. Mach no.
- TBC later.



c) Wing placement: (1) High wing



Applications:

- Light aircraft (old tradition; structural simplicity; high ϵ)
- Large cargo transports (C-5A, C-17: loading issues)
- STOL aircraft (ground effect issues)

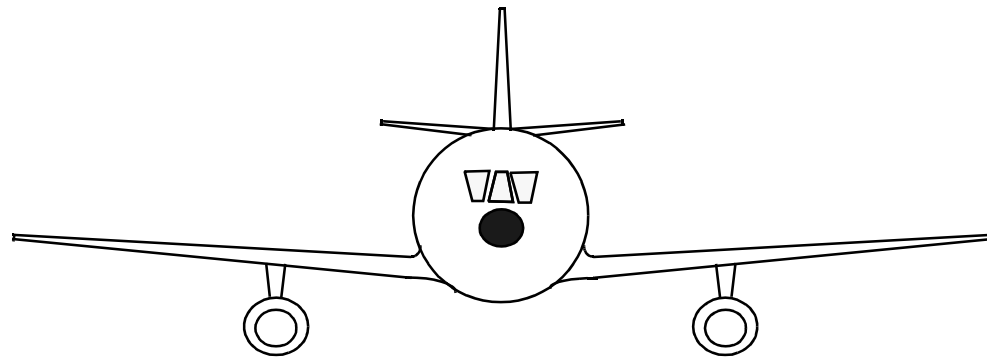
Advantages:

- Low fuselage provides for easy loading (essential for large cargo A/C)
- Good ground clearance (wing; engines; propellers; crash/fire/safety)
- High wing efficiency ϵ

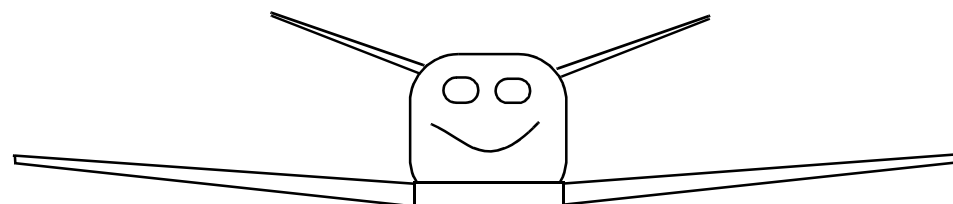
Disadvantages:

- Complex (main) landing gear design, especially for large aircraft
- Difficult engine access on large aircraft (maintenance issues)
- Reduced crew visibility in some cases (light A/C)

(2) Low wing



Subsonic transport



Light aircraft

Applications:

- Large subsonic passenger aircraft
- Business jets
- Some light aircraft

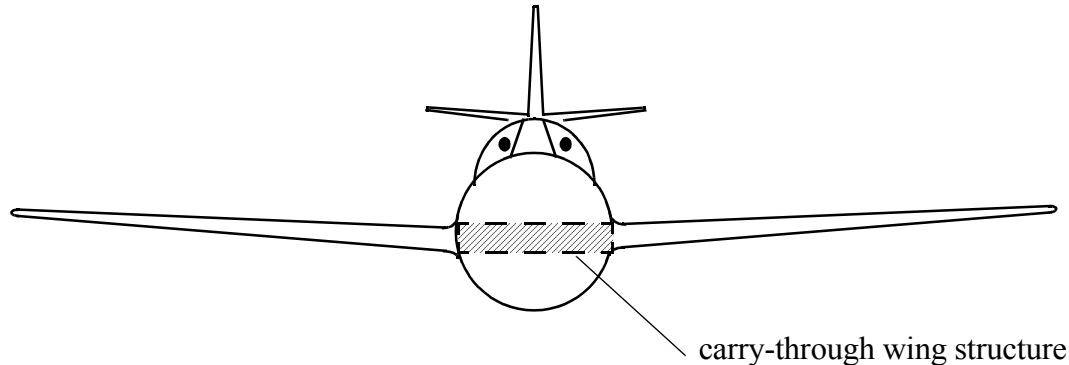
Advantages:

- Well suited for 2- or 3-deck designs (passengers above; cargo below)
- Easy engine access (maintenance)
- Design of landing gear is much less problematic

Disadvantages:

- Ground clearance may become a problem (wing mounted engines)
- Relatively low wing efficiency ϵ ; buffeting at high alpha
- Low ground clearance increases risk of post-crash fires

(3) Mid-wing



Applications:

- High performance military (fighter) aircraft
- Aerobatic aircraft

Advantages:

- Minimizes separation at high alpha (esp. wing root vortex)
- Less buffeting during maneuvers (less tail interference)
- Relatively high wing e (compared to low wing)

Disadvantages:

- More complex and expensive structural design
- Carry-through wing structure wastes space
- Generally not optimal for passenger aircraft (wing carry-through structure wastes valuable space).

d) Engine selection and placement

(1) Type selection:

- Piston (reciprocating) engine
- Turboprop
- Turbojet - with or without afterburners
- Turbofans- with or without afterburners
- Propfan (?)

Choice dictated by:

- Flight envelope (Specs.)
- Reliability & cost

(2) Sizing (BHP, Thrust):

Dictated by performance specs.



(3) Placement (location)

i) Fuselage mounted (fore or aft)



Advantages:

- Clean wing (aero)
- Rel. low propulsive drag
- Good ground clearance

Disadvantages:

- Large c.g. changes
- Inlet losses/separation
- Safety (fire; containment)
- Cabin noise

- In fuselage (single prop. A/C; jet fighters; center engine on 3-eng. A/C)
- Pod mounted (B727; DC-9; business jets; etc.)

ii) Wing mounted

- In wing root or buried (DH Comet; Vulcan bomber)



Advantages:

- Relatively clean wing
- Relatively low propulsive drag
- Lower wing loading (less buffeting during maneuvers)

Disadvantages:

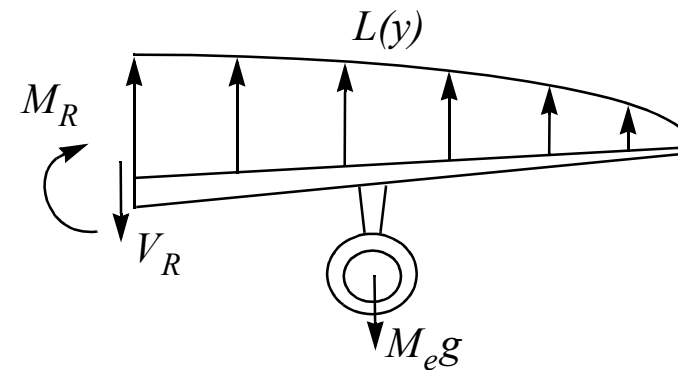
- Poor engine access (maintenance)
- Safety issues (fire; containment)
- Poor gust response
- Cabin noise

- Pod mounted (B707; B747; B767; DC-8; DC-10; etc.)

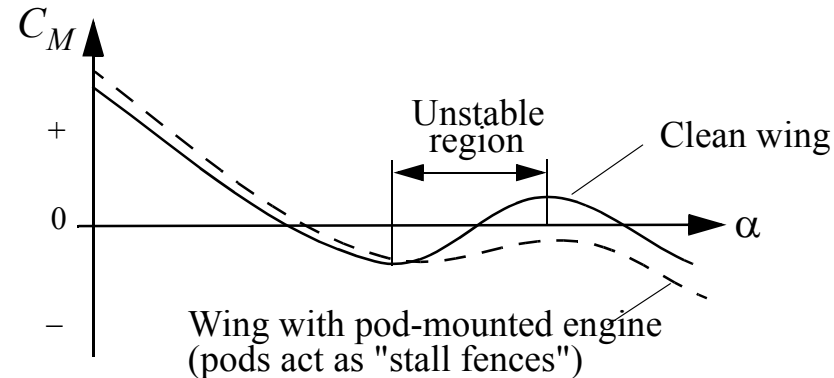


Advantages:

- Fire safety (isolate fire from wing structure)
- Easy engine access
- Low duct losses (inlet & exhaust)
- Wing bending moment reduction



- Reduced post-stall pitch-up of swept wings



- Flutter benefits (mass forward of EA is stabilizing)



Disadvantages:

- Ground clearance problems (smaller A/C; e.g., B737)

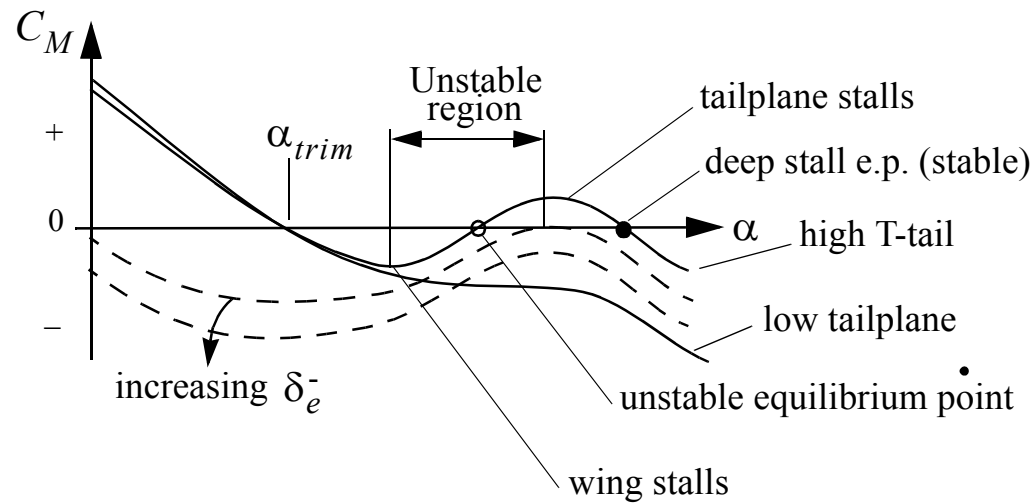


- Higher wing loading (requires high lift devices)
- Wing/nacelle interference
- In-flight TR deployment may lead to loss of control
- Somewhat higher propulsive drag

(e) Tailplane (empennage) design Dictated by stability and control requirements

The following flight conditions must be considered:

- *Low alpha*: cruise; high-speed flight
- *High alpha*: maneuvers; stall; effect of wing slipstream; superstall (T-tails)
- *Spin recovery*: Vertical stabilizer and rudder sizing
- *Engine out condition on multi-engine A/C*: Usually sizes vertical stabilizer and rudder



Canard and Tailless Aircraft

- Different problem, because in trimmed flight, $L_c > 0$.
- Trim issue with flaps (Beech Starship I uses variable sweep)
 - B-2 bomber
 - Tu-144 SST (uses retractable canard)
 - Viggen fighter
 - Various light (home-built) aircraft (e.g., Rutan designs)



Tails, Tails...

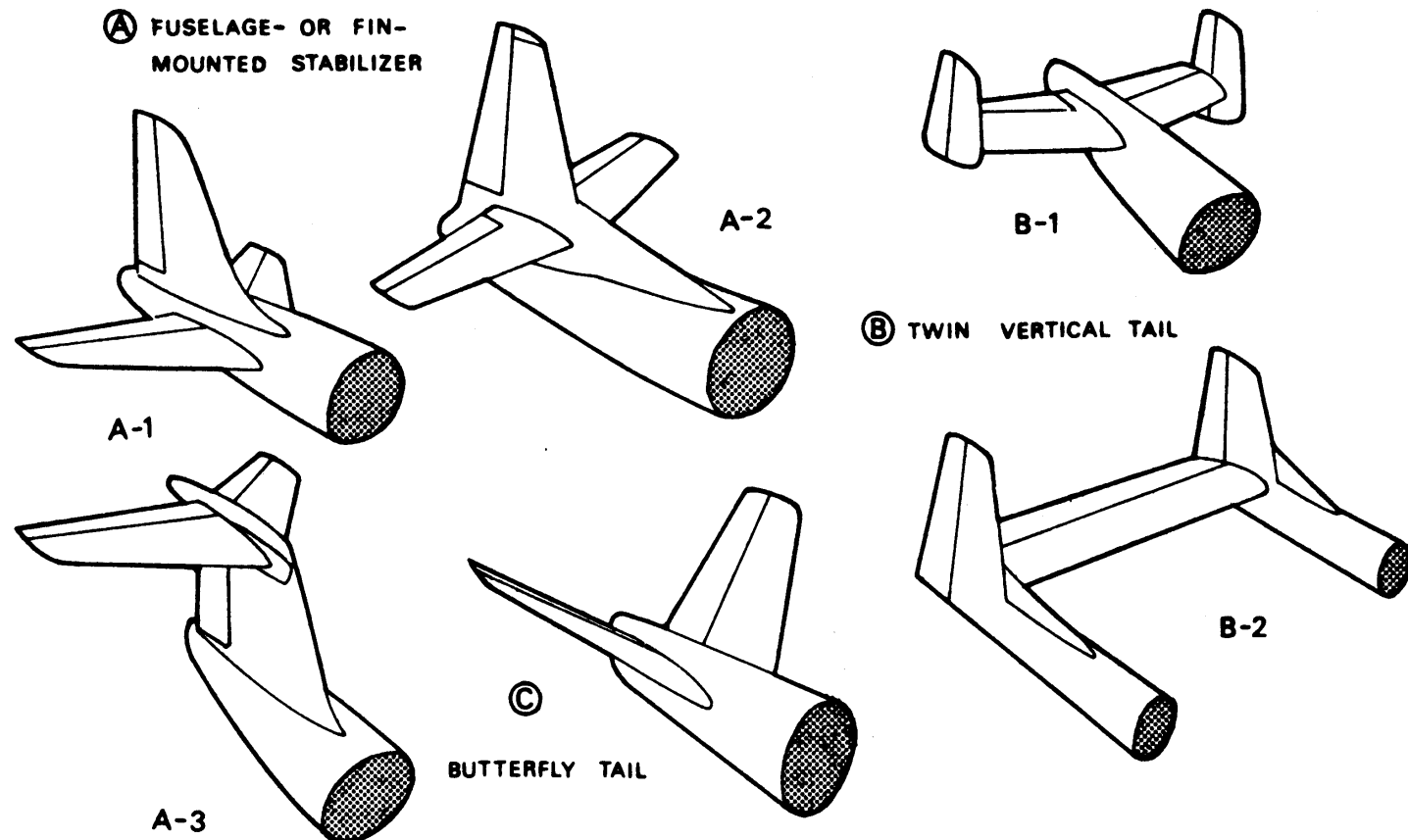


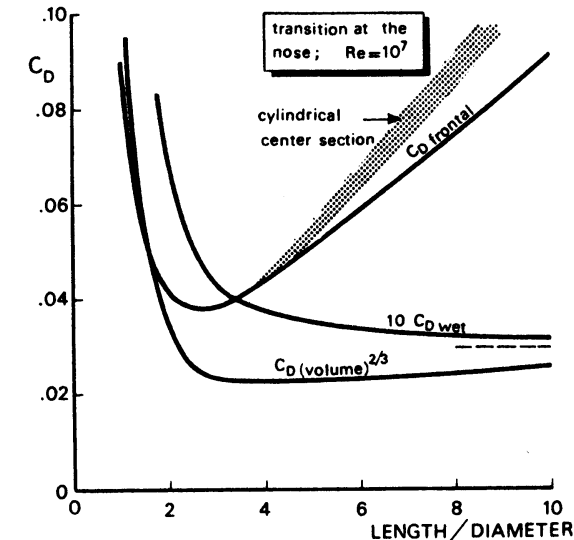
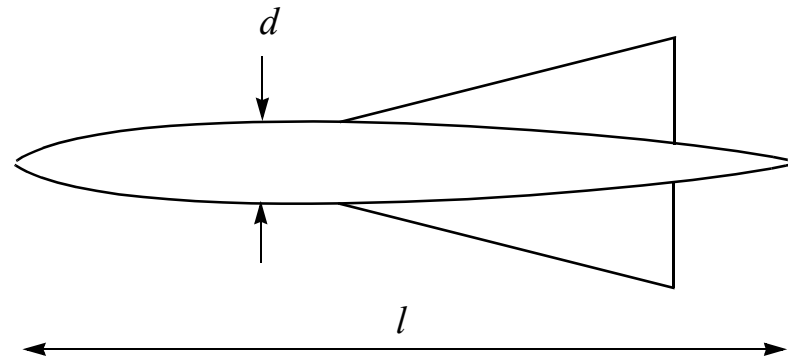
Fig. 2-23. Classification of tailplane configurations

(From Torenbeek)



(f) Fuselage design

- Dictated by application and tradition. Room for new ideas.
- Design considerations:
 - *Aerodynamics (low drag)*: High slenderness ratio l/d .



Fuselage drag vs. slenderness ratio
(from Torenbeek)

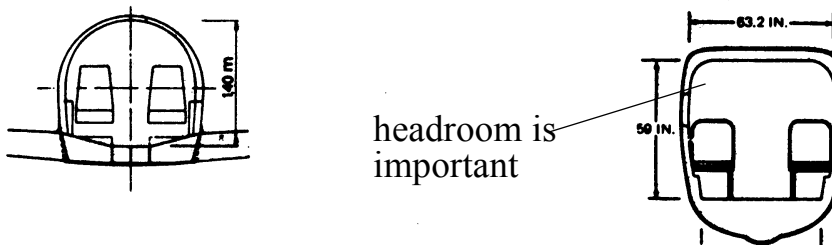
- *Passenger comfort*: Low l/d (wide-body aircraft).



Structural design:

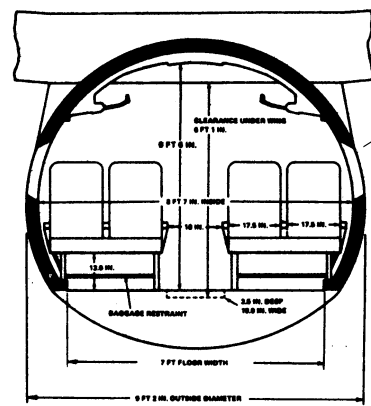
- Slender cylindrical "tubes" tend to be optimal for semimonocoque structures.
- A circular cross-section results in an even distribution of pressurization stresses, which is important from a fatigue life standpoint.

(Adapted from Torenbeek)

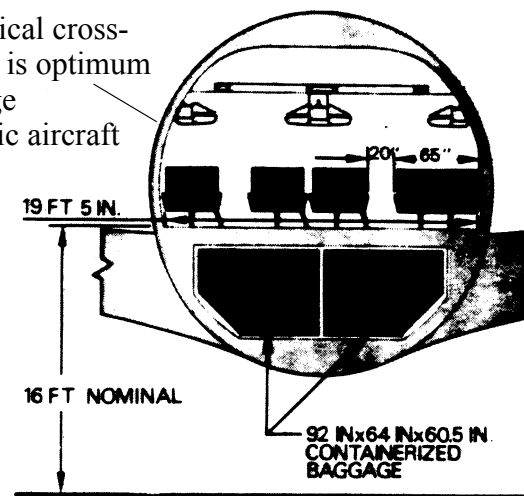


Dassault "Falcon" 10

De Havilland Canada
DHC-6 "Twin Otter"



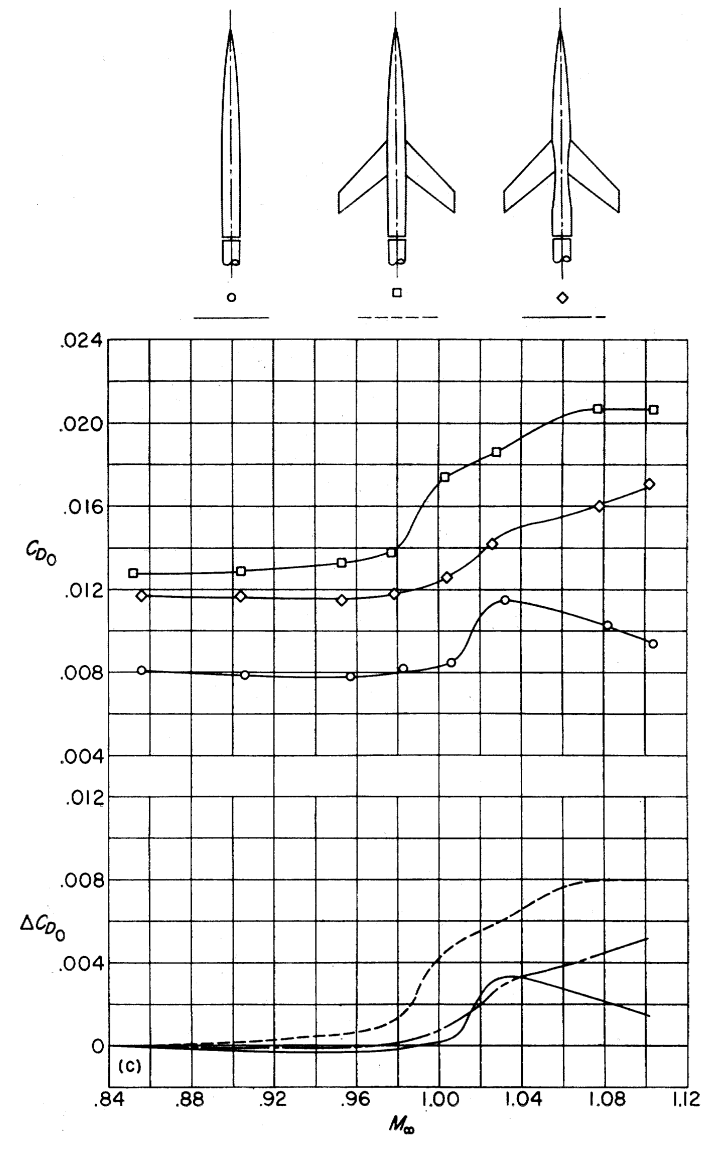
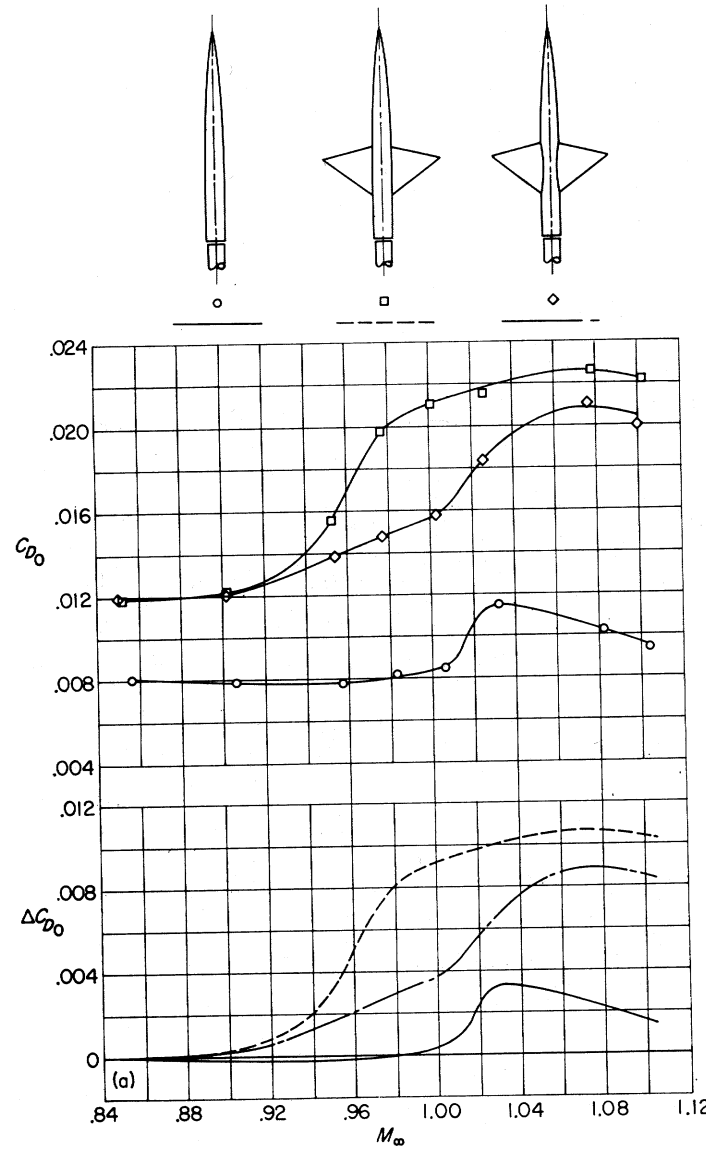
De Havilland Canada DHC-6



Boeing 747

Wing-body wave drag at transonic and supersonic speeds

Transonic and supersonic "area rules"



3.2 Structural and Mechanical Design Considerations

Preliminary Design Considerations

(a) Static and dynamic strength requirements: (*FAR Parts 23, 25, and 27; MIL Specs*)

- Ultimate loads. (Wings must stay on up through 1.5 x limit loads).
- Gust loads. (Also affect fatigue life).
- Flutter (A/C must be flutter-free throughout flight envelope, but LCO-type flutter has been tolerated on some military aircraft, e.g., the F-16).

(b) Fatigue life: (*essentially determines useful service life of aircraft structure*)

- Expected life of *primary* structure.
- Effect of corrosion (corrosion fatigue in marine environment).
- Inspection and maintenance requirements.

Typical aircraft life (non-military):

Economic life: 15 years (IRS write-off).

Design life: 30 years (plus or minus). Actually hrs and cycles.

Consider "what if" economic life or design life is extended.



(c) Reliability of critical components and systems: (can determine economic life of aircraft)

Important issues:

- Fail-safe designs for critical components/systems.
- Redundancies (backup systems).
- "Graceful failures" (where possible).

(d) Learn from history: Examples will be provided in class, including

- Comet
- Lockheed Electra
- C-5A
- DC-10
- Chinook
- Challenger & Columbia

(e) Remember Murphy's Law: What can happen will happen - even the "impossible".



Some Case Histories



De Havilland Comet

Structural Fatigue

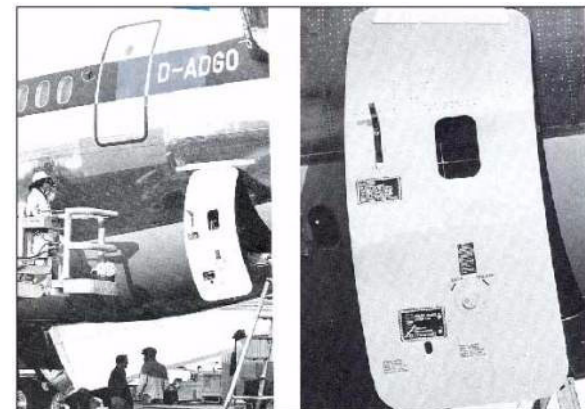
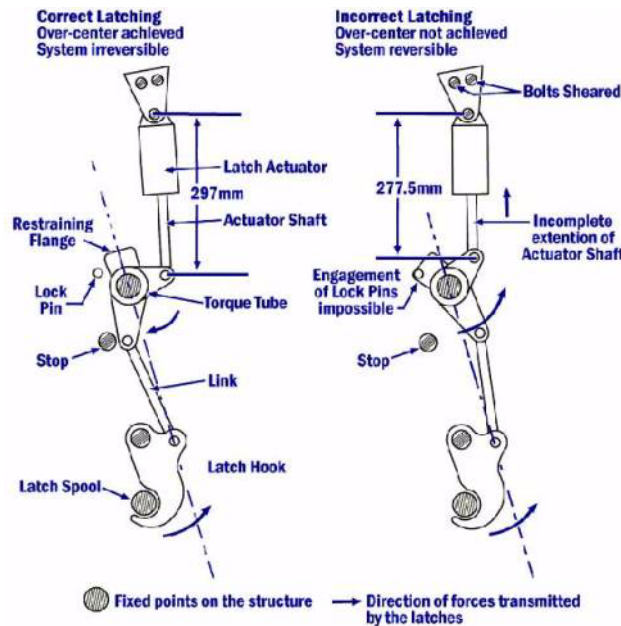


Lockheed Electra Propeller Whirl Flutter Causing Wing Failures



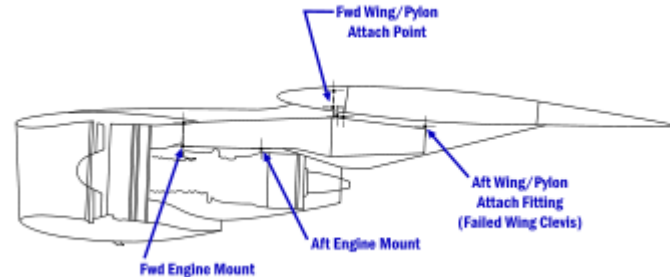
DC-10

Multiple Problems: A Cursed Aircraft?



Cargo Door Problems

DC-10 Engine and Pylon Problems



Lockheed C-5

Wing Fatigue Life Only 25% of Design Life



Lockheed C-5

Thrust Reverser Deployed During Takeoff



Ramstein AFB
August 29, 1990



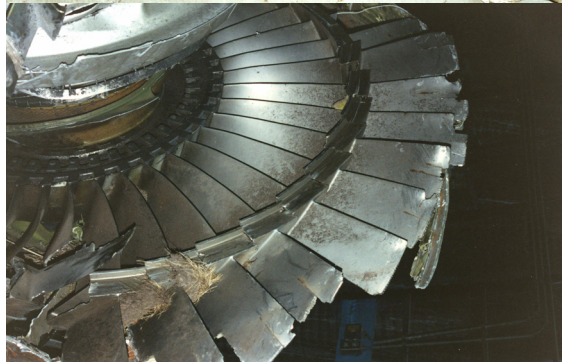
Lockheed C-5

Thrust Reverser Deployed During Takeoff



Lockheed C-5

Thrust Reverser Deployed During Takeoff



Lockheed C-5

Thrust Reverser Deja Vu - Pilot Error



Dover AFB 2006

Aloha Flight 243 - April 1988

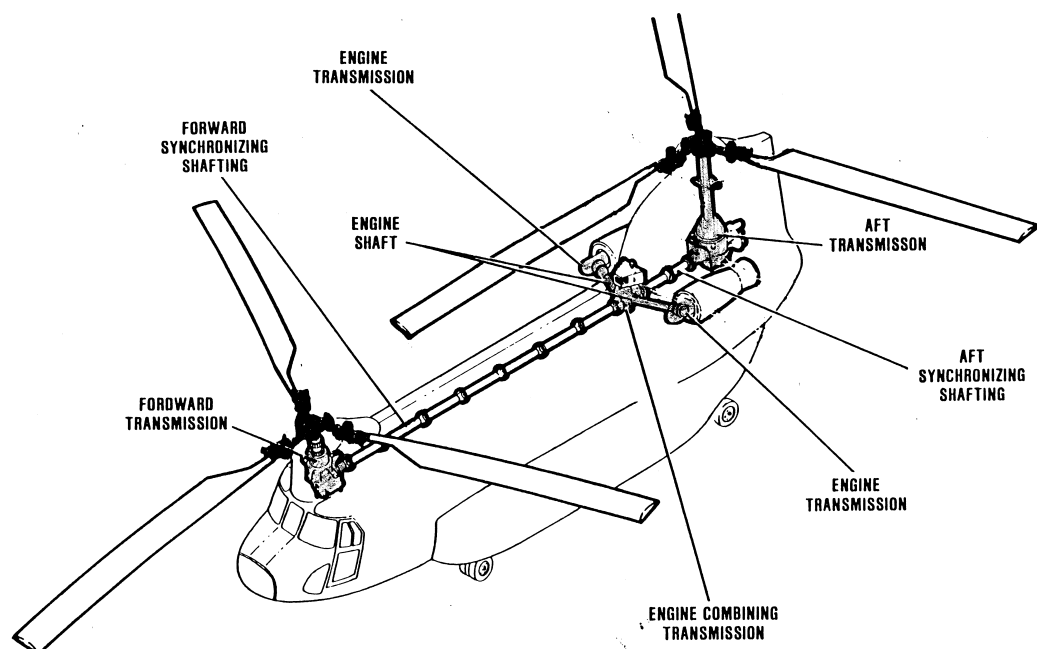
Boeing 737 - Corrosion Fatigue



ALOHA FLIGHT #243
KAHULUI, MAUI, HAWAII
NTSB PHOTOGRAPH

Boeing Chinook 1986 - North Sea Corrosion Fatigue - Spiral Bevel Ring Gear

DRIVE SYSTEM



Boeing Chinook

Corrosion Fatigue - Spiral Bevel Ring Gear



Boeing Chinook Forward Transmission

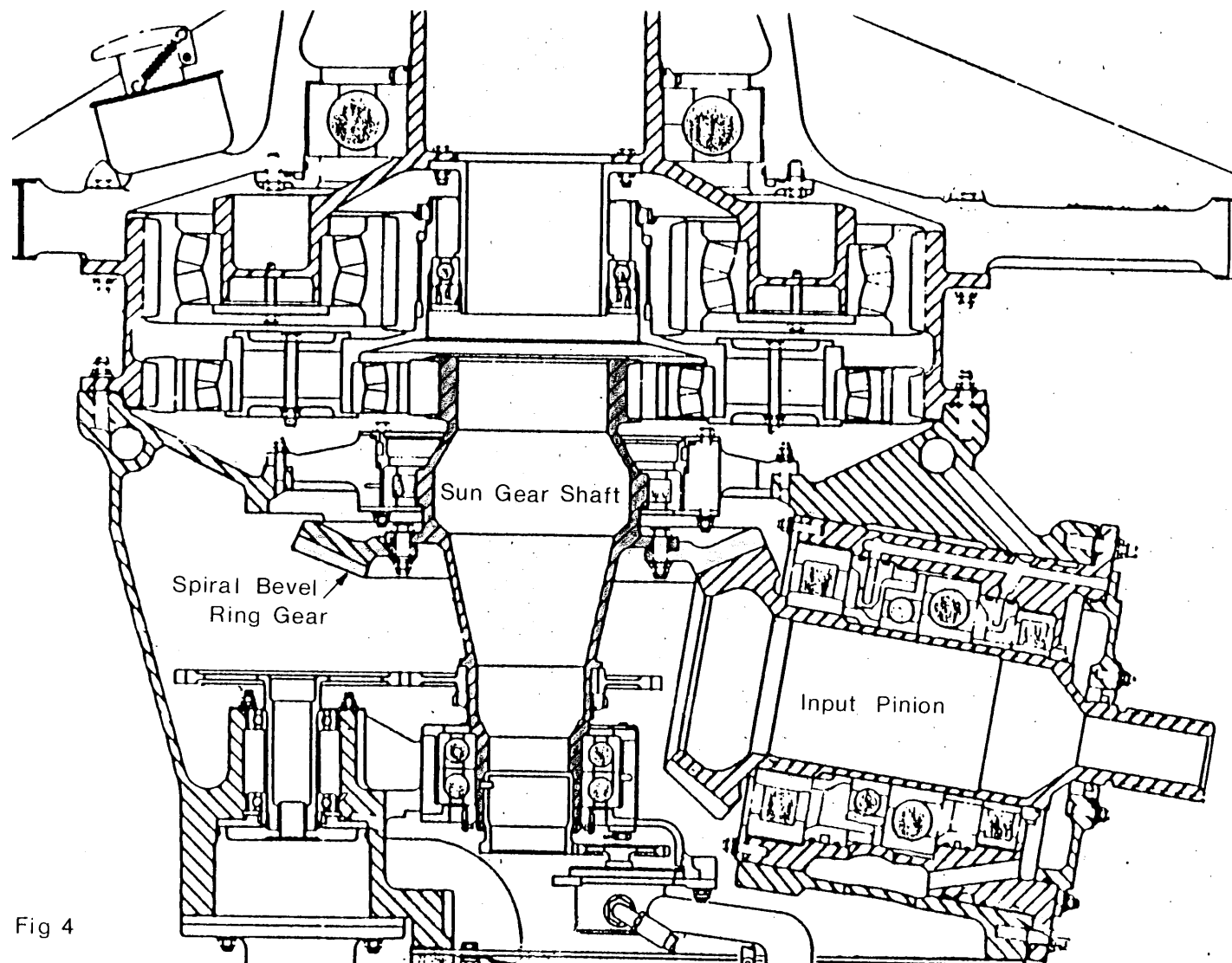
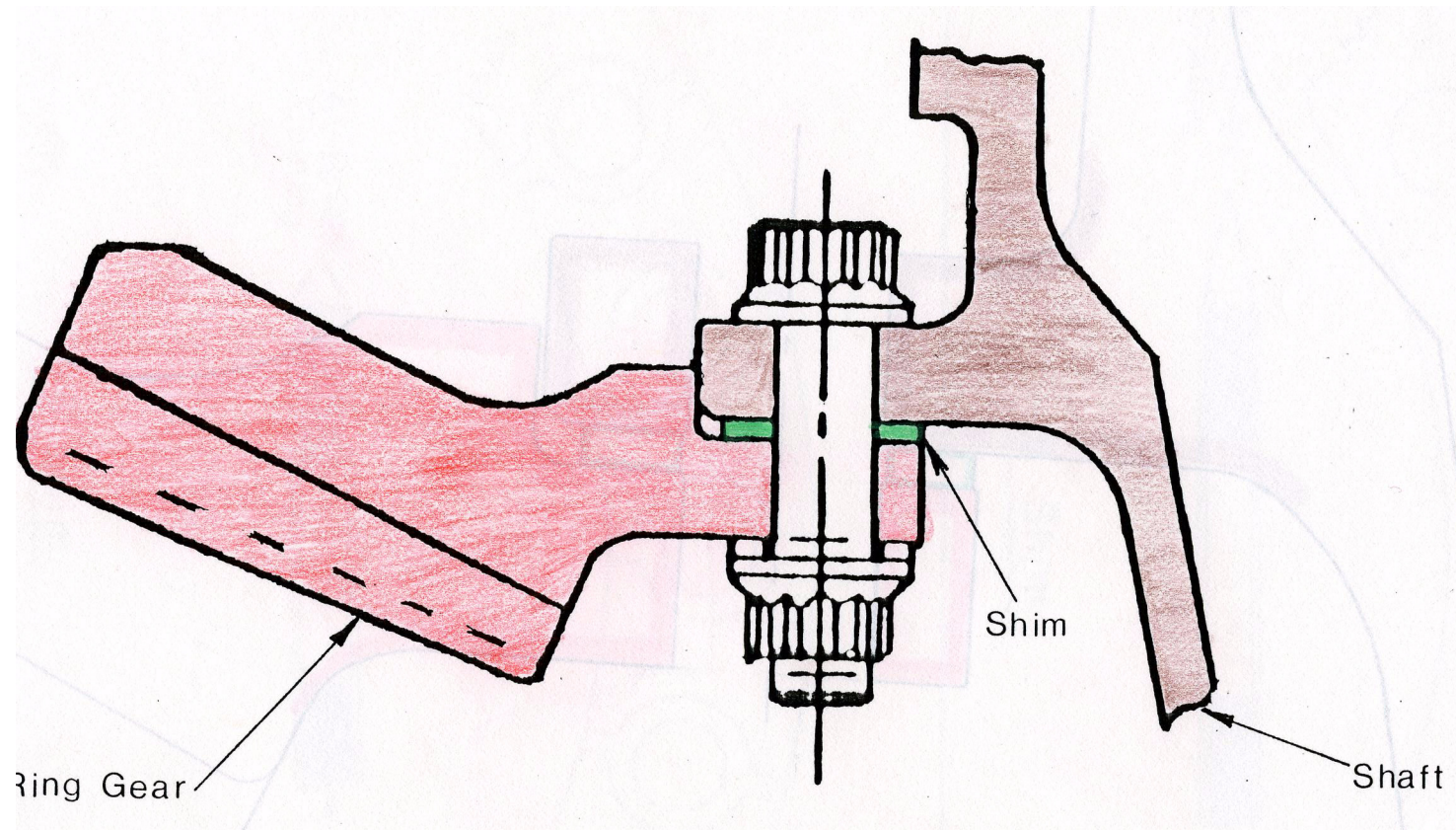


Fig 4



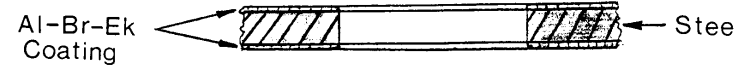
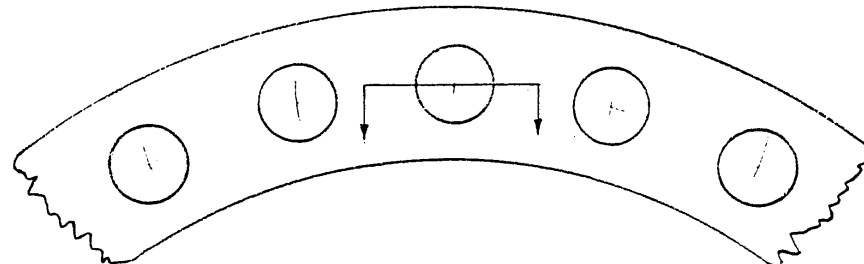
Boeing Chinook

Corrosion Fatigue - Spiral Bevel Ring Gear

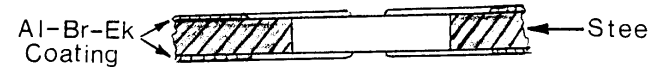
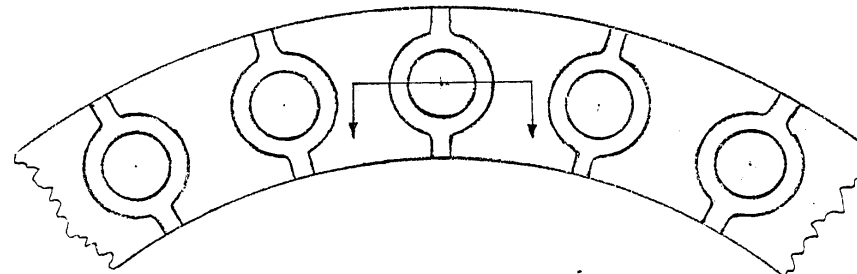


Boeing Chinook

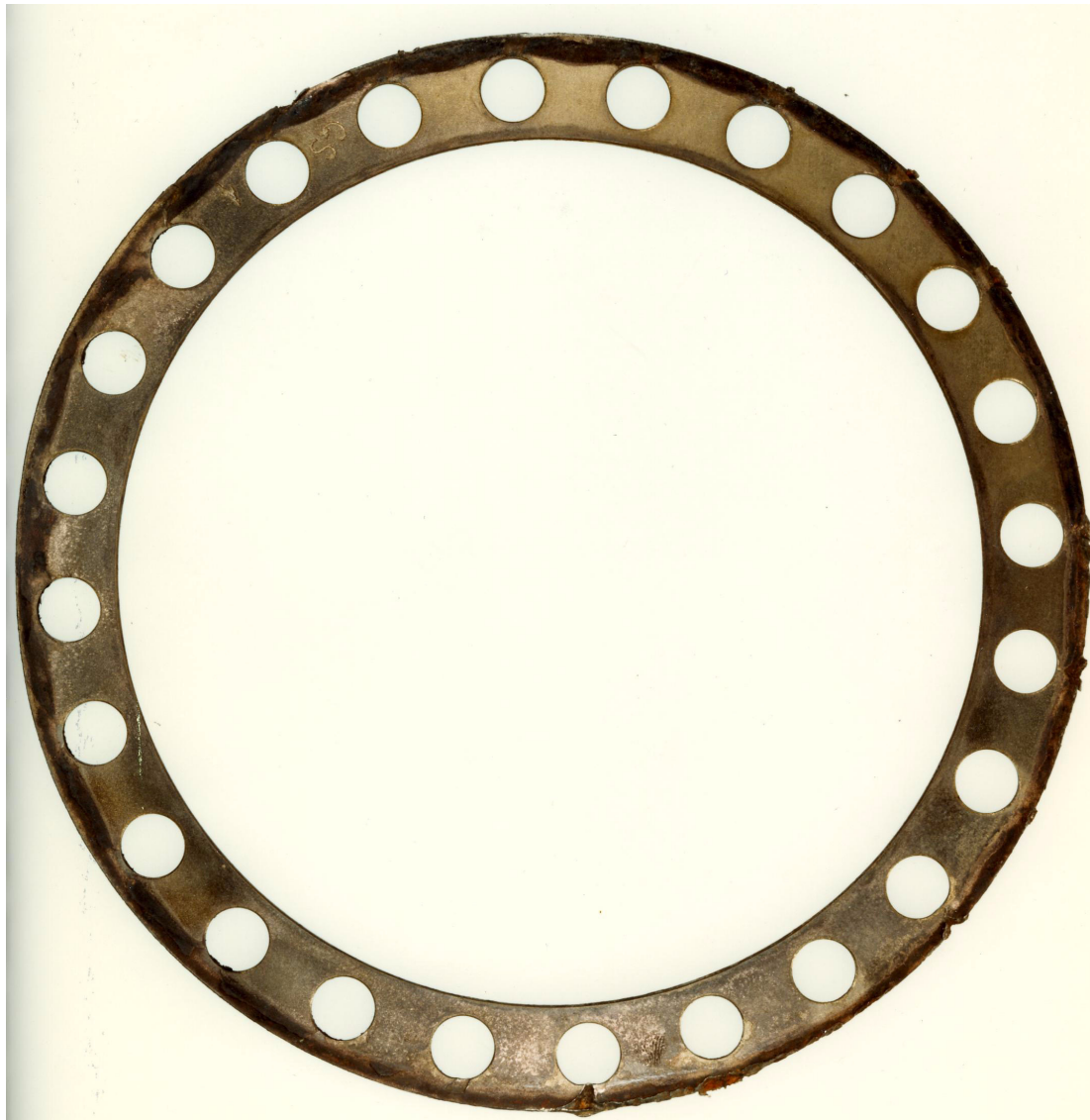
Spiral Bevel Ring Gear Shim Change



- 6 Shim



Boeing Chinook Spiral Bevel Ring Gear Shim



4.0 Airfoil Aerodynamics



4.1 Introduction

- Early studies of wing sections (airfoils) were largely empirical and proceeded by trial and error.
- Joukowski (1910) and Kutta (1911) obtained some theoretical solutions using complex variables, but not much progress was made until World War I, when Prandtl started a series of systematic studies in the Göttingen wind tunnel.
- Prandtl recognized that the airfoil (2D) and 3D wing problems could be studied separately.
- Thin airfoil theory as we know it today was started by Max Munk [2] in 1923, and further developed by Garrick (1926) [3] and Theodorsen (1931) [4], several years after Prandtl had completed his 3D wing theory [1] (1918).

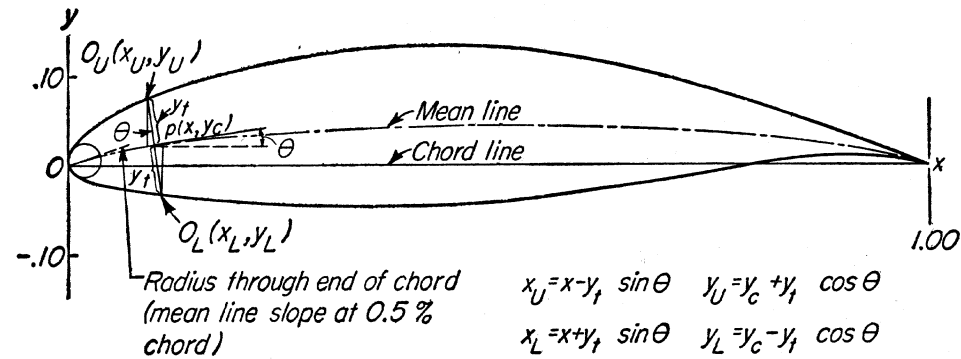


4.2 NACA Airfoil Sections

- Early wind tunnel studies at NACA's Langley Field concentrated on existing Göttingen and RAF sections and the successful Clark Y airfoil.
- Systematic studies of new airfoil shapes started in 1929, after the variable density tunnel at Langley became operational, and continued until about 1945.
- The results were published in a series of NACA reports [6-9], and the airfoils became known simply as *NACA Sections*, classified into “families.”
- The research at Langley extended earlier wind tunnel data obtained in the U.S. and Europe to higher Reynolds numbers, and also made detailed and systematic investigations of the individual effects of camber and thickness distributions.



NACA Airfoil Geometry



Sample calculations for derivation of the NACA 65,3-818 airfoil ($a = 1.0$)											
x	y_t^*	y_c^\dagger	$\tan \theta$	$\sin \theta$	$\cos \theta$	$y_t \sin \theta$	$y_t \cos \theta$	x_U	y_U	x_L	y_L
0	0	0	0	0	0	0	0	0
0.005	0.01324	0.00200	0.33696‡	0.31932	0.94765	0.00423	0.01255	0.00077	0.01455	0.00923	-0.01055
0.05	0.03831	0.01264	0.18744	0.18422	0.98288	0.00706	0.03765	0.04294	0.05029	0.05706	-0.02501
0.25	0.08093	0.03580	0.06996	0.06979	0.99756	0.00565	0.08073	0.24435	0.11653	0.25565	-0.04493
0.50	0.08593	0.04412	0	0	1.00000	0	0.08593	0.50000	0.13005	0.50000	-0.04181
0.75	0.04456	0.03580	-0.06998	-0.06979	0.99756	-0.00311	0.04445	0.75311	0.08025	0.74689	-0.00865
1.00	0	0	0	0	1.00000	0	1.00000	0

* Thickness distribution obtained from ordinates of the NACA 65,3-018 airfoil.

† Ordinates of the mean line, 0.8 of the ordinate for $c_{t_i} = 1.0$.

‡ Slope of radius through end of chord.

Fig. 4.1 NACA airfoil geometry definition and nomenclature. (From Ref. 10).

- All NACA sections use the same methodology and nomenclature for defining the airfoil camber and thickness, and defining the upper and lower airfoil surfaces by specifying the mean camber line $y_c(x)$ and thickness distribution $y_t(x)$.



Airfoil Coordinates

- For convenience, the slope $\theta(x) = dy_c/dx$ of the mean camber line is also given.
- The coordinates for the upper surface are then given by (see Fig. 4.1)

$$\begin{aligned}x_u &= x - y_t \sin \theta \\y_u &= y_c + y_t \cos \theta\end{aligned}\tag{4.1}$$

and on the lower surface by

$$\begin{aligned}x_l &= x + y_t \sin \theta \\y_l &= y_c - y_t \cos \theta\end{aligned}\tag{4.2}$$

- The center for the leading edge radius is set off along a straight line through the origin, with a slope = slope of the MCL at $x/c = 0.005$ (0.5% of chord), and the airfoil surfaces are blended smoothly with the LE circle.
- For cambered airfoil, this results in a small region of the LE radius extending to the left of $x = 0$.



a) Four-digit series (NACA Report No. 460, 1933)

- All airfoils of this family had the same basic thickness distribution, modeled after the efficient Göttingen 398 and Clark Y airfoils (after removing the camber).
- The thickness distribution is given by the following formula [10]:

$$\pm y_t(x) = \frac{t}{0.20} \{ 0.2969 \sqrt{x} - 0.1260x - 0.3516x^2 + 0.2843x^3 - 0.1015x^4 \} \quad (4.3)$$

where t is the maximum thickness, as a fraction of the chord, and x is also nondimensionalized with respect to the chord c .

- The leading edge radius is

$$r = 1.1019t^2 \quad (4.4)$$

- The mean camber line is defined analytically by two parabolic arcs tangent at the position of maximum camber, $y_c(x)_{max}$:



$$y_c(x) = \frac{m}{p^2}(2px - x^2); \quad x \leq p \quad (4.5)$$

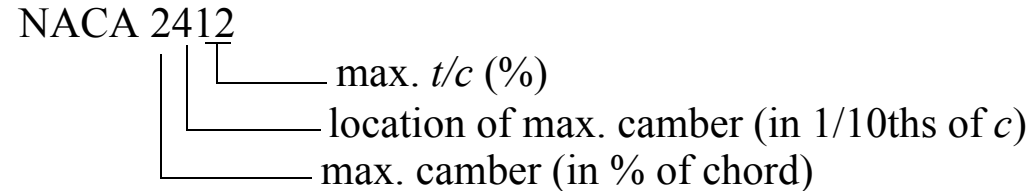
$$y_c(x) = \frac{m}{(1-p)^2}[(1-2p) + 2px - x^2]; \quad x \geq p$$

where

$$\begin{aligned} m &= y_{c_{max}} = \text{max. camber} \\ p &= \text{chordwise location of max. camber} \end{aligned} \quad (4.6)$$

both expressed in fraction of chord c .

- The numbering system is explained in the example below:



- Thus, the NACA 2412 is a 12% thick airfoil with 2% camber ($m = y_{c_{max}} = 0.02$), with the chordwise location of maximum camber at $x = p = 0.4$ (40% of chord).
- The airfoil and its aerodynamic characteristics are shown in Fig. 4.2.



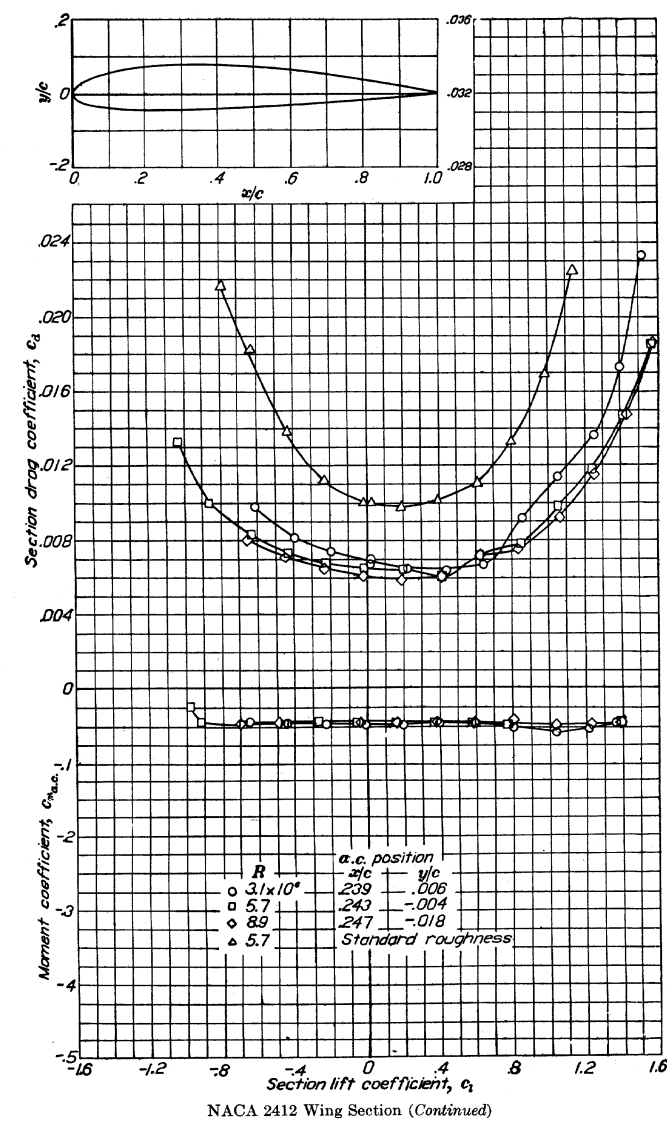
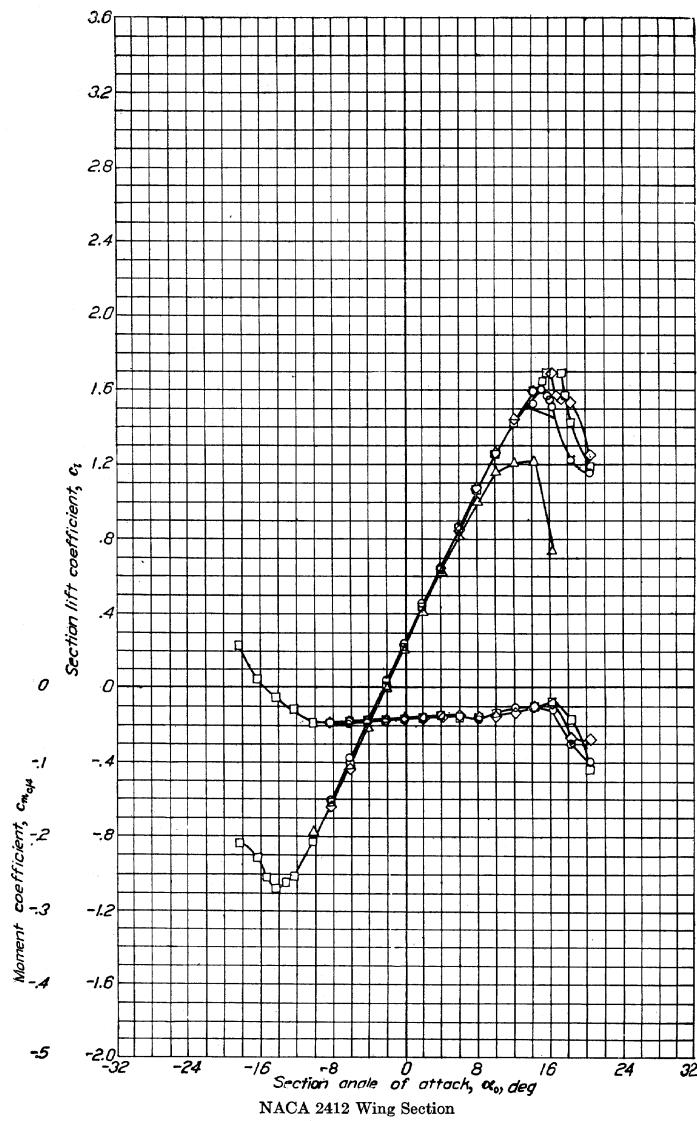
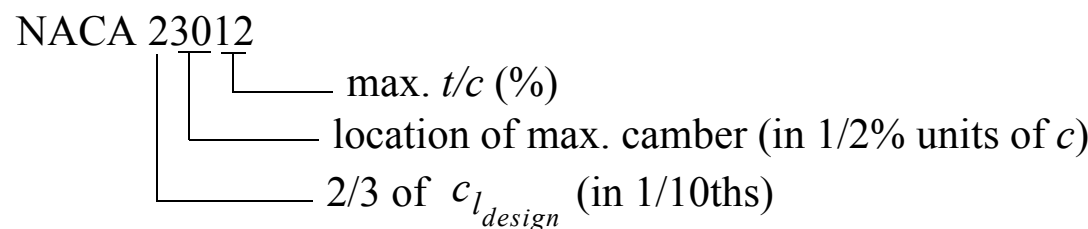


Fig. 4.2 The NACA 2412 airfoil section.



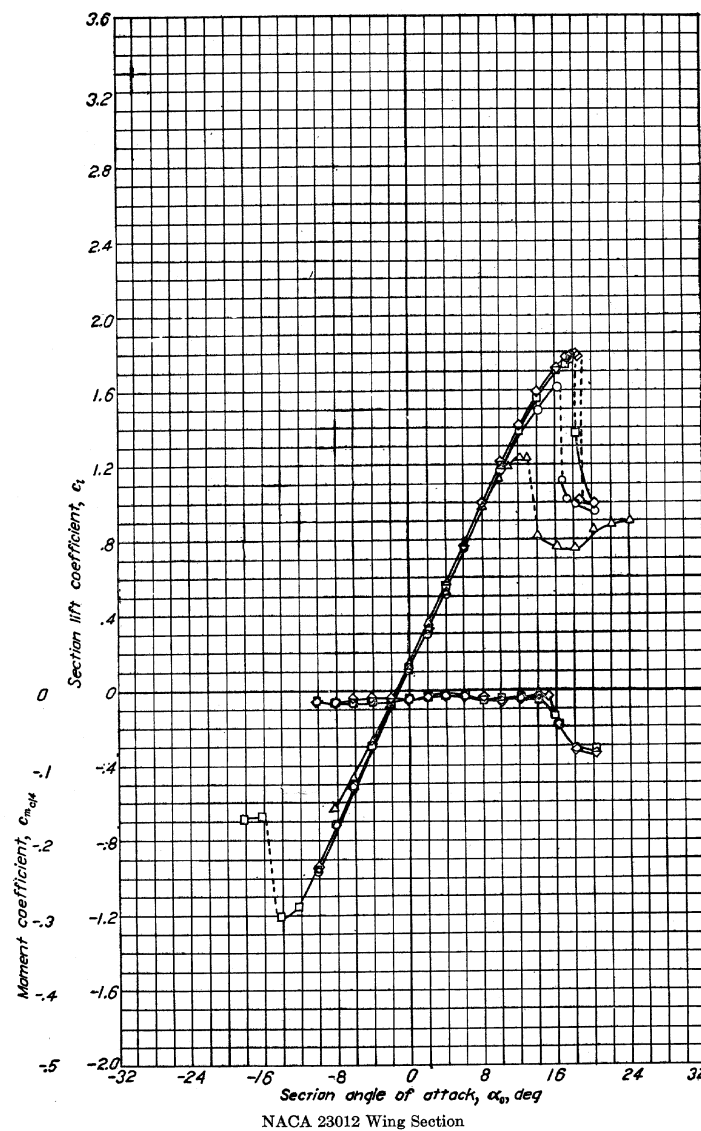
b) Five-digit series (NACA Reports No. 537 and 610)

- All airfoils of this family had the same basic thickness distribution as was used in the four-digit series, Eq. 4.1.
- A new mean camber line was defined, which allowed the position of maximum camber to be moved far forward on the airfoil, in an attempt to increase the maximum lift coefficient.
- The numbering system is explained in the example below:



- Thus, the NACA 23012 is a 12% thick airfoil with a design lift coefficient of $(3/2)(2/10) = 0.3$, with the chordwise location of maximum camber at 15% of chord.
- The airfoil and its aerodynamic characteristics are shown in Fig. 4.3.





NACA 23012 Wing Section

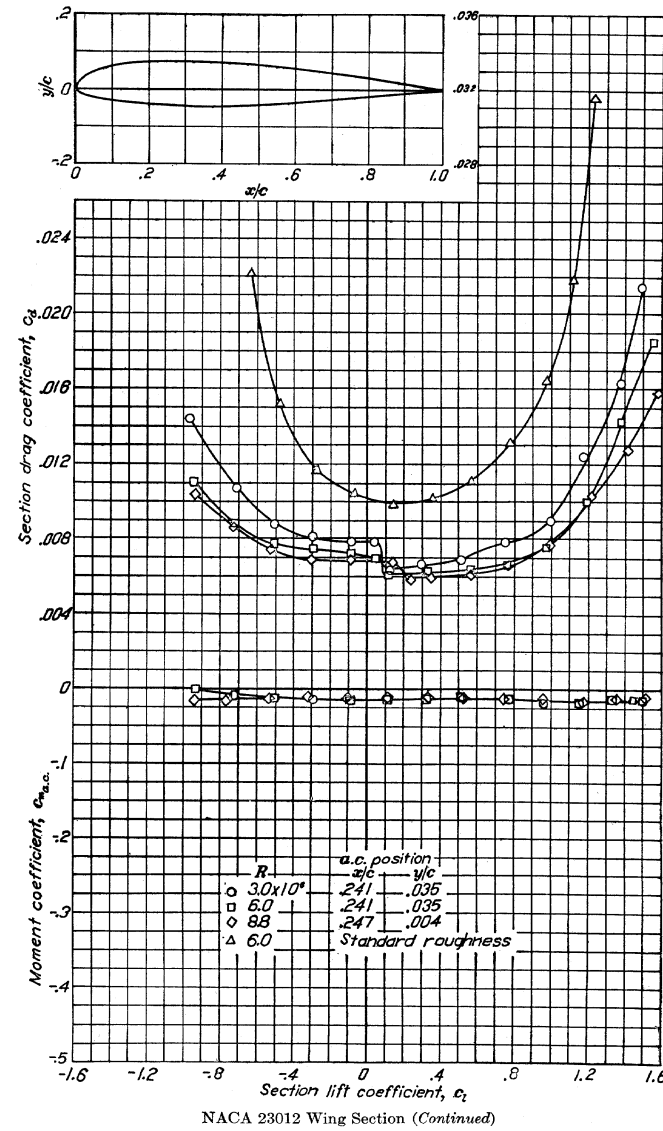
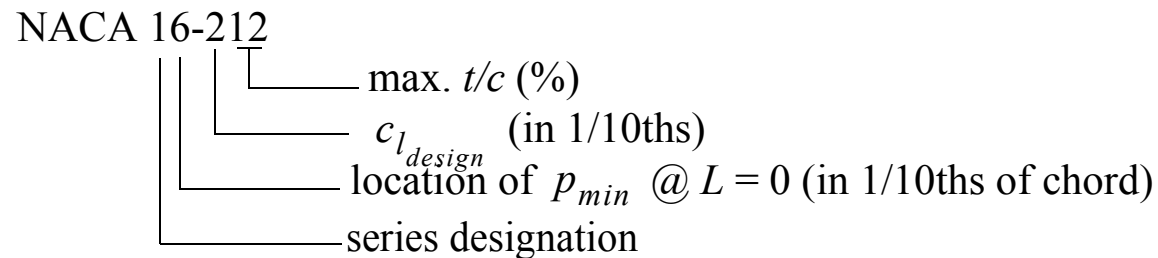


Fig. 4.3 The NACA 23012 airfoil section.



c) One-series (16-series)

- These airfoils represented the first attempt at producing sections with a desired pressure loading, with low drag and a high critical Mach number.
- This was accomplished through empirical modifications of the thickness distribution, using a trial and error approach.
- The mean camber line is of the “uniform load” type, making these sections suitable for propeller blades.
- The numbering system is explained in the example below:

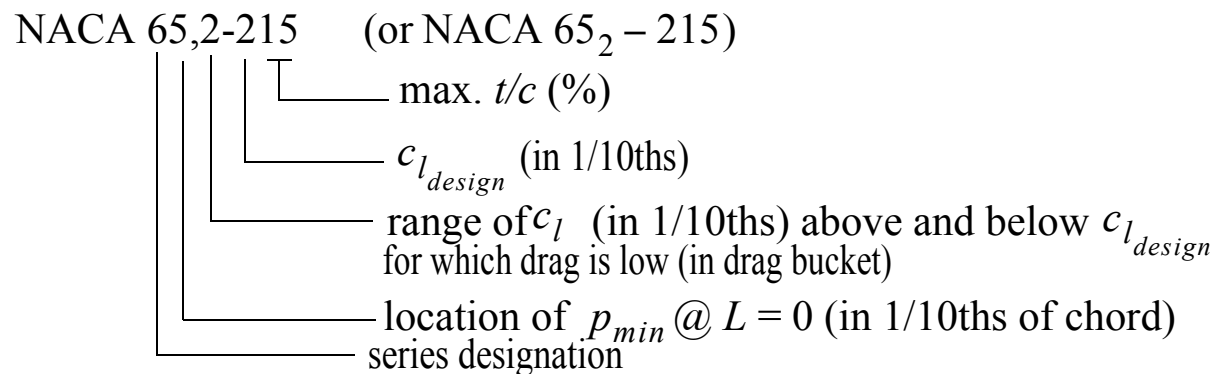


- Thus, the NACA 16-212 is a 12% thick airfoil with a design lift coefficient of 0.2, with the chordwise location of minimum pressure at 60% of chord, at zero lift.



d) Six-series (NACA Report No. 834, 1945)

- The 6-series was the first of the NACA families of airfoils that was designed based on aerodynamic theory, with the specific objective of obtaining airfoils with *low drag, high critical Mach number, and high maximum lift coefficient*.
- Low drag was achieved by obtaining laminar flow over a significant fraction of the airfoil surface (*NACA laminar flow sections*).
- The numbering system is explained in the example below:



- Thus, the NACA 65₂-215 is a 15% thick airfoil with a design lift coefficient of 0.2, with the chordwise location of minimum pressure at 50% of chord, at zero lift, and with low drag for a range of lift coefficients from 0.0 to +0.4.



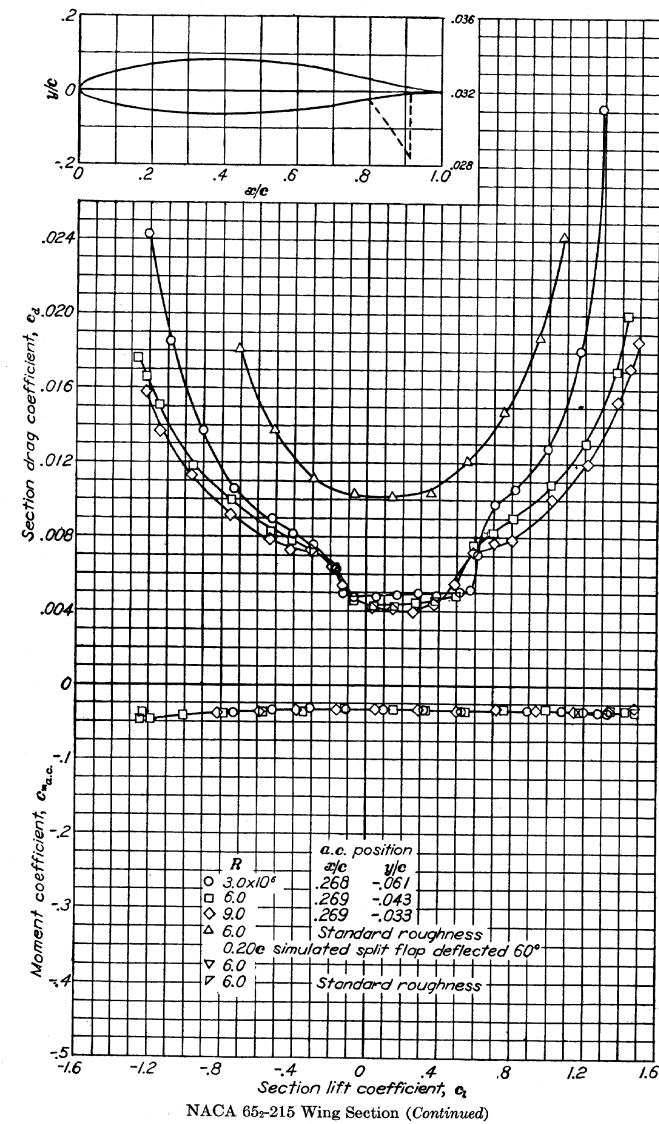
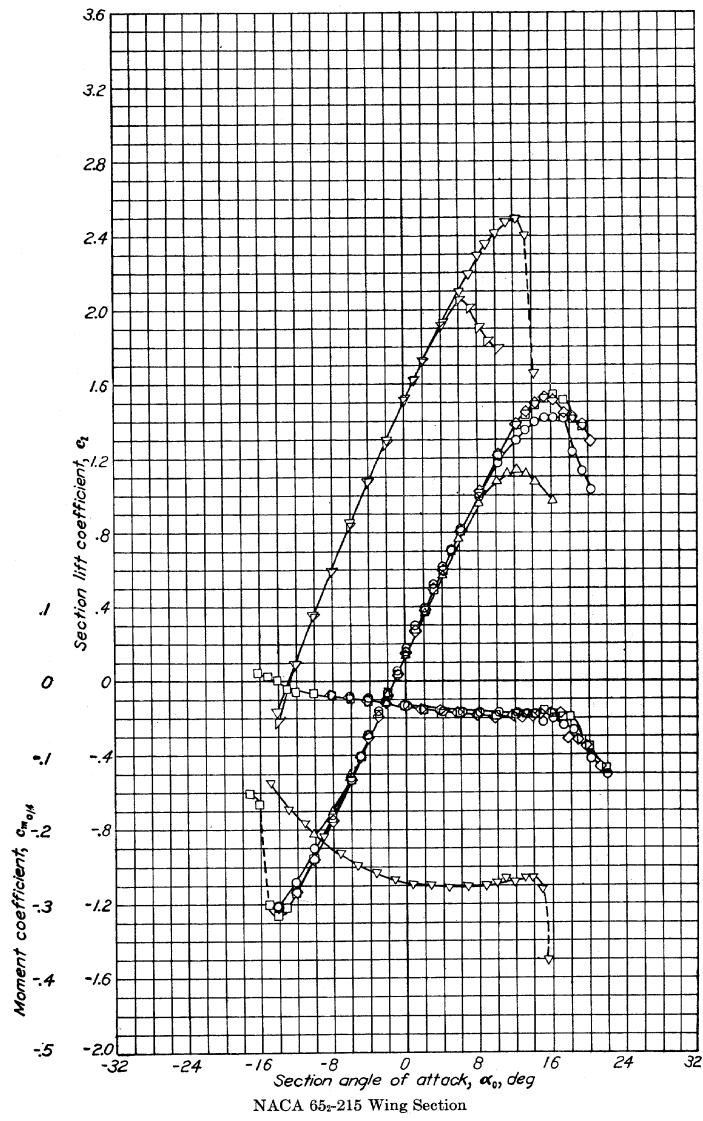


Fig. 4.4 The NACA 65₂ – 215 airfoil section.

Later Designations

- The later 6-series airfoils are designated using the *subscript notation*, and have slightly different thickness distributions than the earlier sections using the comma notation; see the comment in Ref. 10.
- In cases where the airfoil thickness was scaled (linearly) from an airfoil of a different thickness, the following notation was used:

NACA 65(318)-217 or NACA 65₍₃₁₈₎-217

- All numbers *except* those inside the parentheses have the same meaning as before.
- The first number in the parentheses is the range of lift coefficients for which the drag is low.
- The last two digits denote the thickness in percent of chord of the airfoil from which the thickness distribution was obtained by linear scaling of the ordinate.
- For wing sections of thickness less than 12%, the low-drag range is less than 0.1 and the first digit is typically dropped, and one would write NACA 65₍₁₀₎-211.



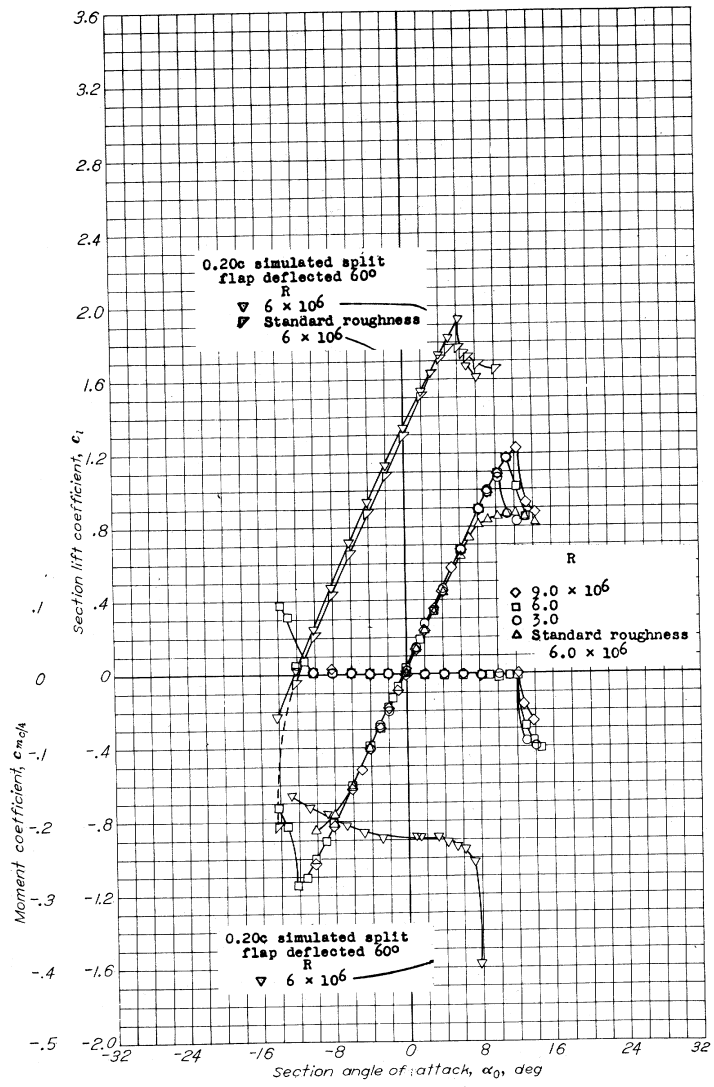
Mean Line Designation

- The letter “ a ” is used to indicate what type of mean line is used; e.g. $a = 0.5$. If no a is listed, it means that $a = 1.0$ (uniform load mean line).
- If a capital letter appears in the designation instead of the dash, e.g.,
NACA 64A010
it means that it is a modified 6-series section.
- Sections with the letter A in this position have essentially straight upper and lower surfaces from about 80% of chord and to the trailing edge.

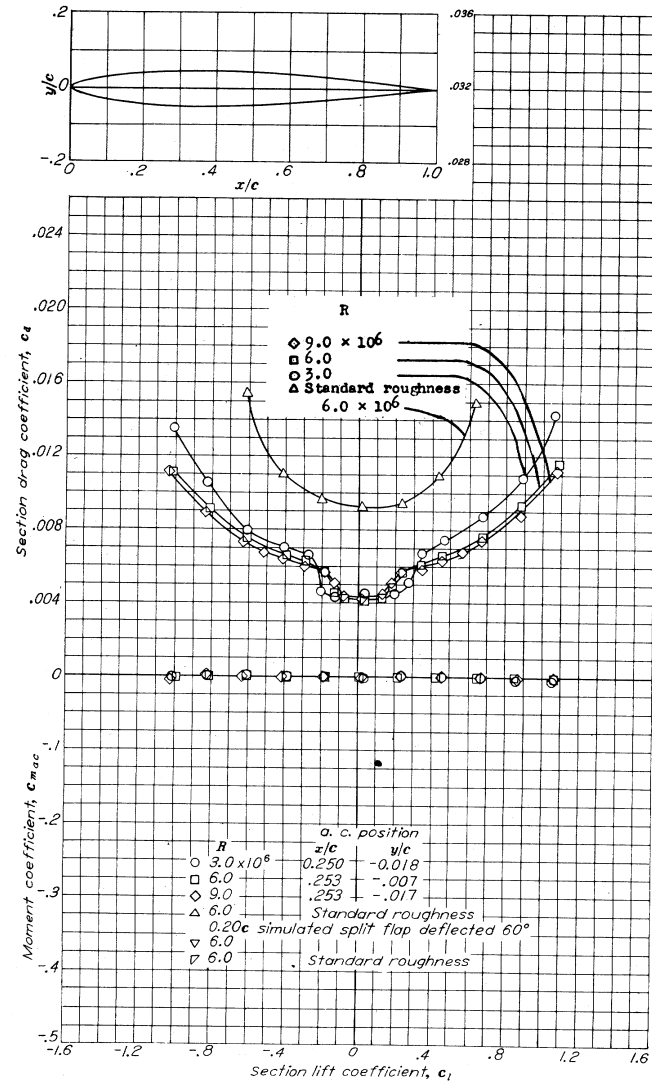
e) Seven-series

- These are also laminar flow sections. For further details, see Ref. 10.





NACA 64A010 Wing Section



NACA 64A010 Wing Section (Continued)

Fig. 4.5 The NACA 64A010 airfoil section.

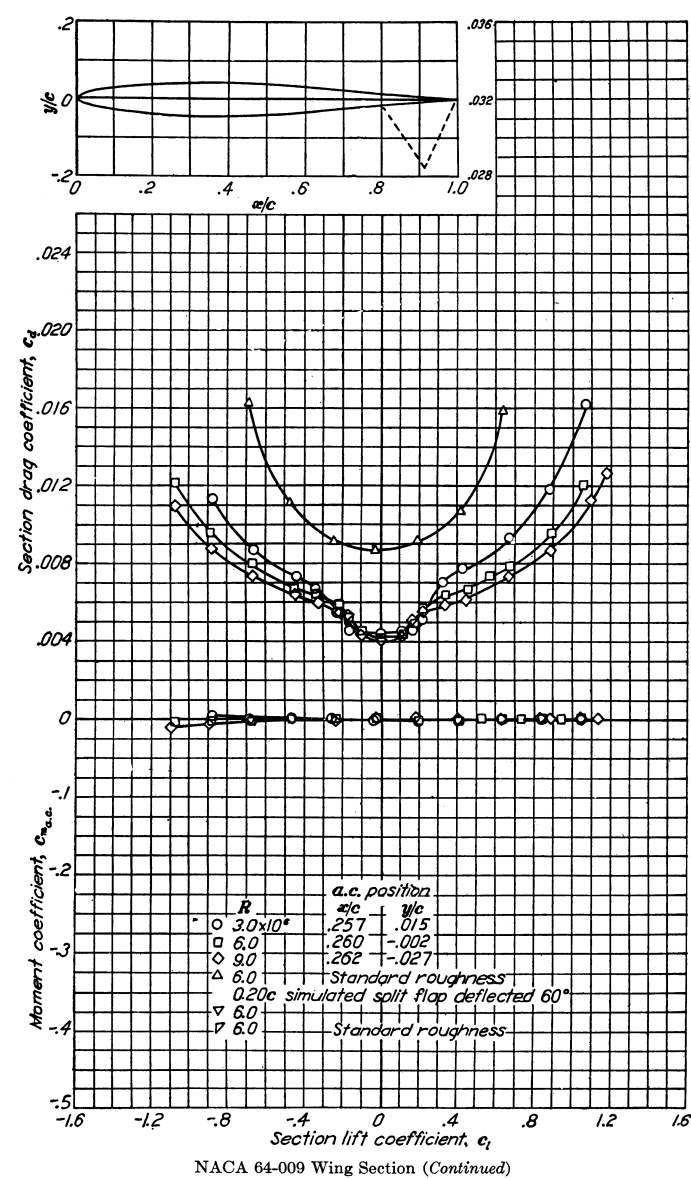
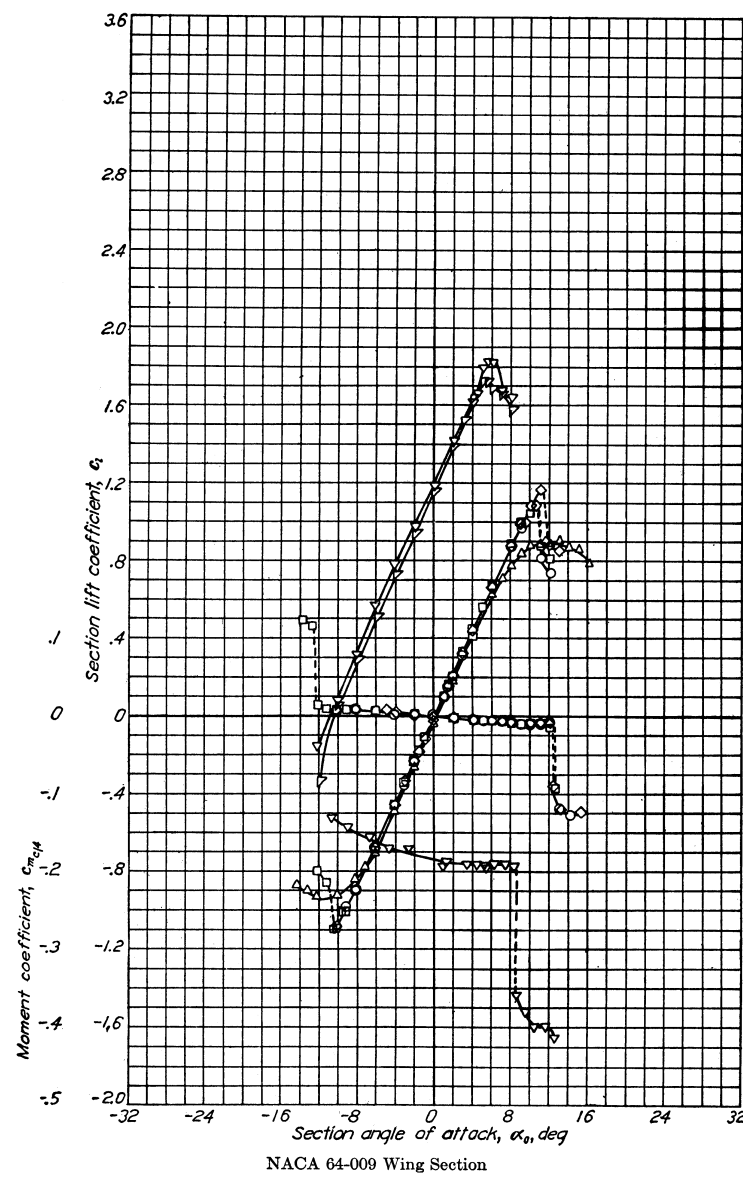
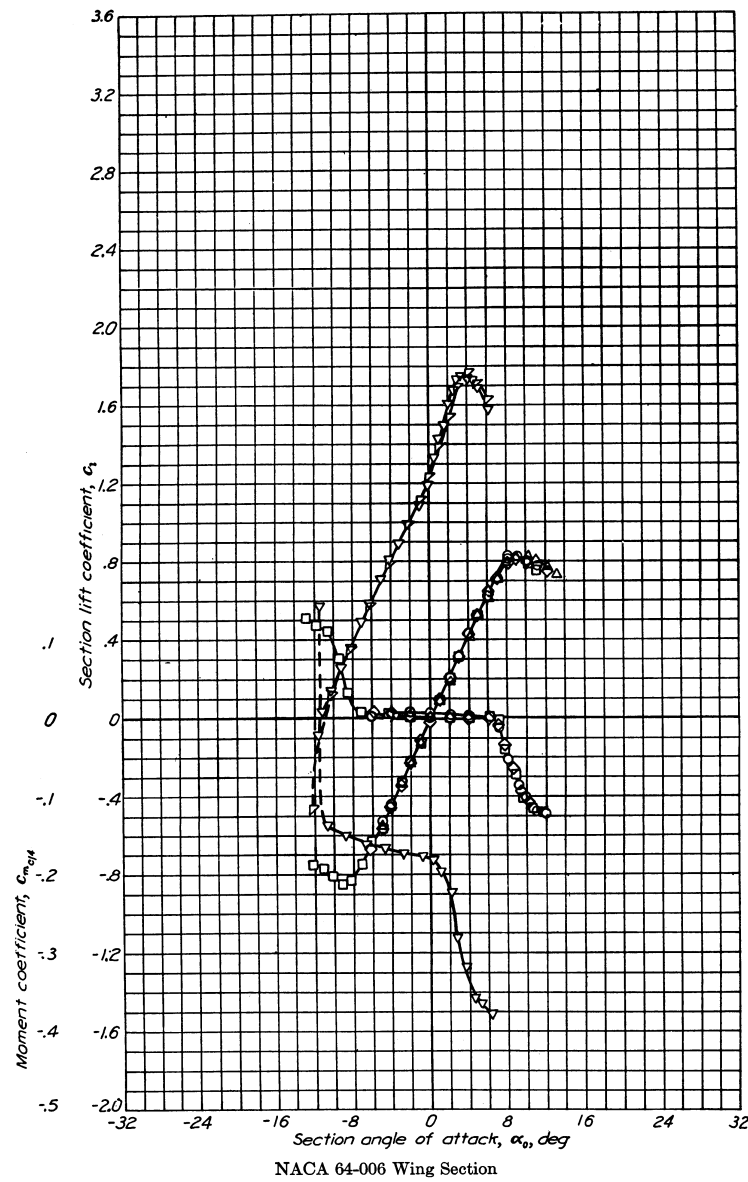
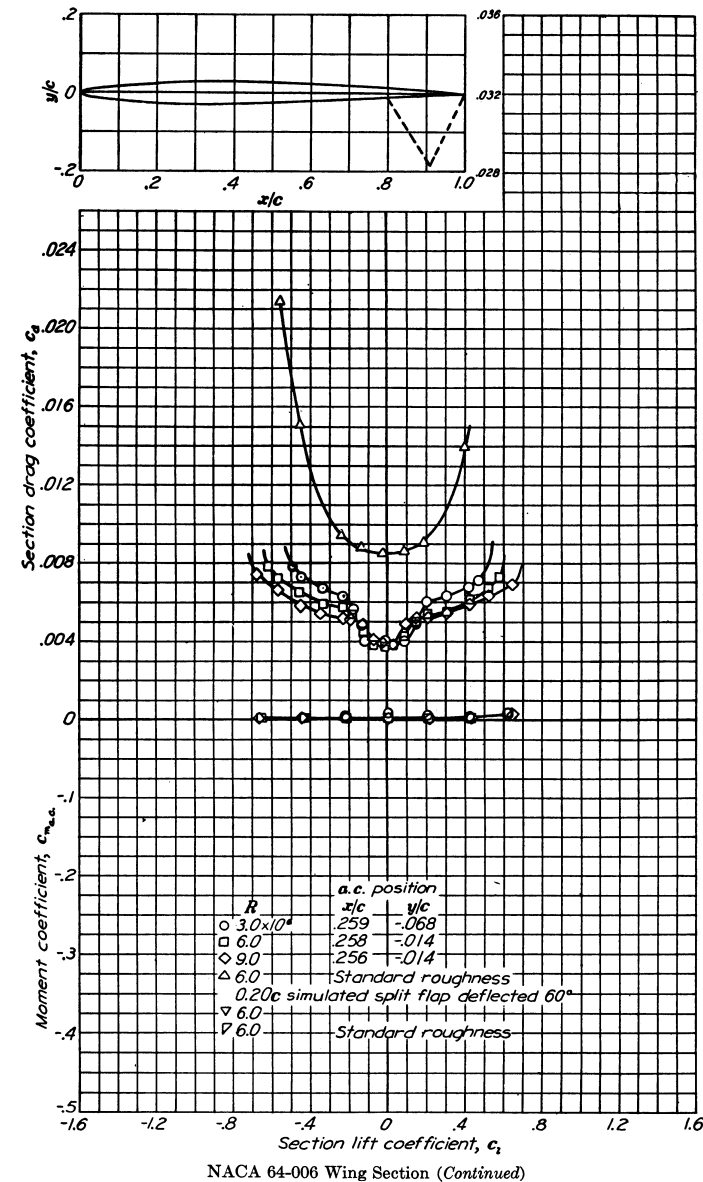


Fig. 4.6 The NACA 64-009 airfoil section.



NACA 64-006 Wing Section



NACA 64-006 Wing Section (Continued)

Fig. 4.7 The NACA 64-006 airfoil section.

4.3 Effect of Reynolds Number, Airfoil Thickness, and Surface Roughness

- Viscosity affects the flow over airfoils and wings through three main mechanisms:
 1. *Boundary layer transition - laminar to turbulent* (mainly a function of pressure gradients and surface curvature, but also of surface roughness)
 2. *Boundary layer separation* (stall characteristics)
 3. *Boundary layer - shock wave interactions* (transonic flows; drag increase, etc.)
- These effects will be discussed in more detail later.



4.3.1 Effect of Reynolds Number and Airfoil Thickness on Maximum Lift

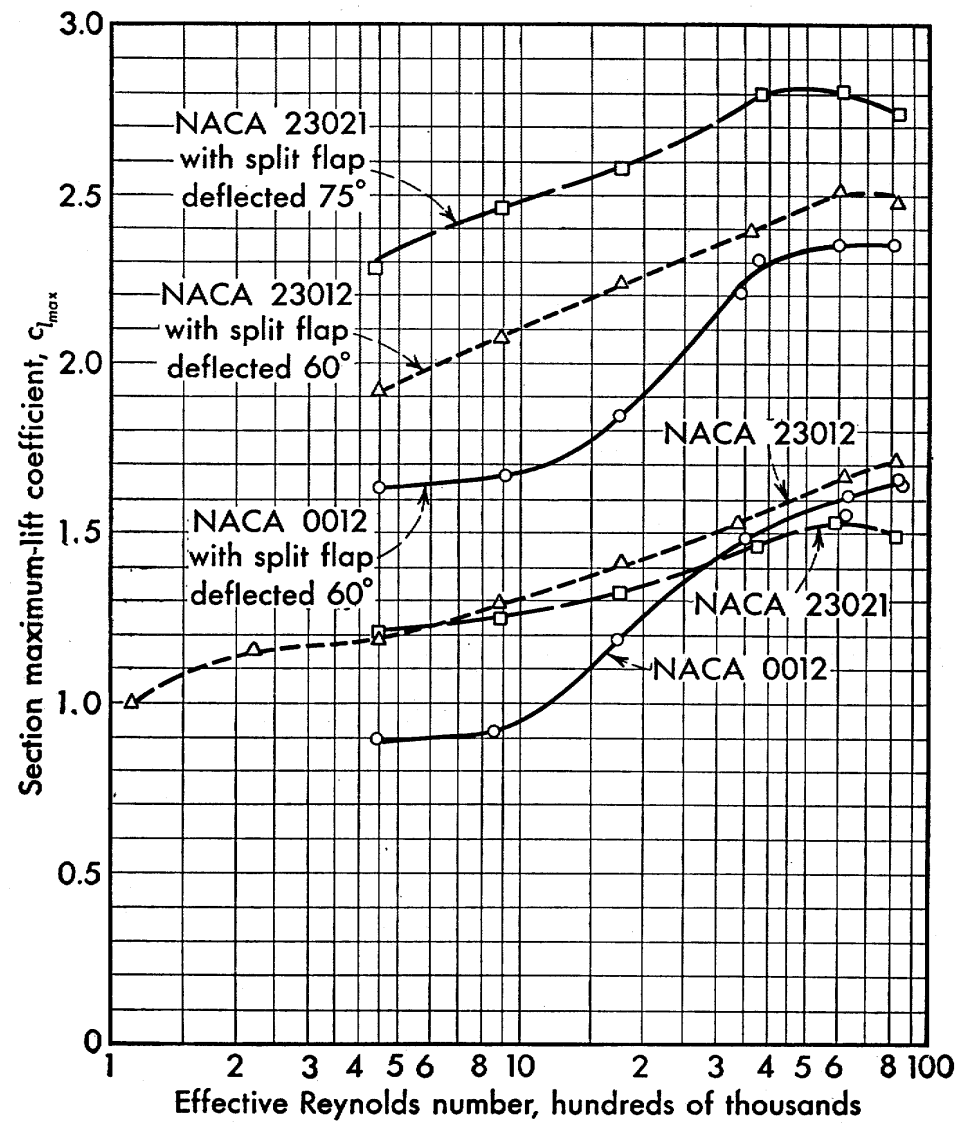


Fig. 4.8 Variation of maximum lift coefficient with Reynolds number for different NACA airfoil sections. (From Ref. 12).



Effect of Thickness

- Note that for the higher Reynolds numbers, a definite maximum of $c_{l_{max}}$ is observed around $t/c \approx 0.12$.

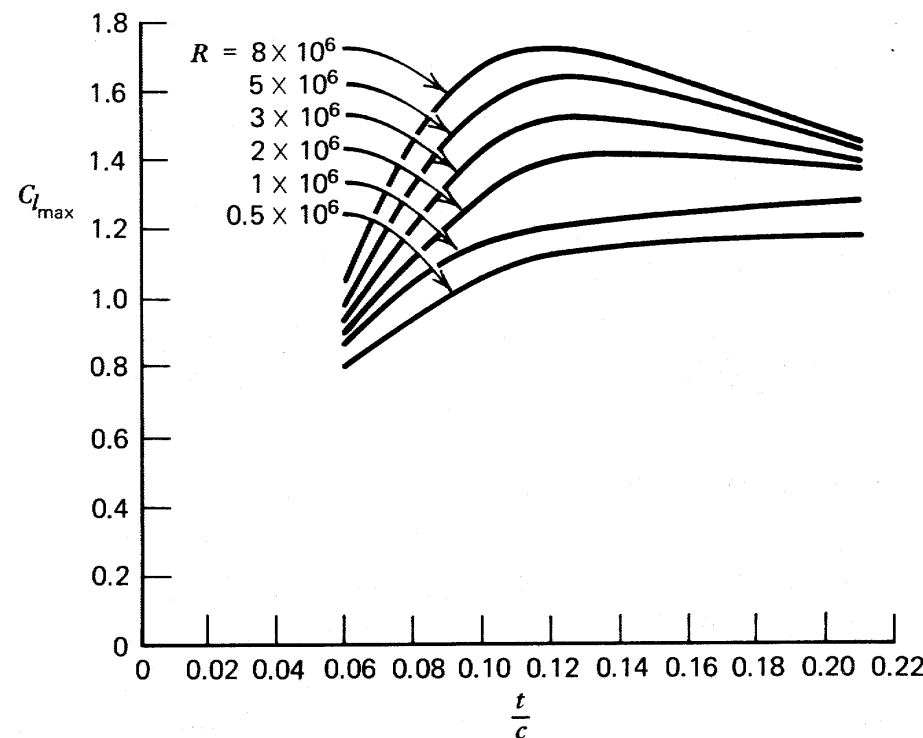


Fig. 4.9 Dependence of maximum lift coefficient on thickness to chord ratio for the NACA 24xx series of airfoils for representative Reynolds numbers. (From Ref. 13).



4.3.2 Effect of Reynolds Number on Drag

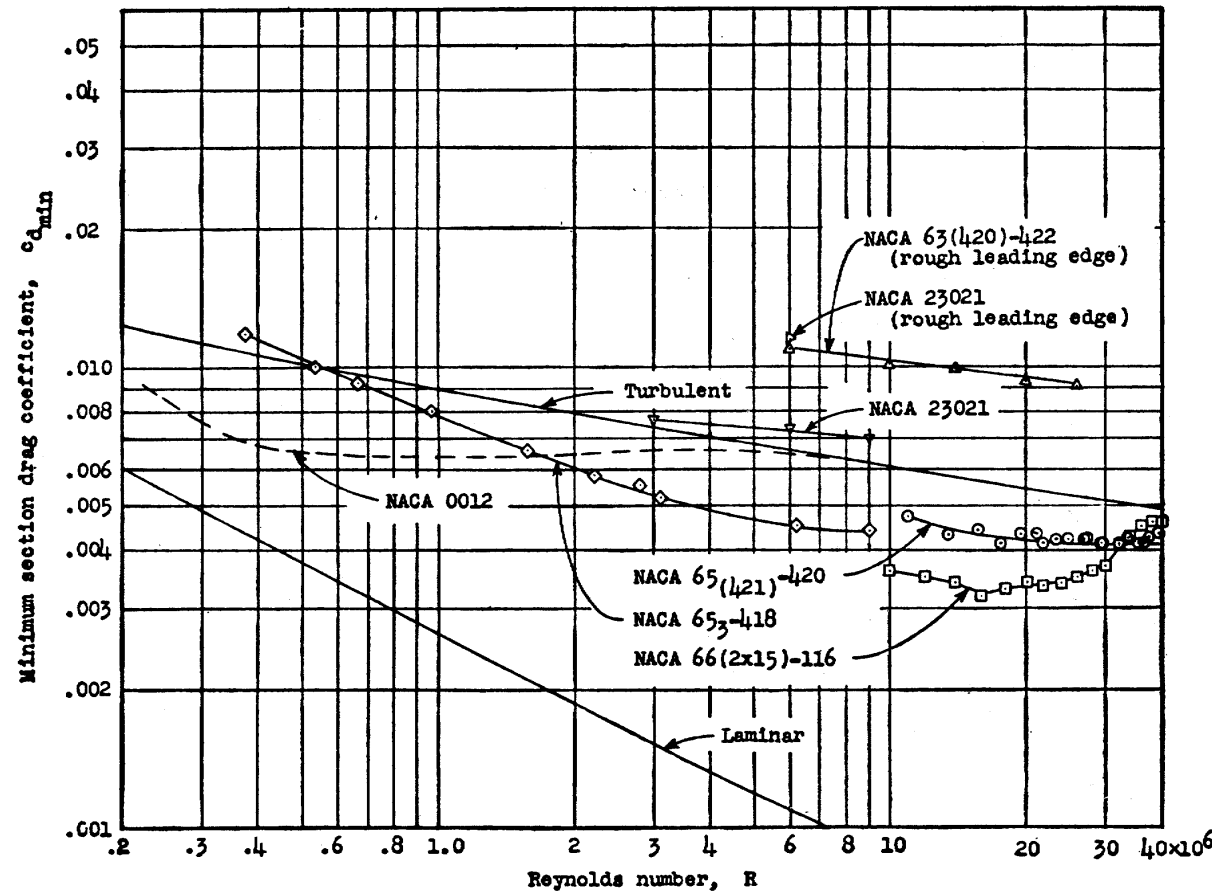


Fig. 4.10 Variation of minimum section drag coefficient with Reynolds number for several NACA sections, and the corresponding laminar and turbulent skin friction coefficients for a flat plate with both sides exposed to the flow. (From Ref. 10).

Observations

- For Reynolds numbers up to about 20 million, the section drag coefficients decrease with increasing Reynolds number.
- Above this Reynolds number the drag coefficient of the NACA $65_{(421)} - 420$ airfoil remains essentially constant up to $R_e \approx 40 \times 10^6$.
- The higher drag coefficient of the laminar flow NACA $65_3 - 418$ airfoil at low Reynolds numbers, compared to the four-digit NACA 0012 airfoil, is caused by a large region of laminar separation downstream of the point of minimum pressure.
- *Low Reynolds number wind tunnel test data should be interpreted with caution*, since it may not give a correct relative merit of various airfoils at actual flight Reynolds numbers.



4.3.3 Effect of Surface Roughness on Drag

- “Standard roughness” consisted of 0.011-inch carborundum grains applied to the airfoil surface at the leading edge, over 8% of chord on both the upper and lower surface, thinly spread over 5 to 10% of this area.

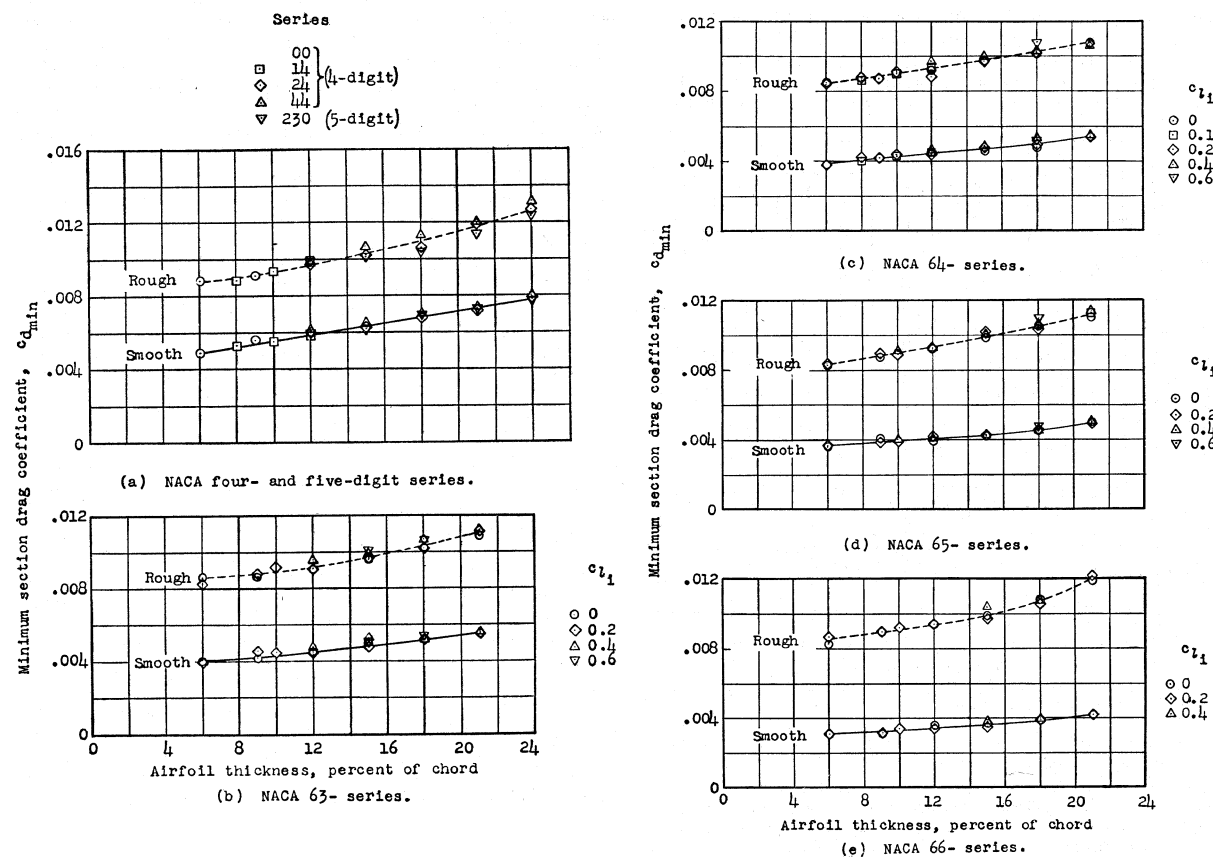


Fig. 4.11 Effect of surface roughness on parasite drag of wing sections. (From Ref. 10).



Sensitivity with Increasing Reynolds Number

- Painting a model with camouflage lacquer introduced sufficient roughness to trigger transition at a Reynolds number of 20 million and a doubling of the drag.
- It is not surprising that laminar flow over practical wings is such an elusive goal.

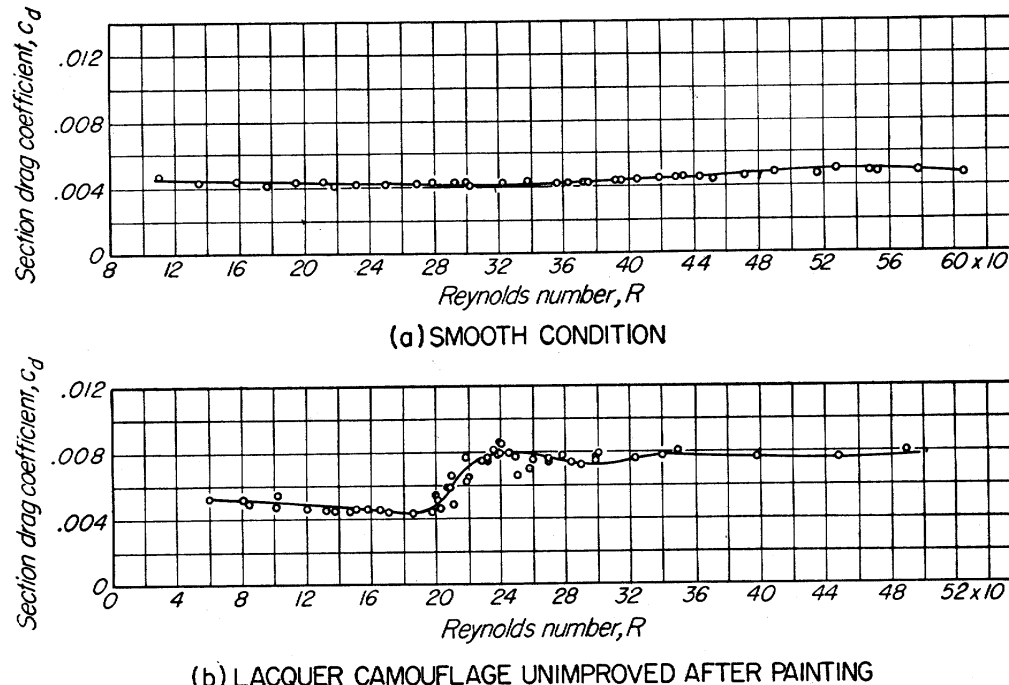


Fig. 4.12 Variation of drag coefficient with Reynolds number for a 60-inch chord NACA 65₍₄₂₁₎-420 airfoil for two surface conditions. (From Ref. 10).



4.4 Thin Airfoil Theory and Design

Superposition Principle

- In the case of a thin wing section or airfoil operating at small angles of attack, the surface of the airfoil can be approximated as follows:

$$z \approx z_c(x) - x\alpha \pm z_t(x) = z_a \pm z_t \quad (4.7)$$

by considering the contribution from *camber*, *angle of attack*, and *thickness*.

- The problem can then be solved by considering the *symmetric (thickness) problem* and the *antisymmetric (lift) problem* separately.

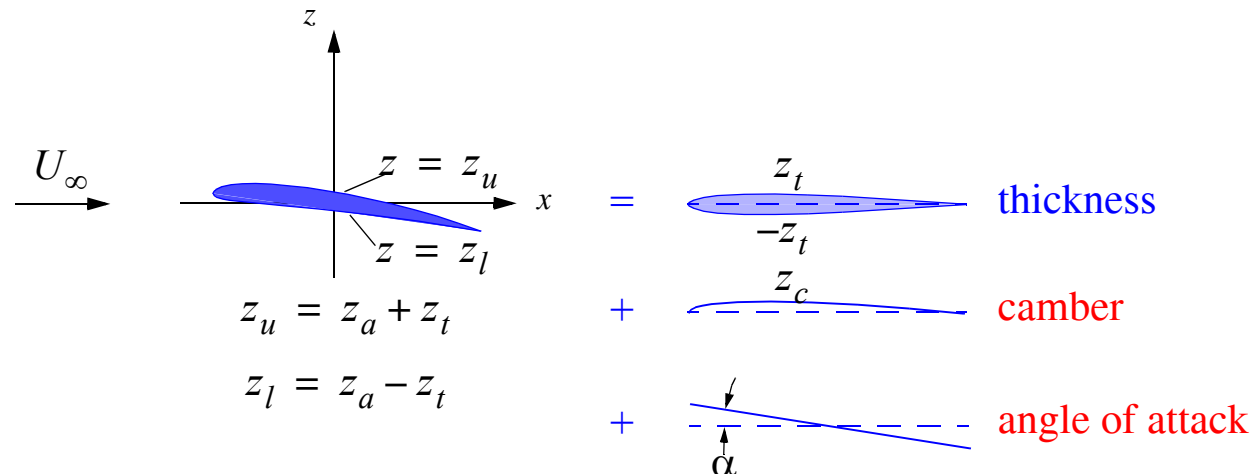


Fig. 4.13 The superposition principle applied to flows over a thin wing section.

a) Symmetric (thickness) problem

- In this case, the flow perturbation velocity in the z -direction is *antisymmetric* in z , which means that the potential and the pressure must be symmetric in z :

$$\begin{aligned} w &= \frac{\partial \phi}{\partial z} \quad \text{is antisymmetric in } z \\ w|_{z=0} &= 0 \\ \phi, p &\quad \text{are symmetric in } z \Rightarrow \text{zero lift} \end{aligned} \tag{4.8}$$

- Because the pressure on the upper and lower surfaces must be identical (symmetry), no lift is produced.
- In transonic flow, aerodynamic nonlinearities void the superposition principle
 - Thickness, camber and angle of attack effects become coupled
 - Must be considered together in overall nonlinear CFD solution



b) Antisymmetric (lifting) problem

- The antisymmetric problem involves a zero thickness camber profile and a flat plate at an angle of attack.
- In both cases the flow perturbation velocity component w in the z -direction is continuous and symmetric in z :

$$\begin{aligned} w &= \frac{\partial \phi}{\partial z} && \text{is symmetric in } z \\ w|_{z=0} & && \text{is continuous} \\ \phi, p & && \text{are antisymmetric in } z \end{aligned} \tag{4.9}$$

- The pressure jump across the airfoil surface becomes

$$\Delta p(x, t) = -[p] = p_l - p_u = -\rho_\infty \left(\frac{\partial \Delta \phi}{\partial t} + U_\infty \frac{\partial \Delta \phi}{\partial x} \right) \tag{4.10}$$

where $\Delta(\) = -[\]$ denotes the jump from the lower to the upper surface.



Lifting Solution

- The corresponding boundary value problem to be solved is, in terms of the velocity potential φ ,

$$\nabla^2 \varphi = 0 \quad (4.11)$$

$$\left. \frac{\partial \varphi}{\partial z} \right|_{z=0} \equiv w_a = U_\infty \frac{\partial z_a}{\partial x} \quad (4.12)$$

- In addition, the Kutta-Joukowski condition at the trailing edge must be satisfied, $\Delta p|_{TE} = 0$, which for a sharp trailing edge is equivalent to requiring finite velocities and pressure at the trailing edge.

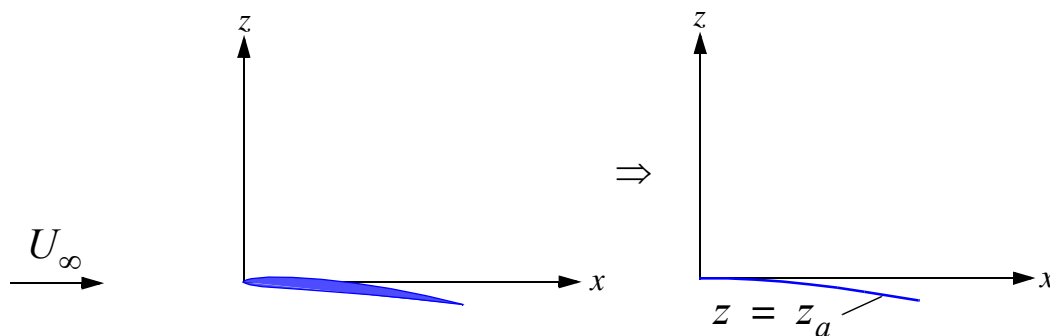


Fig. 4.14 Lifting problem for 2D incompressible flow.

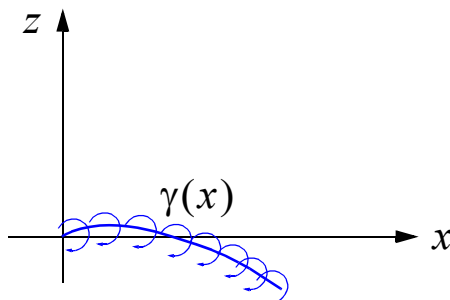


Solution

- The solution of the boundary value problem given by Eqs. (4.11) and (4.12) can be found in most texts on aerodynamics (and our MAE 150B).
- The problem can be recast (see Appendix) as an integral equation for the unknown vortex strength $\gamma(x)$, by replacing the airfoil by an equivalent line of 2D vortices along the mean camber $z_a(x)$, Fig. 4.15.
- Introducing a shift in the x -coordinate and nondimensionalizing,

$$x^* = \frac{2x}{c} - 1 \quad (4.13)$$

the following integral equation is obtained for the unknown distribution $\gamma(x)$:



$$w_a(x^*) = -\frac{1}{2\pi} \int_{-1}^1 \frac{\gamma(\xi^*)}{x^* - \xi^*} d\xi^* \quad (4.14)$$

Fig. 4.15 Replacement of airfoil by an equivalent vortex sheet.



Chordwise Lift Distribution

- The pressure is given by the linearized Bernoulli equation, and the pressure jump across the airfoil becomes

$$\begin{aligned}[p(x)] &= p(x, 0^+) - p(x, 0^-) = -\Delta p(x) \\ &= -\rho_\infty U_\infty \left[\frac{\partial \Phi}{\partial x} \right] = -\rho_\infty U_\infty [u] = -\rho_\infty U_\infty \gamma(x)\end{aligned}\tag{4.15}$$

and is proportional to the vortex sheet strength $\gamma(x)$.

- The solution of the airfoil integral equation (4.14) subject to the Kutta-Joukowski condition

$$\gamma(1) = 0 \Rightarrow [p(1)] = 0\tag{4.16}$$

can be obtained by various methods.

- In airfoil theory the closed-form solution of Söhngen is convenient, given by

$$\gamma(x^*) = \frac{2}{\pi} \sqrt{\frac{1-x^*}{1+x^*}} \int_{-1}^1 \sqrt{\frac{1+\xi^*}{1-\xi^*}} \frac{w_a(\xi^*)}{x^* - \xi^*} d\xi^*\tag{4.17}$$



Example 1: Flat plate at an angle of attack α (or thin uncambered airfoil)

- For the flat plate of zero thickness, Fig. 4.16, we have

$$z_a = -\alpha \frac{c}{2} x^* = -\alpha \frac{c}{2} \left(2 \frac{x}{c} - 1 \right) \quad (4.18)$$

$$w_a = U_\infty \frac{\partial z_a}{\partial x} = -\alpha U_\infty$$

and the solution, Eq. (4.17), becomes

$$\gamma(x^*) = -\frac{2\alpha U_\infty}{\pi} \sqrt{\frac{1-x^*}{1+x^*}} \int_{-1}^1 \sqrt{\frac{1+\xi^*}{1-\xi^*}} \frac{1}{x^* - \xi^*} d\xi^* \quad (4.19)$$

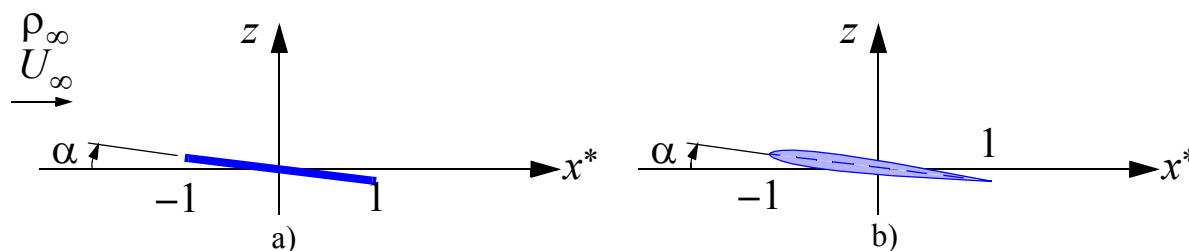


Fig. 4.16 a) Flat plate and b) thin symmetric airfoil in incompressible flow. Linear theory and the superposition principle predict they should have the same lift and moment coefficients.



Solution

- Let

$$\begin{aligned}\xi^* &= \cos\theta, & d\xi^* &= -\sin\theta d\theta, \\ x^* &= \cos\phi\end{aligned}\tag{4.20}$$

and the integral becomes, after multiplying numerator and denominator of the integrand by $\sqrt{1 + \xi^*}$:

$$\int_{-1}^1 \frac{1 + \xi^*}{\sqrt{1 - \xi^{*2}}} \frac{1}{(x^* - \xi^*)} d\xi^* = - \int_0^\pi \frac{1 + \cos\theta}{\cos\theta - \cos\phi} d\theta = -\pi\tag{4.21}$$

which is a special case of the *Glauert integral*

$$\int_0^\pi \frac{\cos n\theta}{\cos\theta - \cos\phi} d\theta = \pi \frac{\sin n\phi}{\sin\phi}, \quad n = 0, 1, 2, \dots\tag{4.22}$$

- The solution for the bound vorticity and the pressure jump become

$$\begin{aligned}\gamma(x^*) &= 2\alpha U_\infty \sqrt{\frac{1 - x^*}{1 + x^*}} \\ \Delta p(x^*) &= -[p(x^*)] = \rho_\infty U_\infty \gamma(x^*) = 2\alpha \rho_\infty U_\infty^2 \sqrt{\frac{1 - x^*}{1 + x^*}}\end{aligned}\tag{4.23}$$



Lift

- The lift is obtained as follows:

$$L = \rho_\infty U_\infty \Gamma = \alpha \rho_\infty U_\infty^2 c \int_{-1}^1 \sqrt{\frac{1-x^*}{1+x^*}} dx^* \quad (4.24)$$

- The integral can be evaluated using regular trigonometric substitution (it is not a Glauert-type integral), to get π . Thus,

$$\begin{aligned} L &= \pi \alpha \rho_\infty U_\infty^2 c = C_L q c \quad (S = c \cdot 1) \\ C_L &= 2\pi\alpha = C_{L_\alpha} \alpha \Rightarrow C_{L_\alpha} = 2\pi \end{aligned} \quad (4.25)$$

- The moment about the quarter-chord point is readily obtained and turns out to be zero and independent of the angle of attack.

The aerodynamic center of the airfoil section is at the quarter chord point.



Example 2: Effect of Camber

- Consider an airfoil with a parabolic mean camber line, as used in the NACA 4-digit series, for example.
- To keep things simple, consider the case where the point of maximum camber is at midchord, and express the *mean camber line* as

$$z_c = z_0[1 - (x^*)^2] \quad (4.26)$$

See Fig. 4.17.

- Note that $z_0/c = m/2$, where m is the maximum camber, in fraction of chord, because the chord in the nondimensional x^* - coordinate is equal to 2.

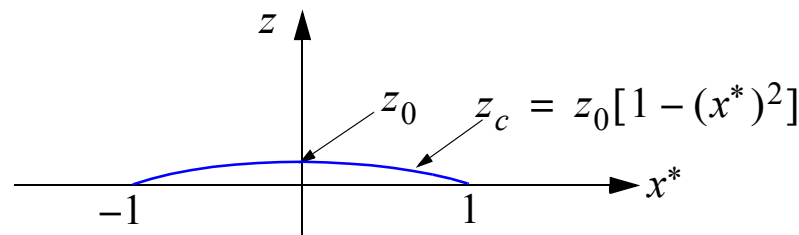


Fig. 4.17 Airfoil with a parabolic mean camber line.



Bound Vorticity

- The upwash on the airfoil and the bound vorticity on the airfoil become

$$w_a = U_\infty \frac{\partial z_c}{\partial x} = U_\infty \frac{\partial z_c}{\partial x^*} \frac{dx^*}{dx} = U_\infty z_0 [-2x^*] \frac{2}{c} = -4U_\infty \left(\frac{z_0}{c}\right) x^* \quad (4.27)$$

$$\gamma(x^*) = \frac{2}{\pi} \left(-4U_\infty \left(\frac{z_0}{c}\right)\right) \sqrt{\frac{1-x^*}{1+x^*}} \int_{-1}^1 \sqrt{\frac{1+\xi^*}{1-\xi^*}} \frac{\xi^*}{x^* - \xi^*} d\xi^* \quad (4.28)$$

- After the trigonometric substitution $\xi^* = \cos\theta$, $x^* = \cos\phi$

$$\begin{aligned} \int_{-1}^1 \sqrt{\frac{1+\xi^*}{1-\xi^*}} \frac{\xi^*}{x^* - \xi^*} d\xi^* &= \int_{-1}^1 \frac{(1+\xi^*)}{\sqrt{1-(\xi^*)^2}} \frac{\xi^*}{x^* - \xi^*} d\xi^* \\ &= \int_{\pi}^0 \frac{(1+\cos\theta)}{\sin\theta} \frac{\cos\theta}{\cos\phi - \cos\theta} (-\sin\theta) d\theta = \int_0^\pi \frac{(\cos\theta + \cos^2\theta)}{\cos\phi - \cos\theta} d\theta \end{aligned} \quad (4.29)$$

- Using the double angle formula $\cos 2\theta = 2\cos^2\theta - 1$, the integral becomes

$$\begin{aligned} \int_0^\pi \frac{\cos\theta}{\cos\phi - \cos\theta} d\theta + \frac{1}{2} \int_0^\pi \frac{(\cos 2\theta + 1)}{\cos\phi - \cos\theta} d\theta &= -\pi - \frac{\pi}{2} \frac{\sin 2\phi}{\sin\phi} \\ &= -\pi(1 + \cos\phi) = -\pi(1 + x^*) \end{aligned} \quad (4.30)$$



Lift due to Camber

- The solution for the bound vortex strength, Eq. (4.28), becomes

$$\gamma(x^*) = 8U_\infty \left(\frac{z_0}{c}\right) \sqrt{\frac{1-x^*}{1+x^*}} (1+x^*) = 8U_\infty \left(\frac{z_0}{c}\right) \sqrt{1-(x^*)^2} \quad (4.31)$$

and the corresponding chordwise distribution of lift becomes

$$\Delta p(x^*) = \rho_\infty U_\infty \gamma(x^*) = 8\rho_\infty U_\infty^2 \left(\frac{z_0}{c}\right) \sqrt{1-(x^*)^2} \quad (4.32)$$

- The lift due to camber becomes

$$L = \int_{-1}^1 \Delta p(x^*) dx^* = 8\rho_\infty U_\infty^2 \left(\frac{z_0}{c}\right) \int_{-1}^1 \sqrt{1-(x^*)^2} dx^* = 8\pi q_\infty \left(\frac{z_0}{c}\right) \quad (4.33)$$

- Expressing the result in terms of the maximum camber $m = 2z_0/c$ as a fraction of chord,

$$L = 4\pi m q_\infty \quad (4.34)$$



Pitching Moment

- The pitching moment about the aerodynamic center is given by

$$\begin{aligned} M_{AC} &= -\frac{c}{2} \int_{-1}^1 \Delta p(x^*) \left(x^* + \frac{1}{2} \right) dx^* \\ &= -4\rho_\infty U_\infty^2 z_0 \int_{-1}^1 \sqrt{1 - (x^*)^2} \left(x^* + \frac{1}{2} \right) dx^* \end{aligned} \quad (4.35)$$

- The integral can be evaluated using the same trig substitution as before, to get

$$\begin{aligned} \int_{-1}^1 \sqrt{1 - (x^*)^2} \left(x^* + \frac{1}{2} \right) dx^* &= \int_{\pi}^0 (\sin \theta) \left(\cos \theta + \frac{1}{2} \right) (-\sin \theta) d\theta \\ &= \frac{1}{2} \int_0^\pi \sin \theta \sin 2\theta d\theta + \frac{1}{2} \int_0^\pi \sin^2 \theta d\theta = \frac{\pi}{4} \end{aligned} \quad (4.36)$$

- The moment about the aerodynamic center becomes

$$M_{AC} = -\pi \rho_\infty U_\infty^2 z_0 = -2\pi q_\infty z_0 = -\pi q_\infty mc \quad (4.37)$$



Lift and Moment

- The (additional) lift and moment coefficients *due to camber alone* become

$$\begin{aligned} C_L &= 4\pi m \\ C_{M_{AC}} &= -\pi m \end{aligned} \tag{4.38}$$

- Note that the lift curve slope is not affected.
- For the NACA 2512 airfoil, the lift and moment coefficients due to the 2% camber are:

$$\begin{aligned} C_L &= 4\pi(0.02) = 0.2513 \\ C_{M_{AC}} &= -\pi(0.02) = -0.0628 \end{aligned} \tag{4.39}$$

- Ref. 10 does not include experimental data for this airfoil. However, the NACA 2412 airfoil only differs in where maximum camber occurs (0.4c vs. 0.5c for the NACA 2512).
- If we compare these predictions to the observed shifts for the NACA 2412 airfoil, Fig. 4.2, we obtain good overall agreement for the lift curve shift and a reasonable average agreement for the moment curve shift.



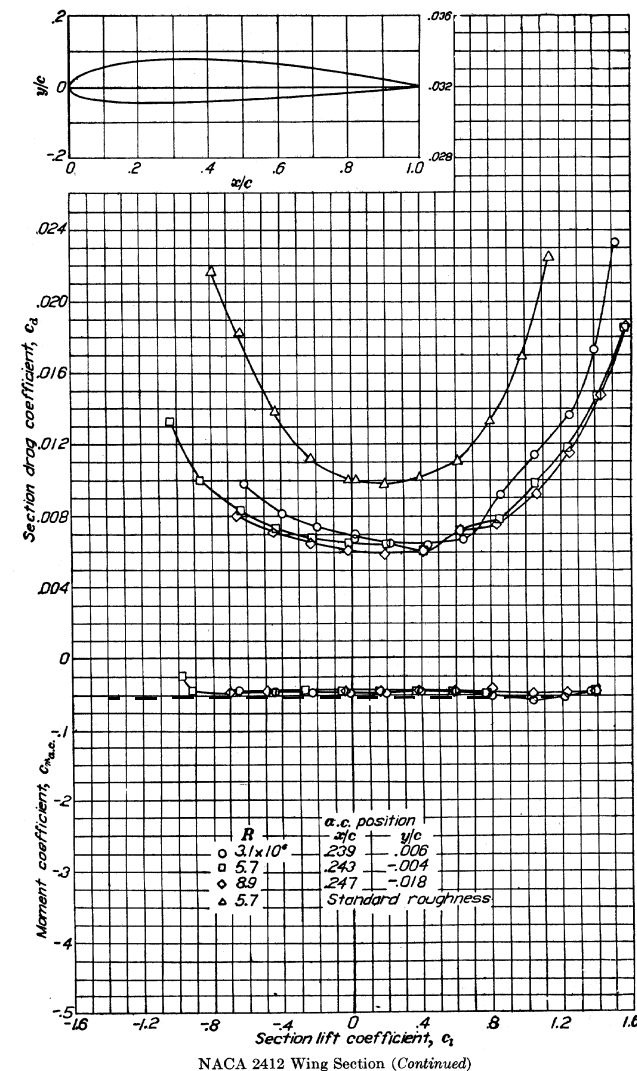
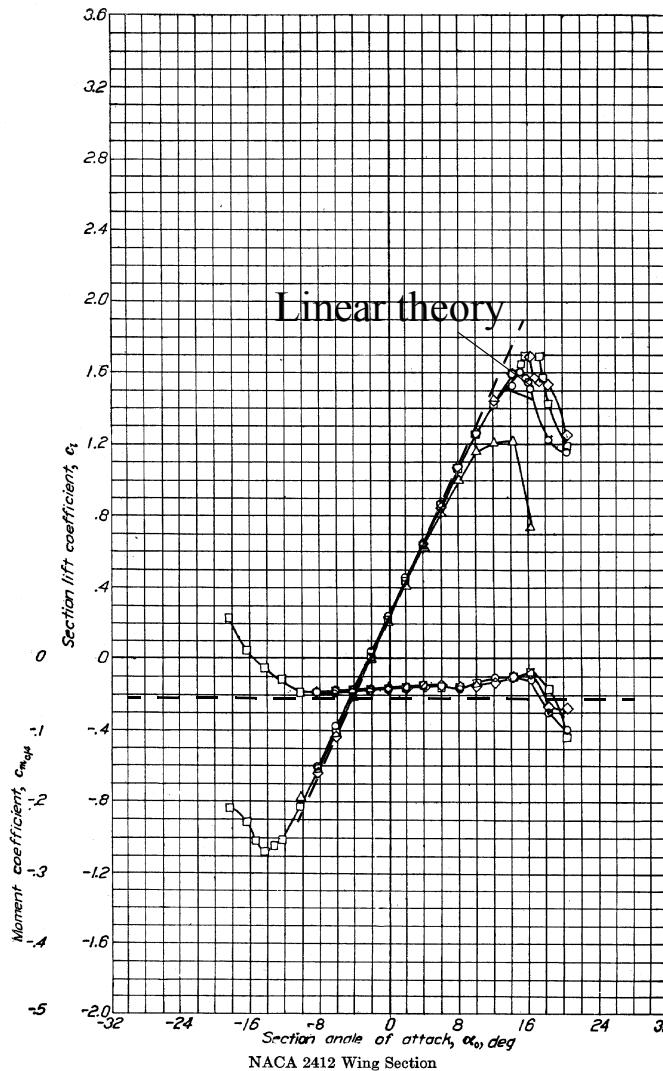


Fig. 4.18 Effect of camber: theory vs. wind tunnel data. (Note: calculations done for NACA 2512 rather than NACA 2412 airfoil, but differences are believed small).

4.5 Effect of Compressibility

Prandtl-Glauert Corrections

- Below the critical Mach number, the effect of Mach number on the aerodynamic coefficients can be determined using the Prandtl-Glauert transformation.
- The transformation involves a stretching of the streamwise x -coordinate by the factor $1/\sqrt{1 - M^2}$, which leads to the following rule for the pressure coefficient

$$C_p \equiv \frac{p - p_\infty}{\frac{1}{2} \rho_\infty V_\infty^2} = \frac{(C_p)_{M=0}}{\sqrt{1 - M^2}} \quad (4.40)$$

and similar formulas for the lift and moment coefficients, and lift curve slope

- Von Karman and Tsien extended the correction to include second-order (nonlinear) effects,

$$C_p = \frac{C_{p_0}}{\sqrt{1 - M^2} + \frac{C_{p_0} M^2}{2 \sqrt{1 - M^2} + 2}} \quad (4.41)$$

- This formula is more accurate, but has a more limited range of validity before the denominator approaches zero and $C_p \rightarrow -\infty$ (the von Karman infinities...)



4.6 Airfoils in Transonic Flow

Background

- As the transonic range is entered, the Prandtl-Glauert as well as the von Karman-Tsien correction formulas break down, and predict “infinite” aerodynamic loads.
- In the case of the Prandtl-Glauert corrections, this occurs as $M_\infty \rightarrow 1$, and no doubt gave rise to the myth of the “sonic wall”.
- The fact that the British test pilot Geoffrey de Havilland, Jr., was killed in an attempt to break the sound barrier in a dive in a tailless aircraft (the *Swallow*) in 1947 only added to the myth.

The aircraft disintegrated at Mach 0.9, as if it had hit “the sonic wall”

- But Mother Nature is not that malicious:

The infinities are of a mathematical rather than a physical nature - they are fictitious.



Why Things Blow up at Mach 1 in Linear Theory

- The reason for this failure can be traced back to the *linear* governing equation, which only permits pressure disturbances to travel away from the wing as linear acoustic waves at a constant speed, the speed of sound a_∞ in the free stream.
- If the wing is traveling with a relative speed U_∞ with respect to the air, upstream propagating wave fronts will accumulate and stay near the wing if the Mach number $M_\infty = U_\infty/a_\infty$ is close to one.
- This results in a large disturbance that violates the small-disturbance assumption.
- A blow-up of the solution at $M_\infty = 1$ occurs, which introduces the well-known $1/\sqrt{1 - M_\infty^2}$ Prandtl-Glauert singularity in the aerodynamic coefficients.



CFD Codes for Transonic Flow

- In the transonic region, no linearization is possible.
- The first-order nonlinear *transonic small disturbance* (TSD) equation was first obtained by von Kármán and Guderley and was the basis for the first transonic CFD codes in the early 1970s (Murman and Cole).
- Modern CFD codes based on the Euler equations are by now highly developed and well suited for use in preliminary design of both airfoil sections and 3-D wings at subsonic, transonic, and supersonic Mach numbers.
- With exception of parasite drag, these codes give reliable predictions of the key aerodynamic properties needed in design, including lift, moment, induced drag, and wave drag.



Transonic Mach No. Distribution Around NACA 0012 Airfoil

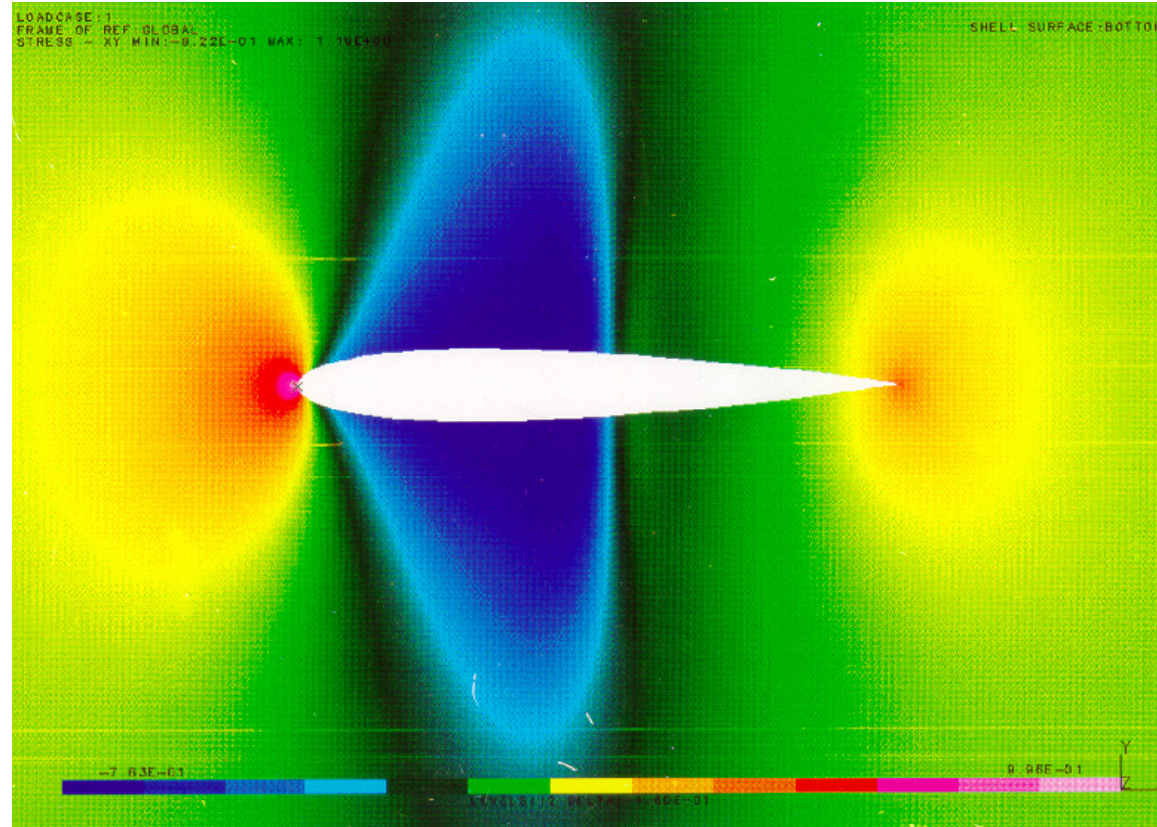


Fig. 4.19 CFD (Euler) calculation for the NACA 0012 airfoil section in transonic flow.
($\alpha = 0$, $M = 0.80$; Mach number contours shown).



Surface Pressure Coefficient

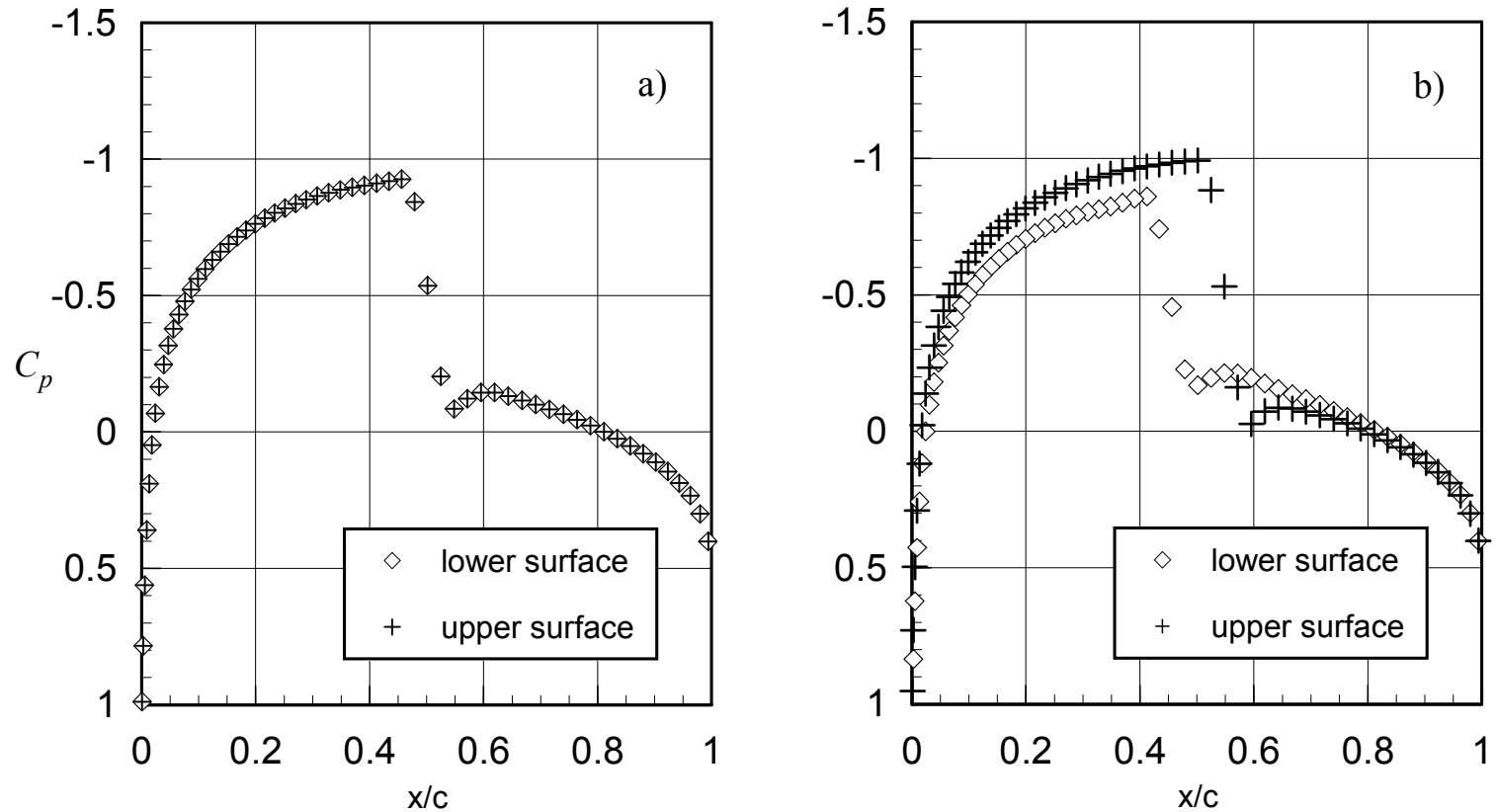
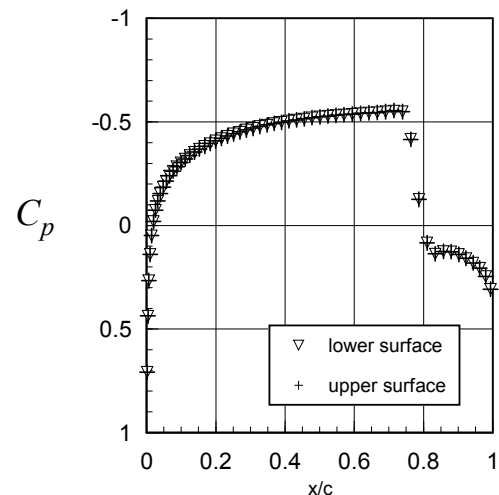
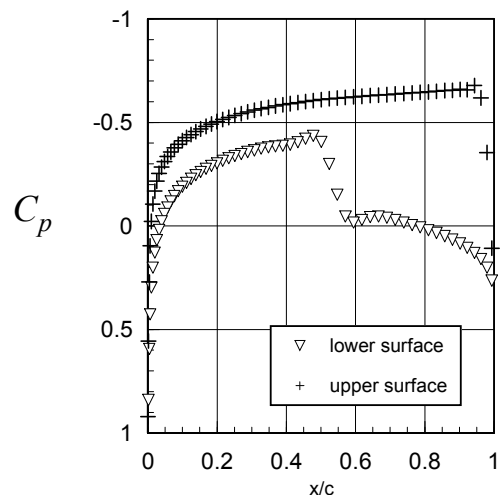


Fig. 4.20 a) Surface pressure coefficient on the NACA 0012 airfoil at Mach 0.80, $\alpha_{\infty} = 0^\circ$
b) Mach 0.80, $\alpha_{\infty} = 0.4^\circ$

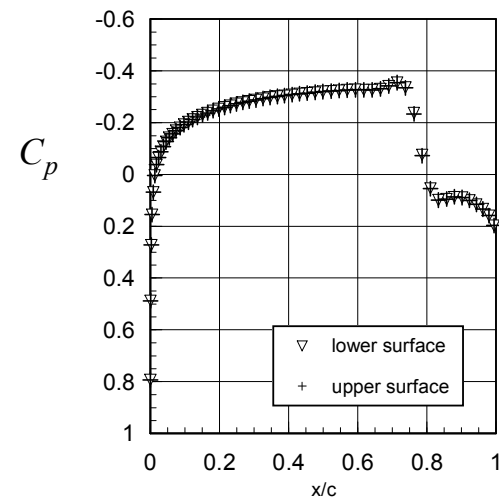
Effect of Thickness



a) NACA 0006 at $M_\infty = 0.90$; $\alpha_\infty = 0^\circ$



b) NACA 0006 at $M_\infty = 0.90$; $\alpha_\infty = 0.8^\circ$



c) NACA 0003 at $M_\infty = 0.935$; $\alpha_\infty = 0^\circ$

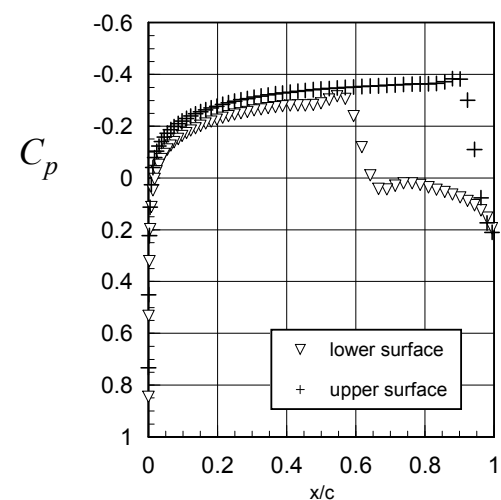


Fig. 4.21 Illustrating the sensitivity of airfoil surface pressure coefficient and shock positions to airfoil thickness and angle of attack in transonic flow.



Lift Curve Slope Breaks

- The Prandtl-Glauert singularity at Mach 1 disappears in a correct nonlinear theory and the lift and moment coefficients remain continuous at Mach 1.
- But the lift curve slope develops an “almost singular” behavior as the airfoil thickness is reduced; see Fig. 4.22.

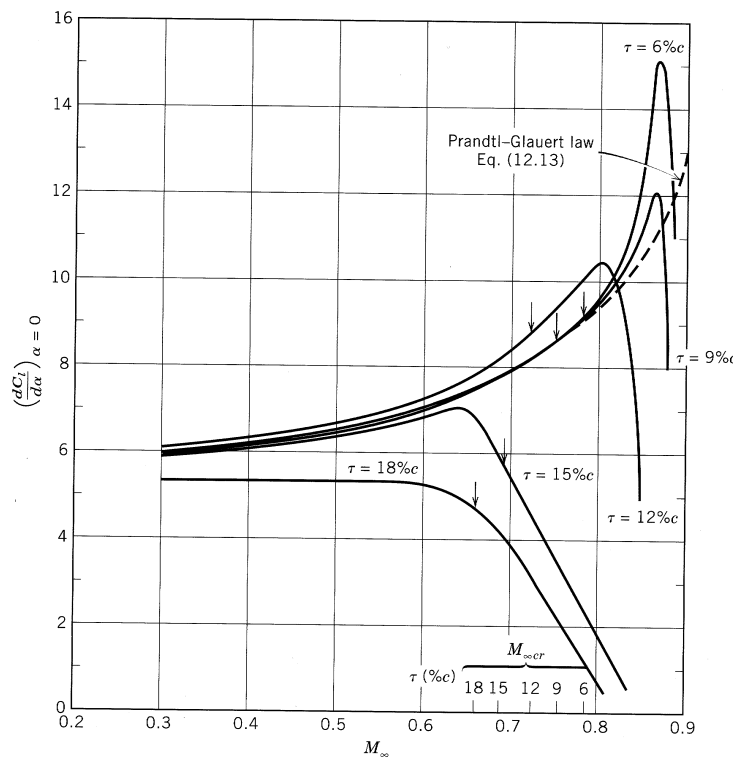


Fig. 4.22 Breaks in the lift curve slopes at transonic Mach numbers. (From Ref. 7; original wind tunnel data from Göthert).



WWII Dive Accidents

- During WWII it was observed that airplanes taken in high-speed dives, where transonic Mach numbers could be reached, had a tendency to “*tuck under*”.
- This phenomenon was associated with a large negative shift in the aircraft trim angle and a significant increase in the stability of the airplane.
- Some airplanes did not have sufficient elevator power to recover from the dive.
- We now know that the “tucking under” effect is caused by the *break in the lift curve slopes* at transonic Mach numbers, and by the gradual aft shift of the A.C.
- Because of the relatively thick and cambered wing sections used on these WWII airplanes, the tucking-under problem occurred at Mach numbers as low as 0.7.



NLR 7301 Supercritical Airfoil Lift Breaks

- For the relatively thick modern supercritical airfoils, such as the NLR 7301, the “force break” also occurs at relatively low transonic Mach numbers, Fig. 4.23.
- Obviously, *linear theory and the corresponding Prandtl-Glauert corrections are pretty much worthless in estimating the transonic lift coefficients.*

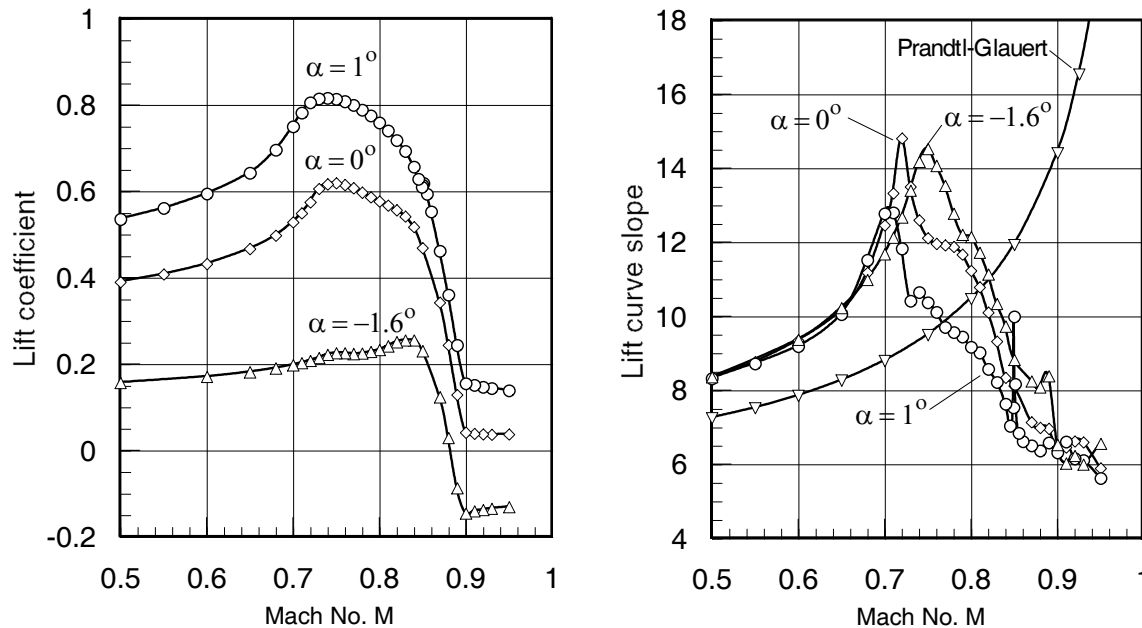


Fig. 4.23 Lift coefficient (left) and lift curve slope (right) vs. Mach number and angle of attack for the supercritical NLR 7301 airfoil (Euler calculations; Prandtl-Glauert comparison curve is based on thin airfoil theory).



4.7 Supercritical Airfoils

Design Objective

- Smooth (shock-free) acceleration from subsonic flow to supersonic flow is possible both theoretically and in practice.
- But the reverse is not true: smooth shock-free (isentropic) deceleration from supersonic to subsonic flow is only possible in theory.
- However, if a given wing shape is capable of admitting a shock-free solution from a theoretical standpoint, then the "real" wing may be expected to have only *weak* shocks and hence the associated (wave) drag penalty should be small.

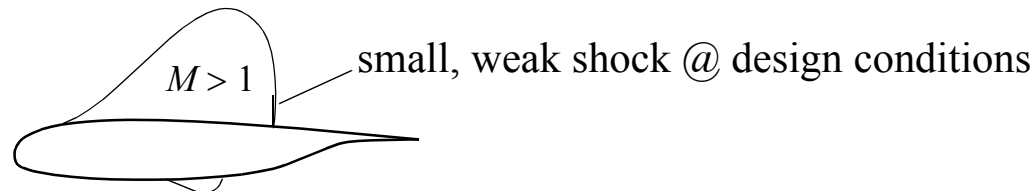
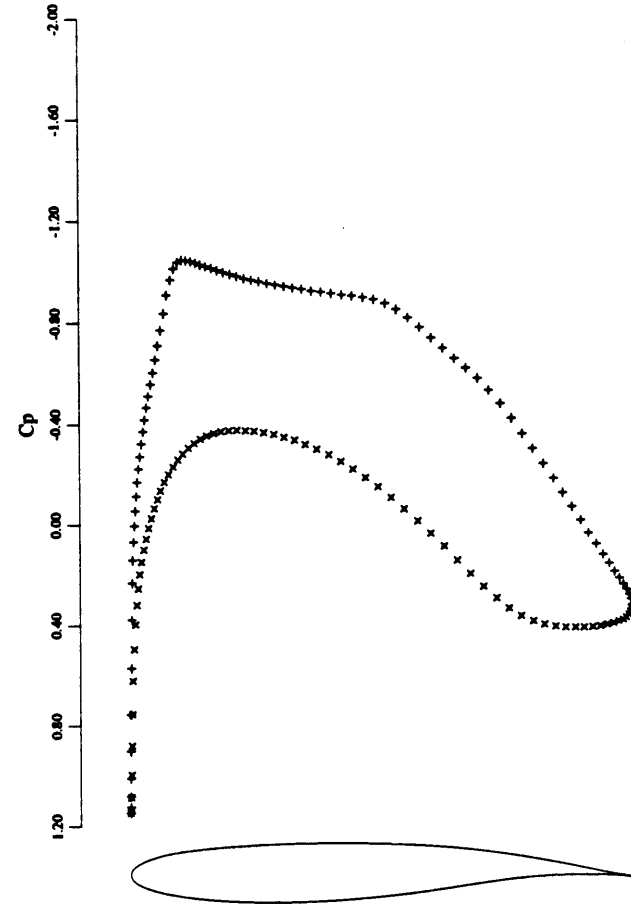
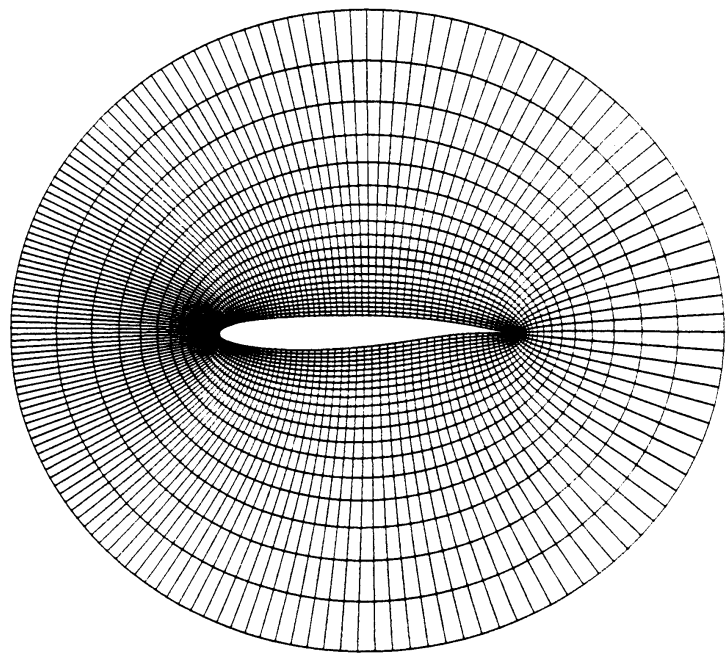
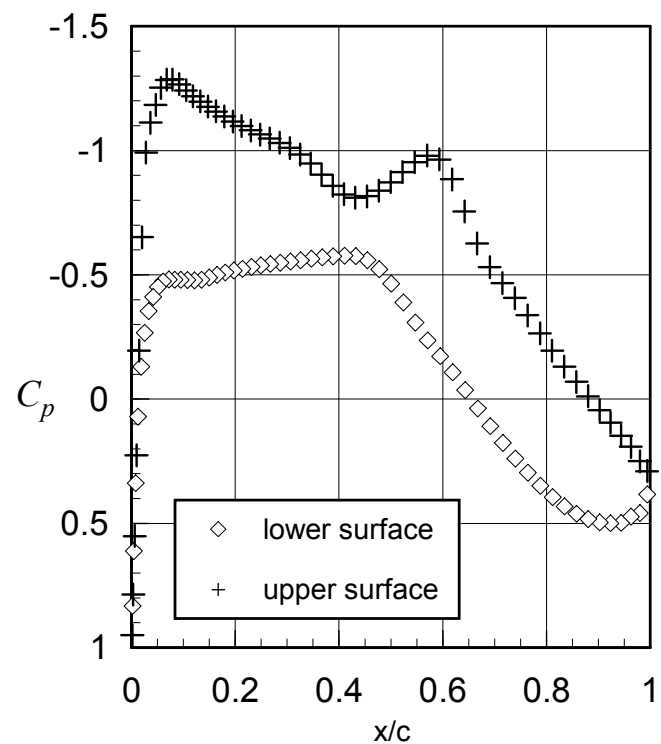


Fig. 4.24 Supercritical airfoil.

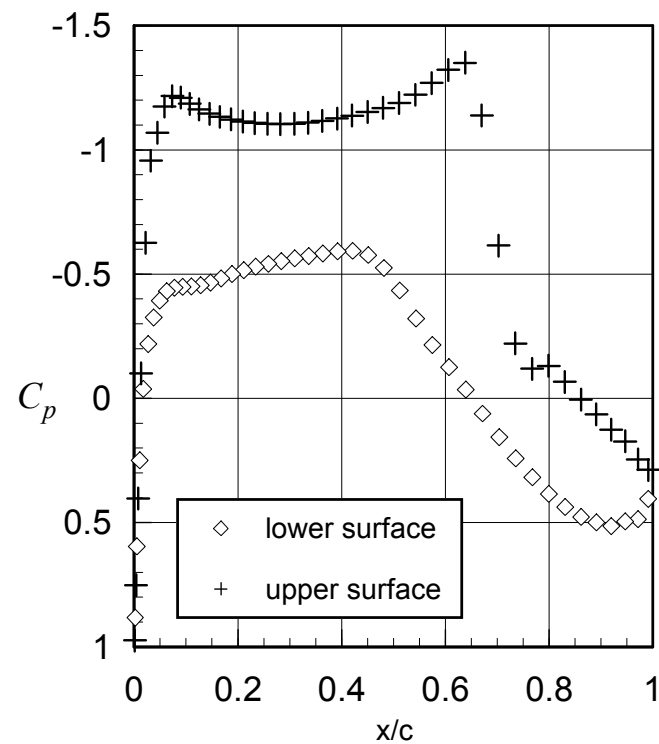


9b: C_p after 50 Cycles.
 $C_l = 0.6314$, $C_d = 0.0000$.

Fig. 4.25 The Korn supercritical airfoil at its design point (Mach 0.75, alpha = 0) [15].



a) $M_\infty = 0.721$; $\alpha_\infty = -0.19^\circ$;
 $C_L = 0.53$; $C_D = 0.0025$



b) $M_\infty = 0.745$; $\alpha_\infty = 0^\circ$;
 $C_L = 0.637$; $C_D = 0.0128$

Fig. 4.26 NLR 7301 supercritical airfoil at a) design condition and b) off-design condition. (Euler calculations).

Pros and Cons of Supercritical Airfoils

- Supercritical airfoils have the additional advantage that they permit the use of greater airfoil thickness ratios in transonic wings, allowing for more room for the internal structure, fuel tanks, etc., making the wing design problem easier.
- However, the supercritical sections have a cusp-like thin trailing-edge region, which brings in its own structural design problem.
- Because shock-free solutions are "isolated" in the sense that they only appear at a fixed design point Mach number and angle of attack, any departure from this design point will produce shocks and hence wave drag.



4.8 Airfoils in Supersonic Flow

Fundamentals

- 2-D supersonic flow is simpler in many respect than the corresponding subsonic case, because the upper and lower airfoil surfaces are completely independent.
- This means that the solutions for the upper and lower surfaces can be determined independently, since no disturbance can be transmitted from one surface to the other.
- Furthermore, the formula for the local surface pressure is remarkably simple, and depends only on the local surface slope in the flow (x) direction.
- In terms of the pressure difference

$$\Delta p = p_l - p_u = -\rho_\infty U_\infty \left[\frac{\partial \varphi_l}{\partial x} - \frac{\partial \varphi_u}{\partial x} \right] \quad (4.42)$$

- The lift and moment about the leading edge, positive nose up, per unit span, become

$$L = \int_0^c \Delta p(x) dx; \quad M_{LE} = - \int_0^c x \Delta p(x) dx \quad (4.43)$$



Lift and Drag Coefficients

- For the flat-plate airfoil, we showed in Sec. 2.7.1 that

$$C_L = \frac{4\alpha}{\beta} = \frac{4\alpha}{\sqrt{M_\infty^2 - 1}} \Rightarrow C_{L_\alpha} = \frac{4}{\beta} = \frac{4}{\sqrt{M_\infty^2 - 1}} \quad (4.44)$$

- The moment about the midchord of the airfoil is zero, independent of the angle of attack; thus the aerodynamic center is at midchord.
- The (wave) drag coefficient can be expressed in terms of the slopes of the upper and lower surfaces, as follows

$$C_D \equiv C_{D_W} = \frac{2}{c\sqrt{M_\infty^2 - 1}} \int_0^c \left\{ \left(\frac{dz_l}{dx} \right)^2 + \left(\frac{dz_u}{dx} \right)^2 \right\} dx \quad (\text{wave drag}) \quad (4.45)$$

- The superposition principle can then be used to separate out the effects of camber, angle of attack and thickness for a general airfoil.



General Case

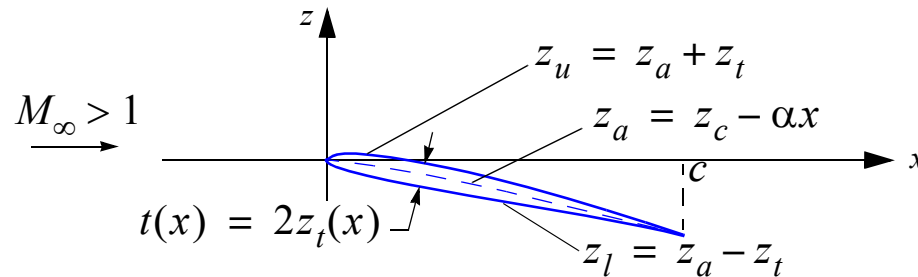


Fig. 4.27 General airfoil in supersonic flow.

- Substituting from Eq. (4.42), the lift integral can be evaluated without knowing the actual shape of the camber line and

$$C_L = \frac{4}{\sqrt{M_\infty^2 - 1}} \left[\frac{z_a(0)}{c} - \frac{z_a(c)}{c} \right] \quad (4.46)$$

- This result shows that camber does not contribute to the lift in supersonic flow, i.e., lift depends only on the angle of attack part $-\alpha x$ of z_a (see Fig. 4.10).

$$C_{D_W} = \frac{4}{c \sqrt{M_\infty^2 - 1}} \int_0^c \left\{ \left(\frac{dz_a}{dx} \right)^2 + \left(\frac{dz_t}{dx} \right)^2 \right\} dx = \frac{4}{\sqrt{M_\infty^2 - 1}} \left\{ \overline{\alpha(x)^2} + \overline{\left(\frac{dz_t}{dx} \right)^2} \right\} \quad (4.47)$$

(a) Doubly symmetric wedge (diamond) airfoil

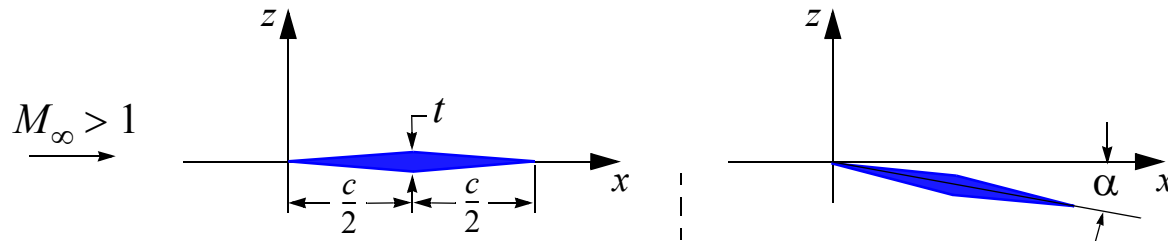


Fig. 4.28 Doubly symmetric wedge airfoil.

- This airfoil can be shown to represent the *optimal shape for minimum drag for a given airfoil maximum thickness*. In this case, the thickness distribution is

$$z_t(x) = \begin{cases} \frac{t}{c}x; & 0 \leq x \leq \frac{c}{2} \\ \frac{t}{c}(c-x); & \frac{c}{2} \leq x \leq c \end{cases} \quad (4.48)$$

and

$$\overline{\alpha(x)^2} = \frac{1}{c} \int_0^c \alpha^2 dx = \alpha^2 \quad (4.49)$$

$$\overline{\left(\frac{dz_t}{dx}\right)^2} = \frac{1}{c} \int_0^c \left(\frac{dz_t}{dx}\right)^2 dx = \frac{1}{c} \int_0^{c/2} \left(\frac{t}{c}\right)^2 dx + \frac{1}{c} \int_{c/2}^c \left(-\frac{t}{c}\right)^2 dx = \left(\frac{t}{c}\right)^2 \quad (4.50)$$



Lift and Drag Coefficients

- The wave drag coefficient becomes

$$C_{D_W} = \frac{4}{\sqrt{M_\infty^2 - 1}} \left[\alpha^2 + \left(\frac{t}{c} \right)^2 \right] \quad (4.51)$$

- The lift coefficient is

$$C_L = \frac{4\alpha}{\sqrt{M_\infty^2 - 1}} \quad (4.52)$$

which is the same as the flat-plate result, as it should be.



c) Double circular arc airfoil

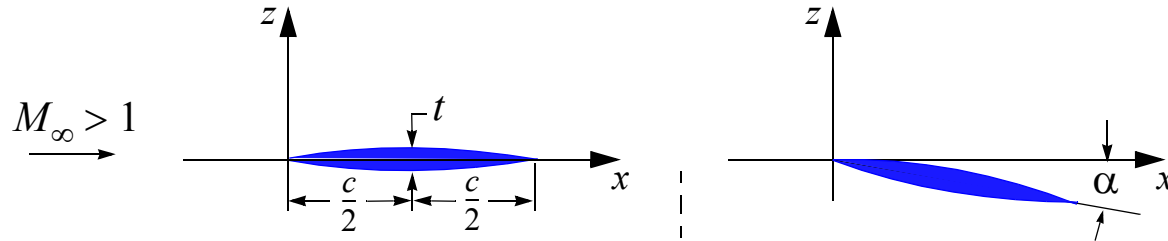


Fig. 4.29 Double circular arc airfoil.

- In this case, it is convenient to introduce an angle variable, defined by

$$R \sin \theta = x - c/2 \quad (4.53)$$

where R is the radius of curvature of the airfoil surface.

- To evaluate R , we have the equation

$$\left(R - \frac{t}{2}\right)^2 + \left(\frac{t}{2}\right)^2 = R^2 \quad (4.54)$$

from which we obtain

$$R = \frac{t}{4} + \frac{c^2}{4t} \quad (4.55)$$

Thickness Distribution and Wave Drag Integrals

- The thickness distribution is then

$$z_t(\theta) = \frac{t}{2} - R(1 - \cos\theta); \quad -\Theta \leq \theta \leq \Theta \quad (4.56)$$

where $\mp\Theta$ represent the LE and TE, respectively, and Θ is given by

$$\cos\Theta = 1 - \frac{t}{2R} = \frac{1 - (t/c)^2}{1 + (t/c)^2} \quad (4.57)$$

- To evaluate the wave drag due to thickness, note that

$$\overline{\left(\frac{dz_t}{dx}\right)^2} = \frac{1}{c} \int_0^c \left(\frac{dz_t}{dx}\right)^2 dx = \frac{1}{c} \int_{-\Theta}^{\Theta} \left(\frac{dz_t}{d\theta}\right)^2 \left(\frac{d\theta}{dx}\right)^2 R \cos\theta d\theta \quad (4.58)$$

$$\overline{\left(\frac{dz_t}{dx}\right)^2} = \frac{1}{c} \int_{-\Theta}^{\Theta} (-R \sin\theta)^2 \left(\frac{1}{R \cos\theta}\right)^2 R \cos\theta d\theta = \frac{R}{c} \int_{-\Theta}^{\Theta} \tan^2\theta \cos\theta d\theta \quad (4.59)$$



Thin Airfoil Approximation

- If we assume that the airfoil is thin, to be within the limitations of linearized aerodynamics, it follows that the angles involved are small, and we may set $\tan \theta \approx \theta$, $\cos \theta \approx 1$, to get

$$\left(\frac{dz_t}{dx} \right)^2 = \frac{R}{c} \int_{-\Theta}^{\Theta} \theta^2 d\theta = \frac{2R}{3c} \Theta^3 \quad (4.60)$$

- Also, because the camber is zero,

$$\overline{\alpha(x)^2} = \frac{1}{c} \int_0^c \alpha^2 dx = \alpha^2 \quad (4.61)$$

- The wave drag coefficient becomes, after making the small-angle approximation consistent with thin airfoil theory

$$\sin \Theta = \frac{c}{2R} \approx \Theta \quad (4.62)$$



Wave Drag and Lift Coefficients

$$\begin{aligned}\frac{2R}{3c}\Theta^3 &= \frac{1}{12}\left(\frac{c}{R}\right)^2 = \frac{1}{12}\left\{\frac{4c}{t+c^2/t}\right\}^2 \\ &= \frac{4}{3}\left[\frac{(t/c)^2}{1+(t/c)^2}\right] \approx \frac{4}{3}\left(\frac{t}{c}\right)^2\end{aligned}\tag{4.63}$$

$$C_{D_W} = \frac{4}{\sqrt{M_\infty^2 - 1}} \left[\alpha^2 + \frac{4}{3}\left(\frac{t}{c}\right)^2 \right]\tag{4.64}$$

which agrees with the value listed in Fig. 2-79 in Perkins and Hage, since $K_1 = 4(4/3) = 16/3 = 5.333$.

- The lift coefficient is obviously

$$C_L = \frac{4\alpha}{\sqrt{M_\infty^2 - 1}}\tag{4.65}$$



Appendix: Formulation and Solution of the Thin Airfoil Equation

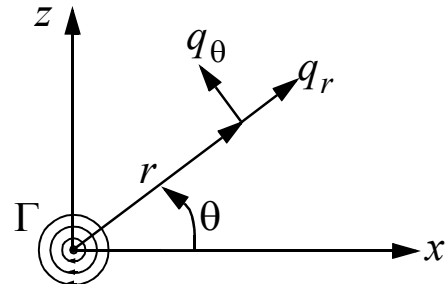


Fig. 4.30 Point vortex.

- For the lifting case, the appropriate singularity solution of Laplace's equation is the point vortex solution, given in polar coordinates by

$$\varphi_V = -\frac{\Gamma}{2\pi}\theta = -\frac{\Gamma}{2\pi} \tan^{-1}\left(\frac{z}{x}\right) \quad (4.66)$$

where Γ is the vortex strength and the polar angle is restricted to $0 \leq \theta < 2\pi$, to give a single-valued solution.

- The point vortex is located at the origin of the coordinate system, Fig. 4.30. The polar velocity components are given by

$$q_r = \frac{\partial \varphi}{\partial r} = 0; \quad q_\theta = \frac{1}{r} \frac{\partial \varphi}{\partial \theta} = -\frac{\Gamma}{2\pi r} \quad (4.67)$$



Representation of Airfoil by Vortex Sheet

- To solve the antisymmetric or lifting problem for the airfoil, we distribute a continuous line of 2D vortices along the skeleton $z_a(x)$ of the airfoil, as illustrated in Fig. 4.31.
- Let $\gamma(x)$ denote the vortex strength per unit chord, then the potential corresponding to this line of vortices (or sheet in cylindrical coordinates) is given by the superposition principle as the integral

$$\varphi(x, z) = -\frac{1}{2\pi} \int_0^c \gamma(\xi) \tan^{-1}\left(\frac{z}{x-\xi}\right) d\xi \quad (4.68)$$

- The distributed vortex strength γ must be determined from the boundary conditions for the problem, Eq. (4.12), plus the Kutta-Joukowski condition.

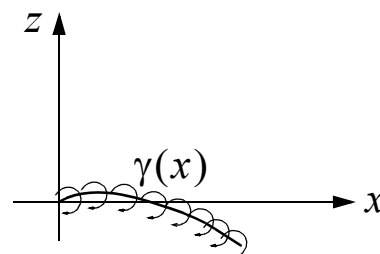


Fig. 4.31 Replacement of airfoil by an equivalent vortex sheet.

Airfoil Equation

- Differentiating with respect to z , and let $z \rightarrow 0^+$ on $0 < x < c$,

$$\frac{\partial \phi}{\partial z} = -\frac{1}{2\pi} \int_0^c \frac{\gamma(\xi)}{x-\xi} \left[\frac{(x-\xi)^2}{(x-\xi)^2 + z^2} \right] d\xi \quad (4.69)$$

$$\left. \frac{\partial \phi}{\partial z} \right|_{z=0^+} = -\frac{1}{2\pi} \int_0^c \frac{\gamma(\xi)}{x-\xi} d\xi = w_a(x) \quad (4.70)$$

where the Cauchy principal value of the integral is implied.

- Introducing a shift in the x -coordinate and nondimensionalizing,

$$x^* = \frac{2x}{c} - 1 \quad (4.71)$$

we obtain the following integral equation for the unknown vortex distribution $\gamma(x)$:

$$w_a(x^*) = -\frac{1}{2\pi} \int_{-1}^1 \frac{\gamma(\xi^*)}{x^* - \xi^*} d\xi^* \quad (\text{airfoil equation}) \quad (4.72)$$

- This is a singular integral equation of the first kind, with a Cauchy kernel.



Airfoil Boundary Value Problem

- The corresponding boundary value problem is shown in Fig. 4.32. The pressure is given by the linearized Bernoulli equation

$$p - p_{\infty} = -\rho_{\infty} U_{\infty} \frac{\partial \phi}{\partial x} \quad (4.73)$$

- The pressure jump across the airfoil becomes

$$\begin{aligned}[p(x)] &= p(x, 0^+) - p(x, 0^-) = -\Delta p(x) \\ &= -\rho_{\infty} U_{\infty} \left[\frac{\partial \phi}{\partial x} \right] = -\rho_{\infty} U_{\infty} [u]\end{aligned}\quad (4.74)$$

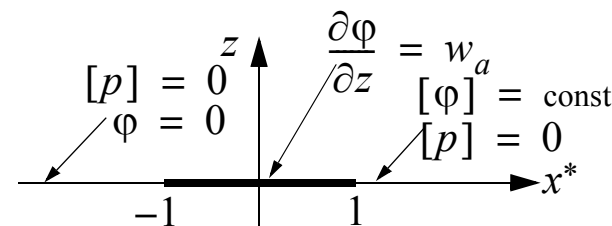


Fig. 4.32 Airfoil boundary value problem.



Chordwise Pressure Loading

- The pressure jump across the airfoil is proportional to the jump in the tangential velocity across the airfoil, which can be related to the vortex sheet strength $\gamma(x)$.
- Detailed calculations lead to the simple relation

$$u(x)|_{z=0^\pm} = \frac{\partial \phi}{\partial x} \Big|_{z=0^\pm} = \pm \frac{\gamma(x)}{2} \quad (4.75)$$

$$[u(x)] = \left[\frac{\partial \phi}{\partial x} \right] = \gamma(x) \quad (4.76)$$

and u is an odd function of z , as it must be in the antisymmetric problem.

- It is now evident why we need not extend the vortex sheet beyond the trailing edge in the *steady* case, because from Eqs. (4.75) and (4.76) we conclude that the pressure jump across the x -axis is

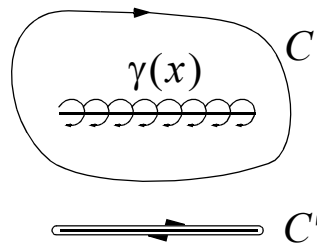
$$[p(x)] = -\Delta p(x) = -\rho_\infty U_\infty \gamma(x) \quad (4.77)$$

- Because the pressure must be continuous off the airfoil, $\gamma(x) \equiv 0$ for $|x^*| > 1$.



Circulation

- The total circulation around the airfoil is given by the integral



$$\Gamma = \oint_C \mathbf{q} \cdot d\mathbf{r} \quad (4.78)$$

where C is any closed contour encircling the airfoil in the clockwise direction; see Fig. 4.33.

Fig. 4.33 Circulation calculation.

The contour can be deformed continuously until it just encircles the airfoil (or its projection on the x -axis in the linearized case), i.e., contour C' .

- Evaluating the circulation integral on C' ,

$$\begin{aligned} \Gamma &= \int_0^c u(x, 0^+) dx + \int_c^0 u(x, 0^-) dx = \int_0^c [u(x)] dx \\ &= \int_0^c \left[\frac{\partial \Phi}{\partial x} \right] dx = \int_0^c \gamma(x) dx \end{aligned} \quad (4.79)$$

Lift

- The lift becomes

$$L = \int_0^c \Delta p(x)dx = -\int_0^c [p(x)]dx = \rho_\infty U_\infty \int_0^c \gamma(x)dx \quad (4.80)$$

- In view of Eq. (4.79), we conclude that

$$L = \rho_\infty U_\infty \Gamma \quad (4.81)$$

- This important relation linking lift and circulation was derived independently by Kutta (1902) and Joukowski (1906), and is fundamental to the understanding of how airfoils and wings generate lift.

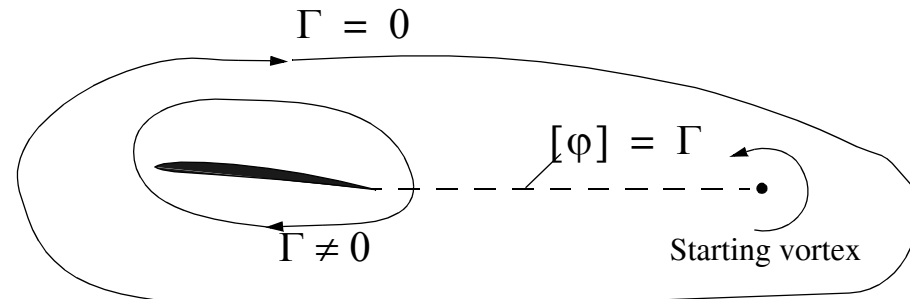


Fig. 4.34 Uniform steady airfoil motion started from rest.

Remarks

- Note that without circulation, there can be no lift.
- Also note that from Eq. (4.79) the circulation is given by the jump in the velocity potential at the trailing edge:

$$\Gamma = \int_0^c \left[\frac{\partial \phi}{\partial x} \right] dx = [\phi]_{TE} - [\phi]_{LE} = [\phi]_{TE} \quad (4.82)$$

since the velocity potential is continuous at the leading edge.

- As a consequence of Eq. (4.82), the velocity potential must have a (constant) discontinuity along the x -axis, from the trailing edge to the starting vortex.
- Unlike the 2D vortex sheet, the discontinuity in the potential persists even after the steady state has been reached.
- In unsteady 2D flows and in all 3D lifting flows, a vortex sheet is present behind the wing.



Solution of the airfoil integral equation

- The solution of the airfoil integral equation

$$w_a(x^*) = -\frac{1}{2\pi} \int_{-1}^1 \frac{\gamma(\xi^*)}{x^* - \xi^*} d\xi^* \quad (4.83)$$

subject to the Kutta-Joukowski condition

$$\gamma(1) = 0 \Rightarrow [p(1)] = 0 \quad (4.84)$$

has been considered by a number of researchers.

- The integral equation (4.83) is a singular integral equation of the first kind, with a Cauchy kernel.
- In airfoil theory the solution of Söhngen is most often quoted, which is given by

$$\gamma(x^*) = \frac{2}{\pi} \sqrt{\frac{1-x^*}{1+x^*}} \int_{-1}^1 \sqrt{\frac{1+\xi^*}{1-\xi^*}} \frac{w_a(\xi^*)}{x^* - \xi^*} d\xi^* \quad (4.85)$$



Nonuniqueness of Solution

- Note that we could add a term of the form

$$\frac{C}{\sqrt{1 - x^{*2}}} \quad (4.86)$$

to the above solution, where C is a constant, without disturbing the upwash boundary condition, because the integral

$$I = \int_{-1}^1 \frac{1}{(x^{*} - \xi^{*})\sqrt{1 - \xi^{*2}}} d\xi^{*} \quad (4.87)$$

vanishes identically for all $|x^{*}| \leq 1$.

- To show this, let

$$\begin{aligned} \xi^{*} &= \cos\theta, & d\xi^{*} &= -\sin\theta d\theta, \\ x^{*} &= \cos\phi \end{aligned} \quad (4.88)$$

then

$$I = \int_{\pi}^0 \frac{-\sin\theta}{(\cos\phi - \cos\theta)\sin\theta} d\theta = - \int_0^{\pi} \frac{1}{\cos\theta - \cos\phi} d\theta \quad (4.89)$$



Kutta-Joukowski Condition Restores Uniqueness

- Eq. (4.89) is a special case of the Glauert integral

$$\int_0^\pi \frac{\cos n\theta}{\cos \theta - \cos \phi} d\theta = \pi \frac{\sin n\phi}{\sin \phi}, \quad n = 0, 1, 2, \dots \quad (4.90)$$

corresponding to $n = 0$. Thus, $I = 0$, by (4.90).

- The Kutta-Joukowski condition restores uniqueness, by requiring that the solution be finite at the trailing edge. This requires that $C = 0$.



References

1. Prandtl, L., *Applications of Modern Hydrodynamics to Aeronautics*, NACA Technical Report No. 116, 1921. See also Prandtl, L. and Tietjens, O.G., *Applied Hydro- and Aerodynamics*, Dover Edition, 1957.
2. Munk, M. M., *Elements of the Wing Section Theory and of the Wing Theory*, NACA Report 191, 1921.
3. Glauert, H., *The Elements of Aerofoil and Airscrew Theory*, Cambridge University Press, New York, 1926.
4. Theodorsen, T., *On the Theory of Wing Sections with Particular Reference to the Lift Distribution*, NACA Report 383, 1931.
5. *Aerodynamic Characteristics of Airfoils-V*, NACA Report 286, 1928. See also Reports Nos. 93, 124, 182, and 244.
6. Jacobs, E.N., et al., *The Characteristics of 78 Related Airfoil Sections from Tests in the Variable-Density Wind Tunnel*, NACA Report 460, 1933.
7. Jacobs, E.N., and Pinkerton, R.M., *Tests in the Variable-Density Wind Tunnel of Related Airfoils Having the Maximum Camber Unusually Far Forward*, NACA Report 537, 1935.
8. Jacobs, E.N., et al., *Tests of Related Forward-Camber Airfoils in the Variable-Density Wind Tunnel*, NACA Report 610, 1937.
9. Abbot, I. H., von Doenhoff, A.E., and Stivers, L.S., Jr., *Summary of Airfoil Data*, NACA Report 824, 1945.
10. Abbott, I.H. and von Doenhoff, A.E., *Theory of Wing Sections*, Dover Publications, 1959.
11. Kuethe, A.M. and Chow, C-Y., *Foundations of Aerodynamics*, John Wiley & Sons, 5th edition, 1998.



-
- 12. Dommasch, D.O., Sherby, S.S., and Connolly, T.F., *Airplane Aerodynamics*, 4th edition, Pitman Publishing Corporation, New York, NY, 1967.
 - 13. McCormick, B.W., *Aerodynamics, Aeronautics, and Flight Mechanics*, 2nd ed., John Wiley & Sons, 1995.



5.0 Subsonic and Transonic Wing Aerodynamic Design



5.1 Wing Geometry and Nomenclature

Span: b (tip to tip)

Area: S (gross)

Dihedral: Γ

Incidence: i_w

Mean aerodynamic chord (MAC): $\frac{2}{S} \int_0^{\frac{b}{2}} c^2 dy$

Aspect ratio: $A = b^2/S$

Sweep: Λ (positive aft)

Taper ratio: $\lambda = c_t/c_r$

Geometric twist (washin/washout): ε

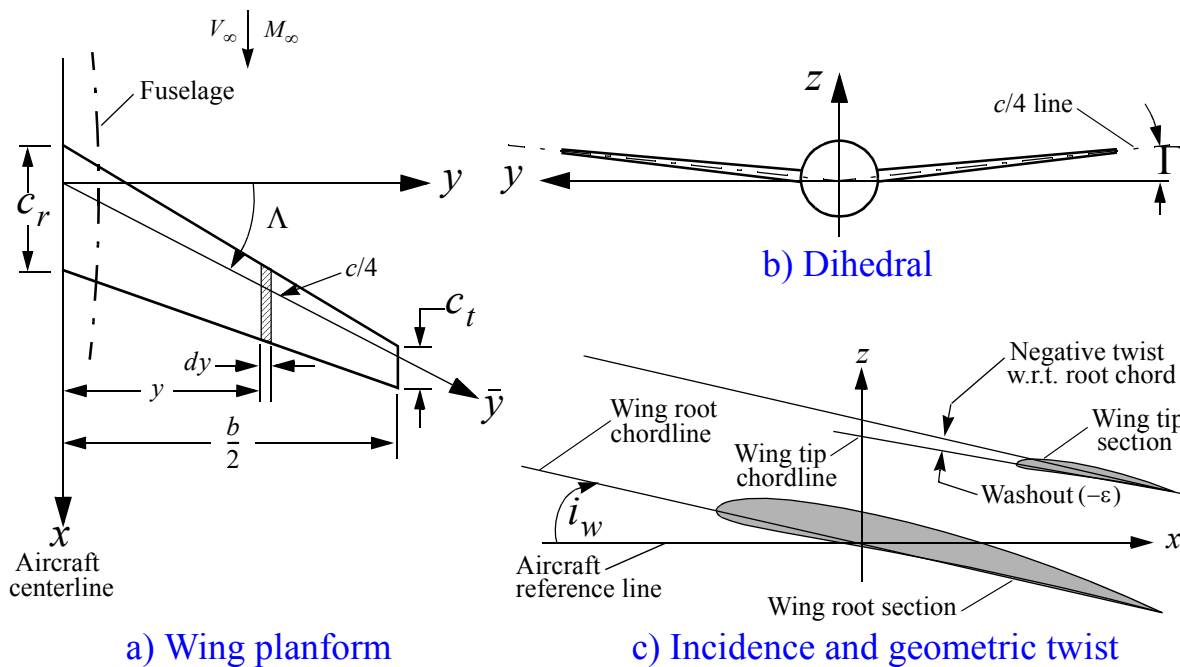


Fig. 5.1 Wing geometry and nomenclature.

5.2 Determination of Wing Aerodynamics

Data needed for design purposes

- 1) C_L , C_{L_α} , and C_D vs. α .
- 2) Aerodynamic center (A.C.) and $C_{M_{AC}}$.
- 3) Spanwise distribution of L , D , and M_{AC} .
- 4) Stall characteristics of wing.



Theoretical Methods

- 1) Lifting Line Theory (Prandtl): Preliminary design of high aspect ratio wings.
- 2) Lifting Surface Methods: Approximate versions are suitable for preliminary design, using design charts for rapid estimation of wing aerodynamics.
- 2) Vortex Lattice and Panel Methods: Preliminary design (and final design). Limited to linear flows (small disturbance; thin wings; no shocks). Codes are very fast and well suited for the iterative environment of preliminary design.
- 3) 3-D Full Potential Equation: Preliminary and final design (sub-transonic). Isentropic flows only; cannot model transonic flows with strong shocks correctly, because entropy production is neglected.
- 4) 3-D Euler Equations: Design of transonic wings with shocks (routine by now). Euler CFD codes model entropy production at shocks; only viscosity is neglected. Not limited to small perturbations (thin wings and bodies).
- 5) 3-D Navier-Stokes Equations: Final design, especially drag calculations and L/D optimizations. CFD codes require some form of turbulence modeling for the high Reynolds numbers encountered in practical wing calculations.



Experimental Methods

1) Wind tunnel data from scaled models:

- Expensive and time-consuming, but still needed.
- CFD methods have cut down on the number of wind tunnel hours required to develop a successful design (but have not yet replaced the good old wind tunnel).

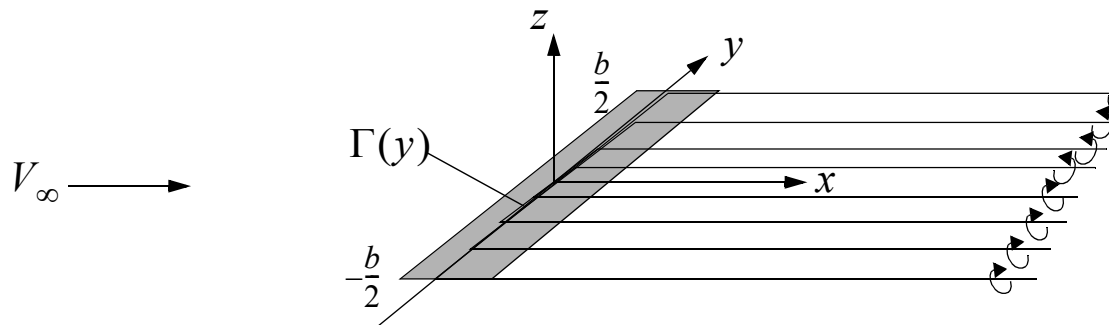
2) Flight test data from prototype aircraft:

- Expensive and late in the design process, but still of vital importance for aircraft certification.
- Flight tests data represent the final proof of the design.
- Provide the designer with a last opportunity to “fine tune” the design, fix problems, or “design out” potential problems discovered during flight tests.
- This data is then added to the manufacturer’s data base for use in the next (or future) design(s).

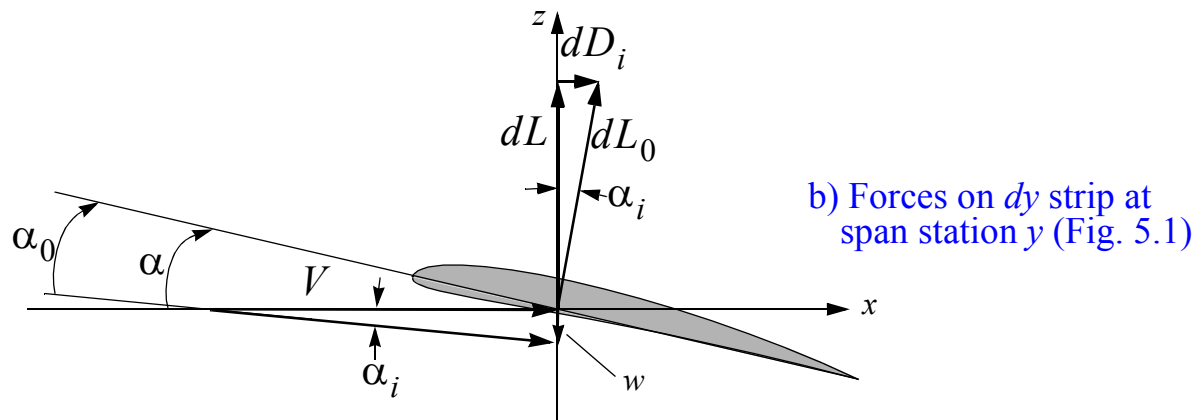


5.3 Prandtl's Lifting Line Theory

- For straight wings of moderate to high aspect ratio, the lifting line theory developed by Prandtl yields results of sufficient accuracy for use in preliminary design.
- For a brief review of the basic formulation, see Sec. 2.6.1.



a) Superposition of horseshoe vortices along quarter chord line



b) Forces on dy strip at span station y (Fig. 5.1)

Fig. 5.2 Prandtl's lifting line theory.

5.3.1 Formulation

- In the lifting line approximation, $\Gamma(y)$ is related to the downwash $w(y)$ on the wing along the quarter-chord line (line of aerodynamic centers), through Prandtl's integral equation:

$$w(y) = \frac{1}{4\pi} \int_{-b/2}^{b/2} \frac{d\Gamma(y_1)}{dy_1} \frac{dy_1}{y - y_1} \quad (5.1)$$

- The induced downwash at the quarter chord gives rise to a corresponding reduction of the local angle of attack, Fig. 5.2, and

$$\alpha = \alpha_0 + \alpha_i \quad (5.2)$$

- Here α_0 is the “effective” angle of attack and α_i is the “induced angle of attack”, given by

$$\alpha_i = \tan^{-1}(w/V) \cong w/V \quad (5.3)$$

$$\alpha_i(y) = \frac{1}{4\pi V} \int_{-b/2}^{b/2} \frac{d\Gamma(y_1)}{dy_1} \frac{dy_1}{(y - y_1)} \quad (5.4)$$



Induced Drag

- The induced drag arises from this redefinition of the local flow angle.
- From Fig. 5.2 we see that the differential forces on a spanwise strip dy at station y is

$$dD_i = dL_0 \sin \alpha_i \approx dL_0 \alpha_i \approx \alpha_i dL \quad (5.5)$$

since $dL = dL_0 \cos \alpha_i \approx dL_0$; see Fig. 5.2b.

- For wings of high aspect ratio, it is reasonable to assume that the spanwise lift distribution can be written in the form

$$\frac{dL}{dy} = c_{l_\alpha} q c [\alpha_{zL}(y) - \alpha_i(y)] \quad (5.6)$$

where α_{zL} is the local geometric angle of attack, measured with respect to the zero lift angle of attack, and c_{l_α} is the local 2D lift curve slope of the wing.



Prandtl's Equation

- The following integro-differential equation is then obtained,

$$\Gamma = \frac{1}{2} c_{l_\alpha} V c \left[\alpha_{zL}(y) - \frac{1}{4\pi V} \int_{-b/2}^{b/2} \frac{d\Gamma(y_1)}{dy_1} \frac{dy_1}{(y-y_1)} \right] \quad (5.7)$$

- The solution of Eq. (5.7) can be most easily obtained by the *inverse method*, by assuming a given spanwise lift or circulation $\Gamma(y)$ and calculating the required wing geometric twist distribution $\alpha_{zL}(y)$ from Eq. (5.7).
- Max Munk showed that the *elliptic lift distribution* corresponding to

$$\Gamma(y) = \Gamma_0 \sqrt{1 - \left(\frac{2y}{b}\right)^2} \quad (5.8)$$

yields a constant downwash w and hence also a constant induced angle of attack α_i over the wing span.



Solution for Elliptic Loading

- The complete solution becomes (see Eqs. (2.46-57)):

$$C_L = \frac{\pi}{2} \frac{\Gamma_0 b}{V S} \quad (5.9)$$

$$\Gamma_0 = \frac{2 V S}{b \pi} C_L \quad (5.10)$$

$$\alpha_i = \frac{w}{V} = \frac{\Gamma_0}{2 b V} \quad (5.11)$$

$$\alpha_i = \frac{2 V S}{2 b \pi b V} C_L = \frac{C_L}{\pi A} \quad (5.12)$$

$$A = b^2/S = \text{aspect ratio}$$

$$D_i = C_L q S \alpha_i = \frac{C_L^2}{\pi A} q S = C_{D_i} q S \quad (5.13)$$

$$C_{D_i} = \frac{C_L^2}{\pi A} \quad (5.14)$$



Optimal Properties of Elliptic Lift Distribution

- Munk showed [2] that the elliptic spanwise lift distribution is optimal, in the following sense:
 - For a given lift L , the lowest induced drag is obtained when the spanwise distribution of lift is elliptic.
 - It can be shown that this result also applies to *general* lifting surfaces in subsonic flow:

To minimize induced drag, the wing should be designed so as to produce an elliptic spanwise distribution of lift.

The chordwise lift distribution does not matter in this respect.

- Most wings are not of the elliptic type, because the improvement in induced drag cannot typically be justified by the added manufacturing costs
- A judicious choice of wing taper ratio will result in a wing with induced drag of only a few percent above the theoretical minimum.



5.3.2 Fourier Series Solution

- In the general case, let

$$y = \frac{b}{2} \cos \theta, \quad 0 \leq \theta \leq \pi \quad (5.15)$$

then the circulation can always be represented as a Fourier sine series,

$$\Gamma = V_\infty b \sum_{n=1}^{\infty} A_n \sin n\theta \quad (5.16)$$

- If we restrict ourselves to an even lift distribution, $\Gamma(-y) = \Gamma(y)$, then it follows that $A_n = 0$ whenever n is an even integer
- For the general case (which includes maneuvers) both even and odd terms contribute to the expansion (5.16).



Lift

- The lift is then

$$\begin{aligned} L &= \rho_\infty V_\infty \int_{-b/2}^{b/2} \Gamma(y) dy = \rho_\infty V_\infty^2 b \int_{-\pi/2}^{\pi/2} \sum_{n=1}^{\infty} A_n \sin n\theta \left(-\frac{b}{2}\right) \sin \theta d\theta \\ &= \frac{1}{2} \rho_\infty V_\infty^2 b^2 \sum_{n=1}^{\infty} A_n \int_0^\pi \sin n\theta \sin \theta d\theta = \frac{\pi}{4} \rho_\infty V_\infty^2 b^2 A_1 \end{aligned} \quad (5.17)$$

from which we conclude that the lift coefficient is given by

$$C_L = \frac{\pi b^2}{2S} A_1 = \frac{\pi A}{2} A_1 \quad (5.18)$$

where A is the aspect ratio of the wing.

- Although the higher terms in the Fourier series do not contribute to the *overall* lift coefficient of the wing, they do affect the *local* or section lift coefficient at a given span location y , since

$$c_l(y) = \frac{2b}{c} \sum_{n=1}^{\infty} A_n \sin n\theta \quad (5.19)$$



Induced Drag

- The induced drag can be calculated from the sectional relation

$$dD_i = \alpha_i dL = \left\{ \frac{1}{4\pi V_\infty} \int_{-b/2}^{b/2} \frac{d\Gamma(y_1)}{dy_1} \frac{dy_1}{(y - y_1)} \right\} \rho_\infty V_\infty \Gamma(y) dy \\ = \frac{1}{2} \rho_\infty V_\infty^2 c_{d_i} c dy \quad (5.20)$$

- Solving for the sectional induced drag coefficient, we get

$$c_{d_i}(y) = \frac{\Gamma(y)}{2\pi c V_\infty^2} \int_{-b/2}^{b/2} \frac{d\Gamma(y_1)}{dy_1} \frac{dy_1}{(y - y_1)} \quad (5.21)$$

- The integral can be evaluated using the same procedure as in Sec. 2.6.1, after substituting from Eq. (5.16) and changing variables to

$$y = \frac{b}{2} \cos \varphi, \quad y_1 = \frac{b}{2} \cos \theta \quad (5.22)$$



Induced Drag Coefficient

- Using the Glauert integral, Eq. (2.53), we obtain

$$c_{d_i}(y) = \frac{b}{c} \left(\sum_{m=1}^{\infty} A_m \sin m\varphi \right) \left(\sum_{n=1}^{\infty} nA_n \frac{\sin n\varphi}{\sin \varphi} \right) \quad (5.23)$$

- The induced drag coefficient for the wing is found by integrating over the span,

$$\begin{aligned} C_{D_i} &= \frac{1}{S} \int_{-b/2}^{b/2} c_{d_i}(y) c(y) dy = \frac{b^2}{2S} \int_0^{\pi} \left(\sum_{m=1}^{\infty} A_m \sin m\varphi \right) \left(\sum_{n=1}^{\infty} nA_n \frac{\sin n\varphi}{\sin \varphi} \right) \sin \varphi d\varphi \\ &= \frac{b^2}{2S} \sum_{m=1}^{\infty} \sum_{n=1}^{\infty} nA_m A_n \int_0^{\pi} \sin m\varphi \sin n\varphi d\varphi = \frac{\pi b^2}{4S} \sum_{n=1}^{\infty} nA_n^2 = \frac{\pi A}{4} \sum_{n=1}^{\infty} nA_n^2 \end{aligned} \quad (5.24)$$

where A is the aspect ratio.

- The last expressions follow from the fact that the integral is zero except when $m = n$. The induced drag becomes

$$D_i = \frac{1}{2} \rho_{\infty} V_{\infty}^2 C_{D_i} S = \frac{\pi}{8} \rho_{\infty} V_{\infty}^2 b^2 \sum_{n=1}^{\infty} nA_n^2 \quad (5.25)$$



Design Formulas Elliptic Case

- If the lift distribution is elliptic, then all coefficients except A_1 in the series (5.16) are zero, and we obtain

$$\begin{aligned} C_L &= \frac{\pi A}{2} A_1 \\ C_{D_i} &= \frac{\pi A}{4} A_1^2 = \frac{C_L^2}{\pi A} \end{aligned} \tag{5.26}$$

- This is clearly a minimum for the induced drag at a given lift, since it is obvious from Eqs. (5.24-25) that:

Every one of the higher harmonics in the series (5.16) adds a positive drag term without adding any lift.

- Oswald (Ref. 2.7) introduced a “wing efficiency factor” to account for the drag penalty incurred for non-elliptic wings, as follows

$$C_{D_i} = \frac{C_L^2}{\pi e A} \tag{5.27}$$

$$\begin{aligned} e &= \text{wing efficiency factor} \\ eA &= \text{effective aspect ratio} \end{aligned} \tag{5.28}$$



Glauert Factors Nonelliptic Lift Distributions

- Glauert (Ref. 2.8) introduced the following correction factors to account for a nonelliptic lift distribution:

$$\alpha_i = \frac{C_L}{\pi A} (1 + \tau) \quad (5.29)$$

$$C_{D_i} = \frac{C_L^2}{\pi A} (1 + \delta) \quad (5.30)$$

- We are now in a position to obtain an expression for δ in terms of the expansion coefficients in Eq. (5.16).
- Comparing Eqs. (5.24, 26, 30), we conclude that

$$\delta = \sum_{n=2}^{\infty} n \left(\frac{A_n}{A_1} \right)^2 \quad (5.31)$$

- If the coefficients of the Fourier expansion for $\Gamma(y)$ or the lift distribution are known, Eq. (5.31) makes it possible to calculate the drag correction factor δ .



Numerical Solution General Case

- To find the coefficients and hence the solution for a given wing, we substitute Eq. (5.16) into Eq. (5.7).
- After some simplification using Glauert's integral, we obtain the equation

$$V_\infty b \sum_{n=1}^{\infty} A_n \sin n\theta = \frac{1}{2} c_{l_\alpha} V c \left[\alpha_{zL}(\theta) - \frac{1}{2} \sum_{n=1}^{\infty} n A_n \frac{\sin n\theta}{\sin \theta} \right] \quad (5.32)$$

or

$$\sum_{n=1}^{\infty} \left[1 + \frac{n c_{l_\alpha} c(\theta)}{4b \sin \theta} \right] A_n \sin n\theta = \frac{1}{2b} c_{l_\alpha} c(\theta) \alpha_{zL}(\theta) \quad (5.33)$$

- If a sectional lift curve slope of 2π is assumed, then Eq. (5.33) becomes

$$\sum_{n=1}^{\infty} \left[1 + \frac{n \pi c(\theta)}{2b \sin \theta} \right] A_n \sin n\theta = \frac{\pi}{b} c(\theta) \alpha_{zL}(\theta) \quad (5.34)$$



Collocation Solution

- Eq. (5.34) can be solved by evaluating the equation at a number of spanwise locations equal to the number of terms kept in the series expansion.
- The result is a set of linear equations for the unknown coefficients A_n .
- For wings with a symmetric load distribution, only odd terms in Eq. (5.34) survive, as already mentioned.
- It then suffices to consider only half of the span and take the collocation points as

$$y_k = \frac{b}{2} \cos \theta_k, \quad 0 \leq \theta_k \leq \frac{\pi}{2} \quad (5.35)$$

- If we take the first N odd terms of the expansion, then

$$\theta_k = \frac{\pi k}{2N}, \quad k = 1, 2, \dots, N \quad (5.36)$$

- For example, with $N = 4$, we would use $\pi/8, \pi/4, 3\pi/8$ and $\pi/2$. This would correspond to the first 7 terms in the general equation (5.34) (since $A_2 = A_4 = A_6 = 0$).



Example: Tapered Wing with Washout

(von Mises, *Theory of Flight*, Ref. 3)

- In this example, both the chord and the angle of attack decrease linearly from the root to the tip, taking on half the root values at the tip.
- In terms of the angle variable $\theta = \cos^{-1}(2y/b)$,

$$c(\theta) = c_r \left(1 - \frac{1}{2} \cos \theta\right) \quad (5.37)$$

$$\alpha_{zL}(\theta) = \alpha_r \left(1 - \frac{1}{2} \cos \theta\right)$$

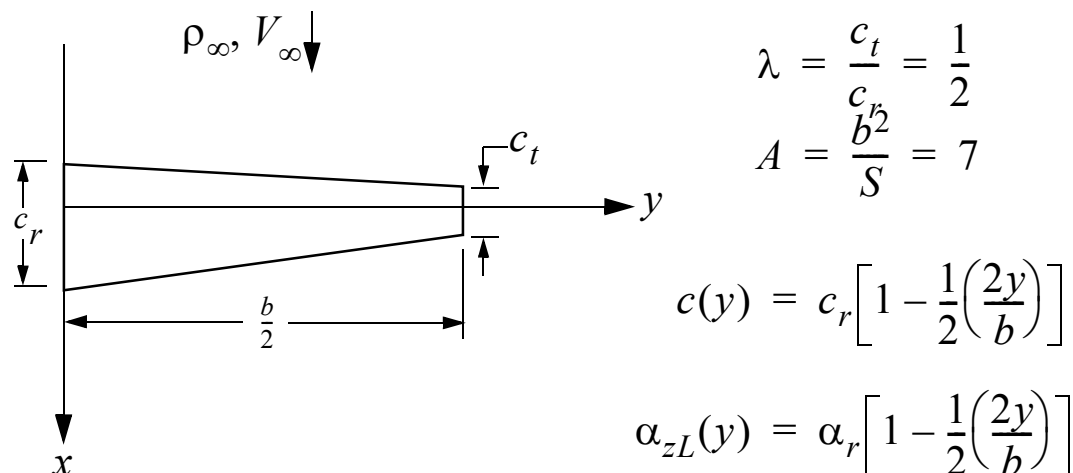


Fig. 5.3 Tapered wing with twist (washout).



Truncated Fourier Solution (4-Term)

- Equation (5.34) becomes, using the first 4 nonzero terms:

$$\sum_{n=1}^7 \left[1 + \frac{n\pi c(\theta)}{2b \sin \theta} \right] A_n \sin n\theta = \frac{\pi}{b} c(\theta) \alpha_{zL}(\theta) \quad (5.38)$$

- For a linearly tapered wing, the aspect ratio can be expressed as

$$A = \frac{2b}{c_r(1 + \lambda)} \quad (5.39)$$

from which it follows that $2b/c_r = A(1 + \lambda) = 7(1 + 1/2) = 21/2$ for this wing.

- Equation (5.38) can now be written in expanded form as

$$\begin{aligned} & \left[1 + \frac{2\pi(1 - \frac{1}{2}\cos\theta)}{21 \sin\theta} \right] A_1 \sin\theta + \left[1 + \frac{6\pi(1 - \frac{1}{2}\cos\theta)}{21 \sin\theta} \right] A_3 \sin 3\theta + \\ & \left[1 + \frac{10\pi(1 - \frac{1}{2}\cos\theta)}{21 \sin\theta} \right] A_5 \sin 5\theta + \left[1 + \frac{14\pi(1 - \frac{1}{2}\cos\theta)}{21 \sin\theta} \right] A_7 \sin 7\theta \\ & = \frac{4}{21} \pi \alpha_r (1 - \frac{1}{2}\cos\theta)^2 \end{aligned} \quad (5.40)$$



Collocation

- To get a numerical solution, we satisfy the equation at the 4 collocation points given by

$$\theta_k = \frac{\pi k}{2N} = \frac{\pi k}{8}, \quad k = 1, 2, 3, 4 \quad (5.41)$$

- The result is a set of linear equations, which can be written in matrix form as

$$[C]\{A\} = \{B\} \quad (5.42)$$

where the coefficient matrix $[C]$ has terms given by

$$C_{kn} = \left[1 + (2n - 1) \frac{2}{21} \pi \frac{(1 - \frac{1}{2} \cos \frac{\pi k}{8})}{\sin \frac{\pi k}{8}} \right] \sin \left[(2n - 1) \frac{\pi k}{8} \right] \quad (5.43)$$

and the column vectors $\{A\}$ and $\{B\}$ are given by

$$\{A\} = \begin{Bmatrix} A_1 \\ A_3 \\ A_5 \\ A_7 \end{Bmatrix}; \quad \{B\} = \begin{Bmatrix} B_1 \\ B_2 \\ B_3 \\ B_4 \end{Bmatrix}; \quad B_k = \frac{4}{21} \pi \alpha_r (1 - \frac{1}{2} \cos \frac{\pi k}{8})^2 \quad (5.44)$$



Numerical Solution

- The solution of the linear equations (5.42) involves the inversion of the coefficient matrix, (which is readily done using available software packages), and

$$\{A\} = [C]^{-1}\{B\} \quad (5.45)$$

- Using information from the example in Ref. 3, the following solution is obtained:

$$\{A\} = \begin{Bmatrix} A_1 \\ A_3 \\ A_5 \\ A_7 \end{Bmatrix} = \frac{4}{21}\pi\alpha_r \begin{Bmatrix} 0.585 \\ -0.056 \\ 0.037 \\ -0.012 \end{Bmatrix} = \alpha_r \begin{Bmatrix} 0.3501 \\ -0.0335 \\ 0.0221 \\ -0.0072 \end{Bmatrix} \quad (5.46)$$

- The lift coefficient becomes, Eq. (5.18),

$$C_L = \frac{\pi A}{2} A_1 = \frac{\pi(7)}{2}(0.3501\alpha_r) = 3.85\alpha_r \Rightarrow C_{L_\alpha} = 3.85 \quad (5.47)$$



- The induced drag is obtained from Eq. (5.24):

$$\begin{aligned}
 C_{D_i} &= \frac{\pi A}{4} \sum_{n=1}^7 n A_n^2 \\
 &= \frac{7\pi}{4} \{ 0.3501^2 + (3)(0.0335)^2 + (5)(0.0221)^2 + (7)(0.0072)^2 \} \alpha_r^2 \\
 &= 0.708 \alpha_r^2
 \end{aligned} \tag{5.48}$$

- If we calculate the Glauert drag correction factor δ using Eq. (5.31), we obtain

$$\delta = \sum_{n=2}^7 n \left(\frac{A_n}{A_1} \right)^2 = \frac{(3)(0.0335)^2 + (5)(0.0221)^2 + (7)(0.0072)^2}{0.3501^2} = 0.0504 \tag{5.49}$$

- This value appears somewhat high, and casts doubt on the accuracy of the values for the A_n 's listed in von Mises' book, where a more reasonable value of $\delta = 0.014$ is also stated but not explicitly calculated.
- As a check, we recalculate C_{D_i} using Eq. (5.30)

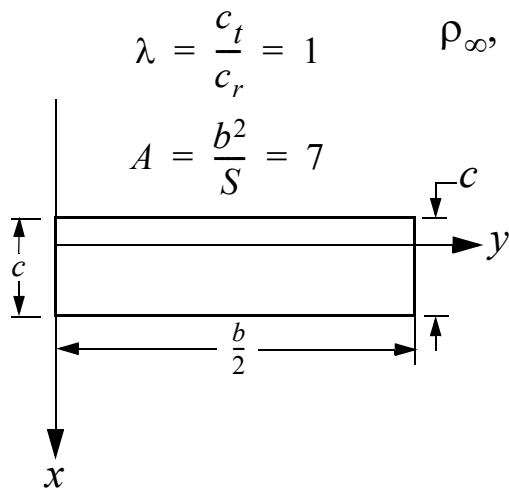
$$C_{D_i} = \frac{C_L^2}{\pi A} (1 + \delta) = \frac{(3.85 \alpha_r)^2}{7\pi} (1 + 0.0504) = 0.708 \alpha_r^2 \tag{5.50}$$

which is higher than the solution of $0.68 \alpha_r^2$ given in von Mises' book.



Computer Calculation of von Mises Wing Examples

- A Fortran program was written to solve the lifting line equation for the tapered wing with linear washout, using the method of collocation.
- The system of equations was solved using the IMSL routine DSLARG.



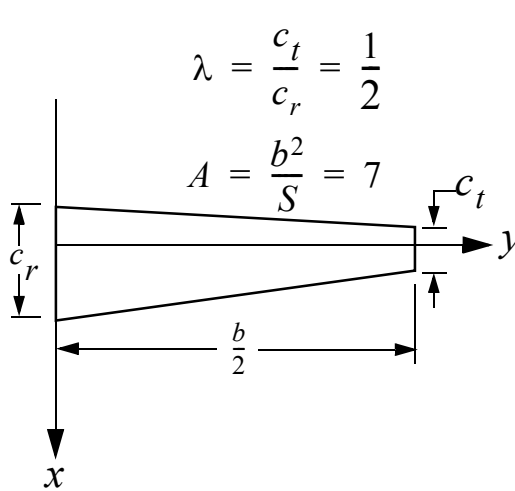
Examples a) and b):

Rectangular wing (zero taper)

Wing a): Zero twist

Wing b): 2.5° linear washout:

$$\alpha_{zL}(y) = \alpha_r \left[1 - \frac{1}{2} \left(\frac{2y}{b} \right) \right]$$



Examples c) and d):

Unswept tapered wing

$$c(y) = c_r \left[1 - \frac{1}{2} \left(\frac{2y}{b} \right) \right]$$

Wing c): Zero twist

Wing d): 2.5° linear washout:

$$\alpha_{zL}(y) = \alpha_r \left[1 - \frac{1}{2} \left(\frac{2y}{b} \right) \right]$$

Fig. 5.4 The von Mises example wings,
Ref. 3, pp. 254-256.



Table 5.1: Lifting Line Calculations^a - von Mises Wings

	C_L	C_{D_i}	δ	$C_{L\alpha}$	$\alpha_{L=0}$	$C_L^{[3]}$	$C_{D_i}^{[3]}$
Wing a)	0.40986	0.00806	0.05546	4.6966	0°	0.410	0.00806
Wing b)	0.31938	0.00468	0.00956	4.8052	1.19°	0.319	0.00472
Wing c)	0.42336	0.00825	0.01252	4.8514	0°	0.422	0.00807
Wing d)	0.33597	0.00540	0.05159	4.9563	1.11°	0.335	0.00518

a. Using first 4 nonzero terms and assuming $\alpha_r = 5^\circ$.

Table 5.2: Convergence of Lifting-Line Solution vs. N

	Wing a) $N=4$	Wing a) $N=10$	Wing a) $N=20$	Wing d) $N=4$	Wing d) $N=10$	Wing d) $N=20$	Wing d) $N=30$
C_L	0.40986	0.41018	0.41018	0.33597	0.33110	0.33040	0.33027
C_{D_i}	0.00806	0.00809	0.00809	0.00534	0.00518	0.00515	0.00515
δ	0.05546	0.05800	0.05806	0.05159	0.03948	0.03776	0.03746
$C_{L\alpha}$	4.6966	4.7003	4.7004	4.9563	4.9387	4.9357	4.9351



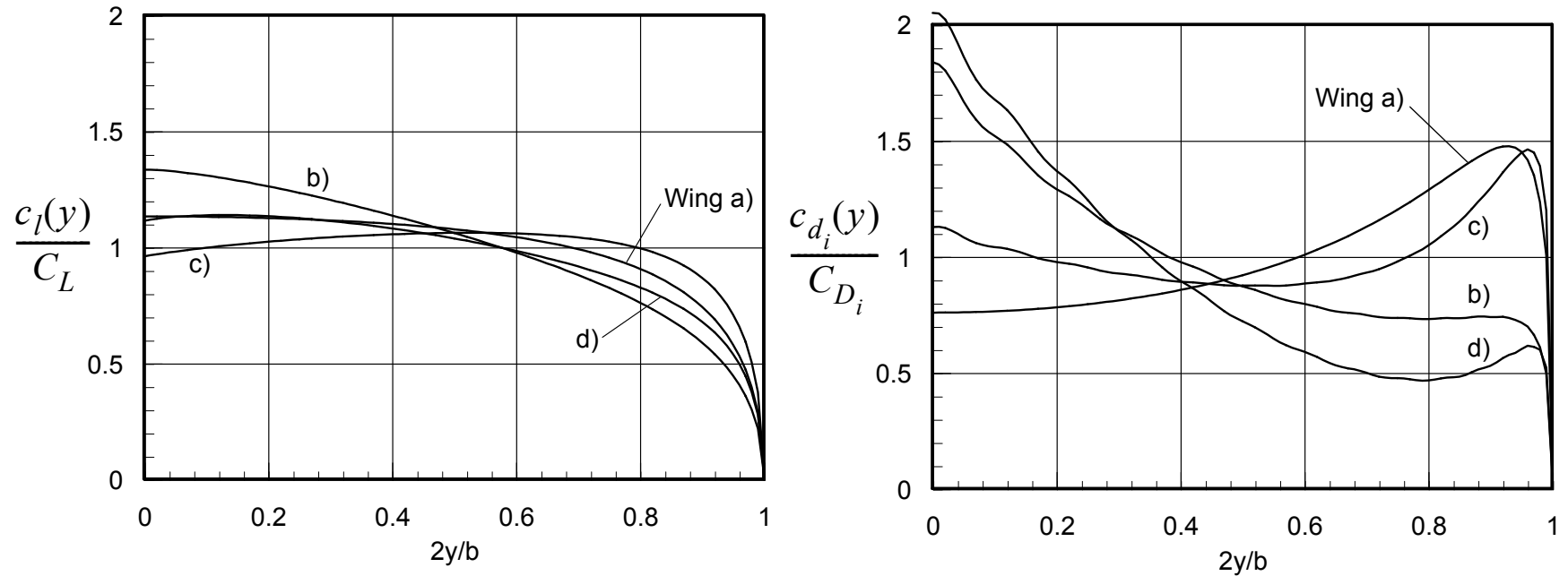


Fig. 5.5 Spanwise variation of lift and induced drag coefficients for wings (a-d).

Glauert Correction Factors

- Using the collocation solution method, values for the Glauert correction factors τ and δ can be computed for any combination of aspect ratio, taper, and washout.
- In preliminary design calculations, an upper limit of $e \leq 0.85$ should be imposed, to provide a performance margin for design uncertainties.
- The parasite drag typically contains a small term that depends on the angle of attack and hence L , because of the sensitivity of the boundary layer to α and L .
- In Oswald's definition, this term is included in the wing efficiency, and we write, using the notation of Perkins and Hage,

$$C_{D_P} = C_{D_{min}} + k'' C_L^2 \quad (5.51)$$

$$C_D = C_{D_{min}} + k'' C_L^2 + \frac{C_L^2}{\pi A} (1 + \delta) = C_{D_{min}} + \frac{C_L^2}{\pi e A} \quad (5.52)$$

$$e = \frac{1}{1 + \delta + \pi A k''} \quad (5.53)$$

where k'' is a small constant (of the order of 0.01 or less) that can be determined directly from curve-fitting a parabola to the two-dimensional wind tunnel data for the airfoil.



Lift Curve Slope

- The lift curve slope can be obtained most easily by differentiating both sides of

$$\alpha = \alpha_0 + \alpha_i = \alpha_0 + \frac{C_L}{\pi A}(1 + \tau) \quad (5.54)$$

with respect to C_L , to obtain

$$\frac{1}{a} = \frac{1}{a_0} + \frac{1}{\pi A}(1 + \tau) \quad (5.55)$$

- Here

$$a = \frac{dC_L}{d\alpha} = C_{L\alpha} = \text{3D lift curve slope} \quad (5.56)$$
$$a_0 = \frac{dC_L}{d\alpha_0} = \text{2D lift curve slope}$$

- The 3D lift curve slope of the wing then becomes

$$a = \frac{a_0}{1 + \frac{a_0}{\pi A}(1 + \tau)} \quad (5.57)$$



5.3.3 Experimental Validation of Lifting Line Theory

- Probably the best data testing the validity of the lifting line approximation comes from Prandtl's original experiments (translated in NACA Report 116, 1921).
- A series of rectangular wings with the same airfoil, with aspect ratio ranging from 7 down to 1.
- In parts (b) and (d) of the figure, the data is “corrected” for aspect ratio, using the wing with $A = 5$ as the reference wing, and the data replotted by changing the angle of attack for each data point consistent with Eq. (5.56).

$$\alpha \rightarrow \alpha + \frac{C_L}{\pi} \left(\frac{1}{5} - \frac{1}{A} \right) \quad (5.58)$$

and rescaling the drag axis in a similar manner, consistent with Eq. (5.14),

$$C_D \rightarrow C_D + \frac{C_L^2}{\pi} \left(\frac{1}{5} - \frac{1}{A} \right) \quad (5.59)$$

- Although deviations from an elliptic lift distribution were neglected, the data points collapse to a single curve in each case, to within the experimental scatter.



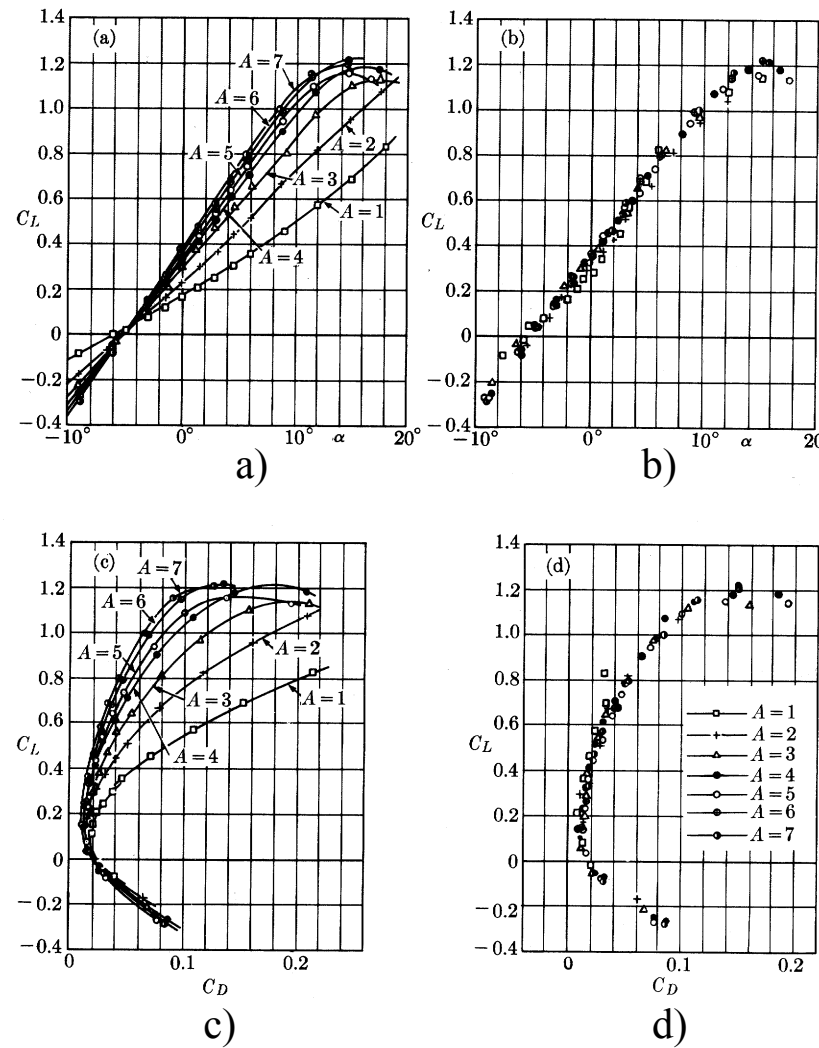


Fig. 5.6 Prandtl's data for lift (a) and drag (c) coefficients vs. angle of attack, for wings of different aspect ratio. In parts (b) and (d), the same data has been corrected for aspect ratio, using $A = 5$ as the reference wing. (Data from NACA Rept. 116, adapted from Ref. 2.12).

5.3.4 Wing Design Calculations: Comparison with Wind Tunnel Data

- Figure 5.7 shows a comparison between wind tunnel data and lifting-line theory for a straight wing of aspect ratio 9.

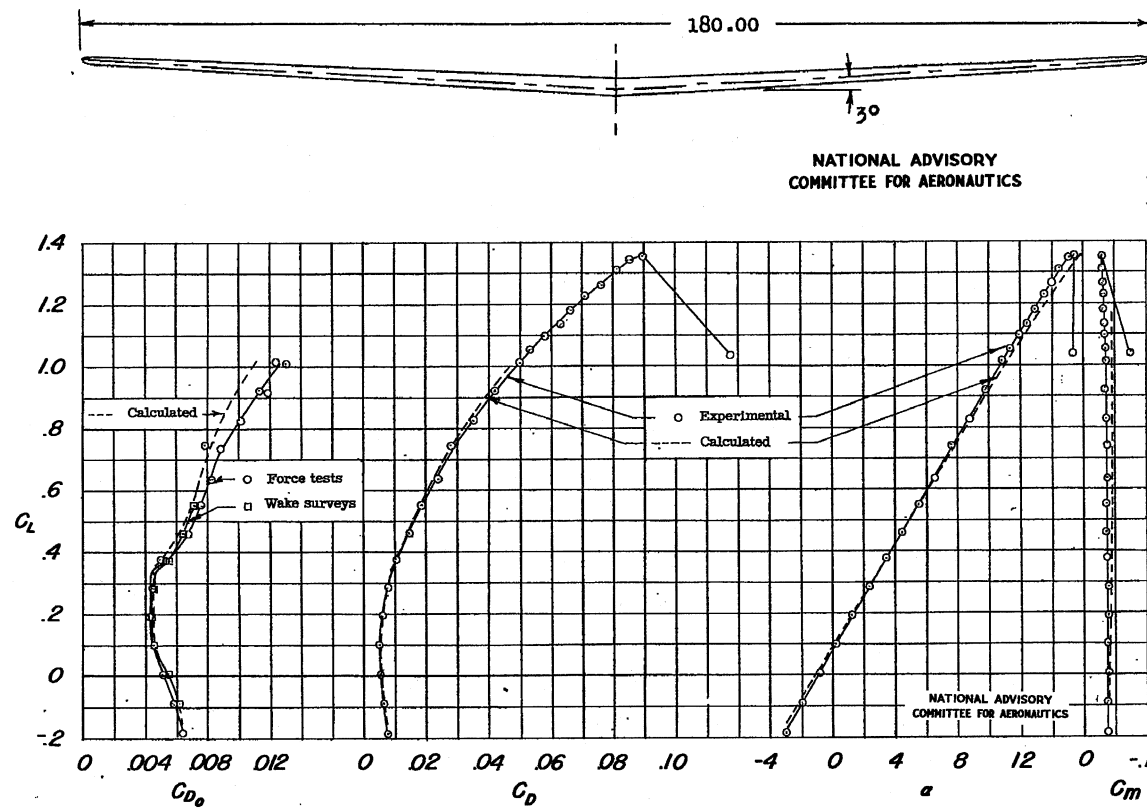


Fig. 5.7 Comparison of lifting line theory and experimental data for the NACA 65-210 wing tested in Ref. 4. ($A = 9$, $\lambda = 0.4$, $\varepsilon = -2^\circ$, $M_\infty \approx 0.17$, $Re \approx 4.4 \times 10^6$).

Remarks

- The wing section is the NACA 65-210 airfoil.
- Lifting line calculations in this comparison were made using the actual nonlinear airfoil section data from wind tunnel tests.
- Agreement between theory and experiment is very good.
- Note that the “drag bucket” observed in the 2-D tests on the NACA 65-210 laminar flow airfoil does not show up on the 3-D drag polar of the wing.
- *This is typical for high Reynolds number wings constructed using normal manufacturing procedures (no extra spit and polish).*



Simplified procedure for determining wing drag polar

- The 2-D drag polar for the NACA 65-210 airfoil is shown in Fig. 5.8, taken from Abbott and von Doenhoff.
- To compare the predicted drag polar to the wind tunnel data, we interpolate between the $R_e = 3 \times 10^6$ and $R_e = 6 \times 10^6$ curves, to obtain an estimate for the corresponding drag polar at the test Reynolds number of 4.4×10^6 .
- The result of a parabolic curve fit (ignoring the drag bucket) gives the following estimates for $c_{d_{min}}$ and k'' :

$$c_{d_{min}} = 0.0060, \quad k'' = 0.0074 \quad (5.60)$$

- Also from the figure,

$$c_l^0 = 0.2 \quad (5.61)$$

- The predicted parasite drag coefficient for the 3-D wing is then

$$\begin{aligned} C_{D_p} &= 0.0060 + 0.0074(C_L - 0.2)^2 \\ &= 0.0063 - 0.0030C_L + 0.0074C_L^2 \end{aligned} \quad (5.62)$$



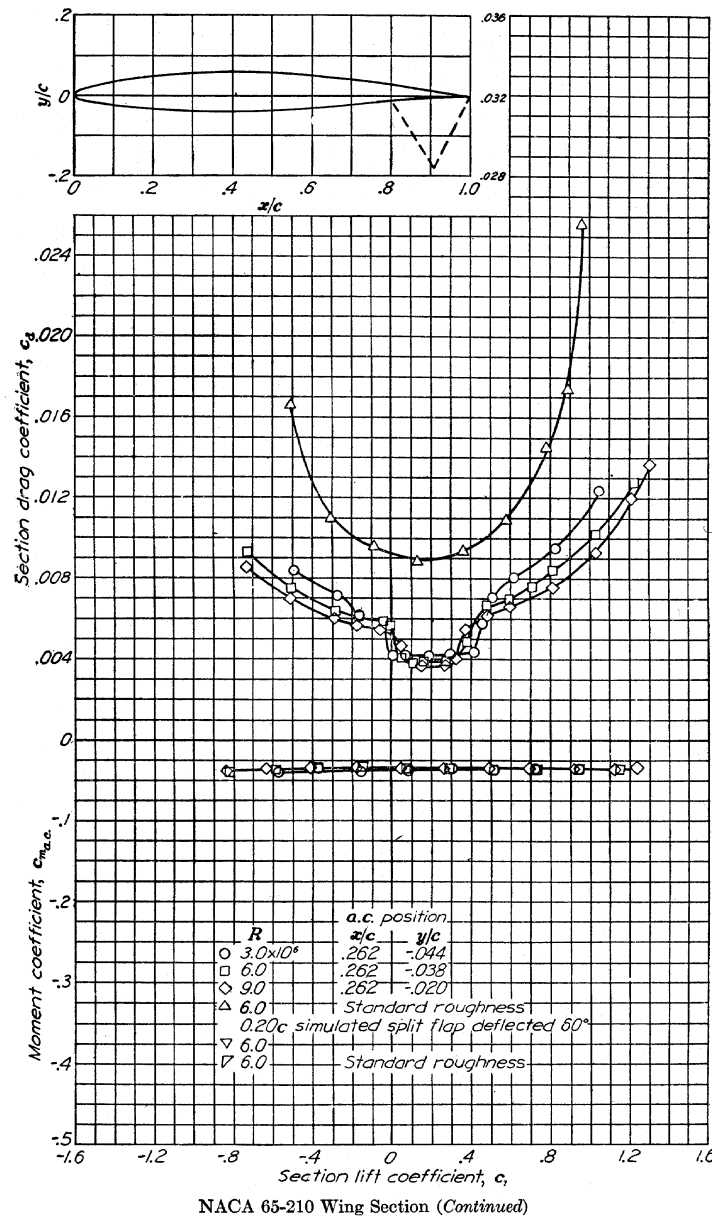


Fig. 5.8 The 2-D drag polar for the NACA 65-210 airfoil. (From Ref. 7).

Common Engineering Approximations

- If we use the common approximation (ignoring linear term) we obtain

$$C_{D_p} = 0.0060 + 0.0074 C_L^2 \quad (5.63)$$

- Adding in the induced drag,

$$C_{D_i} = \frac{C_L^2}{\pi A} (1 + \delta) \quad (5.64)$$

we get, for $A = 9$ and $\delta = 0.0151$ (calculated using the lifting line program, Sec. 5.3, with $\lambda = 0.4$),

$$C_{D_i} = 0.03590 C_L^2 \quad (5.65)$$

- Using approximation (5.63) for the parasite drag, the total drag polar becomes

$$C_D = 0.0060 + 0.04330 C_L^2 \quad (5.66)$$

- A more accurate drag polar would be based on Eq. (5.62), which yields

$$C_D = 0.0063 - 0.0030 C_L + 0.04330 C_L^2 \quad (5.67)$$



A Better Approximation

- For small values of the lift coefficient, the difference between Eqs. (5.66) and (75.67) is negligible.
- At higher C_L 's, the commonly used approximation (7.53) will overpredict the drag somewhat.
- For example, at $C_L = 1$, the difference is 0.0027 (27 drag counts).
- One could of course use the more accurate formula (5.67), but the added accuracy is offset by the disadvantage that most if not all aircraft performance formulas in standard texts assume the simpler form given by Eq. (7.53).
- A quick and not too dirty fix is to simply adjust k'' so that Eqs. (5.66) and (5.67) match at some reference C_L , say at a reasonable design lift coefficient of 0.5.
- For the wing being studied, this results in a “fine-tuned” value of

$$k'' = 0.0050 \quad (5.68)$$

and the simplified fine-tuned drag polar becomes

$$C_D = 0.0060 + 0.04306 C_L^2 \quad (5.69)$$



- The corresponding Oswald efficiency of the wing is calculated as follows:

$$e = \frac{1}{1 + \delta + \pi A k''} = \frac{1}{1 + 0.0151 + \pi(9)(0.0050)} = 0.865 \quad (5.70)$$

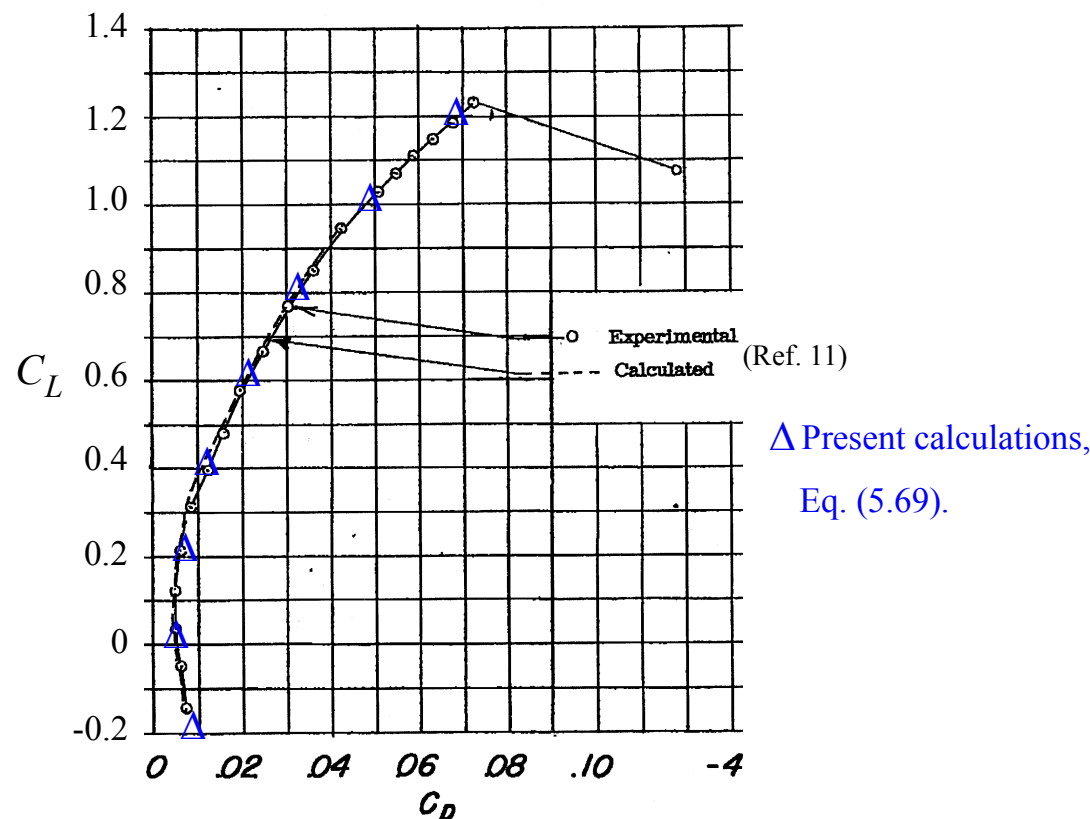


Fig. 5.9 Comparison between predicted and observed drag for the NACA 65-210 wing with zero washout tested in Ref. 11. ($A = 9$, $\lambda = 0.4$, $\varepsilon = 0^\circ$, $M_\infty \approx 0.17$, $Re \approx 4.4 \times 10^6$).

Drag Polar Construction Using CFD Data

- The same procedure can also be used to construct drag polars for more advanced wings, where the induced drag is obtained from a CFD code.
- Although it is possible to calculate a δ factor using Eq. (5.64) and the CFD-calculated C_{D_i} , and then obtain a value for e using Eq. (5.70), it is more convenient to do a curve fit (e.g. cubic splines) to the numerically obtained drag polar.
- This is especially true for transonic and supersonic wings, where the calculated induced drag includes the wave drag and C_{D_i} in the procedure must be replaced by $C_{D_{i+w}}$.
- Also, for these wings the concept of a “wing efficiency” based on the classical lifting line theory is meaningless, since the correct aero theory is nonlinear and fundamentally different.



5.4 Sweepback Theory

- As early as 1935 the German aerodynamicist Busemann noticed that the wave drag of a supersonic wing could be reduced significantly by aft sweep of the leading edge.
- In fact, theoretically at least, *the wave drag vanishes if the leading edge of the wing is swept behind the Mach cone*.

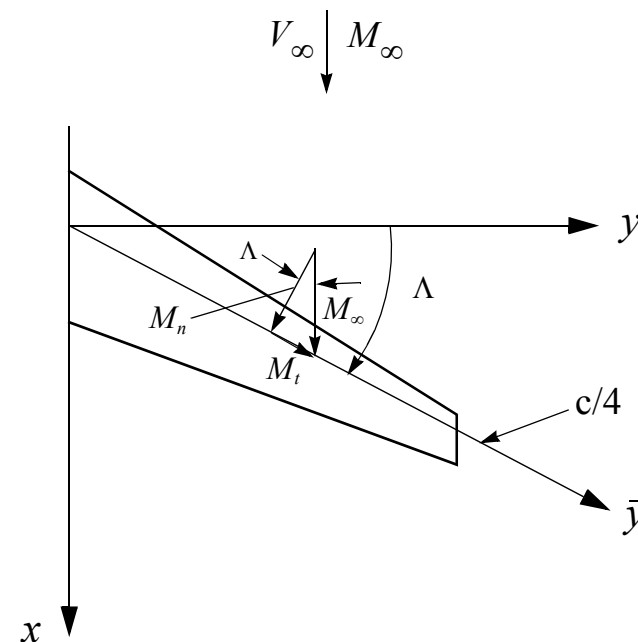


Fig. 5.10 Swept wing.

Performance Implications

- For high speed *subsonic* aircraft, the beneficial aerodynamic effects of sweep are no less important.
- For best range these aircraft should cruise slightly into the drag divergence region, to maximize the range parameter ML/D (jet engine powered aircraft).
- Sweeping the wings aft increases the drag divergence speed by roughly $1/\cos\Lambda$, and hence also the drag divergence Mach number.



Assumptions

- Sweepback theory is based on the assumption that the aspect ratio of the wing is sufficiently large so the “strip theory” assumption is valid and individual wing sections can be assumed independent of each other.
- The flow is resolved into components normal and tangent to the quarter-chord line, as shown in Fig. 5.10:

$$\begin{aligned} M_n &= M_\infty \cos \Lambda \\ M_t &= M_\infty \sin \Lambda \end{aligned} \tag{5.71}$$

- The angle of attack measured with respect to the $c/4$ line is

$$\alpha_n = \alpha_\infty \cos \Lambda \tag{5.72}$$

- In classical sweepback theory, the tangential velocity component is assumed to produce no lift and is ignored.



Lift

- With this assumption, the lift per unit span can be written as

$$l(y) = \frac{dL}{dy} = \frac{1}{2}\rho_\infty V_n^2 c_l^n c = q_\infty \cos^2 \Lambda c_l^n c \quad (5.73)$$

where c_l^n is the local lift coefficient for a wing section taken normal to the quarter-chord line at station y .

- The total lift on the wing can then be expressed as

$$L = q_\infty \cos^2 \Lambda C_L^n S \quad (5.74)$$

$$\begin{aligned} C_L &= C_L^n \cos^2 \Lambda \\ C_{L_\alpha} &= \frac{L}{q_\infty \alpha_n S} = C_{L_\alpha}^n \cos \Lambda \end{aligned} \quad (5.75)$$

- It follows that the critical Mach number and drag divergence Mach number are increased by the factor $1/\cos \Lambda$.
- Sweepback theory must be applied with good engineering judgement, supplemented with wind tunnel data where possible.



Effect of Sweep on Maximum Lift

- Although the relations expressed by Eq. (5.75) are logical from a theoretical standpoint, they do not always correspond to physical reality.
- In particular, the lift coefficient penalty incurred by sweep would suggest that $C_{L_{max}}$ should decrease as $\cos^2\Lambda$ - *not in agreement with wind tunnel data*.
- In fact, many wings show very little sensitivity to sweep angle in this respect; see, for example, the discussion in the text by McCormick.
- Typical wind tunnel results are shown in Fig. 5.11.
- Some authors have argued that the experimental data fits better a $\cos\Lambda$ dependence, but this is rather *ad hoc* and cannot be explained based on any particular theory.



- Because of 3-D effects, the maximum lift coefficient of swept wings is *higher* than would be predicted by classical sweepback theory.

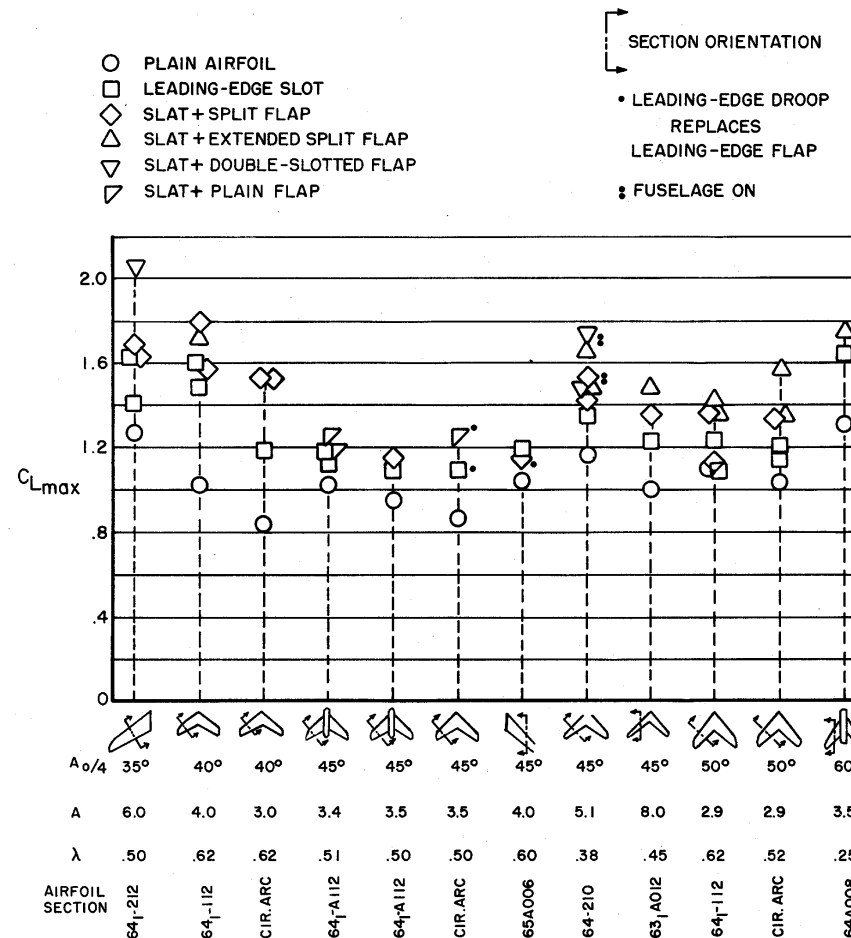


Fig. 5.11 Maximum lift coefficient obtained with various flap-slat systems (NACA TR-1339).

5.5 Spanwise Lift Distribution and Loading Design Requirements

- The determination of the spanwise lift distribution, as well as the sectional (local) coefficient of lift $c_l(y)$, is of importance for three reasons:
 1. To determine if the spanwise lift distribution is close to the optimum elliptic loading.
 2. To determine the stalling characteristics of the wing; that is, where along the span the maximum local lift coefficient is first exceeded and stalling starts.
 3. To determine the internal bending moments and shears for the structural design of the wing.
- Because of *Munk's Stagger Theorem*, the conclusion regarding minimum induced drag (elliptic loading) *holds for wings of any aspect ratio*.
- It also holds for swept wings as well, and for multiple wings (biplanes), wing-canard combinations, etc.



Straight vs. Swept Wings

- For straight wings it is reasonable to use strip theory and assume that local stalling first occurs at the span location y where $c_l(y)$ exceeds $c_{l_{max}}$.
- For tapered wings, that means that $c_{l_{max}}$ decreases towards the tip, on account of the decreasing chord.
- In addition, 3-D effects (spanwise boundary layer flows) tend to amplify the susceptibility towards tip stalls, especially on highly swept wings.
- Tip stalls are especially troublesome on highly swept wings, because they are invariably accompanied by a severe pitch-up of the aircraft.
- The standard design fix for preventing tip stalls is to use washout. For highly flexible swept wings, the structural washout effect is often sufficient to unload the tips and prevent tip stall.



Effect of Taper - Straight Wings

- For the wing in Fig. 5.12, the optimum value is about $\lambda = 0.37$, which yields $\delta = 0.008594$: *The induced drag is only 0.86% above the theoretical minimum.*
- For λ between zero and about 0.05, the induced drag on the tip region of the wing is actually *negative*, because of the strong upwash from the trailing edge vortices from the inboard region.

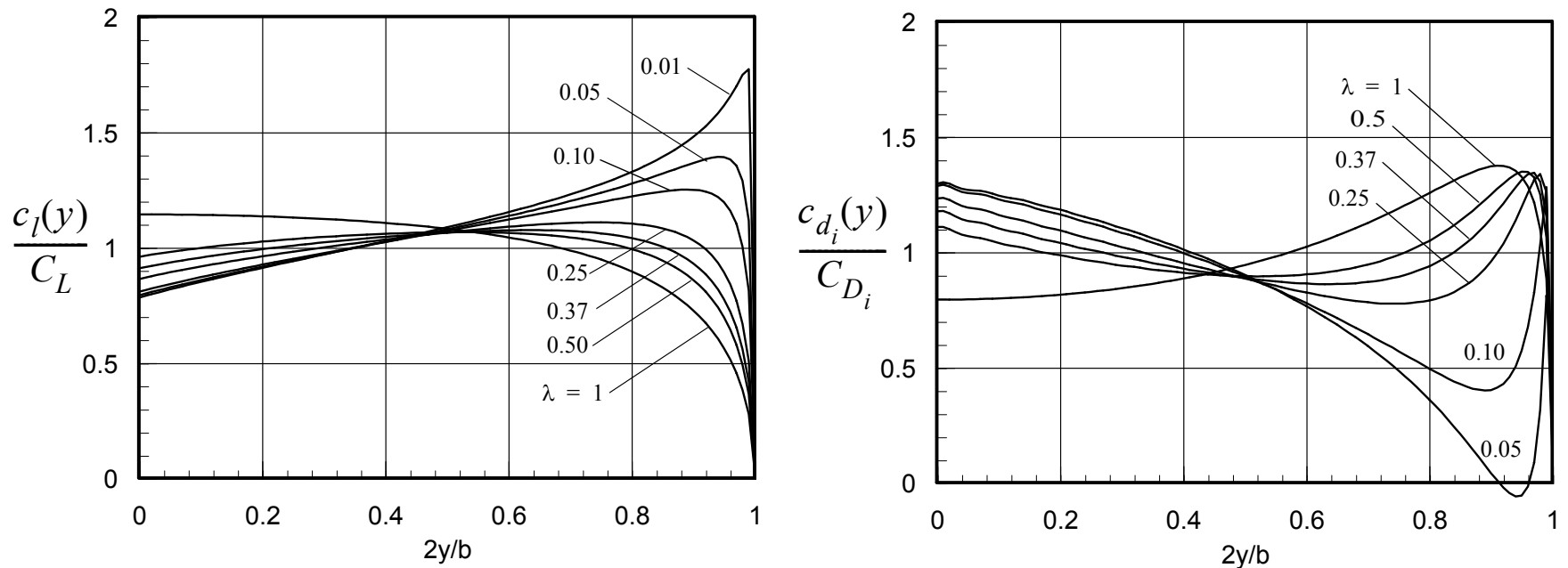


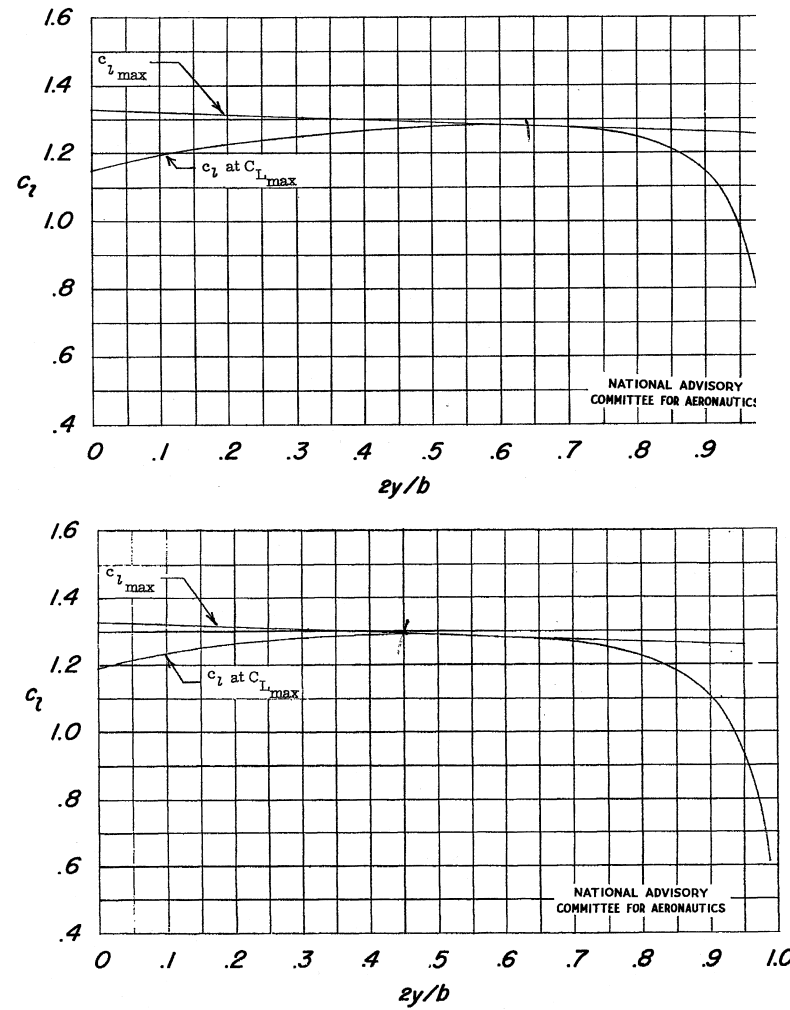
Fig. 5.12 Effect of taper on the spanwise lift and induced drag distribution on a straight wing. (Lifting line calcs., $N = 50$, $A = 6$, $\Lambda = 0$, $\varepsilon = 0$).



Stalling Behavior

- Figure 5.13 shows the predicted stall inception point for the NACA 65-210 wings tested in Ref. 4; see Fig. 5.6.
- Note that the introduction of 2 degrees of washout is predicted to move the stall inception point from about 65% of span to about 45% of span.
- However, it was noted in Ref. 4 that there was not a material difference in the observed stalling behavior (in the wind tunnel) between the two wings.
- The stalling characteristics of all three wings tested are shown in Fig. 5.14.





a) Zero washout

b) 2-degree washout

Fig. 5.13 Spanwise variation of section lift coefficient and maximum section lift coefficient for NACA 65-210 wings tested in Ref. 4. ($A = 9$, $\lambda = 0.4$, $M_\infty \approx 0.17$, $Re \approx 4.4 \times 10^6$).

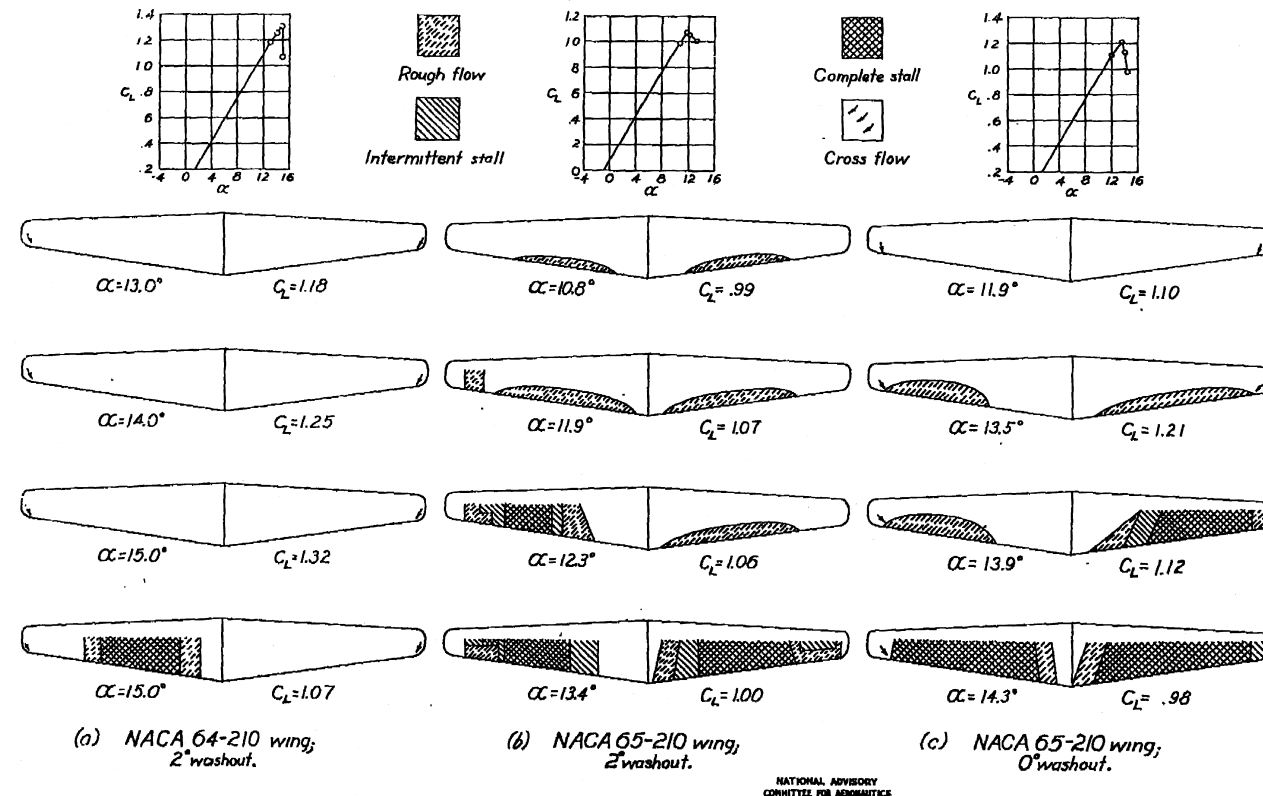


Fig. 5.14 Stalling characteristics of the NACA 64-210 wing and the two NACA 65-210 wings tested in Reference 4. ($A = 9$, $\lambda = 0.4$, $M_\infty \approx 0.17$, $Re \approx 4.4 \times 10^6$).

5.6 Subsonic Lifting Surface Theories

1948-1960+

- For wings of low to moderate aspect ratio, the chordwise loading distribution is also of importance in determining the characteristics of the wing.
- An obvious extension of the Prandtl lifting line theory would be to use a series of “telescoping” horseshoe vortices to model the vorticity on the wing and in the wake (a vortex sheet in the continuous limit).
- Falkner (1948), Watkins, et al. (1959), and others developed integral equation methods for calculating steady and unsteady loads on subsonic wings.
- Since around 1970, more direct “vortex lattice” or “doublet lattice” methods have been developed and implemented on high speed computers.
- These methods are used extensively in preliminary design, since the solutions can be obtained much faster than with modern CFD methods.



Design Charts

- In NACA Report No. 921 (1948), Ref. 2.9, DeYoung and Harper presented an approximate lifting surface method for subsonic wings of arbitrary planform that is of sufficient accuracy to be used in preliminary design.
- Design charts are presented that allow a rapid determination of the lift curve slope, Fig. 2.15.
- The corresponding spanwise lift distribution can also be calculated using the method and design charts presented in NACA Report 921, including the effect of wing washout.



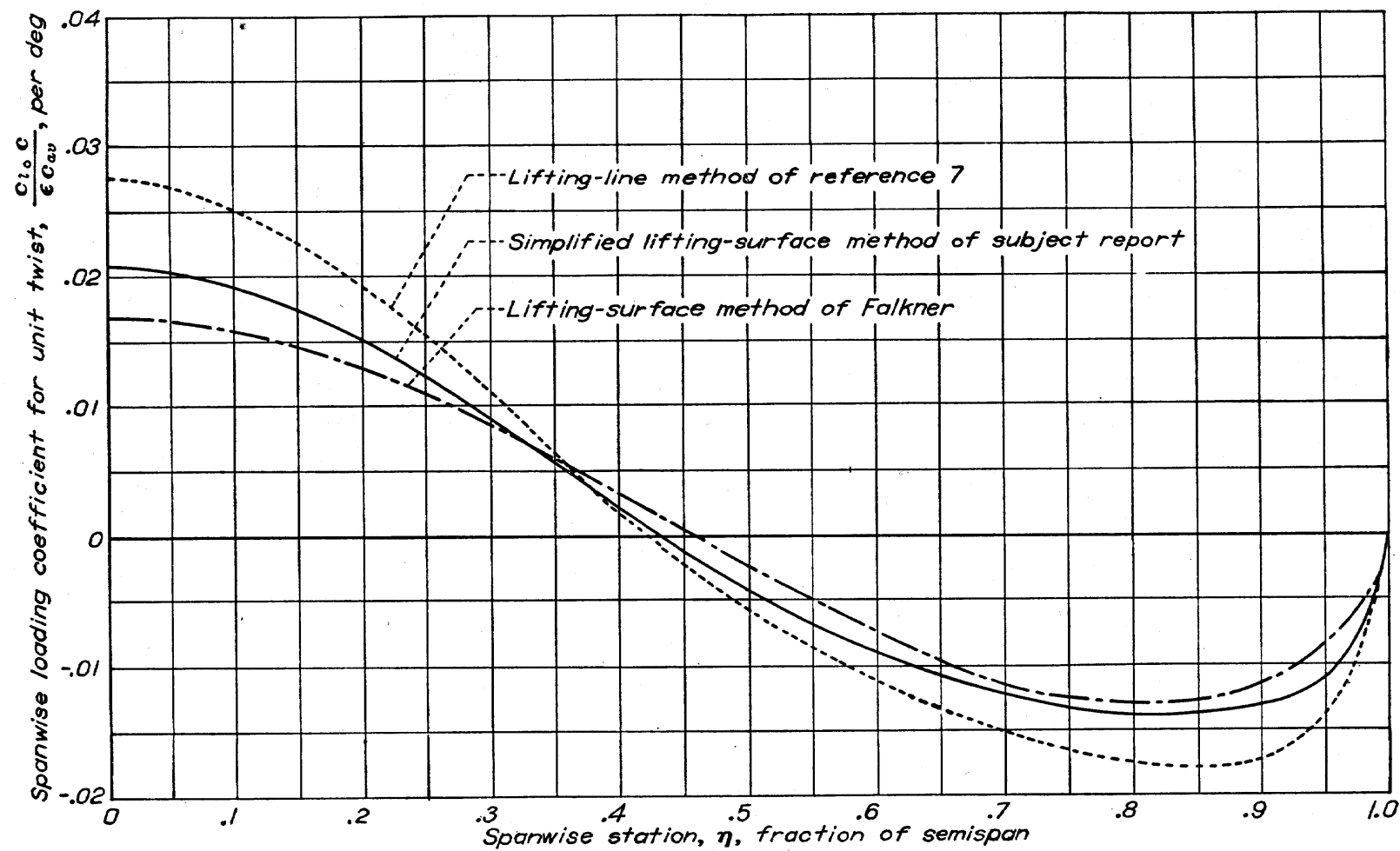


Fig. 5.15 Comparison of spanwise loading predictions for unit twist (washout), for an unswept wing of aspect ratio 6 and taper ratio 0.5.



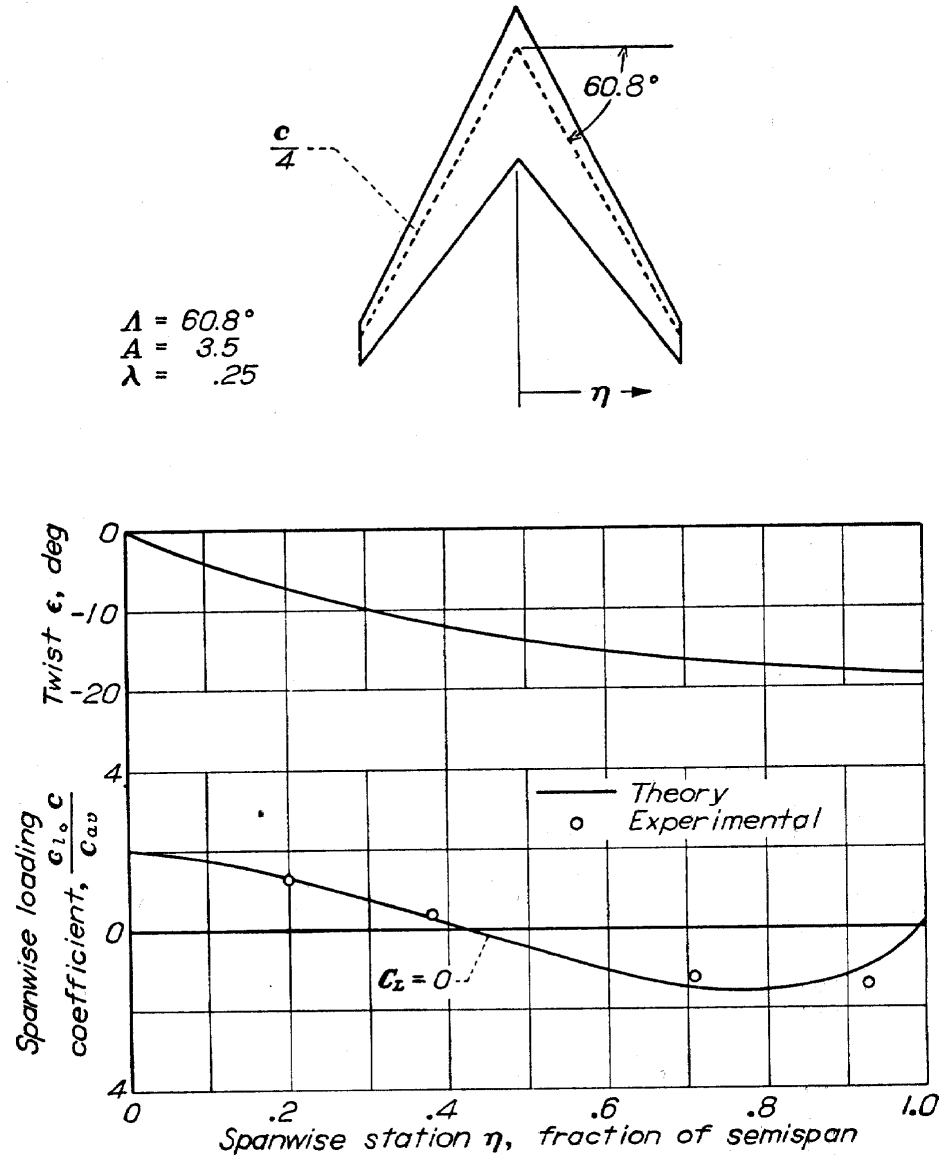


Fig. 5.16 Comparison of predicted vs. experimental spanwise loading distribution for a highly swept wing (NACA Rept. 921).



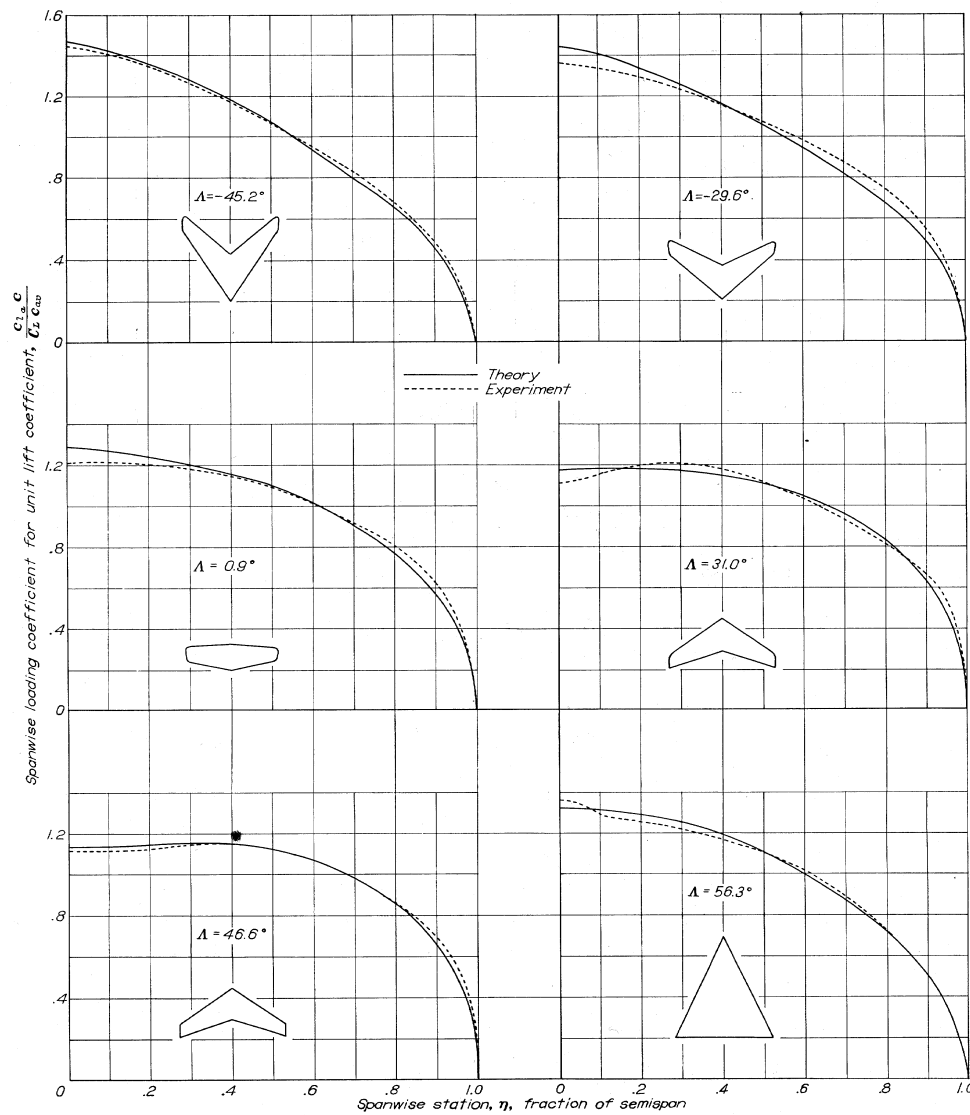


Fig. 5.17 Comparison of predicted vs. experimental spanwise loading distributions for wings of different planform and sweep (NACA Rept. 921).

5.7 Vortex Lattice and Panel Methods

Linear Computer Codes

- These codes emerged as the digital computer became fast enough to solve large linear systems of equations, around the mid-to late 1960s.
- The codes are still used extensively in preliminary design as well as in final design, but are limited to linear flows (small disturbance; thin wings; *no shocks*).
- Because they are relatively easy to write and are very fast on today's computers, they are well suited for the iterative environment of preliminary design.
- The entire aircraft can be modeled without too much trouble and the panel codes generally give good agreement with wind tunnel data, as long as the Mach number is below the transonic range; see, for example, Fig. 5.18.



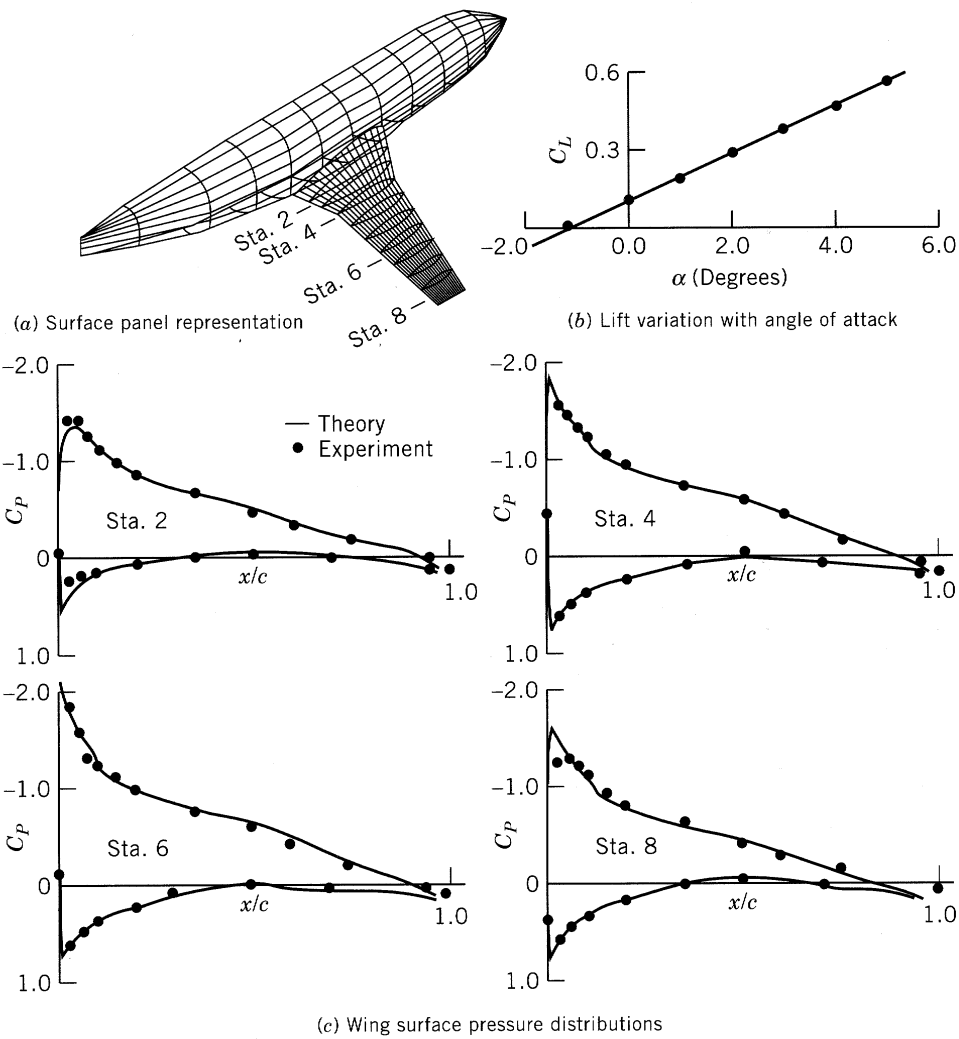


Fig. 5.18 Panel code solution for the flow around a Boeing 737 aircraft, and comparison with experiment. (Adapted from Ref. 7).

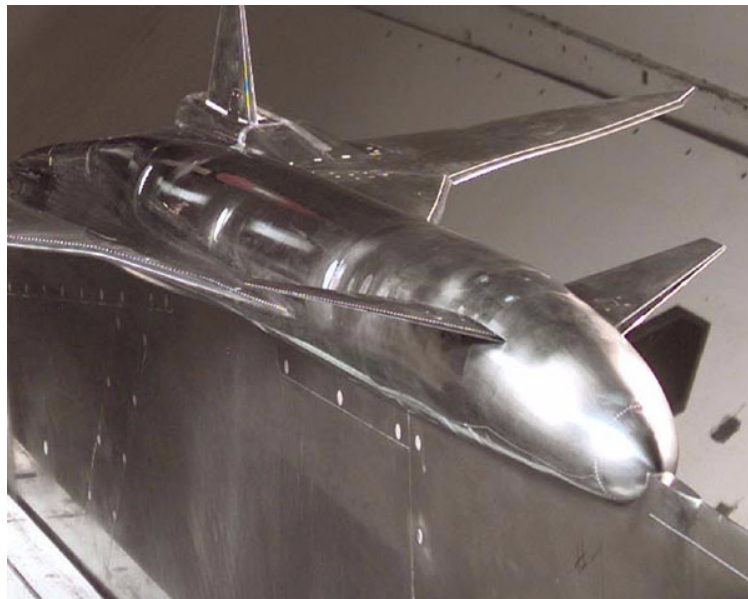
5.8 CFD Methods for Transonic Wings

Present State-of-the-Art

- Design of wings capable of operating efficiently in the transonic region represents the most difficult problem from an aerodynamics standpoint.
- The transonic region is of primary importance in designing large subsonic transports powered by turbofan or turbojet engines.
- To maximize the range parameter ML/D the aircraft needs to cruise slightly into the drag divergence region.
- Computational Fluid Dynamics (CFD) methods have progressed to the point where wing design solutions can be obtained in a matter of minutes or hours.



- The technical feasibility of the Boeing Sonic Cruiser concept, Fig. 5.19, was essentially first established through CFD simulations.
- An SSBJ design must also pay close attention to efficient operation in the transonic region, as long as supersonic overflight of the U.S. remains prohibited.



a) Rigid wind tunnel model



b) Artist's concept

Fig. 5.19 The Boeing Sonic Cruiser was designed to fly close to Mach 1, but alas, never made it off the drawing board. (Courtesy Boeing).

Transonic Flow Characteristics

- Transonic flows with $M_{cr} < M_\infty < 1$ are characterized by embedded supersonic regions on the upper and/or lower wing surface, terminated by shock waves.
- The shocks generate additional drag, because of entropy production and shock-boundary layer interactions.
- Inside the supersonic region(s), the equation is locally hyperbolic and the rules of supersonic flow apply.
- Outside the supersonic regions, the local Mach number is less than one and the governing equation is elliptic and the rules of subsonic flow apply.

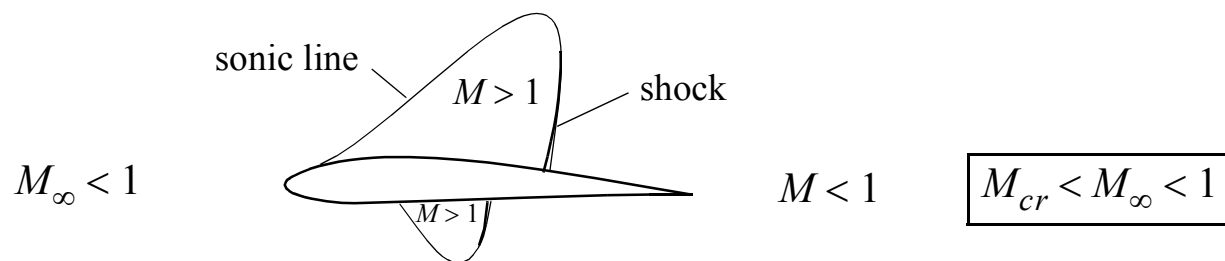


Fig. 5.20 Flow regions about airfoils and wings in transonic flow.

5.8.1 Finite Element Solutions of the Euler Equations

- Modern CFD codes based on the Euler equations are by now highly developed and well suited for use in preliminary design [8].
- The codes are often based on the weak or integral form of the conservation laws.
- Examples of unsteady 2D Euler calculations of transonic flows about the NACA 0012 airfoil are shown in Fig. 5.21.
- The airfoil is oscillating in pitch about the quarter chord, with the angle of attack given by

$$\alpha(t) = \alpha_m + \alpha_0 \sin \omega t \quad (5.76)$$

at a reduced frequency $k = \omega c / (2U_\infty) = 0.0808$.



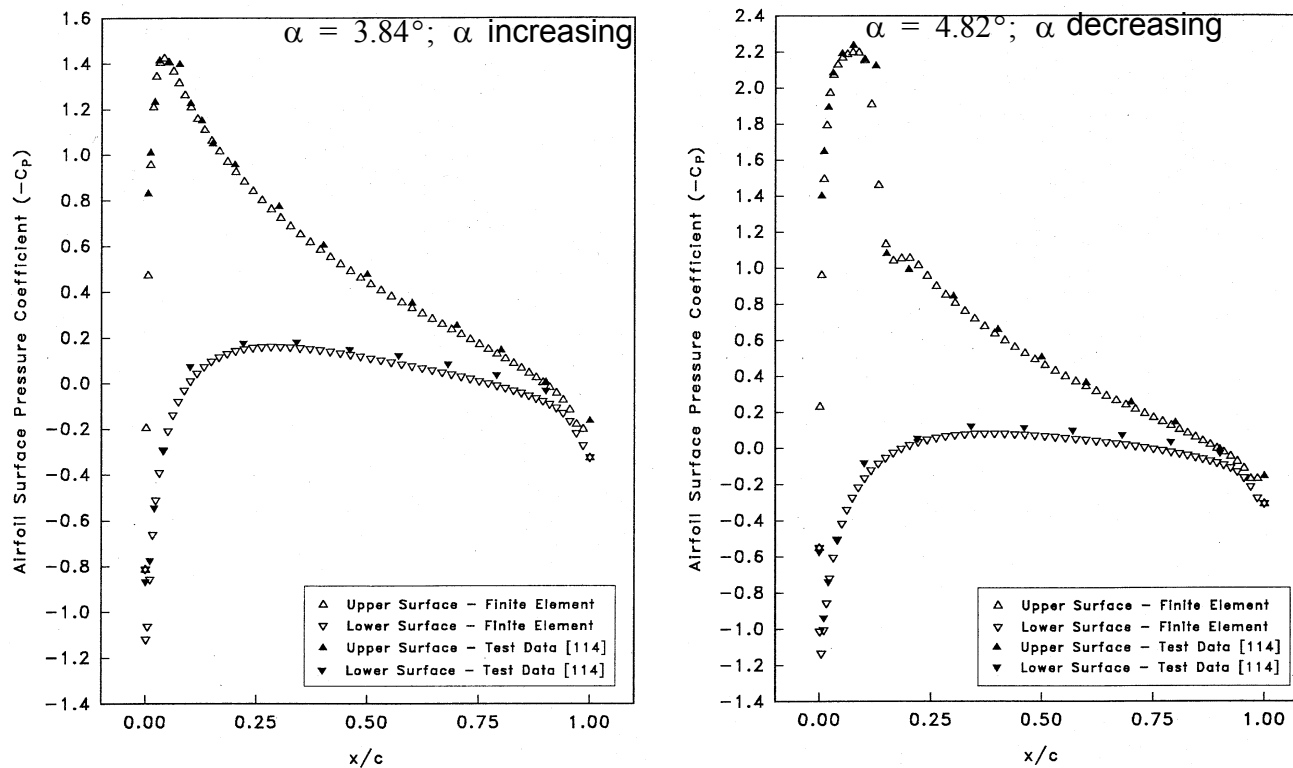
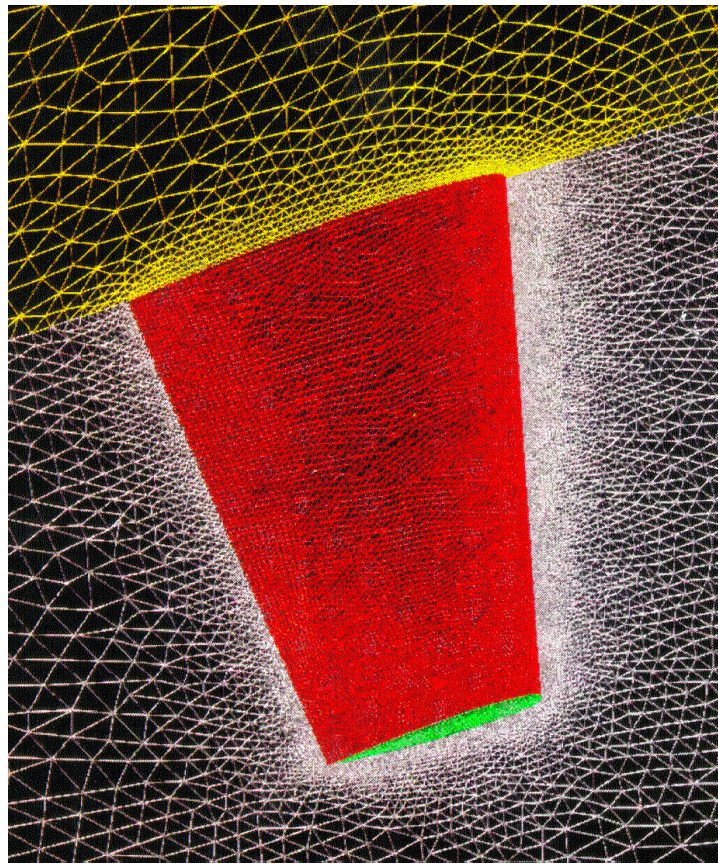


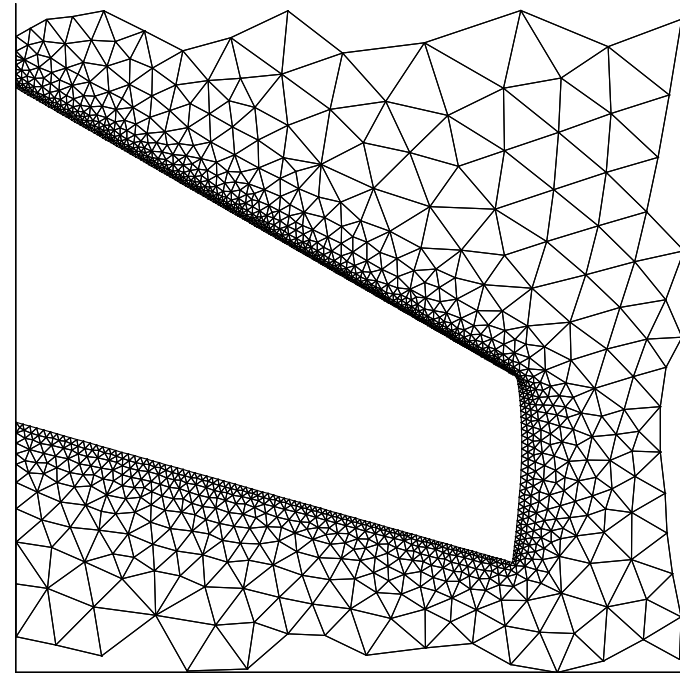
Fig. 5.21 CFD (Euler) calculations for the NACA 0012 airfoil section in transonic flow. Comparison of Finite Element results to AGARD CT1 experimental data for NACA 0012 airfoil pitching about $c/4$ -axis. ($M_\infty = 0.6$, $k = 0.0808$, $\alpha_m = 2.89^\circ$, $\alpha_0 = 2.41^\circ$). (Ref. 9).

- Note that although the Mach number is only 0.6, a shock forms near the leading edge during each pitch oscillation cycle, but does not last for the entire period (intermittent shock motion).

ONERA M6 Wing



a) Near field of Mesh 1



b) Top view of symmetry plane
(near field - Mesh 2)

Fig. 5.22 The ONERA M6 wing showing a typical CFD mesh on projected surfaces. The mesh is made up of 294,041 triangles forming 142,594 tetrahedra and the total number of unknowns is 148,000. ($A = 3.8$, $\lambda = 0.562$, $\Lambda_{LE} = 30^\circ$; ONERA "D" airfoil section).

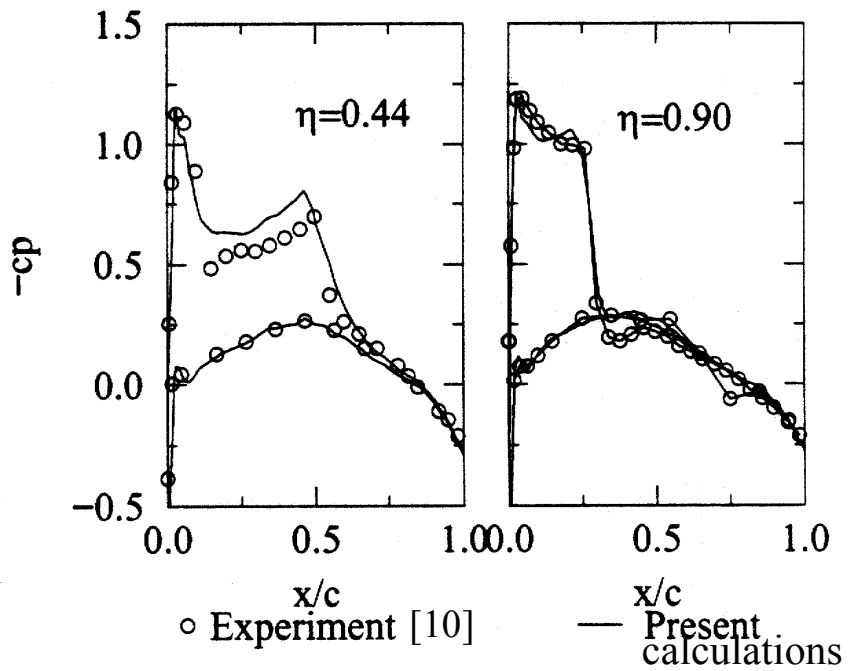
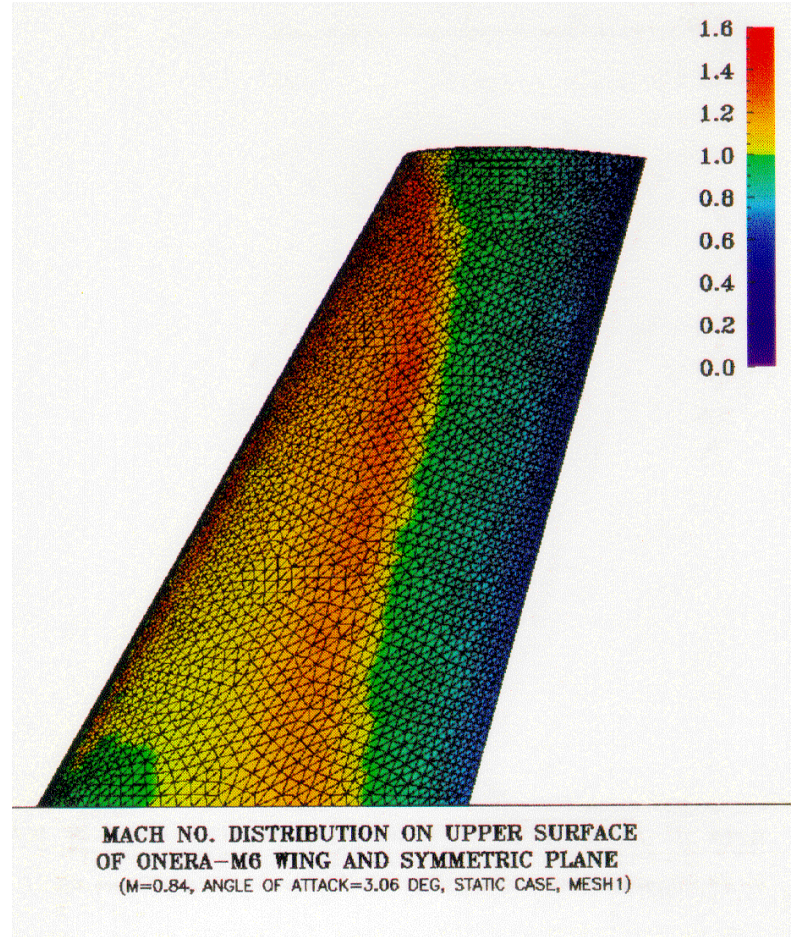


Fig. 5.23 Steady solution at design conditions ($M_{\infty} = 0.84$; $\alpha = 3.06^\circ$. From Ref. 11).

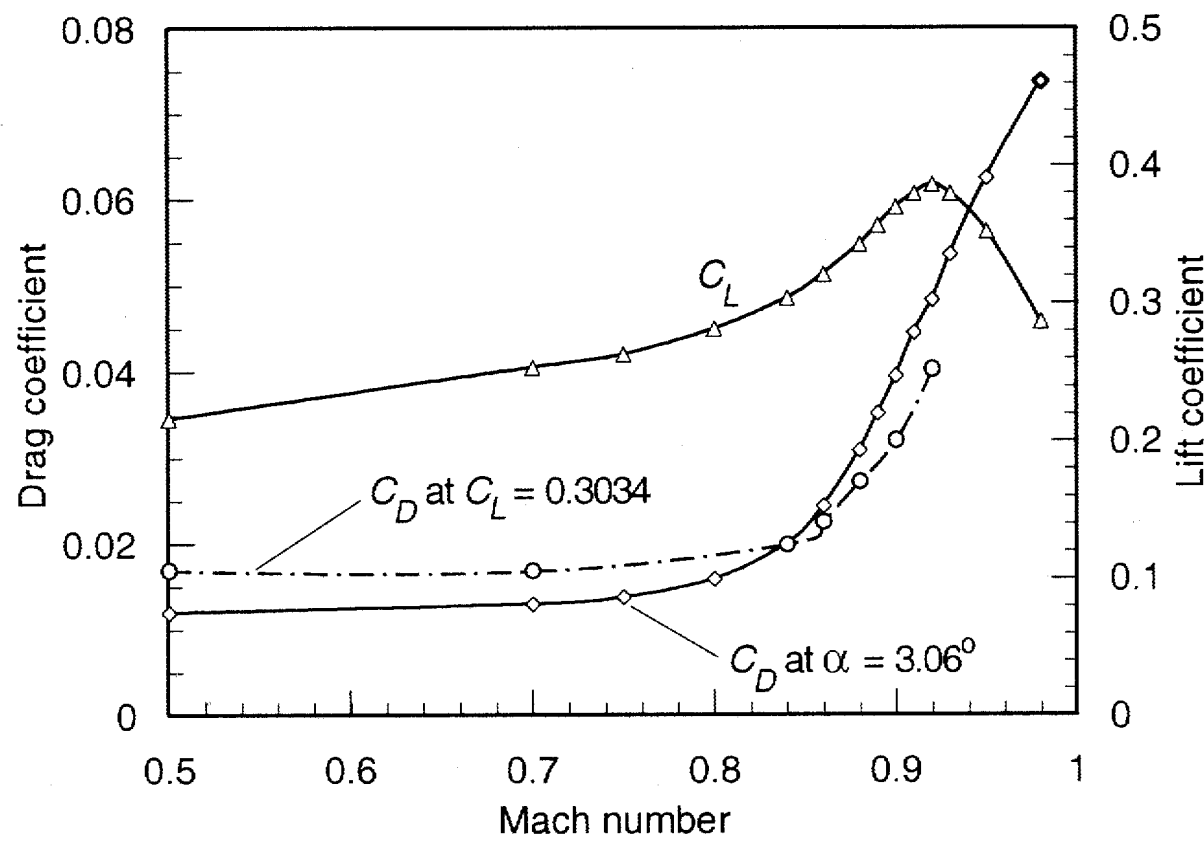
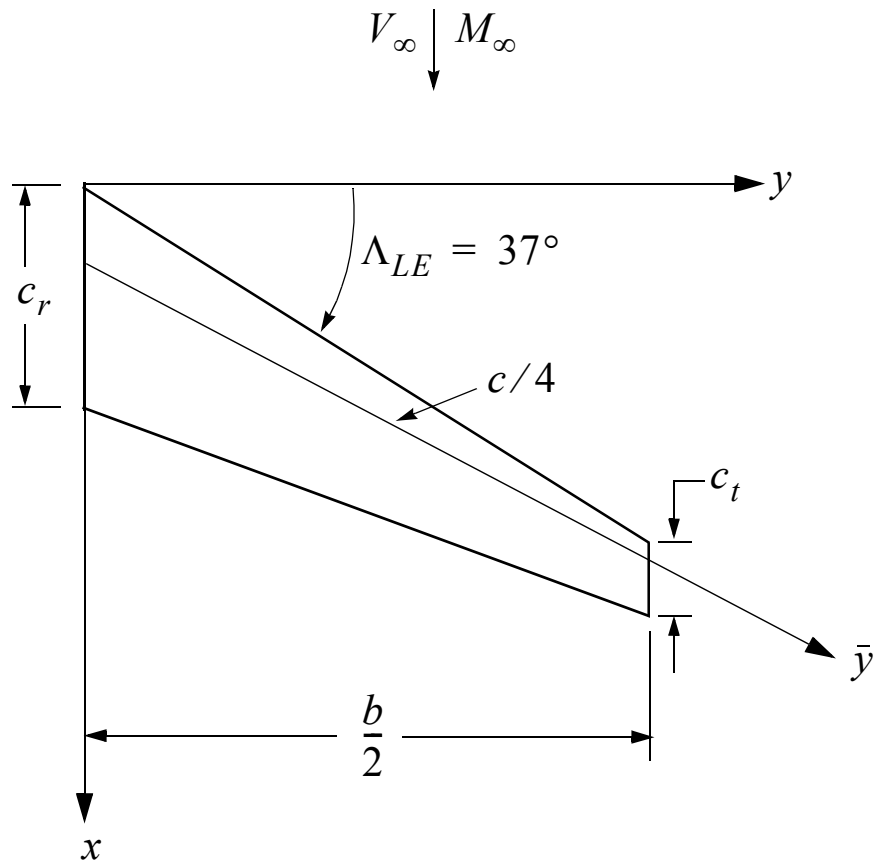


Fig. 5.24 Lift and drag behavior of the rigid ONERA M6 wing at transonic Mach numbers.

Transonic Transport Wing - Mach Number Effects



$$\frac{b}{2} = 2.5c_r$$

$$\lambda = \frac{c_t}{c_r} = 0.3886$$

$$A = \frac{b^2}{S} = 7.2015$$

$$\Lambda_{LE} = 37^\circ$$

$$\Lambda_{TE} = 26.98^\circ$$

$$MAC = 0.73917c_r$$

NACA 64A006 airfoil

No washout.

Fig. 5.25 High subsonic-transonic Mach number wing geometry.



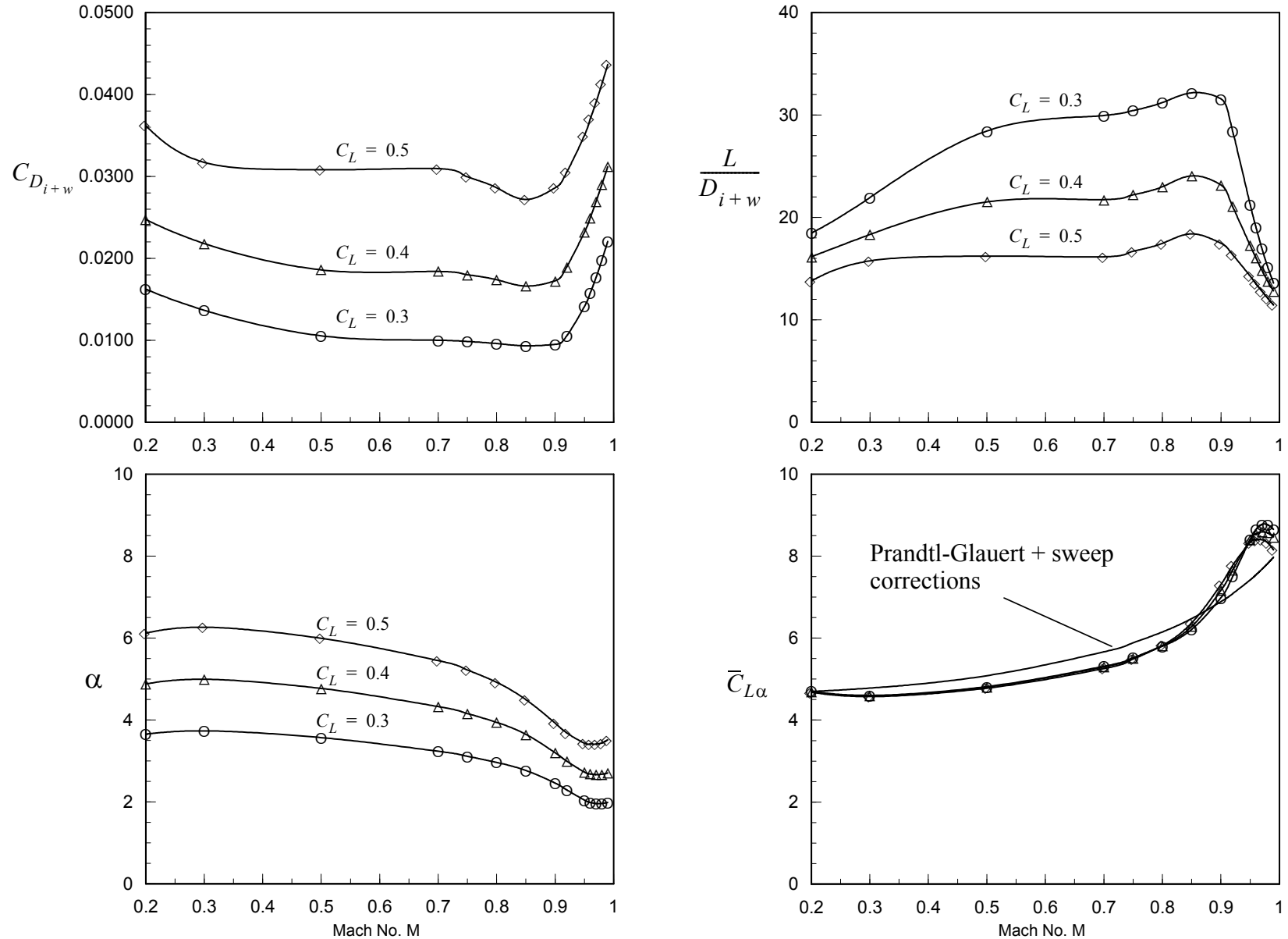


Fig. 5.26 Predicted aerodynamic behavior of wing vs. Mach number (Euler calculations).

5.8.2 Effect of Structural Deformations on Wing Aerodynamics

- For high aspect ratio swept wings, the effect of wing flexibility must be considered even at the preliminary design stage.
- Figures 5.27-29 show similar calculations for swept and unswept high aspect ratio transport wings, with the same ONERA “D” section (10% thick).
- Note that the angle of attack at the tip region of the swept wing *is only about 30% of the wing root angle*, and the spanwise lift distribution of the flexible wing is considerably different than that of the rigid wing.
- From a design standpoint, the calculated optimal wing washout is useless, unless it includes at least an estimate of the structural washout the wing.



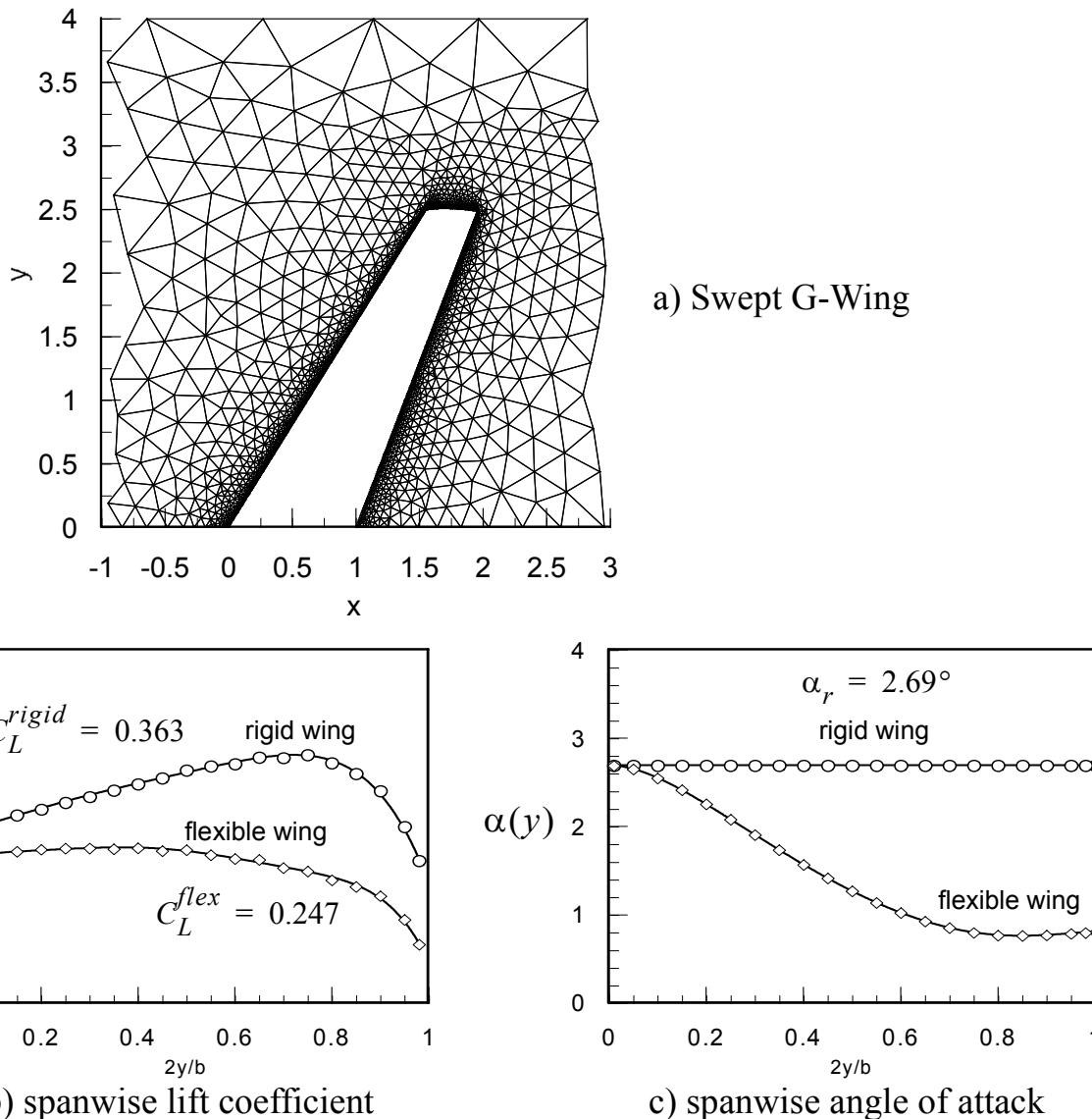


Fig. 5.27 Effect of structural deformations on lift distribution of a high aspect ratio swept wing in transonic flow. ($A = 7.05$, $\lambda = 0.41$, $\Lambda_{LE} = 31.9^\circ$; ONERA "D" airfoil section).

Structural Washout Effect

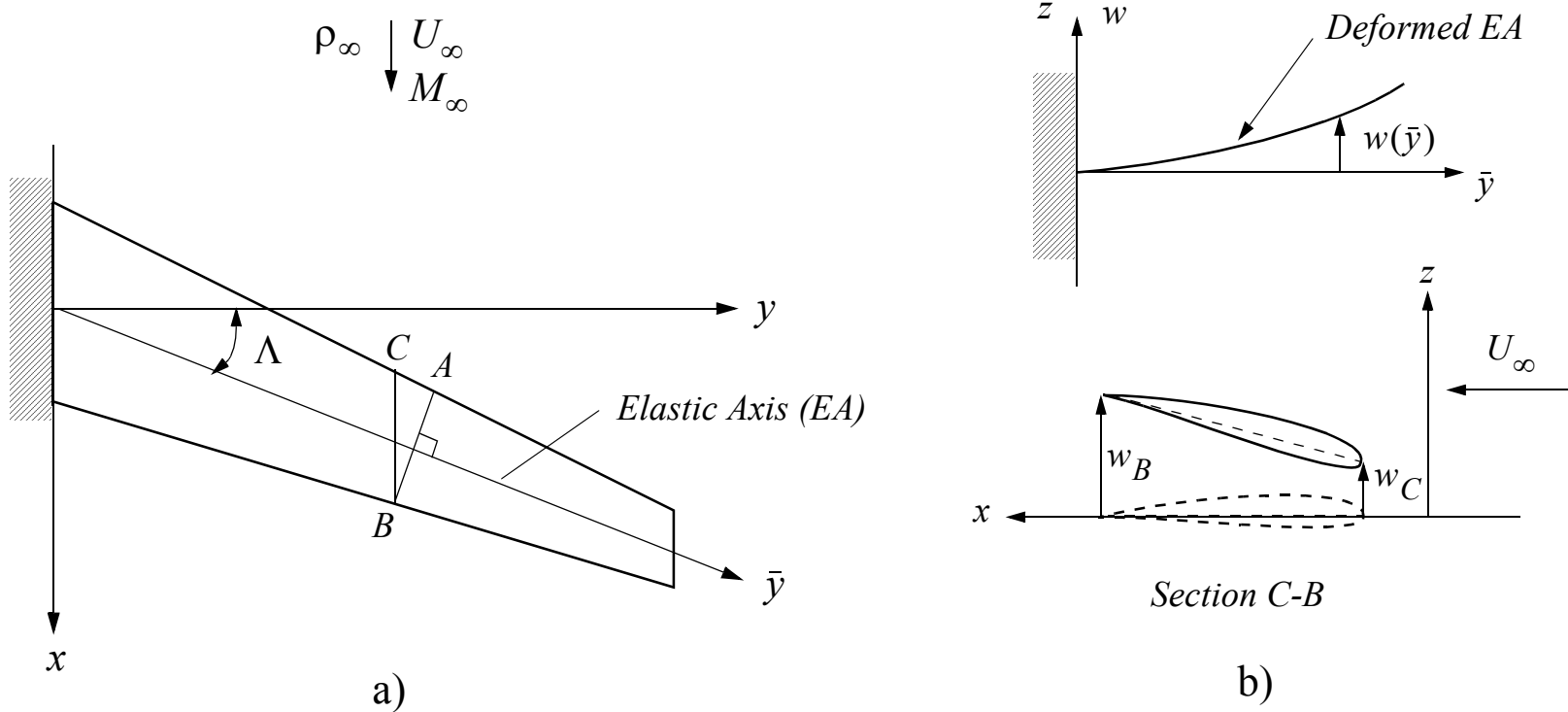


Fig. 5.28

a) Chordwise segment $A-B$ vs. streamwise segment $C-B$ of a swept wing

b) Structural washout effect (reduction of angle of attack of streamwise segment $C-B$, as $w_C < w_B$)

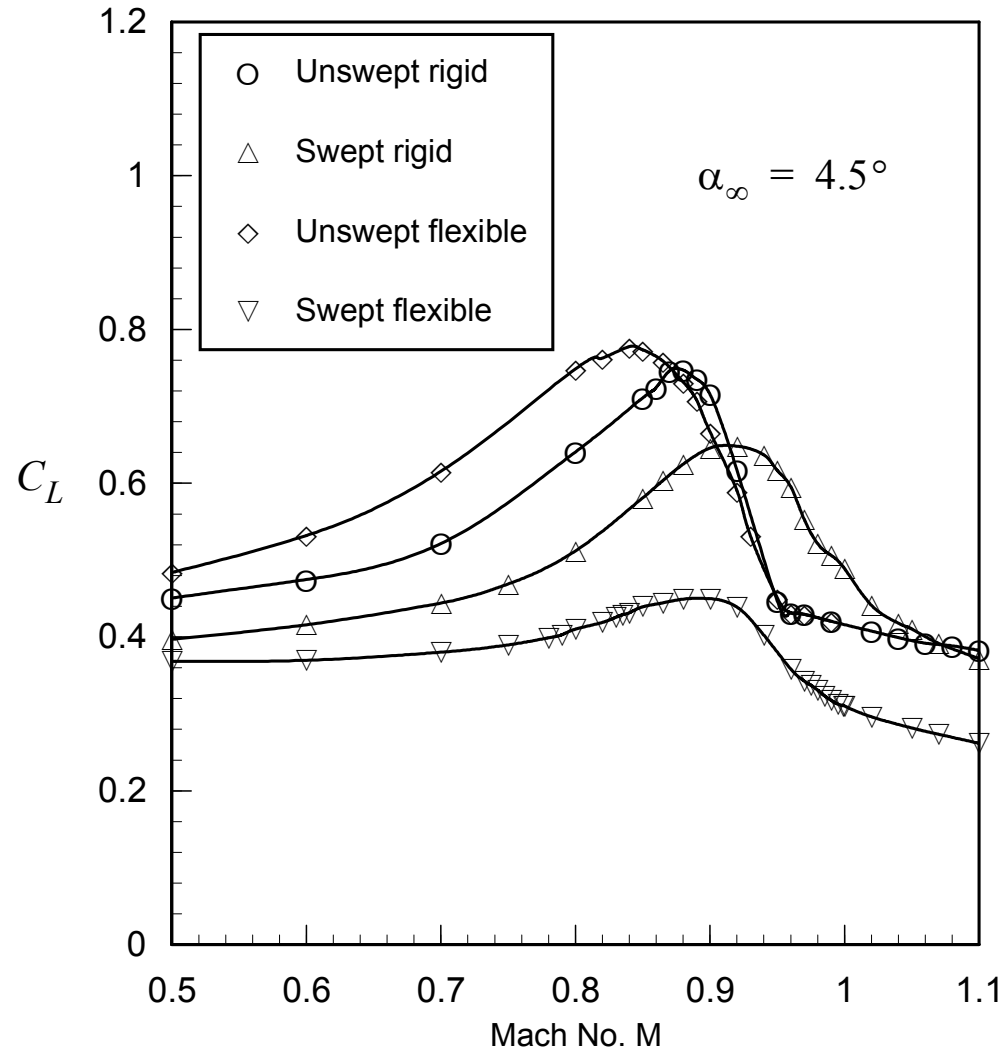
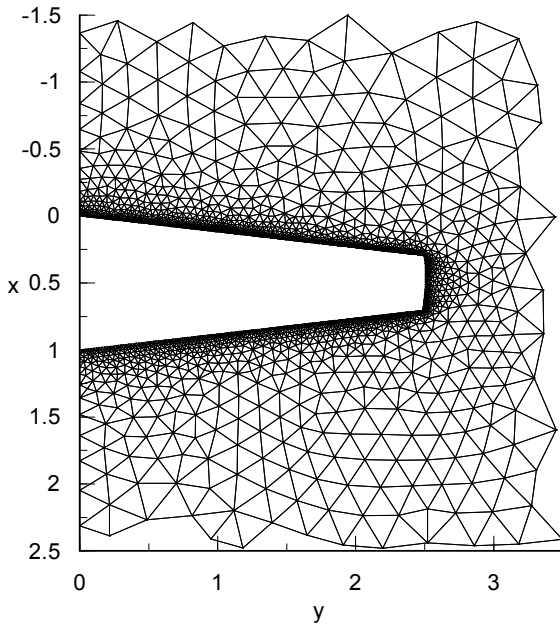


Fig. 5.29 Effect of sweep and flexibility (G-Wings at fixed angle of attack).



Swept and Unswept G-Wings



Unswept G-Wing

$$A = 7.05$$

$$\Lambda_{LE} = 6.77^\circ$$

$$\Lambda_{TE} = -6.77^\circ$$

$$\lambda = 0.41$$

Computational Domain

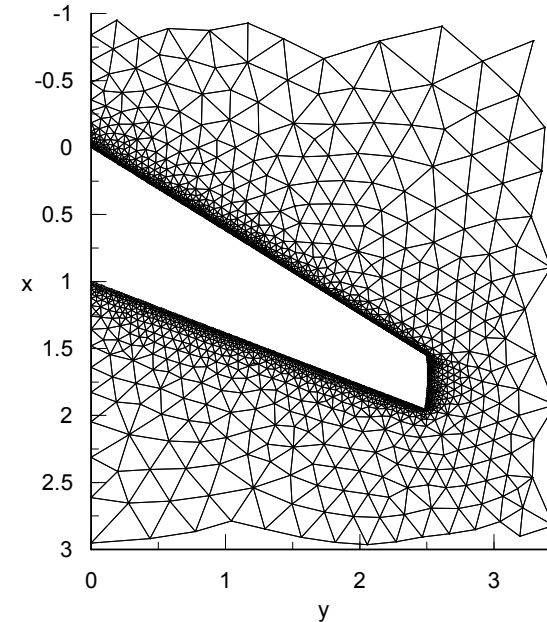
No. of nodes: 43,539

No. of faces: 432,289

No. of cells: 209,896

No. of structural plate elements: 96

No. of structural dof's: 168 (linear)
280 (nonlinear)



Swept G-Wing

$$A = 7.05$$

$$\Lambda_{LE} = 31.86^\circ$$

$$\Lambda_{TE} = 21.02^\circ$$

$$\lambda = 0.41$$

Computational Domain

No. of nodes: 43,344

No. of faces: 430,975

No. of cells: 208,926

No. of structural plate elements: 96

No. of structural dof's: 168 (linear)
280 (nonlinear)

Fig. 5.30



5.8.3 Aerodynamic Shape Optimization

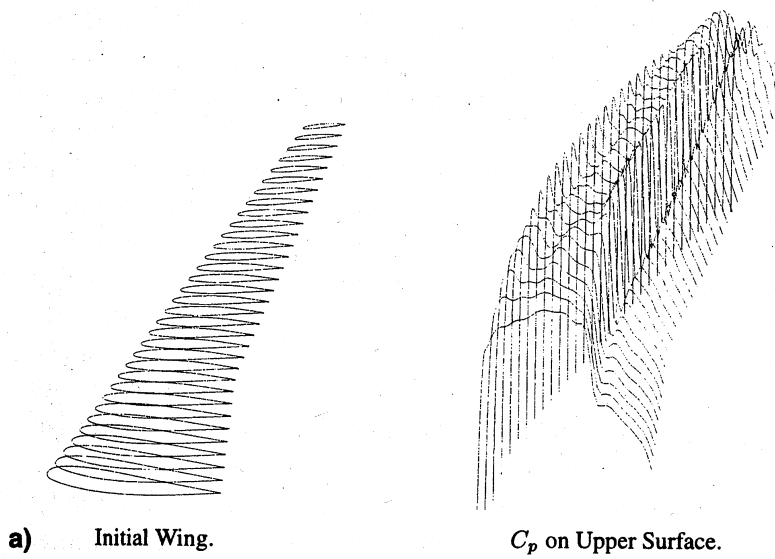
- Efficient CFD codes and faster computers have made it feasible to consider airfoil and wing shape design based on computational optimization procedures.
- Over the past decade, Jameson and his coworkers at Stanford University have demonstrated that CFD-based methods can be coupled with numerical optimization methods to form a basis for *automated aerodynamic design optimization*.
- They have developed a promising approach based on optimal control theory (or calculus of variations), which permits the computations of design sensitivities (gradients with respect to design variables) without having to recalculate the CFD aerodynamic solution.
- This is referred to by the authors as the “adjoint method”, since it involves the solution of the adjoint equation associated with the minimization problem.



Redesign Example: MDXX Aircraft

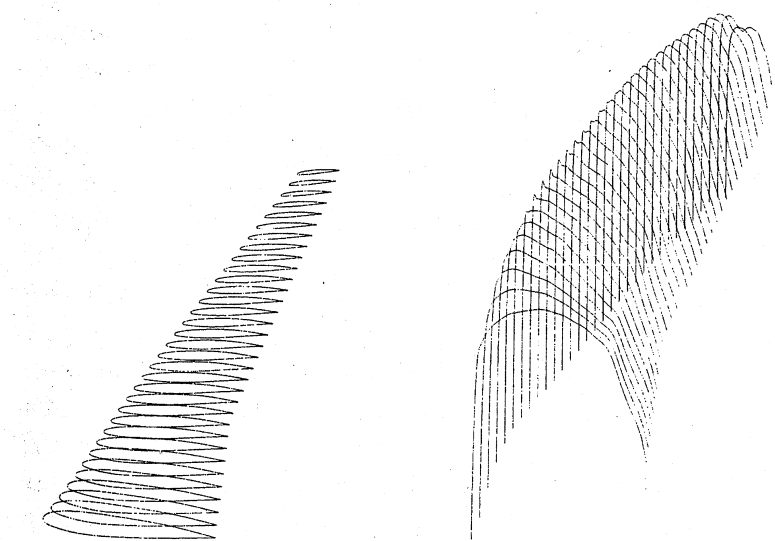
- Figures 5.31 and 5.32 show two aerodynamic wing shape optimization examples, taken from Ref. 12.
- The first is a redesign of a wing of a wide-body transport aircraft, to remove the upper surface shock and hence reduce the wave drag of the wing.
- The second example is taken from a design study that the Jameson group participated in on the MDXX aircraft (the proposed successor to the MD11).
- The study uncovered several areas of difficulty that made it difficult to judge the *actual aircraft* aerodynamic performance benefits that could be realized.
- Chief among these was the complex interaction between fuselage drag and the drag on the inboard region of the wing:
The wing optimization might actually be transferring drag from the wing to the fuselage.





a) Initial Wing.

C_p on Upper Surface.



b) Redesigned wing.

C_p on Upper Surface.

Fig. 5.31 Shape optimization to reduce drag of a transport wing in transonic flow: a) initial design: $M_\infty = 0.83$, $\alpha = 2.410^\circ$, $C_L = 0.5498$, $C_D = 0.0196$ b) redesigned wing after 60 design cycles: $M_\infty = 0.83$, $\alpha = 1.959^\circ$, $C_L = 0.5500$, $C_D = 0.0181$ Redesigned wing is shock-free, resulting in a drag reduction of 15 counts. (From Ref. 12).



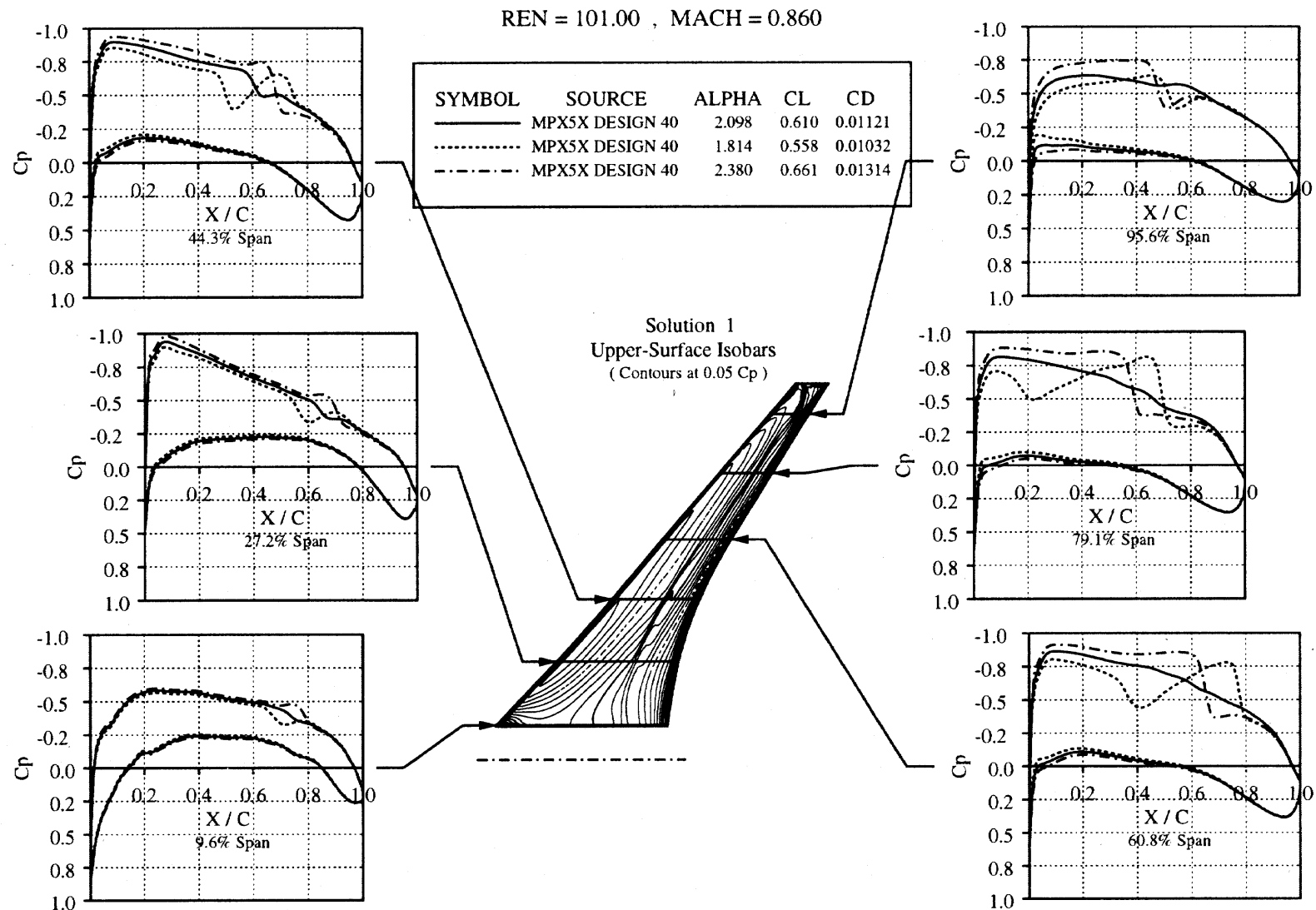


Fig. 5.32 McDonnell Douglas MDXX optimized wing at its design point and at lifts below and above design lift. (From Jameson, Ref. 12).

5.8.4 Transonic Similarity Rules

- The observed sensitivity of the transonic aerodynamic coefficients to wing thickness and angle of attack can be explained using the transonic similarity rules; see Refs. 14-18.
- The idea is to consider a family of “similar” wings of the same airfoil shape, Fig. 5.33, by scaling the wing profile

$$F_{u,l}(x, y) = \delta f_{u,l}(x, y) \quad (5.77)$$

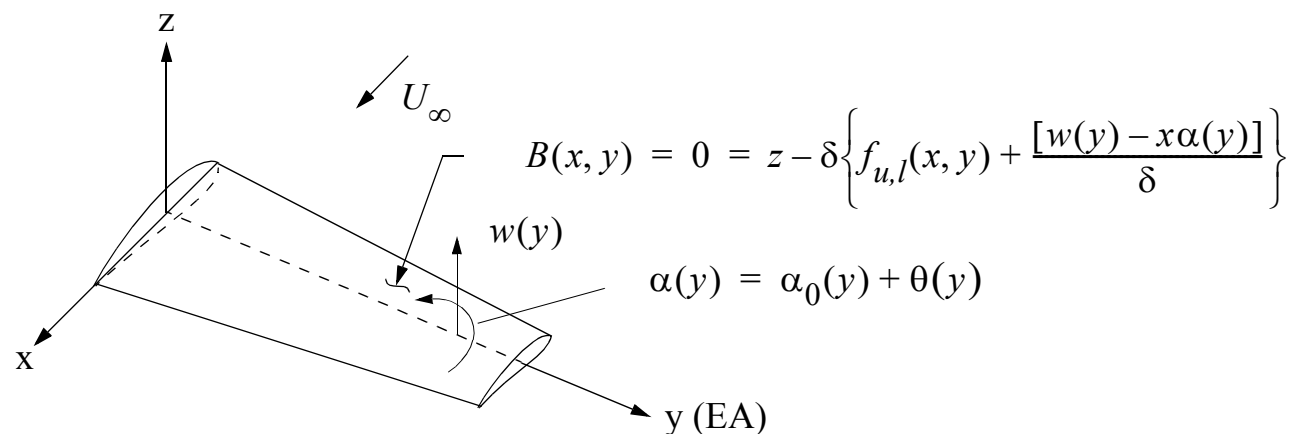


Fig. 5.33 Wing coordinate system and surface definition.

Transonic Scaling Laws

- The similarity rules for the aerodynamic lift and moment coefficients can then be stated in the form [17]

$$\begin{aligned} C_p &= \frac{\delta^{2/3}}{[(\gamma + 1)M_\infty^2]^{1/3}} \tilde{C}_p(\chi, \tilde{A}, \tilde{\alpha}, x/c, 2y/b) \\ C_L &= \frac{\delta^{2/3}}{[(\gamma + 1)M_\infty^2]^{1/3}} \tilde{C}_L(\chi, \tilde{A}, \tilde{\alpha}) \\ C_M &= \frac{\delta^{2/3}}{[(\gamma + 1)M_\infty^2]^{1/3}} \tilde{C}_M(\chi, \tilde{A}, \tilde{\alpha}) \\ C_D &= \frac{\delta^{5/3}}{[(\gamma + 1)M_\infty^2]^{1/3}} \tilde{C}_D(\chi, \tilde{A}, \tilde{\alpha}) \end{aligned} \tag{5.78}$$

- The “similarity functions” \tilde{C}_L and \tilde{C}_M and \tilde{C}_D are functions of the three similarity parameters χ , \tilde{A} , and $\tilde{\alpha}$:

$$\begin{aligned} \chi &= \frac{1 - M_\infty^2}{[(\gamma + 1)M_\infty^2 \delta]^{2/3}}; \quad \tilde{A} = [(\gamma + 1)M_\infty^2 \delta]^{1/3} A \\ \tilde{\alpha} &= \alpha / \delta \end{aligned} \tag{5.79}$$



Interpretation and Applications

- Here γ is the ratio of specific heats and A is the aspect ratio of the wing.
- Similar flows have the same pressure distributions, lift, moment, drag, etc., after they have been rescaled as specified by the similarity rules.
- The locations of the shocks on the airfoil or wing surfaces are also the same.
- The transonic similarity rules are useful in preliminary design calculations, as they provide simple formulas for the effect of wing thickness on lift, drag, etc.
- Using these relations, the effect of reducing the wing thickness, for example, can be estimated based on experimental or calculated data from a single wing of the same airfoil family.



5.8.5 Mach Number Freeze

- Near Mach 1, a curious phenomenon known as “Mach number freeze” occurs in steady two-dimensional flows; namely, the local Mach number at a point on or near the airfoil surface ahead of the shock “freezes” and becomes essentially independent of the freestream Mach number [19].
- In other words, the flow near the airfoil and ahead of the shock can be considered a small perturbation of a sonic flow [20].
- Conversely, a sonic flow can be considered a small perturbation of an off-sonic flow.
- This is also known as the “stabilization law” for transonic flows, and has been the subject of numerous experimental and theoretical investigations; see for example [19-22].
- Mathematically, the stabilization law is usually expressed as

$$\left. \frac{dM}{dM_\infty} \right|_{M_\infty = 1} = 0 \quad (5.80)$$



Transonic Stabilization Law

Steady 2D Flow

- Using the method of matched asymptotic expansions, Cook and Zeigler [20] showed that the local Mach number differs from that at sonic flow ($M_\infty = 1$) only by terms of order χ^3 , where χ is the transonic similarity parameter, Eq. (5.79).
- Thus, in the freeze region,

$$M_{u,l}(x/c, M_\infty) = M_{u,l}(x/c, 1) + O(\chi^3) \quad (5.81)$$

where x/c is the nondimensional chordwise location on the airfoil (ahead of the shock), and the subscripts u,l denote the upper and lower surface, respectively.

- Since $\chi = 0$ at $M_\infty = 1$, Eq. (5.80) follows.
- The stabilization law (or Mach number freeze) for steady 2D transonic flow appears to have been first discovered experimentally [19].
- This interesting flow behavior near Mach 1 is not well-known among aerodynamics engineers, even though it is of considerable practical importance from both an experimental as well as a theoretical standpoint.



Stabilization of Pressure Coefficient Steady 2D Flow

- The pressure coefficient on the airfoil can be expressed in terms of the local and freestream Mach numbers, as follows:

$$C_p = \frac{2}{\gamma M_\infty^2} \left[\left\{ \frac{2 + (\gamma - 1)M_\infty^2}{2 + (\gamma - 1)M^2} \right\}^{\frac{\gamma}{\gamma-1}} - 1 \right] \quad (5.82)$$

- Making use of the stabilization law for the local Mach number, Eq. (5.81), and expanding the denominator using the binomial theorem, we obtain:

$$C_p(x/c, M_\infty) = C_p(x/c, 1) + O(\chi^3) \quad (\text{ahead of shock}) \quad (5.83)$$

- Because the C_p freeze only occurs ahead of the shocks, no freeze (stabilization) of C_L and C_M occurs until the shocks have reached the trailing edge (Fig. 5.34c).
- For an NACA 0012 airfoil at zero angle of attack in inviscid flow, this occurs at roughly Mach 0.9 and corresponds to a transonic similarity parameter of

$$\chi = \frac{1 - M_\infty^2}{[(\gamma + 1)M_\infty^2 \delta]^{2/3}} = \frac{1 - 0.9^2}{[(1.4 + 1)(0.9^2)(0.12)]^{2/3}} = 0.5014 \approx 0.5 \quad (5.84)$$



Stabilization of Lift and Moment Coefficients

Steady 2D Flow

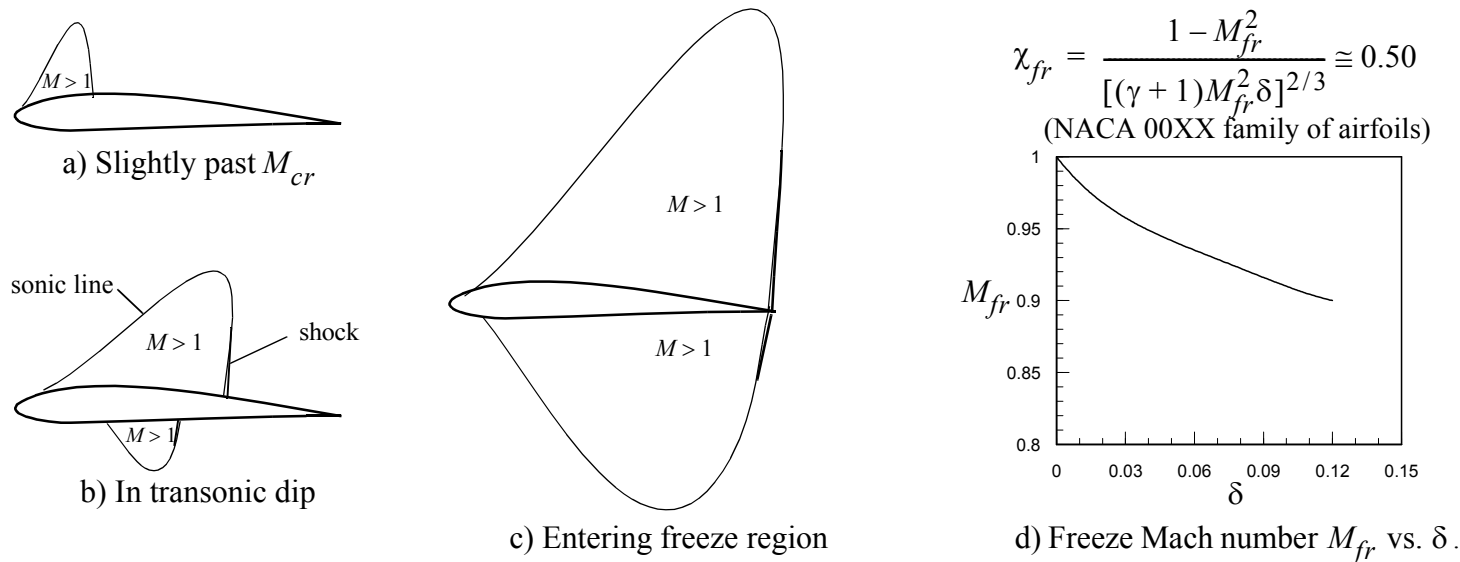


Fig. 5.34 Mach number freeze and transonic stabilization of lift and moment coefficients [24].

- The stabilization laws for C_L and C_M are of the same form as Eq. (5.83)

$$C_L(M_\infty) = C_L(1) + O(\chi^3) \quad (5.85)$$

$$C_M(M_\infty) = C_M(1) + O(\chi^3) \quad (M_{fr} \leq M_\infty \approx 1)$$

- Here M_{fr} is the corresponding freeze Mach number at which both the upper and lower shocks have reached the trailing edge; see Fig. 5.34c).

Lift Curve Slope Nonuniformity

Mach Number Freeze

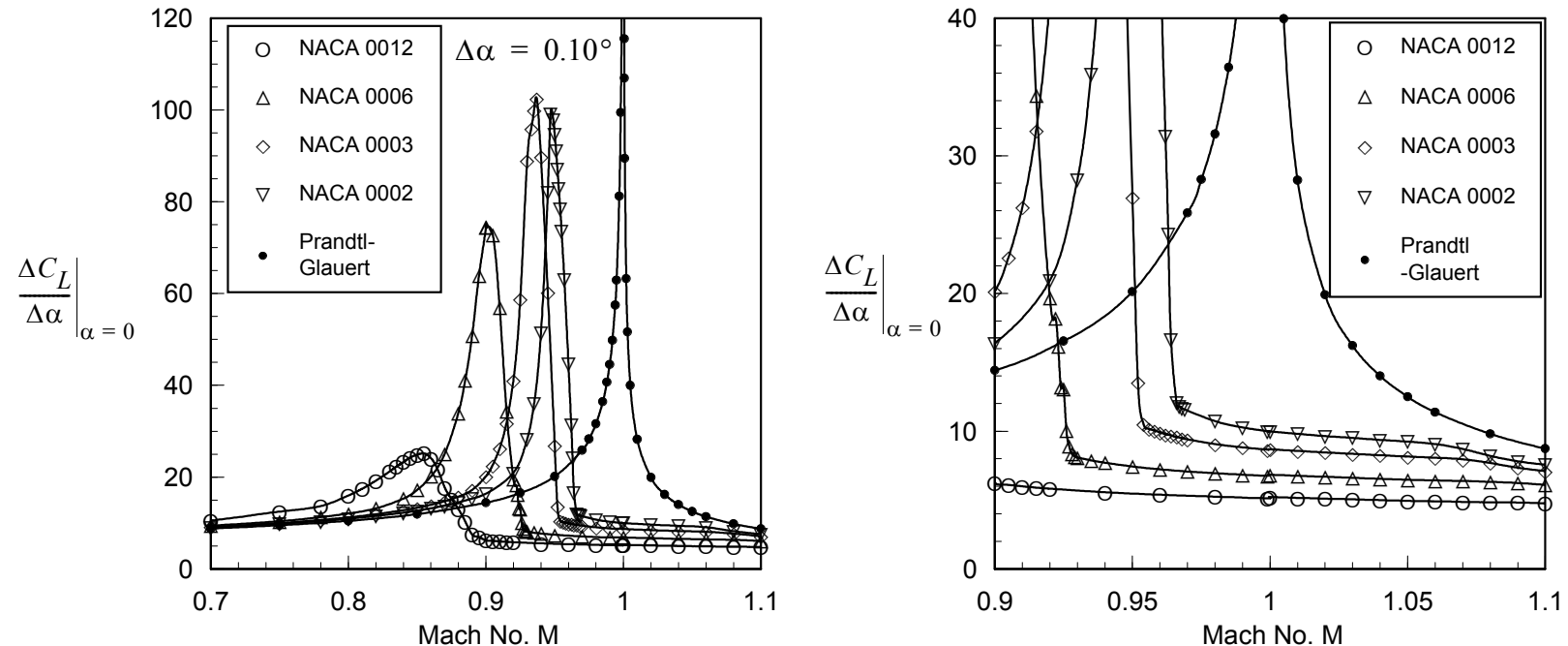


Fig. 5.35 Nonuniform behavior of the calculated lift curve slopes of the NACA 00XX series of airfoils in transonic flow, and comparison with Prandtl-Glauert rule (Euler calculations). Note abrupt lift slope "freeze" past the peaks (right figure) and high sensitivity to airfoil thickness.

- Figure 5.35 shows results of nonlinear Euler calculations of the lift curve slope evaluated at $\alpha = 0$, as a function of airfoil thickness and Mach number [24].
- The peaks and subsequent rapid fall-offs (reversals) are qualitatively similar to experimentally measured behaviors of symmetric 2D sections [23].

Numerical Considerations Near Lift Curve Slope Peaks

- Any computational determination of the lift curve slope $dC_L/d\alpha$ must be based on calculations of the mean slope $\Delta C_L/\Delta\alpha$ for some small but finite $\Delta\alpha$.
- At and near the $dC_L/d\alpha$ peaks, the lift curve slope as $\Delta\alpha \rightarrow 0$ becomes progressively more nonlinear as the airfoil thickness is decreased and the calculated heights of the peaks then become sensitive to the choice of $\Delta\alpha$, especially for thin airfoils.
- Any experimental determination of the lift curve slope near the breaks faces similar problems.
- As can be seen from Fig. 5.35, the lift curve slopes of the NACA 00XX airfoils do indeed become frozen and almost independent of Mach number for $M_{fr} \leq M_\infty \approx 1$.
- The lift coefficient at a fixed angle of attack also becomes frozen.
- The scaling with respect to airfoil thickness follows from Eq. (5.84). For example, as the thickness δ is reduced from 12% (NACA 0012) to 6% (NACA 0006), the freeze Mach number increases from 0.90 to 0.935.
- For the 3% thick NACA 0003 airfoil, the freeze starts at about Mach 0.958.



3D Wings Mach Freeze

- In the case of a 3D wing, the onset of stabilization of the local lift and moment coefficients $c_l(y)$ and $c_m(y)$ would be expected to occur when the shocks at span location y have reached the trailing edge.
- Because of the 3D shock structure, this will occur first at the root of the wing and last at the tip.
- The stabilization of the transonic flow near Mach 1 would therefore be more gradual, but should nevertheless occur for unswept wings as well as for wings of low to moderate sweep.



The Sound Barrier Revisited

The Myth of a Sonic Wall

- Classical linear theory of potential flow has a singularity at Mach one, predicting infinite aerodynamic loads
- The transonic stabilization law (Mach number freeze) comes to the rescue and rules out such a singularity and thus also the old myth of a “sonic wall”
- The strong nonuniformities appearing in the nonlinear aerodynamics immediately before the freeze are largely responsible for the transonic dip and certain curious transonic flutter phenomena
- Had the designers of the Bell X-1 aircraft been aware of the Mach number freeze phenomenon, they would have realized that the critical Mach number from a loads standpoint is not Mach 1, but considerably lower, at or near the lift breaks.



5.9 References

1. Prandtl, L. and Tietjens, O.G., *Applied Hydro- and Aerodynamics*, Dover Edition, 1957.
2. Munk, M. M., *The Minimum Induced Drag of Aerofoils*, NACA Report 121, 1921.
3. von Mises, R., *Theory of Flight*, Dover Edition, 1959.
4. Sivells, J.C., *Experimental and Calculated Characteristics of Three Wings of NACA 64-210 and 65-210 Airfoil Sections With and Without 2° Washout*, NACA TN 1422, 1947.
5. Sivells, J.C. and Neely, R.H., *Method for Calculating Wing Characteristics by Lifting-Line Theory Using Nonlinear Section Lift Data*, NACA TN 1269, 1947.
6. Prandtl, L., *Applications of Modern Hydrodynamics to Aeronautics*, NACA Technical Report No. 116, 1921.
7. Kuethe, A.M. and Chow, C-Y., *Foundations of Aerodynamics*, John Wiley & Sons, 5th edition, 1998.
8. Bendiksen, O.O., “Modern Developments in Computational Aeroelasticity”, *Journal of Aerospace Engineering*, Vol. 218, June, 2004, pp. 157-178.
9. Davis, G.A. and Bendiksen, O.O., “Unsteady Transonic Two-Dimensional Euler Solutions Using Finite Elements”, *AIAA Journal*, Vol. 31, June 1993, pp. 1051-1059.



-
10. Schmitt, V., and Charpin, F., "Pressure Distribution on the ONERA M6 Wing at Transonic Mach Numbers," *Experimental Data Base for Computer Program Assessment*, AGARD-AR-138, Appendix B1, May 1979.
11. Bendiksen, O.O. and Hwang, G., "Nonlinear Flutter Calculations for Transonic Wings," *Proc. International Forum on Aeroelasticity and Structural Dynamics, Vol. II*, June 17-20, 1997, Rome, Italy, pp. 105-114.
12. Jameson, A., "Re-Engineering the Design Process Through Computation", *Journal of Aircraft*, Vol. 36, No. 1, Jan-Feb 1999, pp 36-50.
13. Breitbach, E., "Adaptive Structural Concepts: State of the Art and Future Outlook," *Proc. International Forum on Aeroelasticity and Structural Dynamics*, Rome, Italy, June 17-20, 1997, pp. 69-77.
14. Liepmann, H.W. and Roshko, A., *Elements of Gasdynamics*, John Wiley & Sons, 1957.
15. von Kármán, T. "The Similarity Law of Transonic Flow," *Journal of Mathematics and Physics*, Vol. XXVI, No. 3, October 1947, pp. 182-190.
16. Spreiter, J. R., "On the Application of Transonic Similarity Rules to Wings of Finite Span," *NACA Report 1153*, 1953.
17. Bendiksen, O.O., "Improved Similarity Rules for Transonic Flutter", *AIAA Paper 99-1350*, April 1999.
18. Bendiksen, O.O., "Transonic Flutter Prediction", *Proc. CEAS/AIAA/NVvL Int. Forum on Structural Dynamics and Aeroelasticity (IFASD 2003)*, Amsterdam, The Netherlands, June 4-6, 2003.



-
- 19.Diesperov, V.N., Lipshitz, Y.B., and Ryzhow, O.S., Stabilization Law and Drag in Transonic Range of Velocities," *Symposium Transsonicum II*, Oswatish and Rues, eds., Springer-Verlag, Berlin 1975, pp. 156-164.
- 20.Cook, L.P., and Zeigler, F.J., "The Stabilization Law for Transonic Flow," *SIAM Journal of Applied Mathematics*, Vol. 46, No. 1, February 1986, pp. 27-48.
- 21.Cole, J. D., and Cook. L. P., *Transonic Aerodynamics*, Elsevier Science Publishers, Amsterdam, 1986.
- 22.Zierep, J., "The Freezing Property (Stabilization Law) of Transonic Flows, *Acta Mechanica*, Vol. 108, 1995, pp. 2190223.
- 23.Bendiksen, O.O., "Review of Unsteady Transonic Aerodynamics: Theory and Applications," *Progress in Aerospace Sciences*, Vol. 47, Issue 2, February 2011, pp. 133-167.
- 24.Bendiksen, O.O., "Transonic Stabilization Laws for Unsteady Aerodynamics and Flutter," AIAA Paper 2012-1718, *Proc. 53rd AIAA/ASME/ASCE/AHS/ASCE SDM Conf.*, Honolulu, HI, April 23-26, 2012.

